

THE ROLE OF INDIVIDUAL PROTEIN TURNOVER IN SKELETAL MUSCLE ADAPTATION.

STUART JAMES HESKETH

A thesis submitted in partial fulfilment of the requirements of
Liverpool John Moores University for the degree of
Doctor of Philosophy.

September 2019

Table of Contents

ABSTRACT.....	4
DECLARATION.....	5
ACKNOWLEDGMENTS	6
GLOSSARY OF TERMS.....	7
CHAPTER 1. REVIEW OF THE LITERATURE.	11
1.1 ABSTRACT	11
1.2 MUSCLE PHENOTYPE AND PLASTICITY	12
<i>Objectives</i>	25
1.3 BIBLIOGRAPHY	26
<i>References</i>	26
CHAPTER 2. THE DYNAMIC PROTEOME PROFILING METHOD.....	32
2.1 ABSTRACT	32
2.2 METHODOLOGY DEVELOPMENT RATIONALE.....	33
<i>Objectives</i>	48
2.3 EXPERIMENTAL DESIGN	49
2.4 LABORATORY PROCESSING	51
2.4.1 <i>Laboratory workflow</i>	51
2.4.2 <i>Exemplar experimental methods</i>	53
2.4.3 <i>Measurement of precursor enrichment</i>	53
2.4.4 <i>Muscle processing</i>	54
2.5 ANALYSIS OF MYOFIBRILLAR PROTEINS	55
2.5.1 <i>Top-down proteomic analysis</i>	55
2.5.2 <i>Abundance analysis</i>	55
2.5.3 <i>Matrix-assisted laser desorption ionisation tandem time of flight mass spectrometry</i>	56
2.6 ANALYSIS OF SOLUBLE PROTEINS	58
2.6.1 <i>Bottom-up proteomic analysis</i>	58
2.6.2 <i>Abundance analysis</i>	58
2.6.3 <i>Liquid chromatography-mass spectrometry</i>	59
2.7 TURNOVER CALCULATIONS.....	61
2.7.1 <i>Individual Protein Synthesis rates</i>	61
2.7.2 <i>Individual Protein Degradation rates</i>	63
2.7.3 <i>Absolute Protein turnover rates</i>	64
2.7.4 <i>Statistical Analysis</i>	67
2.8 RESULTS.....	68
2.9 DISCUSSION	74
2.10 CONCLUSION.....	77
2.11 BIBLIOGRAPHY	78
<i>References</i>	78
CHAPTER 3. THE ROLE OF PROTEIN TURNOVER IN SKELETAL MUSCLE ADAPTATION INDUCED BY CHRONIC LOW-FREQUENCY STIMULATION.....	83
3.1 ABSTRACT.....	83
3.2 INTRODUCTION.....	85

<i>Objectives</i>	89
3.3 METHODS	90
3.4 RESULTS	94
3.5 DISCUSSION	120
3.6 CONCLUSIONS	127
3.7 BIBLIOGRAPHY	128
<i>References</i>	128
<i>Supplementary tables</i>	133
<i>Supplementary figures</i>	152
CHAPTER 4. THE ROLE OF PROTEIN TURNOVER IN SKELETAL MUSCLE ADAPTATION INDUCED BY CO-CONTRACTION HIGH-FREQUENCY STIMULATION.	158
4.1 ABSTRACT	158
4.2 INTRODUCTION	160
<i>Objectives</i>	169
4.3 METHODOLOGY	169
4.4 RESULTS	173
4.5 DISCUSSION	197
4.6 CONCLUSIONS	203
4.7 BIBLIOGRAPHY	204
<i>References</i>	204
<i>Supplementary tables</i>	209
CHAPTER 5. GENERAL DISCUSSION	224
5.1 ABSTRACT	224
5.2 GENERAL COMMENTARY	225
5.3 BIBLIOGRAPHY	236
<i>References</i>	236
CHAPTER 6. FUTURE DIRECTIONS	238
<i>References</i>	240

Abstract

Skeletal muscle tissue demonstrates a remarkable malleability and can adjust its metabolic and contractile makeup in response to alterations in functional demands. As a result, great diversity exists in muscle physiology, biochemistry and energy metabolism, all of which are underpinned by the functional changes in the abundance of individual proteins. The proteome represents a highly dynamic and versatile entity that coordinates the adaptive response of skeletal muscle through adjustments in individual protein turnover as well as abundance. Until very recently, research relating to protein turnover was largely limited to average synthesis rates of protein mixtures, e.g. from whole muscle homogenates. This project utilises our new methodology, coined dynamic proteome profiling, combining deuterium labelling and advanced proteomic techniques with computational biology, to investigate muscle protein dynamics at the individual protein level. We have used programmed exercise to perturb skeletal muscle *in vivo* for the purposes of studying two contrasting types of muscle adaptation, each over a chronic 30-day period. The first is an endurance stimulus that induced changes in protein abundance for 50 individual muscle proteins. Of these changes, 30 % were driven by changes in synthesis, 38 % were driven by degradation only and the remaining 32 % by changes in a combination of both synthesis and degradation. We also provide new evidence to demonstrate that in response to resistance exercise training individual proteins increase the rates of protein turnover and can be selectively degraded at varying rates to alter individual protein abundances. As a result, we report, 27 of 91 proteins studied exhibited a change in abundance in response to muscle hypertrophy. Of which 96 % were driven by synthesis and 4 % of proteins were driven by degradation. For the remaining 64 proteins that did not change in abundance, 36 % increased protein turnover, 17 % decreased in protein turnover and 47 % of proteins were unaffected by our resistance exercise training stimulus. This work is the first of its kind and presents a highly novel contribution to the rapidly growing field of exercise proteomics.

Declaration

I Stuart Hesketh declare that all work presented here in this thesis was written by me and is my own. No portion of the work referred to in this thesis has been submitted in support of an application for another degree or qualification of Liverpool John Moores University, any other university or other institute of learning.

A handwritten signature in black ink, appearing to read 'Stuart Hesketh', with a horizontal line extending to the right from the end of the signature.

16/12/19

Acknowledgments

I would like to express my special thanks of gratitude for all of those who have made it possible for me to complete my PhD studies. Firstly, my mentor and director of studies, Professor Jatin Burniston. Jatin's tireless work ethic and astute attention to detail has been my inspiration throughout. His guidance and supervision have been first class, providing endless opportunities to access his deep and quite remarkable subject knowledge both inside and outside of the lab. Jatin has always provided me with timely and detailed feedback of my work which has accelerated my development and understanding allowing me to work through problems for myself in a highly challenging subject area. My two other project supervisors: Professor Jonathan Jarvis and Professor Paulo Lisboa have both been accessible and knowledgeable in their areas of expertise and I thank them deeply for their invaluable contributions and advice. Jonathan in particular I owe special thanks to, as without his vast experience and immense practical skill in working with animals then my PhD would not have been possible. I also sincerely thank his research team, Dr Hazel Sutherland, Mark Viggars and Steffen Eickhoff for all their help with the animal interventions and data collection. I must also thank Steve Broadfoot and his team in the animal facility who came in everyday to care for their wellbeing and whose wealth of experience in animal handling allowed our experiments to run smoothly. I also give my thanks to the team of post-graduate researchers, MSc and undergraduate students that work out of Jatin's lab; who all assisted in some way with lab work during busy periods and offered thoughtful and valuable discussion of my work during many of our lab meetings. Thanks to: Dr Tom Brownlee, Dr Katie Whytock, Alex Brown, Sam Bennett, Jen Barrett, Rob Morton, Denis Kusic, Andrew Noad, Luke Kelly, Connor Stead and Ben Stansfield. Finally, I would like to thank my family who have supported me fully throughout this undertaking, never complaining about my frustrations and long hours of work but selflessly allowing me to totally engage in my research, sometimes to the detriment of themselves. To everybody mentioned above, I reiterate my enormous thanks for your encouragement, advice and support, you have all made the completion of this thesis possible in your own way. Thank-you!

Glossary of Terms

1DGE	One dimensional gel electrophoresis
2D	Two dimensional
2DGE	Two dimensional gel electrophoresis
² H	Deuterium
² H ₂ O	Deuterium oxide
3MH	3-methylhistidine
A-V	arterial–venous balance
AA	Amino acid
AATC	Aspartate aminotransferase, cytoplasmic
AATM	Aspartate aminotransferase, mitochondrial
ACADL	Long-chain specific acyl-CoA dehydrogenase, mitochondrial
ACON	Aconitate hydratase, mitochondrial
ACTH	Adrenocorticotrophic hormone
ACTN1	Alpha-actinin-1
ACTS/ACTC	Actin, alpha skeletal muscle/ Actin, alpha cardiac muscle 1
ADH-1	Alcohol dehydrogenase 1
ADR	Absolute degradation rate
ADT1	ADP/ATP translocase 1
ALBU	Serum albumin
ALBU	Serum albumin
ALDOA	Fructose-bisphosphate aldolase A
ALDR	Aldo-keto reductase family 1 member B1
ANXA4	Annexin A4
ASR	Absolute synthesis rate
AT2A1	Sarcoplasmic/endoplasmic reticulum calcium ATPase 1
AT2A2	Sarcoplasmic/endoplasmic reticulum calcium ATPase 2
ATP5H	ATP synthase subunit d, mitochondrial
ATPA	ATP synthase subunit alpha, mitochondrial
ATPase	ATP synthase
ATPB	ATP synthase subunit beta, mitochondrial
ATPG	ATP synthase subunit gamma, mitochondrial
ATPO	ATP synthase subunit O, mitochondrial
BSA	Bovine serum albumin
Ca ²⁺	Calcium ion
CAH3	Carbonic anhydrase 3
CASQ1	Calsequestrin-1
CHAPS	3-[(3-Cholamidopropyl)dimethylammonio]-1-propanesulfonate hydrate
CHFS	Co-contraction high-frequency stimulation
CISY	Citrate synthase
CLFS	Chronic low-frequency stimulation

CO ₂	Carbon dioxide
COF1	Cofilin-1
COX2	Cytochrome c oxidase subunit 2
CRYAB	Alpha-crystallin B chain
Ctrl	Non-stimulated, contralateral control muscle
CV	Coefficient of variation
CX7A2	Cytochrome c oxidase subunit 7A2, mitochondrial
CYC	Cytochrome c
Da	Dalton
DESM	Desmin
DPP	Dynamic proteome profiling
DTT	Dithiothreitol
ECHA	Trifunctional enzyme subunit alpha
EDL	Extensor digitorum longus
EF1A2	Elongation factor 1-alpha 2
ENOB	Beta-enolase
ESI-Q-TOF	Electrospray ionisation quadrupole time of flight
FABPH	Fatty acid-binding protein, heart
FASP	Filter aided sample preparation
FDL	Flexor digitorum longus
FDR	Fractional degradation rate
FDR	Fractional degradation rate
FHL	Flexor hallucis longus
FHL1	Four and a half LIM domains protein 1
FSR	Fractional synthesis rate
G3P	Glyceraldehyde-3-phosphate dehydrogenase
G6PI	Glucose-6-phosphate isomerase
GAS	Gastrocnemius
GC-MS	Gas chromatography mass spectrometry
GPDA	Glycerol-3-phosphate dehydrogenase [NAD(+)], cytoplasmic
H2B1	Histone H2B type 1
HBA	Hemoglobin subunit alpha-1/2
HBB1	Hemoglobin subunit beta-1
HBB2	Hemoglobin subunit beta-2
HCl	Hydrochloric acid
HS90B	Heat shock protein HSP 90-beta
HSP7C	Heat shock cognate 71 kDa protein
HSPB1	Heat shock protein beta-1
HSPB6	Heat shock protein beta-6
IDH3A	Isocitrate dehydrogenase [NAD] subunit alpha, mitochondrial
IDHP	Isocitrate dehydrogenase [NADP], mitochondrial
IPG	Immobilised pH gradient
<i>k</i>	Synthesis rate constant

KAD1	Adenylate kinase isoenzyme 1
KCRB	Creatine kinase B-type
KCRM	Creatine kinase M-type
KCRS	Creatine kinase S-type, mitochondrial
kDa	Kilo Dalton
KPYM	Pyruvate kinase PKM
LC-MS	Liquid chromatography mass spectrometry
LC-MS/MS	Liquid chromatography mass spectrometry/mass spectrometry
LDHA	L-lactate dehydrogenase A chain
LDHB	L-lactate dehydrogenase B chain
m/z	Mass to charge ratio
m ₀	Monoisotopic peak
m ₁ , m ₂ , m ₃	Heavy isotopomers
MALDI	Matrix-assisted laser desorption/ionization
MALDI-TOF	Matrix-assisted laser desorption/ionization-time of flight
MALDI-TOF/MS	Matrix-assisted laser desorption/ionization-time off fight/mass spectrometry
MDHC	Malate dehydrogenase, cytoplasmic
MDHM	Malate dehydrogenase, mitochondrial
MIDA	Mass Isotopomer distribution analysis
MLRS	Myosin regulatory light chain 2, skeletal muscle isoform
MLRV	Myosin regulatory light chain 2, ventricular/cardiac muscle isoform
MPCP	Phosphate carrier protein
M _r	Relative molecular mass
MS	Mass spectrometry
MS/MS	Tandem mass spectrometry
mTOR	Mammalian target of rapamycin
mTORC1	Mammalian target of rapamycin complex 1
MYG	Myoglobin
MYH4	Myosin-4
MYH8	Myosin-8
MyHC	Myosin heavy chain
MYL1	Myosin light chain 1/3, skeletal muscle isoform
MYL3	Myosin light chain 3
<i>n</i>	Number of exchangeable deuterium/hydrogen sites
NC	No change
NS	Not significant
O ₂	Oxygen
ODPA	Pyruvate dehydrogenase E1 component subunit alpha, somatic form, mitochondrial
ODPB	Pyruvate dehydrogenase E1 component subunit alpha, somatic form
<i>p</i>	Precursor enrichment

PARK7	Protein/nucleic acid deglycase DJ-1
PEBP1	Phosphatidylethanolamine-binding protein 1
PFKAM	ATP-dependent 6-phosphofructokinase, muscle type
PGAM2	Phosphoglycerate mutase 2
PGK1	Phosphoglycerate kinase 1
PGM1	Phosphoglucomutase-1
Phospho S/T p/	Phosphorylation of Serine/Threonine Isoelectric point
PLEC	Plectin
PLN	Plantaris
PRDX5	Peroxiredoxin-5
PRVA	Parvalbumin alpha
PYGB	Glycogen phosphorylase, brain form
PYGM	Glycogen phosphorylase, muscle form
Q-TOF	Quadrapole time of flight mass spectrometry
QCR1	Cytochrome b-c1 complex subunit 1
QCR2	Cytochrome b-c1 complex subunit 2
SAFB1	Scaffold attachment factor B1
SAR	Selective androgen receptor
SD	Standard deviation
SDS	Sodium dodecyl sulfate
SERCA	Sarcoplasmic/endoplasmic reticulum calcium ATPase
SOL	Soleus
Stim	Stimulated muscle
TA	Tibialis anterior
TFA	Trifluoroacetic acid
TIC	Total ion chromatogram
TNNI1	Troponin I, slow skeletal muscle
TNNI2	Troponin I, fast skeletal muscle
TNNT1	Troponin T, slow skeletal muscle
TNNT3	Troponin T, fast skeletal muscle
TPIS	Triosephosphate isomerase
TPM2	Tropomyosin beta chain
TPM4	Tropomyosin alpha-4 chain
TRY1	Anionic trypsin-1
UPLC	Ultra performance liquid chromatography
VDAC	Voltage-dependent anion channel

Chapter 1. Review of the literature.

1.1 Abstract

In mammals ~40 % of total body mass is accounted for by skeletal muscle, commanding ~30 % of resting metabolic rate in adult humans (Wagermakers et al, 1998). Skeletal muscle plays a crucial role in whole body locomotion and is paramount in metabolic homeostasis and glycemic control, being the largest site for glucose disposal (~80 %) (Kraegen et al, 1993). Importantly, skeletal muscle is the site of more than 60 % of whole body protein turnover (Wagermakers et al, 1998). Skeletal muscle is distinguished from other bodily tissues by its unique diversity. This remarkable characteristic is made possible through its design. The heterogeneity of each individual fibre that composes skeletal muscle has a range of physiological characteristics associated with them. It is these functional qualities bestowed on the composition of the individual fibres that is responsible for the basis of muscle plasticity. Exercise capacity is strongly related with all-cause mortality and offsetting the age-associated loss of muscle mass (Cohen et al, 2014). Understanding how exercise causes muscles to adapt is fundamental to improving our health, quality of life and longevity. However, the proportion of different fibre types varies from muscle to muscle and this gives a broad range of different functional properties. This makes the study of skeletal muscle a challenging endeavour because of the wide diversity it exhibits. However, fibre typing has been used as a framework to understand muscle since the 1960's (Barany, 1967). Over the years, the sophistication of fibre typing has developed from gross anatomy to histology and the molecular classification of myosin heavy chain isoforms. More recently, new proteomics techniques have begun to illuminate the full diversity of the muscle proteome and intricacies of changes involved in the response to exercise (Burniston, 2008). This is challenging in itself as the proteome is a highly dynamic entity, but the latest developments have combined proteomics with stable isotope labelling to allow quantification of dynamic changes in the proteome in response to exercise. Such unique advancements allow for an understanding of how muscle coordinates its adaptive response to exercise. Subsequently, such detailed knowledge will position this thesis in a position to provide valuable insights into the mechanisms involved in skeletal muscle adaptation and potentially begin to unpick the physiological and pathophysiological changes within skeletal muscle associated to exercise.

1.2 Muscle phenotype and plasticity

It is clear that skeletal muscle can be classified on the basis of its diversity as early as 1873 when Ranvier distinguished the difference between white and red muscles. White muscles are faster contracting and more specialised for phasic activity, whilst red muscles are slower contracting and better suited to more continuous tonic activity. Grutzner, (1883) and Knoll, (1891) report histological analysis of different muscle fibre types fibre size and appearance, but it was well into the 19th century before histochemical analyses were able to quantify fibre characteristics. Seminal work reported in Barany, (1967) established the intrinsic speed of muscle shortening is a characteristic property of the muscle myosin ATPase activity. This breakthrough justified the use of ATPase as a primary marker for fibre typing and provided a foundation for later studies on the role of myosin heavy chain (MyHC) isoforms as the regulator of the contractile properties across different motor unit types in response to exercise (Petersen et al, 2005), ageing (Barogi et al, 1995) and metabolic dysregulation (Nishida et al, 1992). Muscle fibre typing generated new avenues of research which later established what we now know about muscle e.g. organisation of motor units and metabolic profiles of fast contracting fatigable versus slow contracting fatigue resistance fibres.

We now know that skeletal muscle is composed of a combination of heterogeneous myofibres with specific sub-types established in relation to their contractile and metabolic properties (Schiaffino, 2010). Fast-twitch fibres principally depend on glycolytic metabolism which makes them highly fatigable whereas, slow-twitch oxidative fibres have a relatively larger mitochondrial content and are therefore more fatigue resistant, predominantly depending on oxidative metabolism (Pette and Vrbova, 1992). However, intermediate or fast-twitch oxidative fibres, are also present. These fibres still depend on glycolytic metabolism for energy production but have a preponderant mitochondrial concentration when compared with 'pure' fast-twitch fibres, awarding a greater capacity for endurance; but are sensitive to fatigue at a greater degree than slow-twitch fibres (Schiaffino and Reggiani, 1996). The unique fibre type differences in contractile function are owed to particular alterations in the expression of a diverse range of isoforms from each myofibrillar protein at the individual level (Schiaffino and Reggiani, 1996). Figure 1.1 illustrates the gross to subcellular level of structure in skeletal muscle.

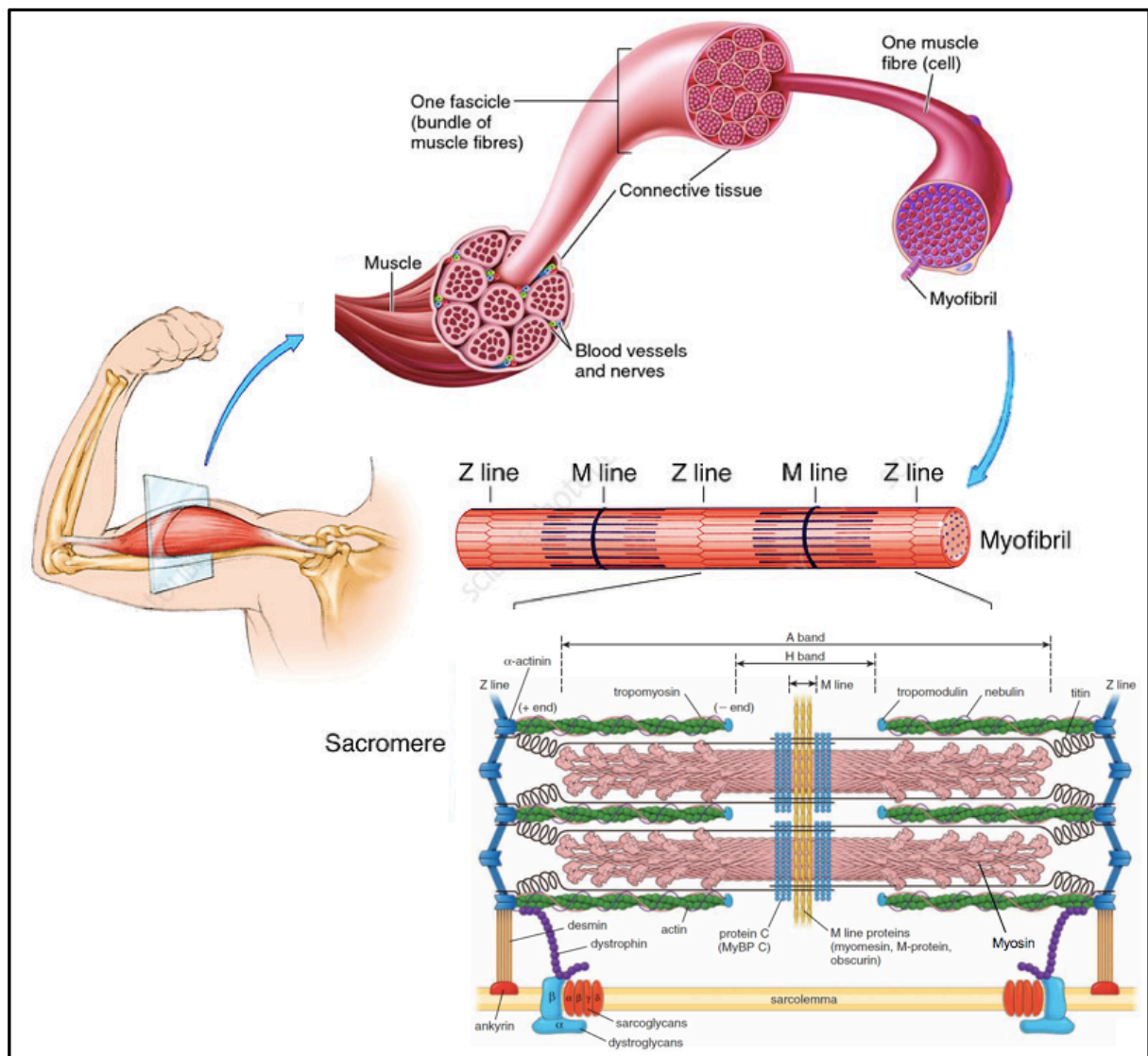


Figure 1.1. The gross to subcellular structure of skeletal muscle anatomy.

The different levels of skeletal muscle anatomy are dissected. Note that many muscle fibres (average cross sectional area $\sim 3000\text{-}6000 \text{ mm}^2$) make up the complete muscle, as many myofibrils (average cross sectional area $\sim 1\text{-}2 \text{ }\mu\text{m}^2$) make up a single muscle fibre. It is within these myofibrils that individual proteins e.g. Actin and Myosin express different isoforms of their protein species that carry very different functional characteristics with them; ultimately impacting on the function of whole muscle physiology to give the muscle a specific phenotype.

Bottinelli et al, (1991) reported the myosin heavy chain (MyHC) composition of single fibres from Soleus, Extensor digitorum longus (EDL) and Plantaris via immunocytochemistry. Four fibre types: slow-twitch (type I), intermediate (type IIA),

fast-intermediate (type IIX) and fast-twitch (type IIB) were distinguished. The maximum shortening velocity of the identified fibres was quantified as muscle lengths per second (L/s) and formed a continuum from 0.35 to 2.84 L/s. The mean values from slowest to fastest fibre type were as follows: type I: 0.639 ± 0.038 L/s, type IIA: 1.396 ± 0.084 L/s, type IIX: 1.451 ± 0.066 L/s and type IIB: 1.8 ± 0.109 L/s. Bar and Pette, (1988) later corroborated these findings by implementing an improved electrophoretic separation technique (Carraro and Catani, 1983) in rat muscle. They discovered a type IIX fibre with corresponding MyHC IIX and concluded the newly detected MyHC IIX is functionally different to MyHC IIB being undetectable in the purely fast-twitch muscle, Levator Ani. However, they did report a concomitant reduction in the expression of MyHC IIB as MyHC IIX increased in chronically stimulated Tibialis Anterior (TA) muscle. Immunohistochemical analysis (Gorza et al, 1990) and biochemical and physiological studies of single fibres (Pette and Staron, 1990) also teach us that muscle fibres adapt in a progressive manner over a spectrum of change in accordance with their MyHC profile, illustrated by the scheme displayed in Figure 1.2.

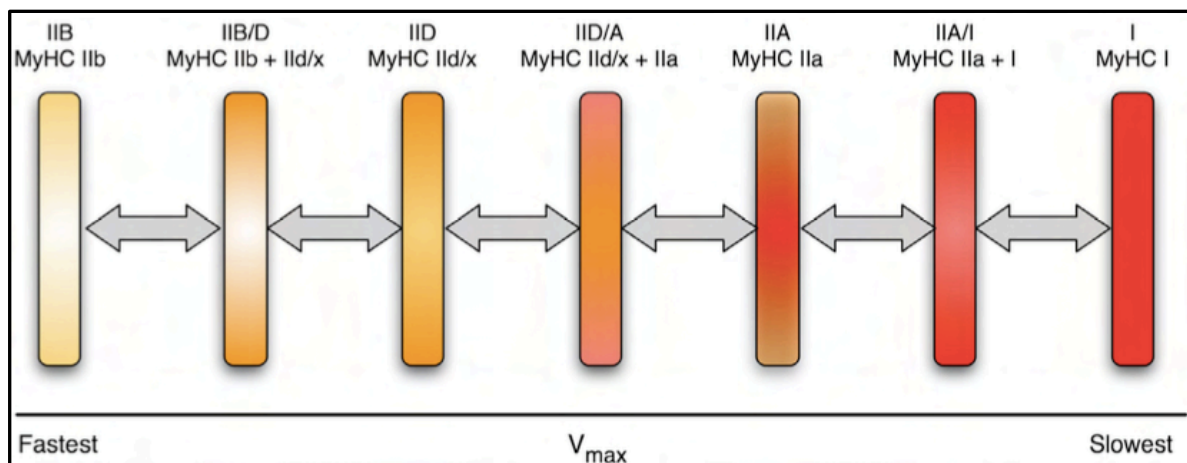


Figure 1.2. Fibre type transitions of skeletal muscle based on Myosin heavy chain profile.

Fibre type transitions occur in a step-wise, progressive manner based on their predominate MyHC isoform composition. This bestows functional and biochemical change on the muscle which enables pure and hybrid fibre expression along the continuum of fibre type transformation.

Close, (1965) showed an intimate relationship between maximum shortening velocity and contraction time, as a result of the association between cross-bridge formation and calcium kinetics of release and re-uptake. As a result, the stimulation frequency necessary to obtain fused tetanic contractions is purported to be higher in small animals when compared to that in large. For example, maximal force is attained at a frequency of 50 Hz in human muscles *in situ* (McComas et al, 1968), while rat fast motor units reach tetanic fusion only above 100 Hz and slow motor units above 70 Hz (Piotrkiewicz and Celichowski, 2007). This evidence suggests that the functional characteristics displayed by skeletal muscle is dictated by the neural demands of the motor unit placed upon the muscle fibre. As a consequence, directly affecting the MyHC isoform composition dominating the muscle. One of the key distinguishing factors between each type of motor unit is cell size, with the fastest motor units commanding the largest cell (Henneman et al, 1974). Henning and Lomo, (1985) investigated single motor units in rat Soleus and EDL muscle by chronically recording the firing patterns of different sized motor units *in vivo*, using implantable electrodes. This work led to the clear identification of three distinct firing patterns in the rat. The first pattern is typically of the motor units found in the relatively slow contracting Soleus muscle. This type of motor unit receives a high amount of impulse activity (300,000 – 500,000 over 24 h) combined with long lasting trains (300 – 500 ms) and a low frequency of firing (~20 Hz). In contrast the motor units innervating the fast fibres of the EDL were sub-divided into two groups (fast to fatigue, FF and fatigue resistance, FR), the first pattern identified for the FF motor units was characterised by a lower impulse activity (3,000 – 10,000 over 24 h) with a very short duration of train (<3 ms) but a high discharge frequency (~90 Hz). The last identified pattern, for the FR motor units had a moderate impulse activity (90,000 – 250,000 over 24 h) with a longer train duration (60 – 140 ms) and an average discharge frequency (~65 Hz). In light of these data, the authors conclude that the motor units found in soleus likely innervate type I fibres, FF type IIB fibres and the FR motor units may correspond to the type IIA and IIX fibres.

The heterogeneity of skeletal muscle fibres throughout the mammalian body primarily reflects the degree of adaptation to the different muscle activity patterns. There is strong evidence (Salmons and Vrbova, 1969) to suggest that the muscle adapts to the neural stimulus placed upon it by the firing pattern; which in turn alters the muscle phenotype by inducing functional change by expression of individual proteins e.g.

myosin heavy chain. This was first demonstrated by the pioneering work of Buller et al, (1960) in a series of nerve cross-union experiments performed in cat. When slow-twitch Soleus is reinnervated by nerve fibres that would normally supply the fast-twitch Flexor Digitorum Longus (FDL), the Soleus adopted contractile characteristics similar to that of the faster contracting FDL. Conversely, when the FDL was reinnervated with the Soleus nerve the muscle became much slower contracting adopting physiological properties consistent to the Soleus. These results helped to establish the notion that motor neurones exert a phenotypic influence on the muscle they innervate.

Many studies have since confirmed the phenotypic influence of fast and slow motor neurones on the contractile properties of adult skeletal muscles. Close, (1969) investigated a host of physiological properties, such as contraction time, sarcomeric shortening, fibre length and cross sectional area in cross-innervated rat EDL and Soleus muscle. Demonstrating that the changes in the speed of contraction from nerve cross-union seem to be brought about directly by neural influence on the muscle, with EDL contraction time lengthening from 13 msec to 25 msec and a complimentary shortening measured in the contraction time of the Soleus from 34 msec to 15 msec. Soon after, Barany and Close, (1970) investigated myosin ATPase activity levels in nerve cross-union experiments in the Soleus and EDL of the rat and discovered it was possible to assign the established neutrally induced changes of contraction speed to alterations in the activity of myosin ATPase, which was consistent with Barany's previous work. Furthermore, the characteristically high levels of SDH in slow-twitch muscles, indicative of a higher mitochondrial content, was also shown to be reversed under cross innervation; with the faster contracting muscle displaying an increased level of SDH under cross innervated conditions (Dubowitz et al, 1967.; Pette and Tyler, 1983). Taken together, this work produced a multitude of evidence that positions skeletal muscle as a highly dynamic, plastic tissue with the ability to adapt to the innervation of its motor units to fulfil the functional demands required of the muscle.

Salmons and Vrbova, (1969) were amongst the first to address muscle adaptation by developing a nerve electrical stimulation technique *in vivo* whereby the motor neurons are stimulated chronically at pre-programmed frequencies and durations in order to alter the neuromuscular function. Chronic low-frequency stimulation (CLFS) in the range of 10 Hz of a rabbit fast twitch muscle such as the extensor digitorum longus (EDL) can transform its fast-type properties into slow-type properties. To help corroborate these findings, new methods in analytical protein chemistry highlighted

that such contractile changes corresponded to altered myosin isoform profiles (Hoh, 1975.; Sreter et al, 1974). Further investigations by Amphlett et al, (1975) utilising a similar protein electrophoresis technique showed that the electrophoretic mobility of protein isoforms in transformed muscle was not exclusive to the Myosins. This evidence indicated that when the contractile speed of the Soleus muscle is increased by cross innervation with EDL, the slow-skeletal muscle isoform for Troponin I is replaced by the fast-skeletal muscle isoform of Troponin I. Furthermore, Heeley et al, (1983) used electrophoresis separation in rabbit Soleus, where only alpha and beta subunits of Tropomyosin were detected and in the EDL, only gamma and delta subunits were observed. Cross innervation of the two muscles revealed that the relative proportions of alpha, gamma and delta subunits altered their expression in accordance with the change in the contraction speed of the muscles. It is now clear that the isoforms of many more myofibrillar and sarcoplasmic/soluble proteins are substituted in response to a change in phenotype of skeletal muscle to account for the contrasting physiological contractile demands placed upon it.

Since the pioneering work performed by Buller et al, (1960) which demonstrated that the contraction speed of skeletal muscle is determined by the nature of its innervation, there is now strong evidence to show that alterations in the biochemical composition and functional properties of muscle are likewise influenced. All of these early physiological investigations in skeletal muscle have taught us that the biochemical changes such as levels of SDH and myosin ATPase activity strongly correlate with changes in the histochemistry and physiological characteristics of transformed skeletal muscle. This highlights the commanding influence of neural input on muscle phenotype and proves that terminally differentiated skeletal muscle is a highly versatile tissue. However, the functional elements within skeletal muscle, with regard to metabolism and contraction, are without doubt attributed to its constituent proteins (Donoghue et al, 2005). With the advent of proteomic investigations, we learn that skeletal muscle has a hugely complex and dynamic proteome which is made up of thousands of individual proteins that each may have multiple splice variants and proteoforms consisting of different post translational states that change in response to environmental stimuli such as exercise (Burniston and Hoffman, 2011). However, the number of proteins that can be mined from skeletal muscle is limited. For instance, Hojlund et al, (2008) were amongst the first to report large scale proteome profiling in skeletal muscle. They used high performance liquid chromatography electrospray

ionization tandem mass spectrometry to identify 945 proteins in human muscle. Burniston et al (2014) later used a more sophisticated instrument (Q-TOF mass spectrometer, which incorporated an additional gas-phase separation) to identify 1514 proteins in rat muscle, encompassing the entire complement of metabolic enzymes and some regulatory kinases. Burniston et al, (2014) also quantified the abundance of these proteins reporting the range to span four orders of magnitude. Due to this scale and complexity seen in the muscle proteome, changes in the abundance of individual muscle proteins contribute towards overt alterations in muscle phenotype, thus changing the characteristics of individual muscle fibres. For example, Murgia et al, (2017) used novel proteomic methods with a high sensitivity to investigate single muscle fibres from human subjects. They were able to categorise muscle fibres based on the protein complement and subsequently measured ~5000 individual proteins. Since the new developments made possible by proteomic methods, we learn that because of the complex design of skeletal muscle, knowledge of the mechanisms that underpin skeletal muscle adaptation and how these processes are coordinated, at the protein level, is not fully understood. Skeletal muscle is one of the most essential tissues in the body and understanding its adaptation is fundamental to physiology and paramount to the understanding of different pathophysiology. In order to comprehend how these adaptive processes are organised in skeletal muscle, proteomics has investigated the effects of exercise on the proteome (Burniston and Hoffman, 2011). The problem with this line of investigation is that existing proteome data are static i.e. report abundance data only. However, the skeletal muscle proteome is a highly dynamic and versatile entity which establishes a need to study protein turnover. As such, a better understanding of individual protein responses is required, for instance, how does the rate of turnover of individual proteins contribute towards muscle adaptation? Figure 1.3 illustrates the factors affecting individual protein turnover within the muscle cell. At present, there are few viable techniques that accurately capture protein degradation. Whilst synthesis measurements are possible, until recently, most data were from gross/mixed muscle.

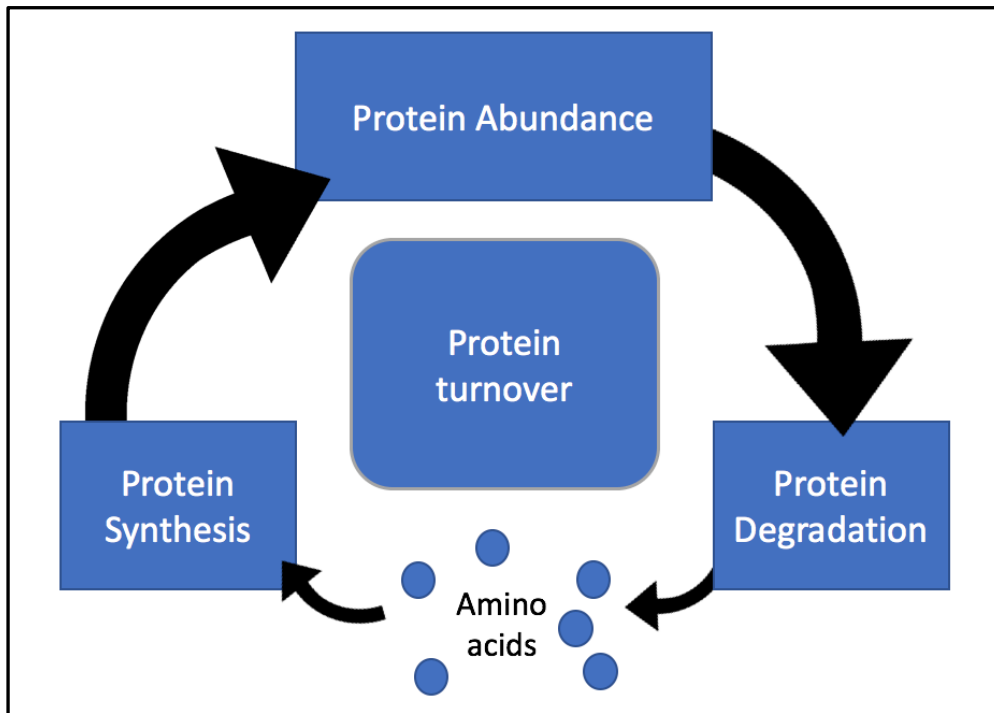


Figure 1.3. Factors effecting individual protein turnover.

All proteins within an organism are being continually broken down (i.e. protein degradation) and remade (i.e. protein synthesis). The abundance of a given protein depends solely on its rate of degradation versus its rate of synthesis. If a protein has a fast synthesis rate and slow degradation rate it will increase in abundance within the cell. Conversely, proteins that have both a swift degradation and synthesis rate have the fastest turnover rates.

Synthesis of new protein *in vivo* has traditionally been investigated by biosynthetic metabolic labelling, using tracers such as stable isotope labelled amino acids e.g. L-[1-¹³C]-leucine (Rennie et al, 1982). This enables the fraction of newly synthesised protein to be calculated from the precursor: product ratio. Incorporation of stable-isotope labelled amino acids in to protein *in vivo* is most commonly combined with gas-chromatography mass spectrometry (GC-MS) analysis of hydrolysed amino acids to measure the average rate of synthesis in protein mixtures extracted from skeletal muscle (Wagenmakers, 1999). In rats, the rate of protein synthesis has been reported to be different, within different skeletal muscles, for example the average half-life for mixed proteins in EDL was 12 days, 14 days in gastrocnemius and 7 days in soleus (Kelly et al, 1984). However, these values represent averages across the entire proteome and can be misleading, as Terjung et al, (1979) gives an account of the

turnover for the mitochondrial protein, cytochrome c, which is more rapid in fast-twitch than slow-twitch muscle. The most important lessons we have learned from the biosynthetic labelling methods is that there are large differences between the fractional synthesis rates in different tissues e.g. 12 %/d in liver (Fearon et al, 1991) compared to 3 %/d in muscle (Nair et al, 1988). Subsequent fractionation of muscle protein has shown that the myofibrillar proteins have the lowest fractional synthetic rates of ~1 %/d (Balagopal et al, 1997) and the highest FSR are seen in the mitochondrial fraction of ~2.5 %/d (Rooyackers et al, 1996). However, FSR has been shown to change in response to external factors such as exercise. For example, resistance exercise can induce a 20 % increase in myofibrillar FSR above basal levels (Brook et al, 2015). Adaptation to exercise is governed by many factors e.g. mechanical load but is mainly a result of the activation pattern delivered to the muscle. High intensity dynamic exercise is known to induce hypertrophy of the muscle fibres and in an attempt to replicate these changes, several models of muscle transformation have been constructed. These models such as tenotomy, synergist ablation and high resistance exercise (Timson, 1990) have clearly demonstrated, using a number of different species (reviewed in greater detail in Chapter 4), that the primary determinant of muscle size is the external load that is applied to it (Booth and Thomason, 1991). In any one of these models a common response to the increased loading is a rise in protein content (Timson, 1990) that asserts a close correlation with increases in protein synthesis (Goldberg, 1968). Wong and Booth, (1990a.; 1990b) used a model of both shortening and lengthening contractions and muscle loading in rat gastrocnemius and TA. It was established that 12-17 h after either eccentric or concentric resistance training protocols protein synthesis was increased to ~40 % higher than control. Interestingly, similar responses have been described in humans with rapid increases in protein synthesis post resistance training (Chesley et al, 1992.; MacDougall et al, 1995) suggesting that activation of protein synthesis is a customary acute response of skeletal muscle following an increased workload. The model utilised by Wong and Booth, (1988) activates the muscles of the distal hindlimb. This model relies on antagonist muscle action resulting in lengthening contractions in the Dorsiflexor muscles and shortening contractions in the Plantar flexor muscles. Baar and Esser, (1999) modified this protocol to ensure that muscle activation occurred through the innervating nerve and all the motor units of the distal hindlimb are recruited. The animals received 100 Hz stimulation in 3 second pulses with a 10 or 50

second rest between repetitions. This continued for 10 sets of 6 stimulations resulting in 60 contractions over a 22 minute period 2 days per week for 6 weeks. They observed increases in muscle mass for TA (14.4 %), EDL (13.9 %) and Plantaris (6.9 %) when compared to control, but no change was recorded in the Soleus (-2.3 %). These findings establish co-contraction as a viable research model to investigate resistance exercise induced changes of the muscle proteome. Baar and Esser, (1999) used a model of co-contraction to discover a key protein (p70s6k) of ribosomal regulation that was associated with muscle hypertrophic response to exercise. This raises questions about whether it is only synthesis that increased or whether degradation could also play a part and should be considered as a possible mechanism. For example, Watt et al, (1982) reported different contributions of synthesis and degradation in fast-twitch muscle EDL and slow-twitch Soleus in rats during a 2-week regimen of high-intensity jump training. The growth rate of both EDL and Soleus increased up to 70 % when compared to control, but growth of the fast-twitch muscle was primarily achieved through greater (28 %) protein synthesis, whereas in the Soleus muscle protein synthesis did not change but there was a 38 % decrease in protein degradation. While it is likely some proteins may not have followed these overall trends, until recently it has not been possible to routinely measure isotope incorporation in large numbers of individual proteins. However, with the application of proteomic separation techniques in striated muscle (Burniston and Hoffman, 2011) along with advances in the sensitivity of mass spectrometers, it is now feasible for these types of investigations to be undertaken in skeletal muscle and in response to stimuli such as exercise.

The first studies in exercise proteomics investigated the acute effects of swimming in rats. For example, Takahashi and Kubota, (2005) performed 2DGE on muscle pooled from rats killed immediately after 150 minutes of swimming and report lesser expression of a gel spot later identified as zinc finger protein 3. In a similar study, Guelfi et al, (2006) isolated gastrocnemius muscles from rats either immediately after or 30 min after a 3 min bout of swimming. Rather than pooled samples, biological replicates were analysed, which enabled statistically significant differences to be identified in the expression of troponin T, creatine kinase and a spot containing both adenylate kinase 1 and heat-shock protein 20. Gandra et al, (2010) also investigated changes in rat gastrocnemius muscles isolated from either 3 or 24 h after an incremental treadmill test to exhaustion, and reported significant changes in glycolytic

enzymes, heat-shock cognate protein 70 and carnitine palmitoyltransferase II. These changes observed in proteins involved in high-energy phosphate (Guelfi et al, 2006) and glycolytic (Gandra et al, 2010) metabolism are consistent with the energy demands of intense exercise. However, because muscles were isolated at different time points or after differing bouts of acute exercise, there is no direct identity among the findings of these studies. Burniston, (2008) investigated rat plantaris muscle using 2DGE after implementing endurance training using intensity-controlled treadmill running and found that endurance training indeed altered the relative expression of individual protein spots; thus, linking changes in spot profile of individual proteins with differences in muscle function. From 80 gel spots, statistical analysis detected significant changes in the expression of 15, which represented the products of 11 individual genes. A total of six of the 11 differentially expressed genes were present as multiple protein spots with endurance training altering the expression of single spots from each of the multi-spot series identified as: transferrin (n = 3 spots), albumin (n = 4 spots), lactate dehydrogenase A (n = 2 spots) and induced changes in multiple spots identified as phosphoglucosyltransferase 1, triosephosphate isomerase and mitochondrial aconitase. Using the same rat model of intensity-controlled treadmill running, Burniston, (2009) reported the effects of a 6-week training programme consisting of four 30 minute sessions per week at approximately 75 % VO₂max. Endurance running resulted in the increase of the animals' VO₂max by an average of 23 % and was associated with an 11 % increase in cardiac mass. Furthermore, 2DGE was implemented to detect changes in the muscle proteome. A spot was identified as heat shock protein 20 and was significantly increased in the hearts of endurance-trained animals, consistent with previous work by Boluyt et al, (2006). However, Burniston, (2009) also used MS/MS analysis to unambiguously identify a phosphorylation of heat shock protein 20 at residue serine 16 unique to endurance trained rat heart. Whilst these findings are important and shed light on quantitative changes in individual protein abundance during adaptation to exercise. They do not inform us about how these changes are brought about i.e. from what are the relative contributions from synthesis and degradation that impacts on changes in protein abundance.

Recent advances in peptide mass spectrometry and deuterium (²H₂O) labelling *in vivo* have created the opportunity to measure changes in the synthesis rates of individual proteins under free living conditions over a long period of time. The classic tracer methods previously described provide only gross measurements of mixed muscle

synthesis rates or employ complex and laborious methodologies. Whereas the advent of $^2\text{H}_2\text{O}$ labelling afford many technical advantages over these techniques, such as length of administration and intracellular labelling of amino acids but also allow the measurement of individual proteins. Xiao et al, (2008) describe a method to determine protein turnover using *in vivo* labelling of individual proteins with $^2\text{H}_2\text{O}$, analysed by matrix-assisted laser desorption ionisation – time of flight mass spectrometry (MALDI-TOF/MS) spectrum. Here, protein synthesis is calculated using mass isotopomer distribution analysis (MIDA) instead of precursor to product amino acid enrichment ratio. This combined with the ability to also identify the protein makes the use of *in vivo* labelling with $^2\text{H}_2\text{O}$ a precise method to determine specific protein synthesis. Kim et al, (2012) implemented a similar methodology to report a large-scale analysis of protein turnover in mouse heart and liver mitochondria using *in vivo* $^2\text{H}_2\text{O}$ labelling and Liquid Chromatography – Mass Spectrometry (LC-MS). Here the synthesis rates of 314 cardiac mitochondrial proteins were reported over a period of 90 days at an enrichment of $\sim 5\%$ $^2\text{H}_2\text{O}$. Protein synthesis rates were approximately 3-fold greater in liver compared to cardiac mitochondria. In addition, while there was a general correlation (Spearman $\rho = 0.50$) between synthesis rates of proteins in heart and liver mitochondria, the synthesis rate of many mitochondrial proteins ranked differently between cardiac and liver mitochondria, which suggest tissue-specific regulation. More recently, we used $^2\text{H}_2\text{O}$ labelling *in vivo* combined with 2DGE and MALDI-TOF/MS to measure synthesis of 8 individual proteins across four different muscle tissues over a 14 day period in the rat (Hesketh et al, 2016). Similar to the work of Kim et al, (2012) we also reported the rank order of synthesis is different depending on the muscle investigated. Furthermore, such work has important implications for future human studies where it is typical for just one muscle to be sampled but the results are often extrapolated to skeletal muscle as a whole. Shankaran et al, (2015) carried out a similar investigation over a 7-day period in the triceps muscle of ovariectomised rats exposed to a selective androgen receptor modulator or vehicle control. Table 1.1 provides a comparison between these data. Of all the proteins investigated within the five different tissues there were no proteins that were completely turned over within this time period. Based on these findings, the duration of future experiments would be wise to extend experimental durations to greater than three weeks in order to capture a more accurate reflection of the individual protein synthesis rates within rat striated muscles.

Table 1.1. Percentage of newly synthesised protein in rat striated muscles after seven days $^2\text{H}_2\text{O}$ administration *in vivo*.

Protein	Heart*	Diaphragm*	EDL*	Soleus*	Triceps †
ALBU	11.9 ± 2.4	20.2 ± 6.1	16.6 ± 2.7	13.6 ± 0.8	-
ATCS	1.3 ± 0.6	2.6 ± 0.8	0.8 ± 0.5	-	7.0 ± 0.3
KCRM	0.4 ± 0.3	5.9 ± 1.7	2.2 ± 1.0	1.0 ± 0.3	13.0 ± 0.4
ENOB	5.3 ± 0.3	4.0 ± 1.0	4.2 ± 1.2	7.5 ± 2.6	13.7 ± 0.3
ATPA	0.3 ± 0.2	3.3 ± 1.0	8.1 ± 4.8	-	30.0 ± 1.2
TPM1	1.6 ± 0.7	1.7 ± 1.6	2.0 ± 1.4	-	14.5 ± 0.4
MLY3	1.2 ± 1.1	2.2 ± 2.1	7.2 ± 2.1	-	13.4 ± 1.6
MLRV	7.9 ± 3.0	6.3 ± 1.3	5.6 ± 1.1	-	9.6 ± 0.3

† From Shankaran et al, (2015); * From Hesketh et al, (2016).

Taken together this work has taught us that not only do protein synthesis rates vary greatly from one tissue to the next, but it appears there is protein-specific regulation within different tissues i.e. muscle, that manifest through a range of synthesis rates that are different from one muscle to the next. This poses some obvious questions in the context of muscle adaptation. For instance, do individual proteins exhibit the same rank order of synthesis rates during muscle adaptation? During muscular hypertrophy is the mechanism of change protein-specific or is there a blanket response for all proteins that results in increased rates of synthesis? How is individual protein turnover regulated when protein abundance i; increases, ii; decreases or iii; stays the same? With these gaps in knowledge driving the research questions, the objective of this thesis is to investigate individual protein turnover during skeletal muscle adaptation. It is clear that skeletal muscle exhibits a wide range of plasticity, this will be exploited to the full by using *in vivo* animal models (chronic low-frequency stimulation, Chapter 3 and co-contraction high-frequency stimulation, Chapter 4) as tools to induce muscle adaptation within the rat. By combining this with the unique exercise proteomic methods our lab has refined (Dynamic proteome profiling, see Chapter 2) we can measure the protein turnover of individual proteins in order to begin to establish the sequence of events that contribute to the alterations in muscle phenotype and the physiological functional changes that are associated with. This will mean we are first to report a comprehensive analysis of the turnover rates of individual proteins in the rat, across striated muscle and in response to adaptation; providing a key insight to the mechanisms of muscle adaptation. This work will utilise the principles of non-

targeted ‘-omic’ science and avoids the temptation to overly reduce complex biological questions to isolated hypotheses or to specify unnecessary constraints by trying to predict which regulatory mechanisms might be dominant. This is expected to provide valuable insights to the mechanisms that underpin muscle adaptation and drive new developments in exercise and clinical physiology.

Objectives

Overarching objective of thesis – To measure individual protein turnover during muscle adaptation.

Specific Aim 1: To successfully implement a method to enable the measurement of individual protein turnover (Chapter 2), over a time series to investigate individual protein responses in a dynamic environment i.e. muscle adaptation (Chapter 3 and 4).

Specific Aim 2: To measure individual protein turnover in a model of endurance-type exercise training to investigate how the relative contributions of synthesis and degradation coordinate changes in protein abundance during skeletal muscle adaptation (Chapter 3).

Specific Aim 3: To measure individual protein turnover in a model of co-contraction induced hypertrophy to investigate how the relative contributions of synthesis and degradation coordinate changes in protein abundance during skeletal muscle adaptation (Chapter 4).

1.3 Bibliography

References

- Amphlett, GW.; Perry, SV.; Syska, H.; Brown, MD.; Vrbova, G. (1975). Cross innervation and the regulatory protein system of rabbit soleus muscle. *Nature*, **257**, 602-4.
- Baar, K.; Esser, K. (1999). Phosphorylation of p70S6K correlates with increased skeletal muscle mass following resistance exercise. *Am J Physiol*, **614**, 120-127.
- Balagopal, P.; Rooyackers, O.E.; Adey, D.B.; Ades, P.A.; Nair, K.S. (1997). Effects of aging on in vivo synthesis of skeletal muscle myosin heavy chain and sarcoplasmic proteins in humans. *Am J Physiol*, **4**, 273-280.
- Barany, M. (1967). ATPase activity of myosin correlated with speed of muscle shortening. *J Gen Physiol*, **50**, 197-218.
- Barany, M.; Close, R. (1971). The transformation of myosin in cross-innervated rat muscles. *J Physiol*, **2**, 455-74.
- Bar, A., Pette, D. (1988). Three fast myosin heavy chains in adult rat skeletal muscle. *FEBS Lett*, **235**, 153–155.
- Barogi, S.; Baracca, A.; Parenti-Castelli, G.; Bovina, C.; Formiggini, G.; Marchetti, M.; Solaini, G.; Lenaz, G. (1995). Lack of major changes in ATPase activity in mitochondria from liver, heart and skeletal muscle of rats upon ageing. *Mech Ageing Dev*, **2**, 139-50.
- Booth, FW.; and Thomason, DB. (1991). Molecular and cellular adaptation of muscle in response to exercise: perspectives of various models. *Physiol. Rev*, **71**, 541 – 585.
- Bottinelli, R., Schiaffino, S., Reggiani, C. (1991). Force-velocity relations and myosin heavy chain isoform compositions of skinned fibres from rat skeletal muscle. *J Physiol*, **437**, 655– 672.
- Brook, M. S.; Wilkinson, D. J.; Mitchell, W. K.; Lund, J. N.; Szewczyk, N. J.; Greenhaff, P. L.; Smith, K.; Atherton, P. J. (2015). Skeletal muscle hypertrophy adaptations predominate in the early stages of resistance exercise training, matching deuterium oxide-derived measures of muscle protein synthesis and mechanistic target of rapamycin complex 1 signaling. *FASEB J*, **29**, 4485–4496.
- Buller, A.J.; Eccles, J.C.; Eccles, R.M. (1960). Interactions between motoneurons and muscles in respect of the characteristic speeds of their responses. *J. Physiol*, **150**, 417-439.
- Burniston, JG. (2008). Changes in the rat skeletal muscle proteome induced by moderate-intensity endurance exercise. *Biochim. Biophys. Acta*, **1784**, 1077–1086.

- Burniston, J.G. (2009). Adaptation of the rat cardiac proteome in response to intensity-controlled endurance exercise. *Proteomics*, **9**, 106-115.
- Burniston, J.G.; Hoffman, E.P. (2011). Proteomic responses of skeletal and cardiac muscle to exercise. *Proteomics*, **8**, 361-377.
- Burniston, J.G.; Connolly, J.; Kainulainen, H.; Britton, S.L.; Koch, L.G. (2014). Label-free profiling of skeletal muscle using high-definition mass spectrometry. *Proteomics*, **14**, 2339-2344.
- Boluyt, M. O.; Brevick, J. L.; Rogers, D. S.; Randall, M. J. (2006). Changes in the rat heart proteome induced by exercise training: Increased abundance of heat shock protein hsp20, *Proteomics*, **6**, 3154–3169.
- Carraro, U.; Catani, C. (1983). A sensitive SDS-PAGE method separating myosin heavy chain isoforms of rat skeletal muscles reveals the heterogeneous nature of the embryonic myosin. *Biochem Biophys Res Commun*, **116**, 793-802.
- Chesley, A.J.; MacDougall, J.D.; Tarnopolsky, M.A.; Atkinson, S.A.; Smith, K. (1992). Changes in human muscle protein synthesis after resistance exercise. *J. Appl. Physiol*, **73**, 1383– 1388.
- Close, R. (1965). The relation between intrinsic speed of shortening and duration of the active state of muscle. *J Physiol*, **180**, 542–559.
- Close, R. (1969). Dynamic properties of fast and slow skeletal muscle of the rat after cross-union. *J Physiol*, **2**, 331-46.
- Cohen, S.; Nathan, J.; Goldberg, A. (2014). Muscle wasting in disease: molecular mechanisms and promising therapies. *Nature Reviews Drug Discovery*, **14**, 58-74.
- Donoghue, P.; Doran, P.; Dowling, P.; Ohlendieck, K. (2005). Differential expression of the fast skeletal muscle proteome following chronic low-frequency stimulation. *Biochimica et Biophysica Acta*, **2**, 166-176.
- Dubowitz, V.; Newman, D.L. (1967). Change in enzyme pattern after cross-innervation of fast and slow skeletal muscle. *Nature*, **20**, 840-1.
- Fearon, K.C.H.; McMillan, D.C.; Preston, T.; Winstanley, F.P.; Cruickshank, A.M.; Shenkin, A. (1991). Elevated circulating interleukin-6 is associated with an acute-phase response but reduced fixed hepatic protein synthesis in patients with cancer. *Annals of Surgery*, **213**, 26-31.
- Gandra, P.G.; Valente, R.H.; Perales, J.; Pacheco, A.G.; Macedo, D.V. (2010). Proteomic analysis of rat skeletal muscle submitted to one bout of incremental exercise. *Scand. J. Med. Sci*, **87**, 765-771.
- Goldberg, A.L. (1968). Protein synthesis during work-induced growth of skeletal muscle. *J. Cell Biol*, **36**, 653–658.

Gorza, L. (1990). Identification of a novel type 2 fiber population in mammalian skeletal muscle by combined use of histochemical myosin ATPase and anti-myosin monoclonal anti- bodies. *J Histochem Cytochem*, **38**, 257–265.

Grutzner, P. (1883), Zur Physiologie und Histologie der Skelettmuskeln. *Breslauer Arztl Z*, **5**, 257-258.

Guelfi, KJ.; Casey, TM.; Giles, JJ.; Fournier, PA.; Arthur, PG. (2006). A proteomic analysis of the acute effects of high- intensity exercise on skeletal muscle proteins in fasted rats. *Clin. Exp. Pharmacol. Physiol*, **33**, 952–957.

Hartner, KT.; Kirschbaum, BJ.; Pette, D. (1989). The multiplicity of troponin T Isoforms Distribution in normal rabbit muscles and effects of chronic stimulation. *Eur. J. Biochem*, **179**, 32 -38.

Hartner, KT.; Pette, D. (1990). Fast and slow isoforms of troponin I and troponin C Distribution in normal rabbit muscles and effects of chronic stimulation. *Eur. J. Biochem*, **188**, 261 -267.

Heely, DH.; Dhoot, GK.; Frearson, N.; Perry, SV.; Vrbova, G. (1983). The effect of cross-innervation on the tropomyosin composition of rabbit skeletal muscle. *FEBS Lett*, **2**, 282-6.

Henneman, E., Clamann, HP., Gillies, JD., Skinner, RD. (1974). Rank order of motor neurons within a pool: law of combination. *J Neurophysiol*, **37**, 1338 –1349.

Hennig, R., Lomo, T. (1985). Firing patterns of motor units in normal rats. *Nature*, **314**, 164 – 166.

Hesketh, S.; Srisawat, K.; Sutherland, H.; Jarvis, J.C.; Burniston, J.G. (2016) On the rate of synthesis of individual proteins within and between different striated muscles of the rat. *Proteomes*, **4**, 1-12.

Hoh, JRY. (1975). Neural regulation of mammalian fast and slow muscle myosins. An electrophoretic analysis. *Biochemistry*, **14**, 742-747.

Hojlund, K.; Yi, Z.; Hwang, H.; Bowen, B. (2008). Characterization of the human skeletal muscle proteome by one- dimensional gel electrophoresis and HPLC-ESI-MS/MS. *Mol. Cell Proteomics*, **7**, 257–267.

Kelly, F.J.; Lewis, S.E.M.; Anderson, P.; Goldspink, D.F. (1984). Pre- and postnatal growth and protein turnover in four muscles of the rat. *Muscle Nerve*, **7**, 235–242.

Kim, S.T.Y.; Wang, D.; Kim, A.K.; Lau, E.; Lin, A.J.; Liem, D.A.; Zhang, J.; Zong, N.C.; Lam, M.P.Y.; Ping, P. (2012). Metabolic Labelling Reveals Proteome Dynamics of Mouse Mitochondria. *Molecular & Cellular Proteomics*, **11**, 1586– 1594.

Knoll, P. (1891). Uber protoplasmaarme und protoplasmareiche Musculatur. *Denkschr Kais Akad Wiss Wien Math Naturwiss Cl*, **58**, 633-700.

Kraegen, E.W.; Sowden, J.A.; Halstead, M.B.; Clark, P.W.; Rodnick, K.J.; Chisholm, D.J.; James, D.E. (1993). Glucose transporters and in vivo glucose uptake in skeletal and cardiac muscle: fasting, insulin stimulation and immunoisolation studies of GLUT1 and GLUT4. *Biochem J*, **295**, 287–293.

MacDougall, J.D.; Gibala, M.J.; Tarnopolsky, M.A.; MacDonald, J.R.; Interisano, S.A.; Yarasheski, K.E. (1995). The time course for elevated muscle protein synthesis following heavy resistance exercise. *Can. J. Appl. Physiol*, **20**, 480 – 486.

McComas, A., Thomas, H. (1968). Fast and slow twitch muscles in man. *J Neurol Sci*, **7**, 301–307.

Murgia, M.; Toniolo, L.; Nagaraj, N.; Ciciliot, A.; Vindigni, V.; Schiaffino, S.; Reggiani, C.; Mann, M. (2017). Single Muscle Fiber Proteomics Reveals Fiber-Type-Specific Features of Human Muscle Aging. *Cell Reports*, **19**, 2396–2409.

Nair, K.; Halliday, D.; Griggs, R. (1988). Leucine incorporation into mixed skeletal muscle protein in humans. *American Journal of Physiology*, **254**, 208-213.

Nishida, K.; Ohara, T.; Johnson, J.; Wallner, J.S.; Wilk, J.; Sherman, N.; Kawakami, K.; Sussman, K.E.; Draznin, B. (1992). Na⁺/K⁺-ATPase activity and its alpha II subunit gene expression in rat skeletal muscle: influence of diabetes, fasting and refeeding. *Metabolism*, **1**, 56-63.

Petersen, A.C.; Murphy, K.T.; Snow, R.J.; Leppik, J.A.; Aughey, R.J.; Garnham, A.P.; Cameron-Smith, D.; McKenna, M.J. (2005). Depressed Na⁺-K⁺-ATPase activity in skeletal muscle at fatigue is correlated with increased Na⁺-K⁺-ATPase mRNA expression following intense exercise. *Am J Physiol Regul Integr Comp Physiol*, **1**, 266-74.

Pette, D.; Tyler, K.R. (1983). Response of succinate dehydrogenase activity in fibres of rabbit tibialis anterior muscle to chronic stimulation. *J Physiol*, **338**, 2-9.

Pette, D.; Staron, R.S. (1990). Cellular and molecular diversities of mammalian skeletal muscle fibers. *Rev Physiol Biochem Pharmacol*, **116**, 1–76.

Pette, D.; Vrbova, G. (1992). Adaptation of mammalian skeletal muscle fibres to chronic electrical stimulation. *Reviews of physiology, biochemistry and pharmacology*, **120**, 115-202.

Piotrkiewicz, M., Celichowski, J. (2007). Tetanic potentiation in motor units of rat medial gastrocnemius. *Acta Neurobiol Exp*, **67**, 35– 42.

Ranvier, L. (1873). Proprietes et structures differentes des muscles rouges et des muscles blancs chez les lapins et chez les raies. *C R Acad Sci Paris*, **77**, 1030-1034

Rennie, M.J.; Edwards, R.H.; Halliday, D.; Matthews, D.E.; Wolman, S.L.; Millward, D.J. (1982). Muscle protein synthesis measured by stable isotope techniques in man: the effects of feeding and fasting. *Clin Sci*, **63**, 519–523.

- Rooyackers, O.; Adey, D.; Ades, P.; Nair, K. (1996). Effect of age on in vivo rates of mitochondrial protein synthesis in human skeletal muscle. *Proc. Natl. Acad. Sci*, **93**, 15364–15369.
- Salmons, S.; Vrbova, G. (1969). The influence of activity on some contractile characteristics of mammalian fast and slow muscle. *J Physiol*, **3**, 535-49.
- Schiaffino, S., Reggiani, C. (1996). Molecular diversity of myofibrillar proteins: gene regulation and functional significance. *Physiol Rev*, **76**, 371– 423.
- Schiaffino, S. (2010). Fibre types in skeletal muscle: a personal account. *Acta Physiol*, **199**, 451– 463.
- Shankaran, M.; Shearer, T.W.; Stimpson, S.A.; Turner, S.M.; King, C.; Wong, P.A.; Shen, Y.; Turnbull, P.S.; Kramer, F.; Clifton, L.; et al. (2015). Proteome-wide muscle protein fractional synthesis rates predict muscle mass gain in response to a selective androgen receptor modulator in rats. *Am. J. Endocrinol. Metab*, **10**, 1152–1201.
- Sreter, FA.; Luff, AR.; Gergely, J. (1974). Effect of cross-innervation on physiological parameters and on properties of myosin and sarcoplasmic reticulum of fast and slow muscles of the rabbit. *J Gen Physiol*, **66**, 811-21.
- Takahashi, M.; Kubota, S. (2005). Exercise-related novel gene is involved in myoblast differentiation. *Biomed. Res*, **26**, 79–85.
- Terjung, R.L. (1979). The turnover of cytochrome c in different skeletal-muscle fibre types of the rat. *Biochem. J*, **178**, 569–574.
- Timson, BF. (1990). Evaluation of animal models for the study of exercise-induced muscle enlargement. *J. Appl. Physiol*, **69**, 1935– 1945.
- Wagenmakers, A. (1998). Muscle Amino Acid Metabolism at Rest and During Exercise: role in human physiology and metabolism. *Exercise and Sport Sciences Reviews*, **26**, 287-314.
- Wagenmakers, A.J.M. (1999). Tracers to investigate protein and amino acid metabolism in human subjects. *Proceedings of the Nutrition Society*, **58**, 987–1000.
- Watt, P.W.; Kelly, F.J.; Goldspink, D.F.; Goldspink, G. (1982). Exercise-induced morphological and biochemical changes in skeletal muscles of the rat. *Journal of Applied Physiology*, **53**, 1144-1152.
- Wong, TS.; and Booth, FW. (1988). Skeletal muscle enlargement with weight-lifting exercise by rats. *J. Appl. Physiol*, **65**, 950– 954.
- Wong, TS.; and Booth, FW. (1990a). Protein metabolism in rat gastrocnemius muscle after stimulated chronic concentric exercise. *J. Appl. Physiol*, **69**, 1709 – 1717.
- Wong, TS.; and Booth, FW. (1990b). Protein metabolism in rat tibialis anterior muscle after stimulated chronic eccentric exercise. *J. Appl. Physiol*, **69**, 1718 – 1724.

Xiao, G.G.; Garg, M.; Lim, S.; Wong, D.; Go, V.L.; Lee, W.P. (2008). Determination of protein synthesis in vivo using labelling from deuterated water and analysis of MALDI-TOF spectrum. *J Appl Physiol*, **104**, 828-836.

Chapter 2. The dynamic proteome profiling method.

2.1 Abstract

Skeletal muscle is one of the most important tissues in the body and understanding its adaptation is fundamental to physiology and pathophysiology. Skeletal muscle consists of a heterogeneous, dynamic mixture of myofibres that express a complex array of protein isoforms. The skeletal muscle proteome is made from thousands of individual genes, many of which have multiple isoforms and splice variants, furthermore each of these gene products may carry numerous different patterns of post-translational modification to give rise to a plethora of proteoforms that underpin muscle function. Due to this complexity, knowledge of the mechanisms underpinning skeletal muscle adaptation and how these processes are coordinated, at the protein level, are not yet well developed. In order to comprehend how these adaptive processes are organised, a better understanding of individual protein responses to muscle transformation will enable a prescription to be tailored for interventions for specific diseases and would provide a valuable contrast against which pathological and physiological situations can be better understood. At present, there are few viable techniques that accurately capture protein degradation. Whilst synthesis measurements are possible, until recently, most data were from gross/mixed muscle. Traditional methods of synthesis measurements, employ amino acid tracers that have limited practical application but have taught us important information about the dynamic nature of body constituents. However, amino acid tracers require intravenous administration that is invasive and can only be implemented over very short duration (<12 h). They are also expensive to administer and the data is not interchangeable due to the labelling of just specific amino acids e.g. phenylalanine and the inability to measure precursor enrichment which often brings complications to the analysis. More recently, there has been renewed interest using deuterium oxide as a biosynthetic label to measure synthesis as it equilibrates with body water quickly, can be easily administered and maintained during free-living conditions. We present a highly novel methodology utilising deuterium labeling in skeletal muscle over a 30-day period, combining established bottom-up and top-down proteomic methods to generate reproducible data for each element of protein turnover i.e. synthesis, abundance and degradation on an individual level.

2.2 Methodology development rationale

Skeletal muscle is known for its high degree of plasticity and its ability to adapt, based on the environment it is exposed to and/or the role it is required for (Coffey and Hawley, 2007). These changes are stimulated by discreet alterations in the muscle proteome; the pioneering investigations by Rudolph Schonheimer in the 1930's helped to establish this, demonstrating that the proteome is constantly in a dynamic state of change, governed by the two processes synthesis and degradation (Schonheimer, 1935). It is now well-established that proteins are continuously recycled through these processes of synthesis and degradation, termed protein turnover. Furthermore, the skeletal muscle proteome is made up of thousands of individual proteins (i.e. gene products) that each have multiple isoforms and can undergo post-translational modification in response to environmental changes of the cell (Burniston and Hoffman, 2011). Due to this complexity, knowledge of the mechanisms underpinning skeletal muscle adaptation and how these processes are coordinated, at the protein level, is not fully understood. Proteomic investigation into muscle adaptation is a new and rapidly growing area of research interest because in order to comprehend how these adaptive processes are organised, a better understanding of individual protein turnover responses i.e. synthesis and degradation to muscle transformation is important, and could eventually be used to provide tailored interventions for specific diseases or training outcomes.

In an attempt to quantify whole muscle protein turnover, several different methods and models have been developed, primarily these have utilised biosynthetic labelling techniques, including radio- or stable-isotope labelling, fluorescent labels and derivatised amino acids (Wolfe and Chinkes, 2005). To achieve turnover measurements in whole tissues, such as muscle, direct incorporation or fractional synthesis rate (FSR) measurements of muscle protein synthesis have been extensively used in the field (Garlick et al, 1994) and for a long time considered the 'gold standard' technique in acquiring protein metabolism measurements. The measurement of FSR may be achieved through the use of either a continuous, bolus or pulsed infusion of a stable isotope labelled amino acid tracer, administered intravenously. However, to measure turnover effectively there is need for a second tracer incorporation to quantify degradation. This is less than ideal, bringing further complexities and can involve complications during the administration making it

challenging to establish the precursor: product ratio. To circumvent such drawbacks, the use of arterial–venous (A–V) balance was introduced (Biolo et al, 1992). The A-V balance method enables both the rates of synthesis and degradation of limb proteins to be estimated by monitoring the rate of disappearance of the tracer from the arterial pool (as a proxy of synthesis) and the rate of appearance of the tracer into the venous pool (as a proxy of breakdown). However, this model is limited to the amino acid being studied, which may be subject to secondary metabolism, and it is not possible to isolate muscle specific responses from those of the surrounding tissues e.g. skin and bone (Biolo et al, 1995). Furthermore, the turnover data are also dependant on measures of arterial blood flow and lean leg mass. This is less than ideal in an exercise context where there are large changes in blood flow during and following exercise, this combined with challenging analyses of lean tissue mass would lead to the acquired data suggesting a potential over or under estimation in muscle protein turnover rates. To date, the majority of studies on muscle protein turnover use L-[ring $^{13}\text{C}_6$]-phenylalanine (e.g. Areta et al, 2013). The calculation of FSR is achieved by comparing the incorporation of tracer into newly made proteins over a period of time against the level of precursor enrichment. Largely, this is achieved by sampling the muscle pool, hydrolysing the protein mixture and then derivatising the amino acid of interest so that the proportion of labelled: unlabelled amino acid can be measured by gas chromatography-mass spectrometry. This combined with similar measurements of the enrichment of free amino acids in the precursor pool gives a precursor: product ratio allowing for the calculation of FSR (Figure 2.1). Furthermore, to gain a measure of fractional degradation rate (FDR), the infusion of a steady state tracer can be stopped and the decay of the tracer enrichment from the protein-bound and free amino acid pools over time can provide a best estimation of FDR (Zhang et al, 1996.; 2002). The application of such techniques has enabled insight into amino acid regulation and the contribution of FSR in tissue-specific and whole-body investigations. In addition, these techniques have made protein metabolism measurements possible through both health and disease states and in response to acute and chronic exercise (Wagenmakers, 1999). However, unlike the FSR methods, measurements of A-V balance are tissue specific and account for changes to blood flow in calculations. Amino acid tracer methodologies, whether AV-balance or direct incorporation, share several key limitations. These methods require intravenous infusion of the amino acid tracer, which restricts measures to acute time periods (<12 h) because of the need for

invasive venous/arterial cannulation. Measurements are generally restricted to a laboratory or clinical settings and the type of exercise or other activities that participants can perform is limited. Investigations that utilise traditional amino acid tracers may also be influenced by the metabolism and transport rates in particular tissues. Synthesis values from amino acid tracer studies represent averages across the entire proteome i.e. data from mixtures containing many hundreds of proteins. The calculation of degradation rate using this technique is less than ideal due to the rate of appearance of the labelled amino acids not being truly reflective of actual degradation rates. This is attributed to the problem of tracer 'label recycling' where tracer can be reincorporated in to new protein; thus, providing end values that are potentially misleading (Nair et al, 1988). Information on the gross turnover of muscle proteins oversimplifies the complexity of biological processes such as muscle adaptation and key information about the turnover of individual proteins is lost. Protein synthesis and degradation are each an intricate process that affect changes in muscle protein abundance. Synthesis and degradation are regulated independently and on a protein-by-protein basis to maintain homeostasis or to facilitate muscle adaptation. It is paramount to accurately capture the contributions of both synthesis and degradation at the individual level to gain a detailed understanding of the mechanisms of muscle adaptation.

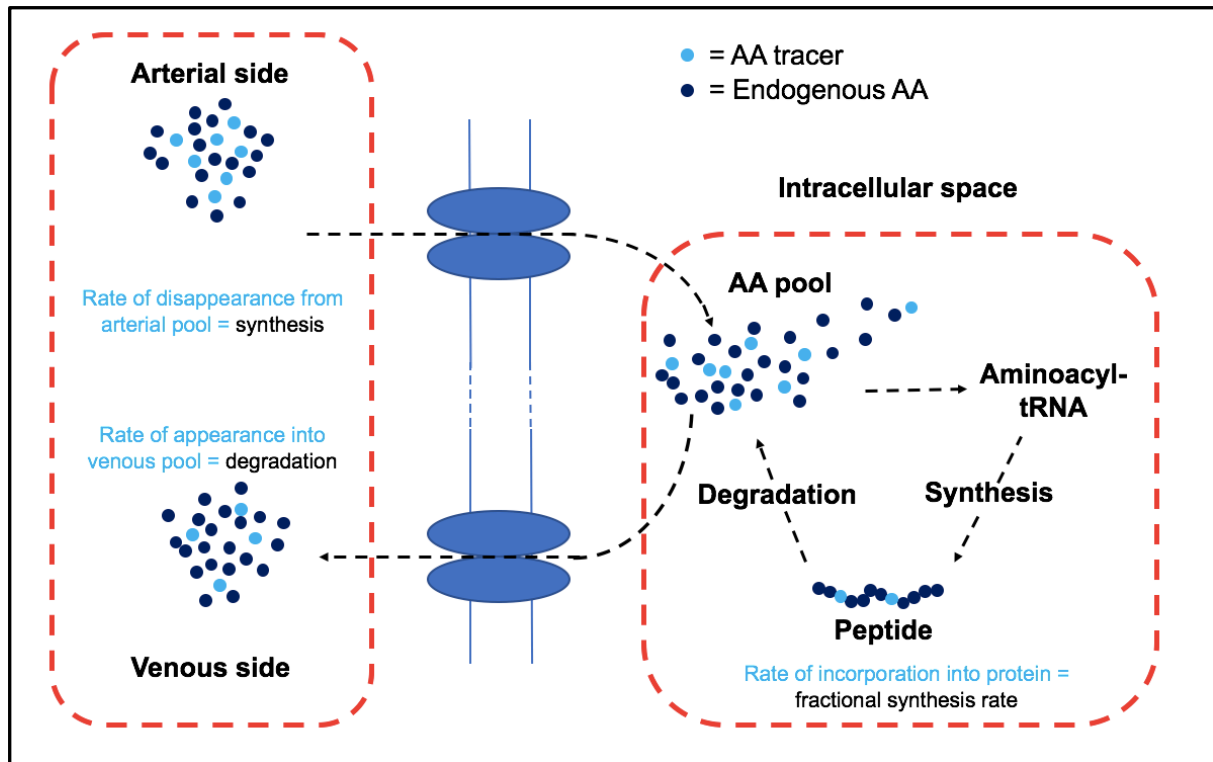


Figure 2.1. Fundamental principle of precursor: product ratio used in tracer studies. Schematic showing the use of stable isotope tracers for the calculation of protein synthesis and degradation utilising the arterial–venous balance and fractional synthesis rate methodologies. The precursor relates to the enrichment of amino acid tracer and the product is the incorporation in the final protein product.

Recent advances in mass spectrometry have brought renewed interest in the use of heavy water, deuterium oxide ($^2\text{H}_2\text{O}$) as a stable isotope amino acid tracer (Gasier et al, 2010). Theory underpinning deuterium labelling is fundamentally the same as the traditional amino acid tracer methods described above, as it still relies on biosynthetic labelling *in vivo* and precursor: product ratio calculation. However, deuterium oxide labelling overcomes the aforementioned limitations of traditional amino acid tracer techniques. Deuterium can be administered orally, consequently equilibrating within the body water quickly <30 min; in rodents (Busch et al, 2006). Almost all amino acids can incorporate ^2H -label and administration of deuterium oxide can be sustained for long periods (but supplementing the drinking water) with no hazardous effects (Jones and Leatherdale, 1991). Therefore, there is no need for intravenous infusion and measurements of turnover of individual muscle proteins can be taken during free-living conditions for acute (hours – days) or chronic (weeks – months) experiments. The use

of deuterium oxide also affords analytical advantages over the previous amino acid tracer methods. Metabolic labelling of newly synthesised proteins with deuterium occurs across almost all amino acid residues and, therefore, gives a proportionally larger signal than previous methods by causing a shift in isotope pattern for any given synthesis rate (Figure 2.2). Furthermore, labelling occurs intracellularly meaning deuterium labelling is not influenced by the metabolism or transport rates of individual amino acids (Gasier et al, 2010). The combination of these factors position the use of $^2\text{H}_2\text{O}$ as an ideal tool for the study of free-living exercise physiology, allowing for the evaluation of muscle protein turnover. Moreover, with its ability to quantify responses of muscle protein synthesis, this technique will prove to be critical in the study of muscle metabolism over longer periods of exercise training, leading to a more complete understanding of the muscle adaptation process.

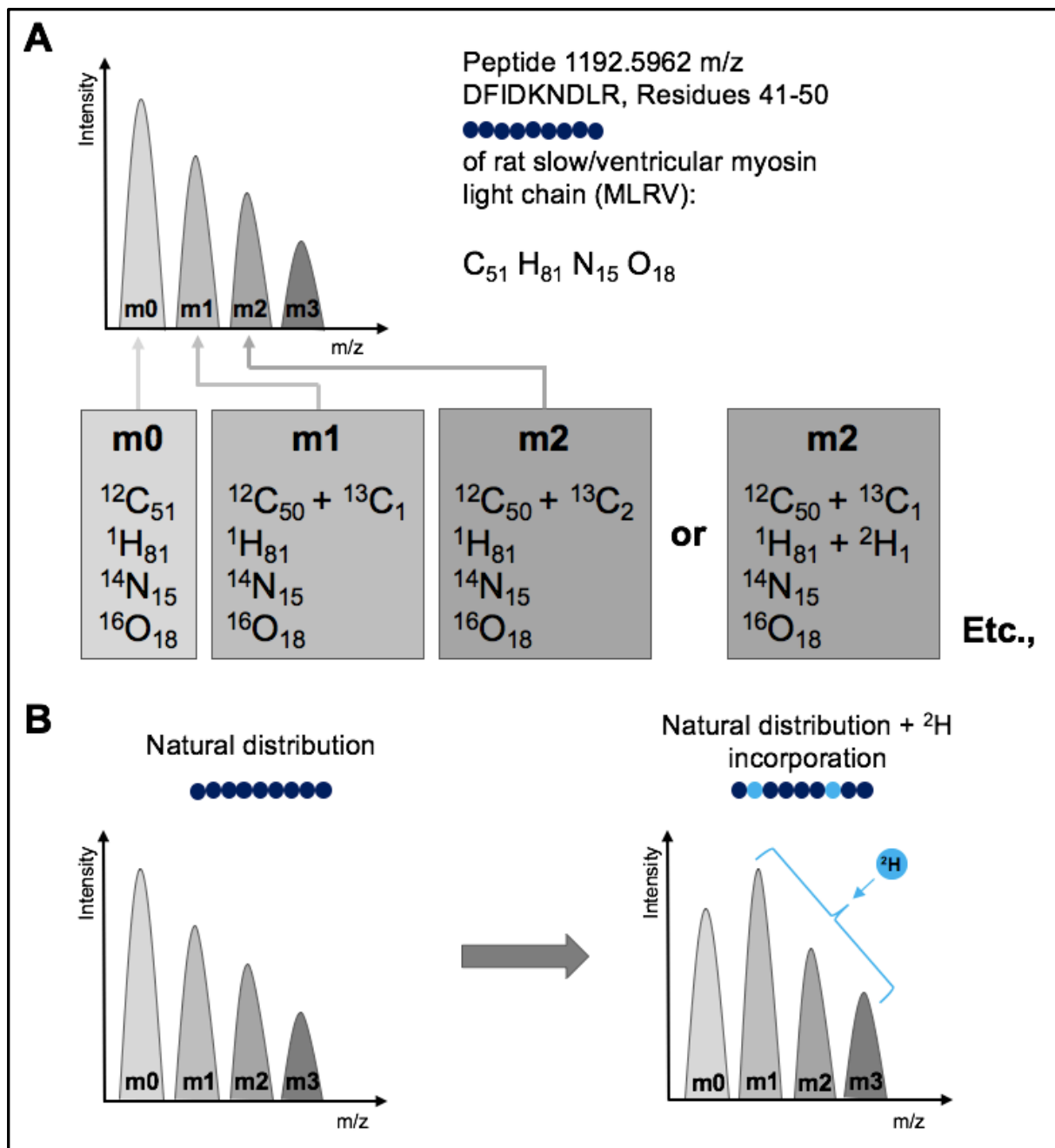


Figure 2.2. Nomenclature and composition of peptide mass isotopomers and how exogenous deuterium is incorporated.

(A) Mass spectrometry resolves peptides as ‘envelopes’ of mass isotopomers, and the relative abundance of the mass isotopomers reflects the natural abundance of C, H, N and O isotopes in the amino acids that were used to synthesise that protein. The first isotopomer in the series has the lowest mass (mass to charge ratio; m/z) and is known as the monoisotopic peak (m_0) because it consists entirely of primary/ ‘light’ isotopes (i.e. ^{12}C , 1H , ^{14}N , ^{16}O etc). The second isotopomer is composed of peptides

that contain one stable secondary/ 'heavy' isotope (i.e. ^{13}C , ^2H , ^{15}N etc) and is labelled the m1 peak, and the next isotopomer is labelled the m2 peak because it contains 2 secondary/ 'heavy' isotopes, which may be ^{13}C or other heavy isotopes such as ^2H . A peptide with the sequence DGFIDKNDLR has an elemental composition of $\text{C}_{51}\text{H}_{81}\text{N}_{15}\text{O}_{18}$ and in the absence of an exogenously applied isotope label, the natural pattern of the mass isotopomers is largely determined by the natural abundance of carbon isotopes because carbon is a major component of amino acids and the 'heavy' ^{13}C isotope has a relatively high natural abundance (~1.1 % of C is ^{13}C and 98.9 % is ^{12}C). The mass isotopomer pattern of a peptide can be roughly predicted based on the probability that 1.1 % of the C will be ^{13}C and therefore cannot contribute to the abundance of the m0 peak. However, accurate and complete prediction of the mass isotopomer pattern also requires the contributions of H, N and O isotopes to be recognised and the diminishing probability of 2, 3 or 4, etc., heavy isotopes occurring with a peptide. (B) For each peptide, deuterium (^2H)-labelled amino acids incorporated in to protein during synthesis *in vivo* cause a shift in the distribution of peptide mass isotopomers. Peptides that contain ^2H -labelled amino acids can only contribute to the abundance of m1, m2 and m3 mass isotopomers, the relative abundance of the m0 mass isotopomer then declines as a function of deuterium incorporation. Consequently, these data can be used to analyse both the relative abundance (based on the intensity of all mass isotopomers) and deuterium incorporation (based on the relative distribution of mass isotopomers) to calculate the rate of protein synthesis for that peptide/protein.

Despite the advances in biosynthetic labelling *in vivo* afforded by deuterium oxide, it is still challenging to determine protein-specific synthesis rates. The hydrolysis of muscle proteins in to individual amino acids destroys the relationship between the protein and its synthesis measurement. Therefore, the majority of the literature (Claydon et al, 2012; MacDonald et al, 2013) report fractional synthesis rates that are essentially averages across the hundreds or thousands of proteins in hydrolysates of whole muscle or sub-cellular fractions such as, myofibrillar, soluble and mitochondrial. This limits the potential to develop knowledge about muscle adaptation because there is now evidence that documents the rate of turnover for individual proteins spans a

broad range (Jaleel et al, 2008.; Hesketh et al, 2016.) and can change in response to exercise interventions (Camera et al, 2017). The use of proteomic applications, including two-dimensional gel electrophoresis (2DGE) combined with analytical techniques such as peptide mass spectrometry have facilitated the advancement of research at the protein-specific level. Our laboratory has pioneered the application of proteomic techniques in exercise physiology and reported data on the changes in the abundance of individual proteins in response to, moderate-intensity endurance exercise in rats (Burniston, 2008), cardiac adaptation of rats (Burniston, 2009), high and low running capacity in the rat (Malik et al, 2013) and interval training in humans (Holloway et al, 2009). Data such as these present information on individual proteins and even their post-translation states (Burniston, 2009), but largely these are static proteome data that quantifies protein abundance only. Jaleel et al, (2008) reports the separation of individual proteins using 2DGE from rat gastrocnemius that had been labelled by an infusion of ring- $^{13}\text{C}_6$ phenylalanine *in vivo*. Gel spots were identified by peptide mass spectrometry, whereas incorporation of the stable isotope label into new protein was measured in mixtures of hydrolysed amino acids using gas chromatography-mass spectrometry (GC-MS) of derivatised amino acids. The marriage of these established techniques enabled synthesis rates to be calculated for 68 mitochondrial proteins in rat skeletal muscle. Despite this work confirming the synthesis of proteins within a muscle differs on a protein-by-protein basis, of the proteins investigated beta enolase had the greatest synthesis rate (11 %/day) while myosin light chain regulatory had the lowest (3 %/day). However, this is a complex and laborious solution to acquiring data on protein-specific turnover rates and was not widely adopted in the field. In contrast, advances in the sensitivity of mass spectrometers and the ability to mass analyse peptides, presented new opportunities for investigation of protein turnover based on mass spectrometry data. The mass analysis of peptides offers a more straight forward solution for the calculation of protein-specific turnover rates. Using peptide mass spectrometry, it is possible to identify the parent protein that the peptide has derived from, measure the level of incorporation of isotopically labelled amino acid in that protein and determine the relative enrichment of isotopically labelled amino acids in the precursor pool.

During my MSc studies, we (Hesketh et al 2016) used 2DGE analysis of deuterium labelled proteins to measure protein-specific synthesis rates in four different striated muscles in the rat (EDL, SOL, cardiac and diaphragm). Two dimensional gel

electrophoresis is an advanced biochemical method that separates proteins based on isoelectric point (pI) and relative mass (M_r) (Kelleher et al, 1999). This technique enables the semi-quantitative analysis and identification of specific proteoforms via the use of peptide mass fingerprinting. 2DGE is nicknamed a 'top-down' approach because it provides separation of individual proteoforms prior to mass spectrometry analysis. Gel-based methods are robust and provide a highly efficient visual platform for the separation of protein proteoforms (Padula et al, 2017). The separation of protein into discrete spots (proteoforms) by 2DGE provides a swift and reliable way for determining the characteristic combination of the M_r and the pI of a proteoform of interest (Dowling et al, 2019). A proteoform is the same product of an individual protein species that normally occurs at a different isoelectric point. This is usually the result of a post-translation modification e.g. phosphorylation (Burniston, 2009) but can also be caused from a shift in isoform. The visualisation of these protein spots also offers a semi-quantitative measure of protein abundance using spot density, analysed by computer software. After 2DGE separation, in-gel proteolytic digestion is performed on each protein-spot to digest protein into their constituent peptides. Peptide mass spectrometry is then used to identify each 2D-gel spot against gene or protein databases. For example, peptide mass fingerprinting (PMF) is used to compare mass spectrometry data that contains multiple peptide peaks against a protein database such as SwissProt (<https://www.uniprot.org>). A successful PMF search returns a protein identification and a probability-based (MOWSE) score of the certainty of the protein identification. An acknowledged limitation of 2DGE is that the range of protein separation is restricted to high abundance, complex mixtures of proteoforms. There can also be technical issues with gel-to-gel variations and the possible underestimation of the presence of certain types of proteins. For example, high-molecular-mass proteins, low-abundance proteins or very hydrophobic proteoforms (Burniston, 2008; Murphy et al, 2016). However, top-down proteomics that utilise gel-based approaches are well suited to the investigation of proteins in the myofibrillar fraction. This collection of proteins are highly abundant and therefore well represented on gel-based techniques. Furthermore, most myofibrillar proteins (e.g. myosin, troponin etc.) exist as many different isoforms which can be expressed as multiple proteoform patterns. Changes in muscle phenotype are underpinned by complex patterns of such proteoform expression which are clearly resolved by 2DGE.

Currently, the majority of muscle proteome data comes from 2DGE (e.g. Burniston

and Hoffman, 2011), which affords robust comparative analysis of protein species but does not easily resolve proteins at the extremes of the molecular mass and isoelectric point ranges. Moreover, because 2DGE separates proteins to their constituent species, the number of non-redundant proteins identified may be relatively small (e.g. <300 proteins). In contrast, liquid chromatography mass spectrometry (LC-MS) is able to catalogue larger numbers of muscle proteins. For instance, Burniston et al, (2014) identified 1514 proteins encompassing the entire complement of metabolic enzymes and some regulatory kinases. The method of proteome profiling provides that basis of a contrasting technique to gel-based 'top-down' proteomic strategies.

An alternative approach for proteome profiling is nicknamed 'bottom-up' analysis and involves in-solution digestion of proteins from the muscle homogenate followed by delivery of the peptide mixture in to the mass spectrometer by reverse-phase liquid chromatography. The peptide mixture is resolved in time and a chromatogram is produced wherein the intensity of the peptide peaks provide a measure of abundance. This can be further quantified with use of a protein 'spike' where a known quantity of spiked protein is incorporated into the chromatogram so the peaks of the experimental peptide can be compared to provide a measure of abundance in absolute (fmol) terms. Label-free quantitation is performed, which defines the isotopic envelope of each peptide and records the abundance of all mass isotopomers over the duration of the chromatographic peak for that peptide. Bottom-up proteomic approaches can also be combined with deuterium labelling which means that the mass isotopomers can be used to calculate protein synthesis utilising the same principles described in Figure 2.2. Despite this approach affording greater levels of automation compared to top-down approaches there are still several challenges associated with this type of analysis. Firstly, all proteins are digested in one mixture and it can be a time-consuming process to identify individual proteins from the resulting peptides. Furthermore, because all proteins are digested in the same mixture, this means that individual proteoform identifications or information on post translation modifications is lost. This means that bottom-up proteomics is better suited to the analysis of muscle proteins from the soluble fraction where differences in proteoforms may be less extensive compare to myofibrillar proteins. Sophisticated software platforms exist which assist with bottom-up label-free quantitation of individual proteins. Our lab uses commercial software (Progenesis QI-P; Waters Corp.), which normalises mass spectrometry by inter-sample abundance ratio and generates log-transformed protein

data that can be used to investigate differences in protein abundance (Malik et al, 2013.; Burniston et al, 2014). However, there are currently no commercially available software applications for automated analysis of protein synthesis rates, therefore researchers working in this area need to do this work manually and develop their own solutions for computing synthesis rates from peptide mass isotopomer data.

Mass spectrometers are cutting edge, analytical machines that are constantly improving to encompass a greater range of biological applications. In recent years, exercise proteomics has exploited these developments by measuring large numbers of proteins of individual proteins (Burniston et al, 2014) and in response to exercise training (Sollanek et al, 2017). The advances in peptide mass spectrometry combined with stable isotope techniques such as deuterium oxide labelling, now mean information can be gained on the synthesis rate of individual proteins. Xiao et al, (2008) were the first to combine MALDI-TOF MS data collection with established (Hellerstein and Neese, 1992) mass isotopomer distribution analysis. Xiao et al, (2008) reported the measurement of albumin synthesis *in vivo* via $^2\text{H}_2\text{O}$, labelling and peptide analysis by matrix-assisted laser desorption ionisation – time of flight mass spectrometry (MALDI-TOF/MS). Furthermore, Price et al, (2012) devised a method to isolate deuterated peptides using liquid chromatography-mass spectrometry (LC-MS) and calculate the rates of turnover for ~100 individual proteins within humans. Similar techniques using $^2\text{H}_2\text{O}$ and peptide mass spectrometry have been used to provide information on tissue proteome dynamics in response to exercise. Shankaran et al, (2016) quantified synthesis rates for over 139 individual muscle proteins in response to 3 weeks of sprint interval training, reporting 20 proteins with greater synthesis rates in exercised muscle, highlighting individual differences in synthesis rates across the muscle proteome. Kim et al, (2012) implemented a similar deuterium oxide labelling *in vivo* with bottom-up analysis to report a large-scale analysis of protein synthesis rates in mouse heart and liver mitochondria. The synthesis rates of 314 cardiac mitochondrial proteins were characterised over a period of 90 days and were approximately 3-fold greater in liver compared to cardiac mitochondria (Kim et al 2012). A general correlation (Spearman $\rho = 0.50$) between synthesis rates of proteins in heart and liver mitochondria was reported, but the synthesis rate of many mitochondrial proteins ranked differently between cardiac and liver mitochondria, suggesting tissue-specific regulation. In Hesketh et al (2016), we developed this technique further by combining it with 2DGE, which enabled us to investigate a

collection of different proteins across different striated muscles of the rat. Deuterium labelling *in vivo* of 8 individual proteins across fast- and slow-twitch, cardiac and diaphragm muscles were used over a 14-day period. Similar to the work of Kim et al, (2012) we also reported the rank order of synthesis is different depending on the muscle investigated. While all of this work is unique, implementing deuterium labelling and mass spectrometry proteomics still fails to report individual abundance. This research has taught us valuable information by demonstrating that there is a broad range of fractional synthesis rates of muscle proteins and a specific rank order of individual protein synthesis rates across different muscle tissues i.e. fast vs slow-twitch. This raises questions about previous work that used mixed protein data where it is typical for just one muscle to be sampled but the results are often extrapolated to skeletal muscle as a whole. By just measuring protein synthesis rates means we cannot ascertain whether a change in synthesis rate represents a greater turnover of the protein pool or accretion of a given protein. This becomes especially important when we consider that changes to the balance between the rate of synthesis and breakdown can alter the net abundance of a protein within the cell and the rate of turnover can vary from one protein to the next (Figure 2.3).

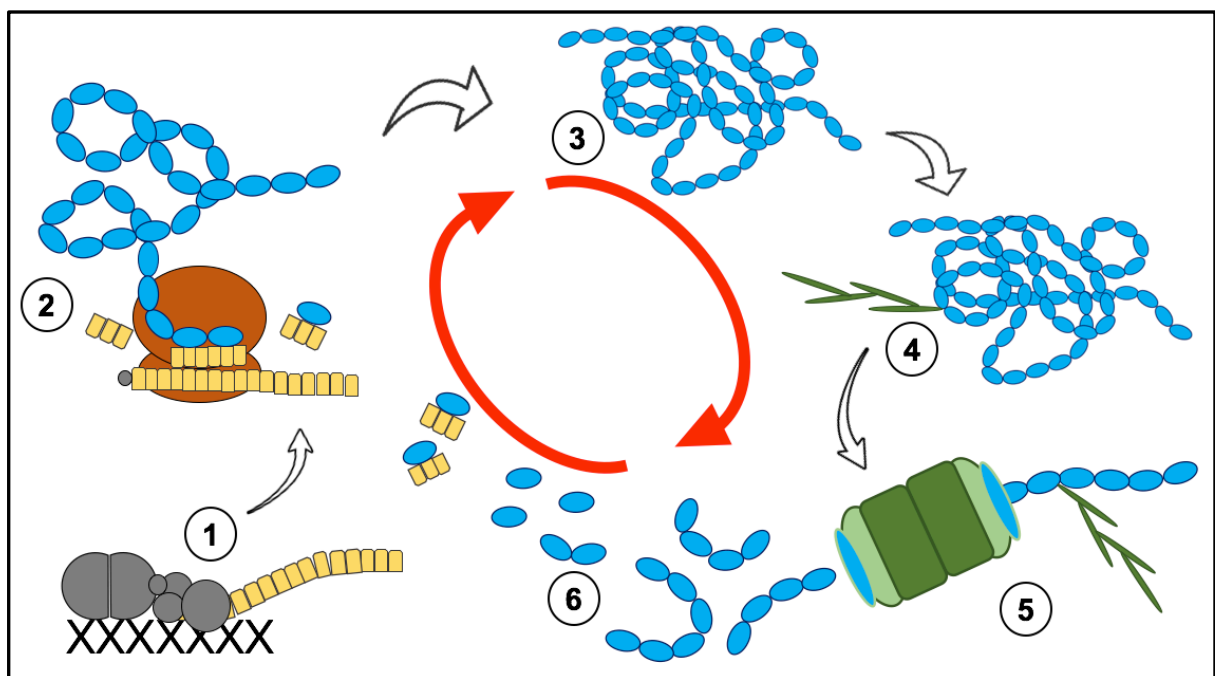


Figure 2.3. Protein turnover: The lifecycle of a protein.

(1) Genetic information contained in the DNA sequence is transcribed into messenger RNA (mRNA). This message contains all of the information necessary to build a

particular protein. (2) The mRNA is used to direct the synthesis of the new protein at the ribosome. The ribosome translates the genetic information contained in the mRNA sequence into the appropriate sequence of amino acids. How quickly this process is coordinated is the synthesis rate of that protein. (3) The chain of amino acids forms folds and other complex shapes and becomes a mature protein (Balchin et al, 2016). The amount of this functional protein in the cell is the protein abundance. Often proteins are modified by covalent attachment of molecules such as phosphate (i.e. phosphorylation) and this changes their functional properties. (4) Proteins are marked for degradation by the attachment of chains of ubiquitin. (5) Ubiquitylated proteins are degraded by the 26S proteasome, which cleaves the protein into peptides. The speed that this process occurs is the rate of degradation for that protein. (6) The peptides are digested into single amino acids by endopeptidases and the amino acids are attached to transfer RNA (tRNA) ready for use by the ribosome.

The data generated from the recent advent of $^2\text{H}_2\text{O}$ labelling combined with peptide mass spectrometry and proteomics give rise to new opportunities to investigate tissues, such as muscle, at the individual protein level. However, it is also important to consider the contributions of protein degradation (Figure 2.3) at the individual level in order to achieve complete insight into the turnover of muscle proteins *in vivo*. Protein degradation is yet more challenging to study. A variety of techniques purport to measure degradation (Biolo et al, 1995, 1997; Pasiakos et al, 2014), but these methods are associated with important confounding factors. For example, the A-V balance method may underestimate the rate of degradation because of reutilisation of labelled amino acids for protein synthesis. Other stable isotope tracer methods have also been developed to assess protein degradation *in vivo* that do not require such invasive methods (Zhang et al, 1996). The principle behind these methods is that the appearance of unlabelled amino acids from protein degradation will dilute the tracer enrichment in the muscle intracellular pool but not the arterial blood pool, allowing the relationship of label enrichment in the muscle intracellular fluid and arterial blood to be used to calculate the fractional degradation rate (Chinkes, 2005). More recently, a pulse-chase version for determination of protein degradation was developed (Zhang et al, 2002). This method requires fewer biopsies and does not require an infusion of amino acids. However, physiological steady state is a crucial component of this

models is to allow protein degradation to be determined. Without maintaining this steady state, the relationship between degradation and amino acid transport is variable meaning that interpretation of the data can be easily confounded (Tuvdendorj et al, 2013). Thus, the technique is not appropriate for quantifying protein degradation rates in response to exercise. Furthermore, these methods that attempt to measure fractional degradation rates and the A-V methods are both limited to degradation rates of mixed muscle proteins with no capacity to quantify individual proteins or even protein sub-fractions e.g. myofibrillar or soluble. Measurement of 3-methylhistidine (3MH) in the urine is one approach that attempts to address this limitation. 3MH is a post translationally methylated histidine found in myofibrillar proteins. This is used as a marker of myofibrillar degradation because it cannot be further metabolised and cannot be recycled for use in protein synthesis (Vesali et al, 2004). 3MH methods are controversial (Rennie et al, 2008) and the routine measurement of 3MH in urine means the degradation information is not specific to a specific muscle or muscle type. More recently, attempts have been made to investigate degradation of individual proteins in muscle. This method involves the measurement of decay of isotopic enrichment of protein mixtures (Holm et al, 2010). However, despite this method allowing for measurements to last up to as long as 2 weeks, methodologies like deuterium labelling cannot be employed simultaneously because this method relies on no labelled amino acids being re-incorporated into new proteins and means that the net muscle protein balance cannot be determined. This positions the utility of this method with a very limited scope, especially when trying to study adaptive models where there is a changing protein mass.

The next challenge would be to gain this level of insight i.e. individual protein turnover responses, into muscle adaptation. Even with the introduction of mass spectrometry driven methods to measure protein synthesis, all previous studies have been conducted in a 'stable environment' with no intervention or 'change' in the system. Therefore, protein abundance is assumed to be stable throughout the experimental period. However, during patho-physiological or physiological change, such as muscle adaptation, there are quantifiable differences in individual protein abundance (Burniston, 2009; Holloway et al, 2009) to change the desired characteristics of the muscle i.e. faster contracting or more fatigue resistant (Burniston 2008). We know that changes such as these occur in response to exercise and are documented extensively in whole muscle physiology (Burniston and Holloway, 2011). However, there is little or

no information on how these processes of change are orchestrated on the individual protein level. In order to investigate this level of detail and elucidate the mechanisms responsible, a shift in paradigm must be introduced. Programmed exercise would provide a 'changing environment' to give a platform where individual protein turnover can be investigated in response to altered protein abundance; challenging the status quo of how traditional tracer studies are normally conducted. In a changing system, protein degradation can be calculated as the difference between the measured synthesis rate and change in protein abundance (Burniston and Chen, 2019).

Our lab has previously achieved in humans, the combination of $^2\text{H}_2\text{O}$ labelling and proteomic investigation with a changing system to permit investigation of how protein synthesis and degradation contribute to muscle adaptation (i.e. changes in abundance) on an individual level (Camera et al, 2017). This implements a robust method of measuring protein synthesis and abundance of individual proteins and can therefore accurately calculate protein degradation. However, further optimisation of this technique is required as the degree of adaptive change that is quantified in this work is not reflective of the whole muscle. In this regard, absolute measurements are not possible in humans even with multiple biopsies. This is due to that fact we cannot extract whole muscles in humans for analysis and because the fibre type characteristics (and therefore the individual proteins) differ from one biopsy to the next, even within the same muscle of one individual (Elder et al, 1982).

Muscle phenotypes are determined by complex patterns of co-expression of fast and slow isoforms of myofibrillar proteins that share high levels of sequence homology. This makes peptide level studies particularly challenging because isoform-specific peptides must be detected in order to study adaptations of the myofibrillar proteome. Furthermore, the bottom-up approach utilised in such work (e.g. Camera et al, 2017) means that to quantify this level of peptide-specific data is challenging. Therefore, future work and consequently the aim of this chapter is to present a method that can incorporate peptide-specific data to give insight in to domain-specific rates of turnover, e.g. for peptide domains that may be cleaved or subject to post-translational modifications that alter their rate of turnover. Further limitations of human studies include problems with larger body mass meaning slower uptake of deuterium making curve fitting more complex. Whereas, the use of small laboratory animals means that precursor enrichment is rapid and stable. This makes the calculation of synthesis rate

more robust and subsequently enabling us to calculate both relative (FSR) and absolute synthesis rates for individual proteins.

To circumvent limitations associated with human administration of deuterium, we present the implementation of animal models which allows for the extraction of the whole muscle for analysis, thus making absolute measurements possible and providing a greater amount of tissue sample to permit both bottom-up and top-down proteomic analysis, in order to capture peptide-specific changes in turnover. This also has the added benefit of using a programmable stimulation protocol to exploit the unique characteristics of muscle plasticity to the full, whilst utilising the contralateral non-stimulated muscle as an internal control. The implementation of introducing a dynamic system to study muscle adaptation will be the main aim of future chapters. The proposed methodology will calculate protein turnover on not just an individual protein scale but to also shed light on proteoform-specific turnover, providing information on whether a particular post translational modification is associated with a change to the synthesis or degradation rate of that specific protein. Thus, allowing us access to a deeper understanding of muscle adaptation by providing important quantitative information, at the absolute cutting edge, of how muscle adaptation is orchestrated.

Objectives

Objective of chapter – To establish the dynamic proteome profiling method.

Specific Aim 1: To implement a robust technique that combines common proteomic approaches to exploit the fractionation of skeletal muscle to increase the number of non-redundant protein identifications and to increase the analytical space allowing for proteoform specific analysis.

Specific Aim 2: To combine biosynthetic labelling with mass spectrometry analysis during a period of adaptation (30 d), using multiple sampling points to quantify the relative abundance changes and synthesis rates of individual proteins during muscle adaptation.

Specific Aim 3: To use mathematics to calculate the rate of change for individual

protein abundances to allow for calculation of degradation rates of individual proteins for each experimental time point.

Specific Aim 4: To calculate values that reflect the state of the whole muscle, generating absolute protein turnover data for all individual proteins.

2.3 Experimental design

In order to interrogate complex proteoform-specific responses it will be necessary to further optimise experimental designs for generating protein turnover rates from peptide mass spectrometry data. Experiments that collect only baseline and post-intervention samples are less appropriate for detailed interrogation of protein responses because they do not chart the time-course of changes in deuterium incorporation and, therefore cannot establish whether the labelling of a protein has reached equilibration. For a study to accurately measure muscle protein turnover at the level of the individual protein in response to skeletal muscle adaptation, there are several key factors that must be considered when designing the experimental investigation. Firstly, there must be a baseline or control group to establish the profile of unlabelled peptides. Secondly, it is paramount to include multiple sampling points in a time-series analysis (Figure 2.4) to minimise the risk that aspects of the adaptation process might be missed because the asymptote of the synthesis and abundance measures are not detected. Finally, there must be biological replication within groups, and across the experimental time series to allow for adequate comparison at incremental periods throughout the adaptive process.

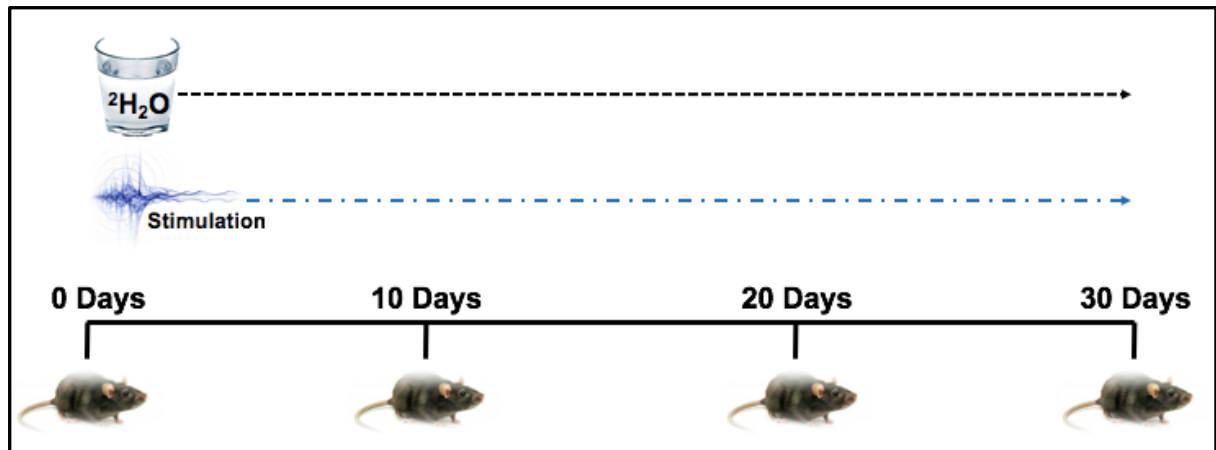


Figure 2.4. Schematic overview of theoretic experimental design.

A theoretic experimental design shows a time series with independent groups of rats in each group. After a post-operative recovery period the animals in the 0 d group (baseline/sham control) are killed and muscles from both the left and right limb are extracted for analysis. The animals in the subsequent groups: 10 d, 20 d and 30 d then receive deuterium oxide ($^2\text{H}_2\text{O}$) labelling and the implanted stimulators are switched on to administer a programmed stimulation pattern designed to induce adaptation to the target left limb muscle. At each of the experimental time periods, the respective group of animals are killed in the same way as the 0 d group and both the left (stimulated) and right limb (non-stimulated control) muscles are extracted for further analysis.

In addition to the main components of the experimental design an appropriate labelling protocol must be adhered to. For all the experimental investigations that include animal models and/or handling described here. All aspects of the animal husbandry were conducted by the LJMU animal facility staff. Surgery procedures and the electrical stimulation models were part of a collaborative effort in a wider project. As a result, work conducted within this thesis focused solely on aspects associated with dynamic proteome profiling of muscle samples. All animal procedures are conducted under the British Home Office Animals (Scientific Procedures) Act 1986 and are part of a subset of experiments from a larger investigation (licence holder Prof. Jonathan Jarvis). Animals assigned to our experimental procedures were all male Wistar rats that were bred in-house in a conventional colony, housed in controlled conditions of 20 °C, 45 % relative humidity, and a 12 h light (0600–1800 hours) and 12 h dark cycle, with water and food available *ad libitum*.

We have previously used $^2\text{H}_2\text{O}$ in rats (Hesketh et al, 2016) and found ~4 % body water enrichment sufficient enough to allow for the tracking of $^2\text{H}_2\text{O}$ in to newly synthesised peptides. To achieve this level of enrichment the animals must receive deuterium oxide ($^2\text{H}_2\text{O}$; Sigma-Aldrich, St. Louis, MO) that is initiated by an intraperitoneal loading injection of 10 $\mu\text{l/g}$ of 99 % $^2\text{H}_2\text{O}$ -saline, which is then maintained over the course of the investigation by administration of 5 % (v/v) $^2\text{H}_2\text{O}$ in the drinking water, available to the animals *ab libitum* and refreshed daily. Findings from our previous work (Hesketh et al, 2016) were also used to optimise the duration of the current experiments. Based on the calculated half-life of serum albumin, ALBU, half- 14.4 d (Hesketh et al, 2016) we chose to use a 30-d experimental period.

2.4 Laboratory processing

2.4.1 Laboratory workflow

The methodology described in this chapter has been developed to study models of muscle adaptation, combining stable isotope labelling using deuterium oxide and proteomic techniques. Figure 2.5 gives an overview of the processing involved in the proteomic workflow. This approach affords in-depth analysis of muscle adaptation by analysing both the contractile apparatus of the muscle (myofibrillar) and the enzymes/energy producing proteins (soluble) on an individual level.

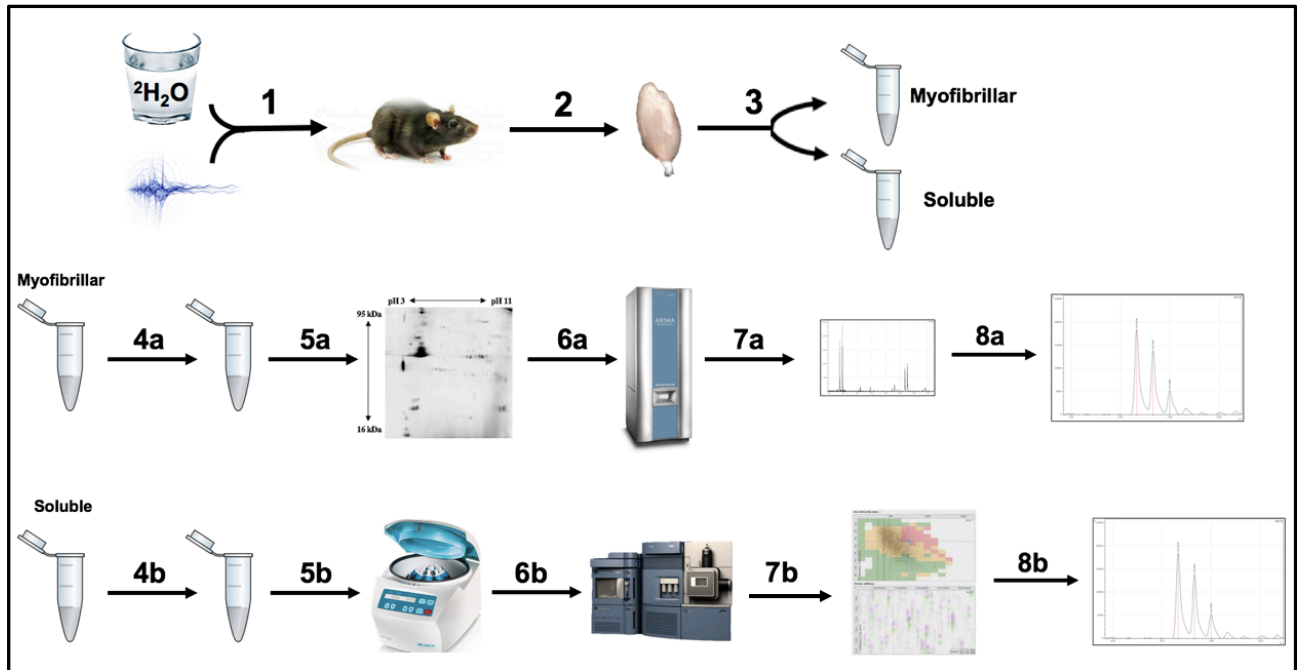


Figure 2.5. Established workflow sequence to measure protein turnover during skeletal muscle adaptation.

(1) Deuterium oxide ($^2\text{H}_2\text{O}$) administration to independent groups of rats for given period of time (i.e. 0, 10, 20 or 30 days). N.B. in subsequent experimental chapters, the animals also receive *in vivo* stimulation to bring about transformation of left hind limb muscles only. (2) Animals are sacrificed and both the left stimulated and right non-stimulated muscles are excised for analysis. The contralateral, non-stimulated muscle is taken to serve as internal control. (3) Muscles are then homogenised and fractionated to myofibrillar proteins and soluble proteins. (4a/b) Muscle fractions are processed via biochemical techniques to establish the amount of protein per sample. (5a) Proteomics techniques e.g. 2DGE is used to separate myofibrillar proteoforms and quantify abundance changes. (5b) Homogenised soluble proteins undergo in-solution digest to separate samples into peptides. (6a) Gel spots are cut and digested before peptide mass fingerprinting is used via MALDI-TOF/MS to identify each individual protein. (6b) Peptides are loaded onto LC-MS where proteins can be identified and abundance quantified. (7a) MALDI-TOF/MS provides raw data of peak intensities for individual peptides specific to each protein. (7b) Alignment of raw data is required using Progenesis software to perform calculations. (8a/b) After extracting the raw data for each protein/peptide mass isotopomer, a computer programme is used so the rate of synthesis for each protein can be calculated.

2.4.2 Exemplar experimental methods

The data presented in the current chapter were from Male Wistar rats ($n = 16$) aged 3 months, 500 ± 69 g body weight were bred in-house in a conventional colony, housed in controlled conditions of $20\text{ }^{\circ}\text{C}$, 45 % relative humidity, and a 12 h light (0600–1800 hours) and 12 h dark cycle, with water and food available *ad libitum*. All aspects of animal husbandry were conducted by the LJMU animal facility staff conducted under the British Home Office Animals (Scientific Procedures) Act 1986.

These animals provided example data using soleus and plantaris muscles that did not receive any kind of stimulation or adaptation induced change. The purpose of which was to test our relative and absolute calculations fit the expected outcomes before applying them to a model of muscle adaptation (subsequent chapters). An experimental design using the same time-series described in Figure 2.4 was utilised, this included independent grouping of the rats ($n = 4$, in each) that received deuterium oxide ($^2\text{H}_2\text{O}$), in line with the labelling protocol described in section 2.3, at 0 d, 10 d, 20 d and 30 d. At each of these time points the Soleus (SOL) and Plantaris (PLN) muscles of the hindlimb were extracted and processed according to the methods detailed in sections 2.4 and 2.6. From which we provide data to show the two methods of calculating fractional synthesis rate (FSR) described in section 2.7.1 as well as documenting the comparisons in FSR of slow-twitch muscle (SOL) and fast-twitch muscle (PLN).

2.4.3 Measurement of precursor enrichment

Body water ^2H enrichment was measured in plasma samples collected at the time of muscle isolation. Plasma water was measured against external standards that were constructed by adding $^2\text{H}_2\text{O}$ to phosphate buffered saline over the range from 0.0 to 5.0 % in 0.5 % increments. Deuterium enrichment of aqueous solutions was determined after exchange with acetone (McCabe et al, 2006). Samples were centrifuged at $12\ 000 \times g$, $4\text{ }^{\circ}\text{C}$ for 10 min, and 20 μl of plasma supernatant or standard was reacted overnight at room temperature with 2 μl of 10 N NaOH and 4 μl of 5 % (v/v) acetone in acetonitrile. Acetone was then extracted in 500 μl chloroform and water was captured in 0.5 g Na_2SO_4 before transferring a 200 μl aliquot of chloroform to an autosampler vial.

Samples and standards were analysed in triplicate using an Agilent 5973N mass selective detector coupled to an Agilent 6890 gas chromatography system. A CD624-GC column (30 m x 0.25 mm x 1.40 μ m) was used in all analyses. Samples (1 μ l) were injected using an Agilent 7683 autosampler. The temperature program begins at 50 °C and was increased by 30 °C/min to 150 °C, and was held for 1 min. The split ratio is 50: 1 with a helium flow of 1.5 ml/min. Acetone was eluted at approximately 2.0 min. The mass spectrometer was operated in the electron impact mode (70 eV) and selective ion monitoring of m/z 58 and 59 was performed using a dwell time of 10 ms/ion.

2.4.4 Muscle processing

Muscles were fractionated into myofibrillar and soluble fractions according to Camera et al, (2017). Samples were pulverized under liquid nitrogen using a mortar and pestle, 100 mg of the tissue powder was homogenized on ice in 10 volumes of 1 % Triton X-100, 50 mM Tris pH 7.4 including phosphatase inhibitor and complete protease inhibitor cocktails (Roche, Indianapolis, USA) using a PolyTron homogenizer. Samples were incubated on ice for 15 min, then centrifuged at 1000 x g , 4 °C, for 5 min. The supernatants containing the soluble/sarcoplasmic proteins were decanted and stored on ice, and the myofibrillar pellet was resuspended in 0.5 ml of homogenization buffer and then centrifuged at 1000 x g , 4 °C, for 5 min. The washed myofibrillar pellet was solubilized in 10 volumes of 7 M urea, 2 M thiourea, 4 % CHAPS, 30 mM Tris, pH 8.5 and cleared by centrifugation at 12 000 x g , 4 °C, 45 mins. Protein concentrations of each myofibrillar and soluble protein sample were measured using the Bradford assay (Sigma-Aldrich, Poole, Dorset, United Kingdom). The reference protein used was Bovine serum albumin (BSA) plotted on a standard curve over a range of increments in concentration: 0.000 mg/ml (Blank), 0.125 mg/ml, 0.250 mg/ml, 0.500 mg/ml, 0.750 mg/ml and 1.000 mg/ml. Standards were pipetted in triplicate into a microtitre plate. Myofibrillar samples were diluted (distilled water) 1:10 and proteins of the soluble fraction diluted 1: 20 to bring them in range of the standard curve. 5 μ l of each sample was pipetted in duplicate and 250 μ l of Bradford reagent was added to each well. The sample absorbance was captured at a wavelength of 595 nm and protein concentrations were calculated using linear regression from the changes in absorbance.

2.5 Analysis of myofibrillar proteins

2.5.1 Top-down proteomic analysis

Homogenates of the myofibrillar fraction were prepared for 2-dimensional gel electrophoresis (2DGE) as described previously in Burniston, (2008). Gels were produced in batches of 8 comprising of an individual gel for each experimental and contralateral control muscle over the time series of 4 points (0 d, 10 d, 20 d and 30 d) so there is no technical bias. For each batch of gels, identical stock solutions were used, gels were loaded equivalently and were electrophoresed under the same conditions. An aliquot of each supernatant was precipitated in 5 volumes of acetone at -20 °C for 1 hour and then resuspended in 7 M urea, 2 M Thiourea, 2 % (w/v) CHAPS, 20 mM dithiothreitol, 0.5 % (v/v) and ampholytes (pH 3-11). Samples, containing 250 µg protein, were loaded on to 13 cm pH 3–11 nonlinear IPG strips (GE Healthcare, Chalfont St Giles, UK) and resolved using an “active rehydration” and isoelectric focusing protocol comprising: 150 Vh at 30 V, 300 Vh at 60 V, 500 Vh at 500 V, 1000 Vh at 1000 V and 48 000 Vh at 8000 V; conducted on an IPGPhor II (GE Healthcare) at 20 °C, maximum 50 mA per strip. IPG strips were equilibrated in 50 mM Tris-HCl pH 8.8, containing 6 M urea, 30 % (v/v) glycerol, 70 mM sodium dodecyl sulfate (SDS) and a trace of bromophenol blue. Dithiothreitol (DTT) (65 mM) was present as a reducing agent in the first equilibration and iodoacetamide (135 mM) in the second. Proteins were then electrophoresed from the IPG strip through 16 cm linear 12 % polyacrylamide gels at 20 °C; at a constant current of 15 mA per gel for 30 min, then 30 mA per gel until the tracking dye reached the bottom edge of the gel. Gels were washed and stained with colloidal Coomassie blue (Bio-Safe; BioRad, Hercules, CA, USA) according to the manufacturer’s instructions. Gels were subsequently scanned on to a computer and digitised images (8-bit greyscale, 300 dpi) of the stained gels were saved as tagged-image file format (.TIFF) files.

2.5.2 Abundance analysis

Image analysis (Samespots, v3.0, Nonlinear Dynamics, Newcastle, UK) was performed on all individual 2DGE images, representing the myofibrillar protein fraction from the experimental and contralateral control muscles of every animal included in the experiment over a time series of 4 points e.g. 0 d, 10 d, 20 d and 30 d. Prominent

spots were manually identified to avoid including gel artefacts in the data and the gel images were warped to align the spot positions to a common reference gel. The resulting spot outlines were applied to each parent image and manually verified consistent with our previous work (Burniston, 2008). Statistical analysis was performed on log-transformed spot volume data that were normalised relative to total spot density for each individual gel.

2.5.3 Matrix-assisted laser desorption ionisation tandem time of flight mass spectrometry

Protein spots were cut from each 2D-gel and processed using an Xcise robot (Proteome Systems, North Ryde, Australia) as described previously (Burniston et al, 2007.; Burniston, 2008.; Hesketh et al, 2016). Gel plugs were destained in three changes of 25 mM ammonium bicarbonate in 50 % acetonitrile and were dehydrated before being incubated with 35 μ L of 1.25 mg/mL porcine trypsin (Promega, Madison, WI, USA) in 50 mM ammonium bicarbonate.

Peptide solutions were de-salted and concentrated (Zip-tips; Millipore, Billerica, MA, USA) before being mixed with matrix (3.5 μ g α -cyano-4-hydroxycinnamic acid in 50: 50 acetonitrile and 0.1% trifluoroacetic acid) and spotted on to 384-well stainless steel target plates. A calibration mix (Laserbio Labs, Sophia Antipolis, France) consisting of angiotensin II (m/z 1046.2), angiotensin I (m/z 1296.5), neurotensin (m/z 1672.9), ACTH fragment {1–17} (m/z 2093.5) and ACTH fragment {18–39} (m/z 2465.19) was mixed 1: 1 with matrix solution and spotted (0.5 μ L) between every four sample-wells. Peptide mass spectra were recorded using a matrix-assisted laser desorption ionisation tandem time of flight mass spectrometer (MALDI-TOF/MS), (Axima TOF2; Shimadzu Biotech, Manchester, UK) in positive reflectron mode over a mass/charge (m/z) range of 900–3000. Data was smoothed (Gaussian, 2 chan peak width), baseline subtracted (100 chan peak width) and an adaptive (8.0[^]) threshold applied. Peptide mass lists (restricted to 20 peptides over 900–3000 m/z) were produced using the peak selection tool of the instrument's Launchpad software (Version 2.8.4) and searched against the Uniprot database restricted to "Rattus" using the online MASCOT (www.matrixscience.com) server v.2.2.03. The enzyme specificity was set as trypsin allowing one missed cleavage, carbamidomethyl modification of cysteine (fixed), oxidation of methionine (variable) and an m/z error of \pm 0.3 Da. Protein

identifications were accepted subject to performing quality controls on the data. Firstly, the signal: noise ratio was <30 and secondly, each protein had a MOWSE score of above 54, signalling the significant identity threshold, our exclusion criteria was set at >60 .

Mass spectrometry data were recorded from every gel spot from the 2DGE in every experimental and contralateral control muscle for every animal included in the experiment over the time series of 4 points (i.e. 0 d, 10 d, 20 d and 30 d). Raw mass spectra were exported in mzXML format and mMAss software (Version 5.5.0, <http://www.mmass.org>) was used to extract intensity data for the monoisotopic peak (m_0), m_1 and m_2 mass isotopomers of 5 selected peptides for each protein/ proteoform, as previously described (Hesketh et al, 2016).

2.6 Analysis of soluble proteins

2.6.1 Bottom-up proteomic analysis

Soluble proteins in lysis buffer at a concentration of 5 µg/µl of protein were processed for mass spectrometry analysis by in-solution digestion according to the filter aided sample preparation (FASP) method described by Wisniewski et al, (2009). An aliquot (200 µg) of each sample was precipitated in 5 volumes of acetone at -20 °C overnight and then resuspended in UA buffer (8 M urea in 0.1 M Tris-HCl, pH 8.5). Proteins were diluted with 200 µl of UA buffer in a 30 kDa MW filter cup (Micron-30/ Ultracel PL-30), the filter cup was placed in a waste collection tube and was centrifuged at 10, 000 x g, at room temperature for 30 mins. Subsequently, 100 mM of dithiothreitol in UA buffer was added to each sample filter cup, agitated for 5 mins and incubated at 37 °C for 15 mins before being centrifuged at 10, 000 x g, at room temperature for 30 mins. 50 mM of iodoacetamide in UA buffer was then added to each sample filter cup, agitated for 2 mins and incubated at 4 °C for 20 mins before being centrifuged at 10, 000 x g, at room temperature for 30 mins. The samples were then washed twice by adding 100 µl of UA buffer to each sample filter cup which was centrifuged at 10, 000 x g, at room temperature for 30 mins after each wash. One-hundred microlitres of 50 mM ammonium bicarbonate was then added to each sample filter cup which were agitated for 2 mins and centrifuged at 10, 000 x g, at room temperature for 30 mins. Waste collection tubes were then discarded and clean labelled tubes used for collection of the samples after proteolytic digestion by porcine trypsin (Promega, Madison, WI, USA). Trypsin was prepared in 50 mM ammonium bicarbonate for a 1: 50 enzyme: protein ratio. The trypsin solution was then added to each sample filter cup and agitated for 5 mins before overnight incubation at 37 °C in a humidified chamber. Following the overnight digestion, the samples were centrifuged at 10, 000 x g, at room temperature for 30 mins. After which, 40 µl of 50 mM ammonium bicarbonate was then added to each sample filter cup before centrifugation at 10, 000 x g, at room temperature for 30 mins. The trypsin reaction was then stopped by adding 20 µl of 1 % trifluoroacetic acid (TFA) to each sample collection tube.

2.6.2 Abundance analysis

After FASP digest, 4 µl of peptides (equivalent to x 4 ug) from each sample was mixed with 11 µl of 0.1 % trifluoroacetic acid. After which, each peptide solution was de-

salted and concentrated using Zip-tips (Millipore, Billerica, MA, USA) according to the manufacturer's instructions. The eluents were then subject to drying using a SpeedVac (Thermo Scientific Savant, United Kingdom) for 20 mins at 60 °C with the lids open. Yeast protein ADH-1 was then spiked into all samples at a concentration of 10 fmol per μl before each sample was transferred into autosampler vials for LC-MS/MS analysis.

2.6.3 Liquid chromatography-mass spectrometry

Label-free liquid chromatography-mass spectrometry analysis was performed using nanoscale reverse-phase ultra-performance liquid chromatography (UPLC; Nano Acquity; Waters) and online electrospray ionization quadrupole–time-of-flight mass spectrometry (ESI-Q-TOF; QTOF Premier; Waters). Samples (400 ng tryptic peptides) were loaded in aqueous 0.1 % (*v/v*) formic acid via a Symmetry C₁₈ 5 μm , 2 cm X 180 μm trap column (Waters). Separation was conducted at 35 °C via a BEH C₁₈ 1.7 μm , 25 cm X 75 μm analytical reverse-phase column (Waters). Peptides were eluted using a gradient that rises to 37 % acetonitrile 0.1 % (*v/v*) formic acid over 90 min at a flow rate of 300 nl/min. For all measurements, the mass spectrometer was operated in positive electrospray ionization mode at a resolution of >10, 000 full width at half maximum (FWHM). Before analysis, the time-of-flight analyser was calibrated using fragment ions of [Glu-1]-fibrinopeptide B from *m/z* 50 to 1990. Mass spectra (MS) for liquid chromatography-mass spectrometry profiling was recorded between 350 and 1600 *m/z* using mass spectrometry survey scans of 0.9 s durations with an inter scan delay of 0.1 s. In addition, equivalent data-dependent tandem mass spectrometry (MS/MS) spectra was collected from each 0 d (control) sample. MS/MS spectra of collision-induced dissociation fragment ions were recorded for the 5 most abundant precursor ions of charge 2+ or 3+ detected in the survey scan. Precursor fragmentation was achieved by collision-induced dissociation at an elevated (20–40 eV) collision energy over a duration of 0.15 s per parent ion with an inter scan delay of 0.05 s over 50–2000 *m/z*. Acquisition was switched from MS to MS/MS mode when the base peak intensity exceeds a threshold of 30 counts per second, and returned to the MS mode when the total ion chromatogram (TIC) in the MS/MS channel exceeds 7, 500 counts per second or when 1.0 s (5 scans) were acquired. To avoid repeated selection of peptides for MS/MS, the program used a 30 s dynamic exclusion window.

For data processing Progenesis Quantitative Informatics for proteomics (Water Corp, United Kingdom) was used to perform label-free quantitation that was consistent with our previous work (Malik et al, 2013.; Burniston et al, 2014.; Camera et al, 2017.; Sollandek et al, 2017). Prominent ion features (>600 per chromatogram) were used as vectors to align each data set to a common reference chromatogram. An analysis window of 15–105 min and 350–1500 m/z was selected, which encompasses features with charge states of +2 or +3. Log-transformed MS data were normalised by an inter-sample abundance ratio, and differences in relative protein abundance were investigated using nonconflicting peptides only.

MS/MS spectra were exported in Mascot generic format and searched against the Swiss-Prot database (2016.7) restricted to Rattus (8,071 sequences) by using a locally implemented Mascot server (v.2.2.03; www.matrixscience.com). Enzyme specificity was trypsin, which allows for 1 missed cleavage, carbamidomethyl modification of cysteine (fixed), deamination of asparagine and glutamine (variable), oxidation of methionine (variable) and an m/z error of ± 0.3 Da. Mascot output (xml format), was restricted to nonhomologous protein identifications, was recombined with MS profile data, and peptides modified by deamination or oxidation were removed before quantitative analysis.

2.7 Turnover calculations

2.7.1 Individual Protein Synthesis rates

After MALDI-TOF/MS analysis, raw mass spectra for the myofibrillar proteins is exported in mzXML format and mMAss software (Version 5.5.0, <http://www.mmass.org>) is used to extract intensity data for the isotopomer envelope, including the monoisotopic peak (m_0), m_1 and m_2 mass isotopomers for each peptide from each protein/ proteoform, as previously described (Hesketh et al, 2016). For each myofibrillar protein a minimum of 5 selected peptides are used to calculate the molar fraction of m_0 as shown in Figure 2.6.

After LC-MS analysis, mass isotopomer abundance data for the soluble proteins are extracted from MS only spectra using Progenesis Quantitative Informatics (Nonlinear Dynamics). Peak picking is performed on ion features with +2, or +3 charge states within an analysis window of 15–105 min and 350–1500 m/z . The abundance of the monoisotopic peak (m_0), m_1 and m_2 mass isotopomers are collected over the entire chromatographic peak for each non-conflicting peptide that is used for label-free quantitation in the aforementioned Progenesis Quantitative Informatics for proteomics analysis, as previously described (Camera et al, 2017). For each soluble protein, a minimum of one unique peptide is used to calculate the molar fraction of m_0 as shown in Figure 2.6.

Fractional synthesis rate (FSR) is then derived for all identified myofibrillar and soluble proteins. Synthesis rates are calculated in both control (right, non-stimulated) and stimulated (left) muscles in two primary ways. Fitting mass isotopomer data collected at each of the 4 experimental time-points using a semi-log plot and fitting the same data to a 2-point (0 d and 30 d) non-linear first-order equation. These calculations provide the rate constant (k) for the decay of the molar fraction of the m_0 mass isotopomer across the specified time points. The rate constant (k) is then divided by the number (n) of exchangeable hydrogen sites reported in standard tables (Commerford et al, 1983) and finally by the level of precursor enrichment (p) measured by GC-MS analysis of plasma samples. Protein FSR is then reported as the mean of the peptide values assigned to each protein or proteoform.

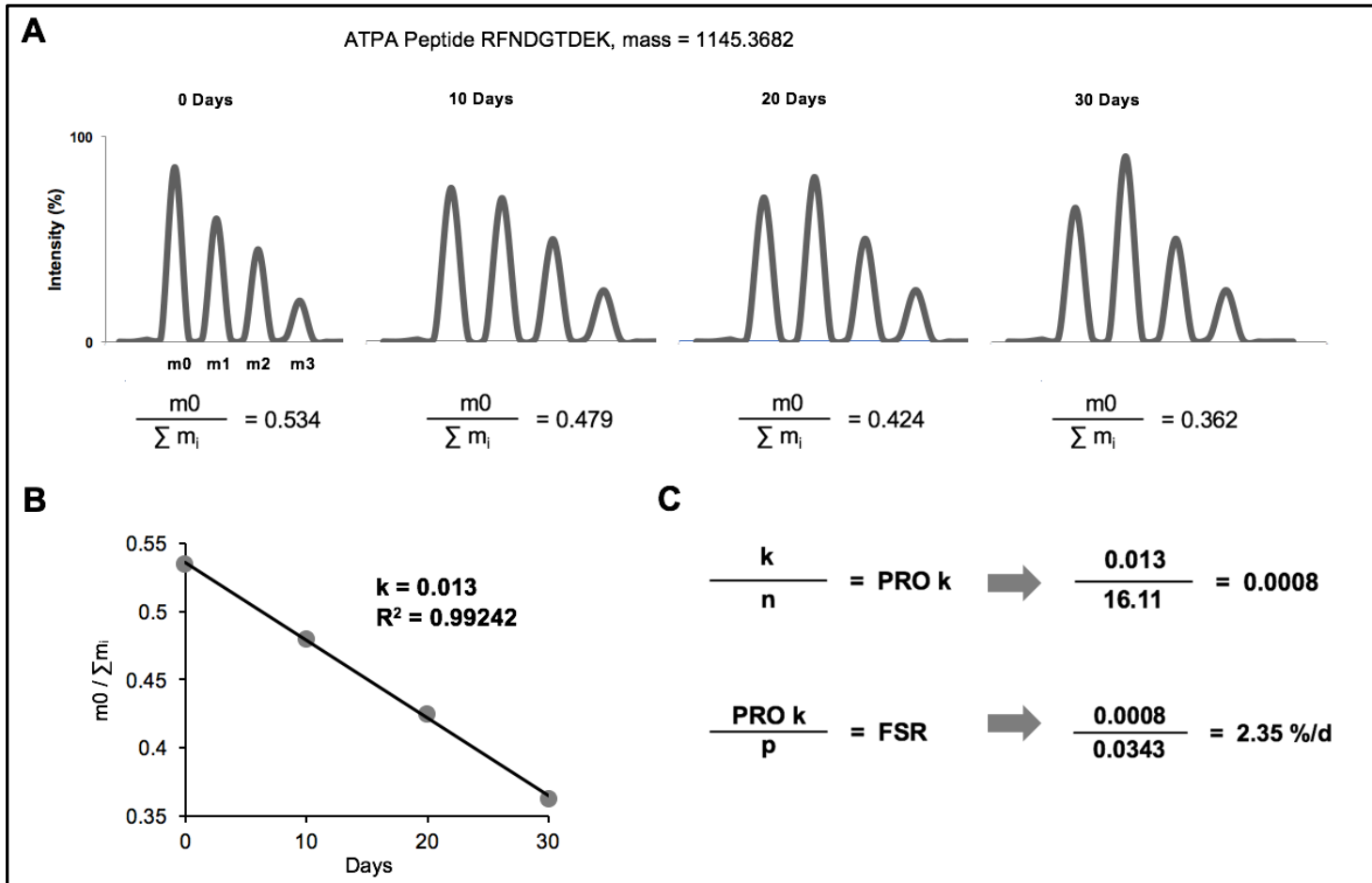


Figure 2.6. Fractional synthesis calculations from mass spectra analysis.

(A) Example mass spectra of peptide RFNDGTDEK (1145.3682 m/z) from ATP synthase alpha (ATPA). Relative abundances of m^0 (monoisotopic), m_1 , m_2 and m_3 mass isotopomers at days 0, 10, 20, and 30 are presented. Incorporation of deuterium into newly synthesized protein is evident in the proportional increase in the heavy isotopomers (m_1 , m_2 , and m_3) and relative decrease in the fractional abundance of the monoisotopic peak (i.e., $m_0 / \sum m_i$). (B) Rate constant (k) of synthesis is calculated by fitting mass

isotopomer data ($m_0 / \sum m_i$) to a nonlinear model of steady state precursor enrichment and incorporation of deuterium into the product peptide, taking into account the amino acid composition of the peptide. (C) The rate constant (k) is then divided by the number (n) of exchangeable hydrogen - deuterium sites which is then finally divided by the level of precursor enrichment (p) measured by GC-MS analysis of the plasma samples to give the fractional synthesis rate for the example peptide in percent per day.

To calculate the synthesis rate constant (k) using our 2-point calculation used for time point intermediaries, we implement the following non-linear first-order equation:

$$k = \frac{1}{t - t_0} \cdot -\ln \left(\frac{Fm_{0t}}{Fm_{0t_0}} \right)$$

Where Fm_{0t} is the molar fraction of m_0 at time t , and Fm_{0t_0} is the molar fraction of m_0 at time t_0 . By using protein abundance data at times t and t_0

2.7.2 Individual Protein Degradation rates

The rate of change in the abundance of a protein is dependent on the difference between its rate of synthesis (R_s) and the rate of degradation (R_d). Our model assumes first-order kinetics that followed the standard formula:

$$A = A_0 e^{(R_s - R_d)(t - t_0)}$$

Where A is the abundance at time t , and A_0 is the abundance at time t_0 . By using protein abundance data at times t and t_0 , the net rate of change in abundance can be calculated by rearranging the above to give:

$$s - d = \frac{1}{t - t_0} \cdot -\ln \frac{A}{A_0}$$

Converting differences in abundance between day zero and day 30 to rates of change in abundance enables the rate of degradation of each protein to be calculated as the difference between its rate of synthesis and its rate of change in abundance.

2.7.3 Absolute Protein turnover rates

Absolute protein turnover is calculated for individual proteins in both the control (right, non-stimulated) and stimulated (left) muscles of both the myofibrillar and soluble fractions. To calculate values that reflect the state of the whole muscle i.e. protein turnover; firstly, the protein content of the muscle must be calculated (Equation 1).

Equation 1:

$$\left(\frac{HV \cdot PC}{MA} \right) \cdot \text{muscle wet weight} = \text{Protein content (mg)}$$

Where MA is the muscle aliquot (mg) of the mass from the muscle powder that was taken and weighed after the whole muscle is pulverised under liquid nitrogen. HV is the homogenisation volume (ml) that is measured after the homogenisation process. PC is the protein concentration value (mg/ml) derived from the protein assay. This gives the protein extraction in mg of protein per mg of muscle mass. This value is then multiplied up by the mass of the whole muscle (mg) to give the protein content for the entire muscle.

Once the absolute protein content is determined, absolute protein abundance can then be calculated for each individual protein. This is achieved in two similar ways for the soluble (Equation 2) and myofibrillar (Equation 3) fraction. It is necessary to calculate absolute abundance in this way for the two fractions because relative abundance changes are quantified in different ways between the two fractions. The soluble fraction proteins contain a protein 'spike' utilised by the LC-MS to give a measure of protein abundance in units i.e. fmol/ μ g of protein. However, relative abundance changes in the myofibrillar fraction proteins are quantified by densitometry and require manual conversion to mg units.

Absolute abundance (ABD) of proteins in the soluble fraction was calculated by Equation 2.

Equation 2:

$$i \quad \frac{\text{Protein content} \cdot AA_{\text{QIP}} \left(\frac{\text{fmol}}{\mu\text{g}} \right)}{1000} = \text{ABD (pmol)}$$

$$ii \quad \frac{1}{d} \cdot \ln \left[\frac{\text{ABD}_{30}}{\text{ABD}_0} \right] = \text{ABD (k)}$$

(i) Total protein content (ug) is multiplied by the absolute abundance value (AA_{QIP}) generated from the Progenesis Quantitative Informatics software normalised to the ADH-1 protein spike (fmol). This value is divided by one thousand to convert into more manageable units (pmol). (ii) The experimental period in days (d) is converted to a decimal by dividing by one and is then multiplied by the natural log of the absolute abundance of the muscle at 30 days (ABD_{30}) is divided by the absolute abundance of the muscle at zero days (ABD_0). This gives the rate constant (k) of absolute abundance change from day-0 to day-30.

Absolute abundance (ABD) for the myofibrillar fraction is calculated by Equation 3.

Equation 3:

$$\left(\left(\ln \left(\frac{\text{MM}_0}{\text{SD}_0} \right) \cdot \left(\frac{\text{MM}_{30}}{\text{SD}_{30}} \right) \right) \cdot \frac{1}{d} \right) \cdot 100 = \text{ABD (\%/d)}$$

Fold change is calculated between muscle mass (MM_0) and spot density (SD_0) at day 0 and multiplied by the fold change at day-30. For each value, one is divided by the experimental period in days (d) to convert it in to a decimal and multiplied by the natural log (ln) of the product between the fold changes of 0 days and 30 days. This is then multiplied by 100 to convert the final value into percent per day (%/d).

Before absolute synthesis rate can be calculated the units of both the soluble fraction proteins (fmol/d) and myofibrillar proteins (mg/d) must be normalised (Equation 4) to achieve comparable data.

Equation 4:

$$MW \cdot C \cdot V = \text{pg}$$

The molecular weight (MW) of each protein is multiplied by C, the protein concentration (pmol) and finally by the sample volume (pl) to give the final units as pictograms.

Absolute synthesis rate (ASR) for individual proteins are calculated by using the absolute abundance of the protein which gives two similar equations for both the myofibrillar and soluble fraction proteins (Equation 5).

Equation 5:

$$\left[\frac{\text{FSR}}{100} \right] \cdot \text{ABD}_{30} = \text{ASR (pg/d)}$$

The fractional synthesis rate (FSR in %/d) for each individual protein is divided by 100 and multiplied by ABD, derived from Equation 2 for the soluble fraction proteins, and from Equation 3 for the myofibrillar proteins to give ASR in pg/d.

Absolute degradation rate (ADR) is calculated for both soluble and myofibrillar fractions using Equation 6.

Equation 6:

$$\text{ASR} - \text{ABD} = \text{ADR (pg/d)}$$

2.7.4 Statistical Analysis

Statistical analysis of myofibrillar protein abundances are conducted on normalised spot abundances from 2D-gel spots. Normalised protein abundance from LC-MS label-free quantitation are used for soluble protein abundance. Relative synthesis rates are analysed as percent per day (%/d) and absolute synthesis rates are analysed as picograms per day (pg/d) in the soluble fraction proteins and as pg/d in the myofibrillar fraction proteins, all values are averages of the analysed peptides for each protein and subsequent analysis is at the protein level. All statistical testing is conducted using SPSS (SPSS, v23, Chicago, USA) and the statistical significance level is set at $P < 0.05$. To assess the degree of consistency across control situations (right limb, non-stimulated muscle) for all time points (10 d, 20 d and 30 d) and sham operated animals (0 d) a one-way ANOVA is used to analyse protein abundance, synthesis and degradation data.

2.8 Results

The first method used to calculate is described by Figure 2.7 illustrates the semi-log plot method for calculating protein FSR. For each protein, a minimum of 5 selected peptides was used to calculate the molar fraction of m_0 . Synthesis rates are then calculated for each individual peptide by fitting mass isotopomer data collected at each of the 4 experimental time-points (0 d, 10 d, 20 d and 30 d) using a semi-log plot (Figure 2.7). The rate constant (k) of the change in the molar fraction of m_0 , across the experimental time points can then be used to derive the FSR of the selected peptides and subsequently the whole protein. The rate of change in the mass isotopomer distribution is also dependant on the number of hydrogen to deuterium exchangeable sites (n) each peptide contains and the body water enrichment of $^2\text{H}_2\text{O}$ in the animal (Figure 2.6). The change in mass isotopomer distribution is a result of the incorporation of ^2H labelled amino acids in to newly synthesised peptides. This leads to the changes in mass isotopomer distribution following an exponential plateau, which can then be used to determine the rate of change of the monoisotopic peak over the 30-day experiment (Figure 2.7).

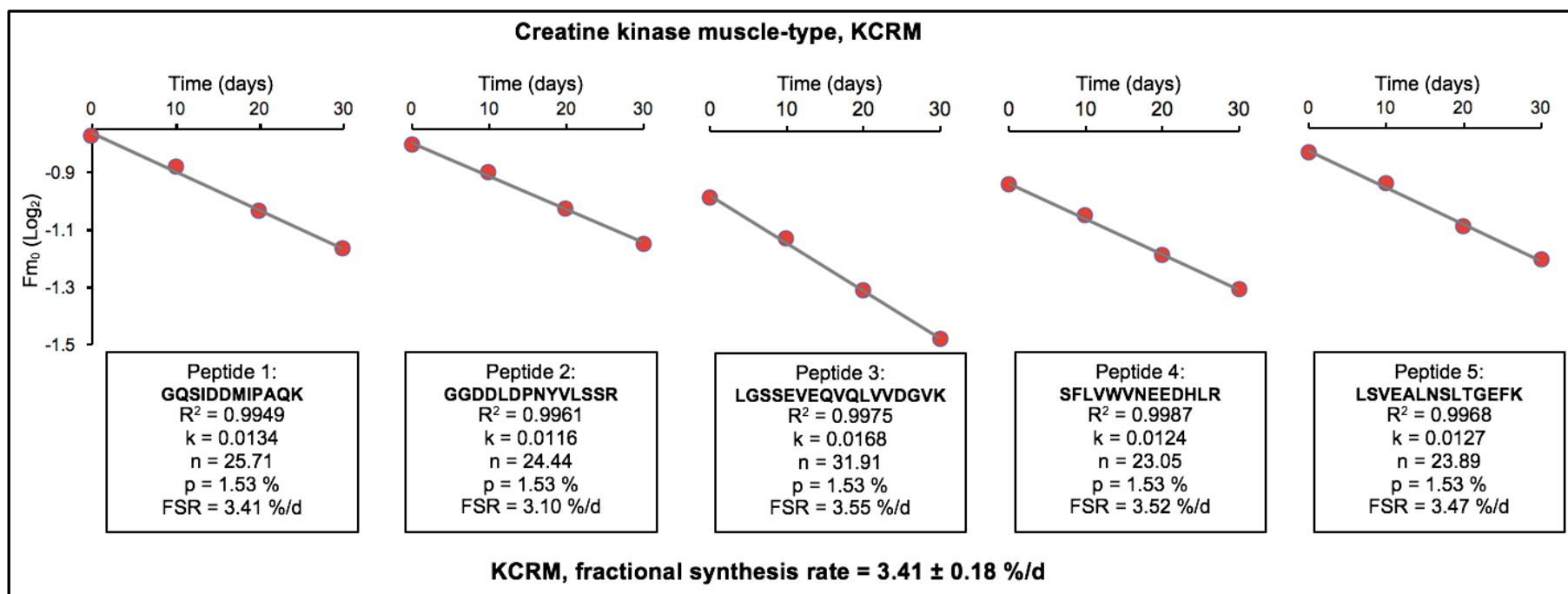


Figure 2.7. Peptide semi-log plot calculations to determine FSR for muscle creatine kinase (KCRM).

Each figure represents a semi-log plot for an individual peptide. The data is presented as the log-transformed fraction of the monoisotopic peak (Fm_0) over 0 d, 10 d, 20 d and 30 d for each peptide. This represents the relative decrease in the fractional abundance of the monoisotopic peak, due to the incorporation of deuterium into newly synthesized protein resulting in a proportional increase in the heavy isotopomers. The rate constant (k) of synthesis is calculated by linear regression of the mass isotopomer data (Fm_0), taking into account the amino acid composition of the peptide (sequence in bold for each peptide) and precursor enrichment (p) to give the fractional synthesis rate (FSR) for each peptide. From which the mean \pm SD can be calculated to inform the final FSR in percent per day (%/d) for Creatine kinase (KCRM).

Mixed muscle FSR in the SOL (3.77 ± 0.41 %/d) is greater ($P = 0.019$) than mixed muscle FSR in the PLN (2.55 ± 0.25 %/d), Figure 2.8. A difference between the two muscles is further extended at the level of the individual protein. Table 1 shows there is a clear difference in FSR rank order between the two muscles. However, for both the SOL and PLN the protein with the fastest FSR was ALBU (7.25 ± 0.79 , 7.60 ± 0.68 %/d respectively). Yet, beyond ALBU the SOL displays its greatest FSR rates in mitochondrial and calcium handling proteins such as ATPA (5.71 ± 0.35 %/d) and AT2A2 (5.03 ± 0.76 %/d). Whereas the PLN has greater FSR values for proteins more associated with glycolysis; for example, PYGM (4.14 ± 0.14 %/d) and ALDOA (3.63 ± 0.18 %/d). In SOL, the protein with the slowest FSR was ENOB (1.13 ± 0.14 %/d) and in the PLN muscle, CASQ1 had the slowest FSR (0.81 ± 0.09 %/d).

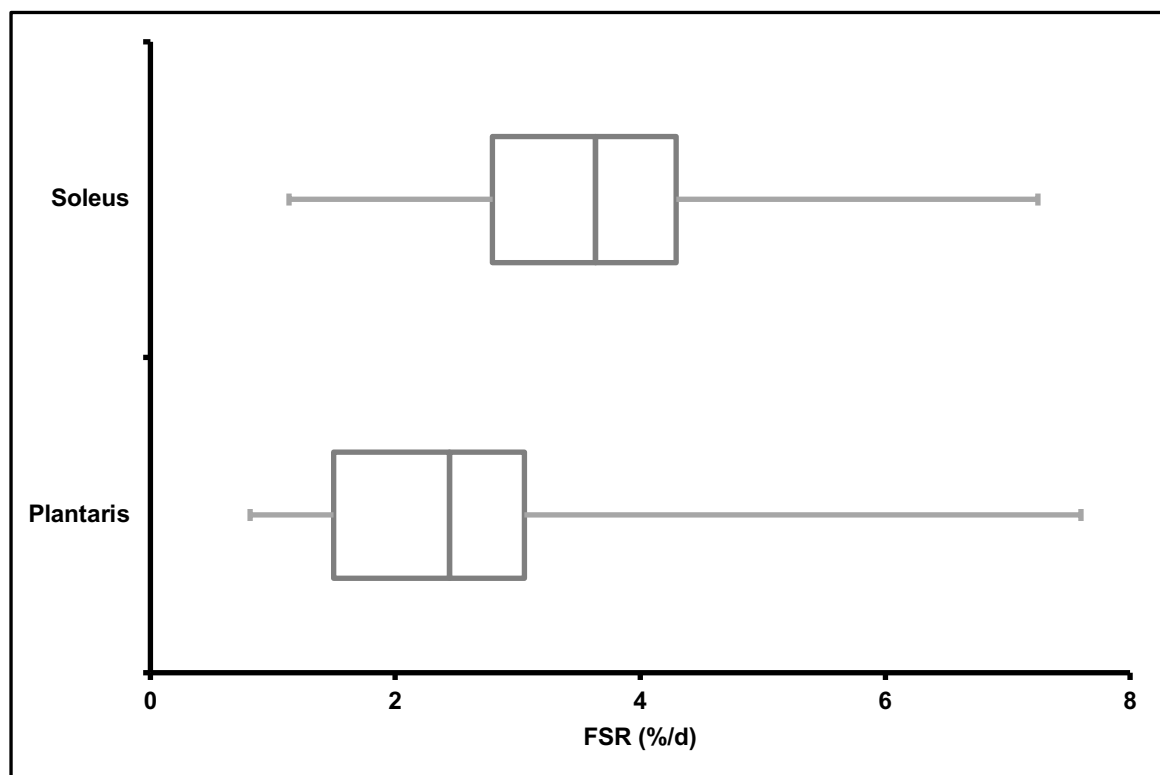


Figure 2.8. Fractional synthesis rate of mixed muscle proteins in Soleus and Plantaris muscle over 30 days.

All data is reported and calculated by fitting mass isotopomer data using a semi-log plot for individual proteins. Data is presented in box and whisker plots with fractional synthesis (FSR) data in percent per day (%/d), of the 24 detected proteins in soleus muscle and the 28 detected proteins in plantaris muscle (Proteins detailed in Table 1).

FSR was greater in soleus than in plantaris detected by independent t-test, P-value was set at <0.05.

Table 2.1. The rank order of individual protein FSR in Soleus and Plantaris muscle after 30 days.

Soleus			Plantaris		
Protein I.D.	FSR (%/d)	CV (%)	Protein I.D.	FSR (%/d)	CV (%)
ALBU	7.25 ± 0.79	10.95	ALBU	7.60 ± 0.68	8.92
CAH3	6.57 ± 0.80	12.14	PYGB	4.46 ± 0.23	5.16
HSPB1	5.73 ± 0.57	9.90	PYGM	4.14 ± 0.14	3.42
ATPA	5.71 ± 0.35	6.11	KPYM	3.72 ± 0.28	7.45
AT2A2	5.03 ± 0.76	15.06	ALDOA	3.63 ± 0.18	5.06
KCRS	4.34 ± 0.21	4.81	KAD1	3.62 ± 0.63	17.50
MGHM	4.28 ± 0.62	14.60	PGAM2	3.06 ± 0.51	16.79
HSPB6	4.10 ± 0.33	8.09	KCRM	3.05 ± 0.06	1.92
LDHB	4.08 ± 0.27	6.66	TPIS	3.04 ± 0.26	8.42
FHL1	3.76 ± 0.39	10.31	G3P	2.66 ± 0.13	4.80
MYL3	3.72 ± 0.37	9.87	TNNT3	2.65 ± 0.26	9.76
G3P	3.69 ± 0.73	19.77	MDHM	2.60 ± 0.11	4.08
PEBP1	3.58 ± 0.42	11.67	CAH3	2.51 ± 0.30	12.03
MDHC	3.48 ± 0.50	14.51	ENOB	2.49 ± 0.09	3.59
KCRM	3.41 ± 0.18	5.28	ATPB	2.40 ± 0.23	9.48
ALDOA	3.39 ± 0.58	16.99	MYH4	2.25 ± 0.20	9.10
TPIS	2.98 ± 0.03	0.84	ATPA	2.18 ± 0.29	13.39
MLRV	2.84 ± 0.31	10.78	MYL3	2.00 ± 0.33	16.74
FABPH	2.65 ± 0.35	13.15	MYG	1.94 ± 0.18	9.40
HBA	2.44 ± 0.33	13.33	PRVA	1.70 ± 0.22	13.24
HBB1	2.17 ± 0.05	2.22	TPM2	1.50 ± 0.11	7.44
PGK1	2.11 ± 0.32	15.39	MYH8	1.49 ± 0.20	13.21
MYG	2.09 ± 0.36	17.16	ADT1	1.44 ± 0.25	17.53
ENOB	1.13 ± 0.14	12.57	MYL1	1.27 ± 0.15	12.04
-	-	-	H2B1	1.15 ± 0.11	9.84
-	-	-	HBB1	1.09 ± 0.19	17.08
-	-	-	AT2A1	1.07 ± 0.18	16.94
-	-	-	CASQ1	0.81 ± 0.09	11.08

Protein I.D. relates to the Uni-Prot database, entries returned using the MASCOT search engine. FSR is the fraction synthesis rate representative of the selected peptides for each protein, reported as mean ± SD in percent per day (%/d). CV represents the coefficient of variation expressed as a percentage.

Alternative methods for calculating k is through applying a two-point calculation between time points to give a rate of decline in the monoisotopic peak without the influence from the excluded time points. In addition, a series of two-point calculations were used 0 d – 10 d, 10 d – 20 d and 20 d – 30 d for KCRM across both SOL and PLN muscles (Figure 2.9).

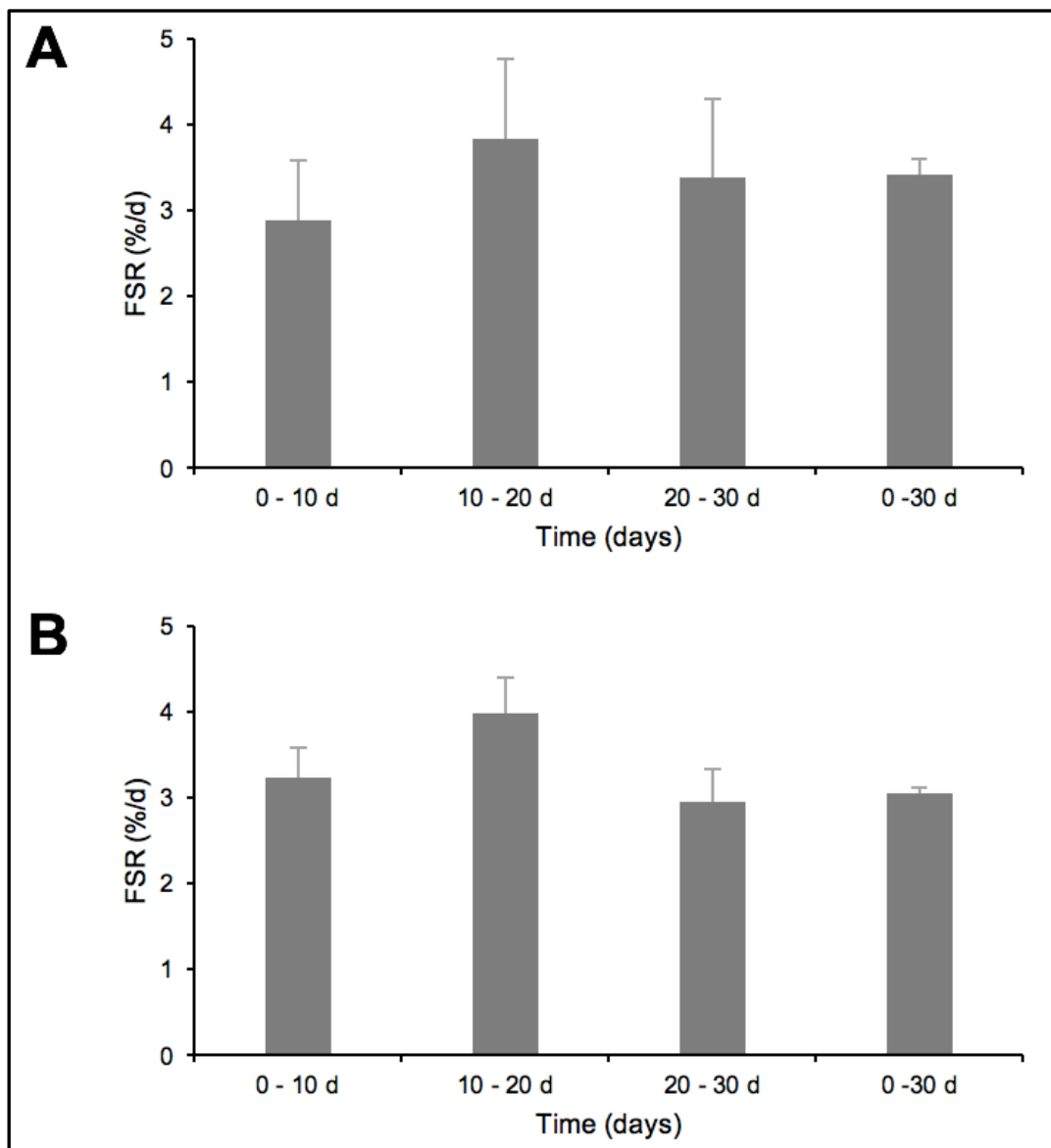


Figure 2.9. Fractional synthesis rate of KCRM at each experimental time-series duration for Soleus and Plantaris muscle.

All data is presented is fractional synthesis rate expressed as present per day (%/d) as mean \pm SD. FSR values are calculated by the two-point calculation over each incremental time-series 0-10 days, 10-20 days and 20-30 days with the addition of

FSR calculated via semi-log plot method (0-30 days) for comparison for (A) Soleus muscle and (B) Plantaris muscle.

Statistical analysis was performed in SPSS (SPSS, v23, Chicago, USA) and the statistical significance level was set at $P < 0.05$. One-way ANOVA was conducted on KCRM FSR to assess for differences between each time point within each muscle. Tukey's HSD post-hoc testing was conducted ($P = 0.361$) as were independent t-tests to assess the differences within time points between muscles. There were no differences between the semi-log plot calculation (0-30 d) and any of the other time points for both SOL and PLN. In addition, there were no significant differences between any of the time points in SOL ($P = 0.231 \pm 0.071$), or between the time points for PLN ($P = 0.159 \pm 0.066$).

2.9 Discussion

The aim of this chapter was to develop a protocol that will enable us to investigate skeletal muscle adaptation at the level of synthesis, abundance and degradation of individual proteins. To evaluate whole muscle changes over a period of time (i.e. 30 days) that will provide insight to changes that occur in the context of whole muscle adaptation; we present an experimental design that utilises an animal model over a time series analysis (Figure 2.4). This allows us to create an experiment with a robust statistical analysis by filtering out proteins that do not fit to the expected exponential plateau across the four sampling points. Not only does our methodology equip us with the investigatory tools to quantify changes in individual protein turnover of enough myofibrillar and soluble proteins ($n = \sim 30$ myofibrillar and ~ 40 soluble proteins after stringent filtering) to begin to inform the mechanism of how muscle adaptation is coordinated. It also provides access to a deeper understanding of how muscle transformation is orchestrated, allowing us to gather unprecedented information on proteoform-specific turnover. This is highly unique as almost all previous biosynthetic labelling experiments have been designed so that protein abundance does not change during the investigatory period and have therefore assumed that synthesis rates are equivalent to degradation rates (Wagenmakers, 1999).

We can subsequently present exemplar data that document expected differences (Kelly, 1984; Lewis et al, 1984) between the synthesis rate of fast and slow muscle, with a different rank order of synthesis between tissues, consistent with our previous work (Hesketh et al, 2016). This gives us great confidence to report our semi-log plot calculation method (Figure 2.7) performs comparably with existing literature. Independent groups of rats were subject to deuterium labelling during a time series of 30 days. We analysed deuterated peptides to compute FSR data in both the soleus (SOL) and plantaris (PLN) muscles (Figure 2.8). The soleus muscle is a slow-twitch muscle in the rat, containing $\sim 95\%$ type 1 fibres which express MyHC type 1 isoforms (Soukup et al, 2002). Whereas, plantaris represents a faster twitching muscle with $\sim 12\%$ type 1 fibres, $\sim 28\%$ type 2a and $\sim 60\%$ type 2b (Burniston et al, 2007). Figure 2.8 reveals a greater ($P = 0.019$) mixed muscle protein FSR in the SOL and PLN. This equates to an average half-life in SOL of 18.7 days and PLN of 27.7 days. Consistent with previous data (Lewis et al, 1984) that demonstrate slow-twitch muscle (SOL, half-life of 12.1 days) in developing rats to have a greater turnover rate than fast-twitch

muscle (TA, half-life of 18.3 days). Furthermore, this is supported by further tissue-specific investigation that reports protein turnover is generally more rapid in slow than fast-twitch muscle. The average half-life of proteins is reported to be ~14 days in mixed fibre locomotive muscles and ~7 d in slow-twitch postural muscles (Kelly, 1984). However, these values represent averages across the entire proteome and so are a gross simplification of events at an individual protein level. For example, contrary to the average turnover rate, turnover of the mitochondrial protein, cytochrome c, is more rapid in fast than slow-twitch muscle (Terjung 1979). During such investigations, these differences in individual protein turnover rate suggests protein degradation is selective and thus, should also be considered for these types of experiments. For example, the turnover of rabbit myosin heavy chain is ~29 days and actin is ~75 days (Koizumi, 1974). Even amongst the troponin complex, which consists of 3 subunits: troponin T, troponin I and troponin C, the rates of turnover are different. Troponin T and troponin I turnover in about 12 days, whereas troponin C turnover is almost twice as long (i.e. ~22 days). Furthermore, we have also previously shown that the synthesis rates of individual proteins change depending on which muscle is analysed. Hesketh et al, (2016) investigated four different muscle tissues in the rat over a 14-day period using deuterium labelling and found the rank order of protein synthesis was different across all muscles. For example, KCRM had a FSR of 3 % over 14 days in fast twitch EDL and 9.5 % over 14 days in the slower contracting SOL. These data are corroborated by our exemplar data as we report 24 proteins detected in the SOL compared to 28 in the PLN, both with contrasting rank orders for protein synthesis (Table 1), corresponding to large ranges in FSR for the SOL (1.13 – 7.25 %/d) and the PLN (0.81 – 7.60 %/d), underlining the significance of analysing muscle at the protein level and relying on mixed muscle data.

One of the main challenges of studying skeletal muscle on an individual protein level is that there is a small number of high abundance proteins present in skeletal muscle that tend to mask the expression of the majority of other proteins by dominating the analytical space (Murphy et al, 2019). Challenges are also encountered with peptide-level studies due to isoform-specific peptides being co-expressed within different skeletal muscle phenotypes that share high levels of sequence homology (Blaauw et al, 2013). The methodology presented here attempts to overcome these technical issues and greatly enhance the number of proteins we can detect for analysis. This is achieved by using the fractionation of samples into soluble and myofibrillar fractions

that subsequently allow us to employ separate, more optimised workflows for each fraction. The soluble fraction generally contains many different metabolic enzymes e.g. mitochondrial and glycolytic which do not tend to be expressed as multiple proteoforms thus allowing for a bottom-up proteomic approach combined with tandem mass spectrometry to quantify abundance changes and synthesis rates of individual proteins. Subsequently, the myofibrillar fraction that contains the contractile apparatus of the muscle, with proteins such as troponin and myosin that display many different proteoforms, position a top-down proteomic approach as a more optimised technique for investigation of this fraction (Burniston, 2008, 2009; Nishikawa et al, 2018.; Dowling et al, 2019).

Using our refined methods of dynamic proteome profiling we are able to assess each muscle on an individual level and calculate protein synthesis rates between each time sampling point to interrogate the degree of change over time. This is important to establish gaining a further level of detail to ensure no acute adaptive responses are missed over a 30-day time course. We can report that our semi-log plot data (Figure 2.7) is consistent with previous work (Hesketh et al, 2016) and our 2-point calculation methods appear consistent with our semi-log plot data (Figure 2.9). Therefore, validating our use of the 2-point calculation. Furthermore, Table 1 suggests a high level of repeatability reporting the coefficient of variation encompassing the technical and biological variability for SOL $10.9 \pm 4.8 \%$ and $10.6 \pm 5.7 \%$ for PLN with none of the proteins analysed in either muscle exceeding 20 %.

2.10 Conclusion

The methodology presented here allows for the robust calculation of protein synthesis over a time-course with subsequent calculation of synthesis rates at intermediary sampling points. This allows us to establish individual protein turnover measurements during a time-course of muscle adaptation. In future chapters, we have employed established proteomic techniques to quantify abundance changes of individual proteins (Burniston, 2008; 2009) with robust models of adaptation e.g. chronic low-frequency stimulation (Jarvis et al, 1996). These methods can then be coupled with the biosynthetic labelling technique we describe, using deuterium, that permits rapid equilibrium within rodents and can accurately measure incorporation into new protein through mass spectrometry analysis (Hesketh et al, 2016). Furthermore, we will also combine this with the marriage of both top-down and bottom-up proteomic analysis to allow a deeper investigation of skeletal muscle adaptation. Subsequently, exemplar data is provided to show that the calculations we use are consistent and robust meaning the degradation values derived from the abundance and synthesis calculations will be precise.

2.11 Bibliography

References

- Areta, J.L.; Burke, L.M.; Ross, M.L.; Camera, D.M.; West, D.W.D.; Broad, E.M.; Jeacocke, N.A.; Moore, D.R.; Stellingwerff, T.; Phillips, S.M.; et al. (2013). Timing and distribution of protein ingestion during prolonged recovery from resistance exercise alters myofibrillar protein synthesis. *J. Physiol*, **591**, 2319–2331.
- Balchin, D.; Hayer-Hartl, M.; Hartl, U. (2016). In vivo aspects of protein folding and quality control. *Science*, **353**, 1654-1664.
- Biolo, G.; Chinkes, D.; Zhang, X.J.; Wolfe, R.R. (1992). A new model to determine in vivo the relationship between amino acid transmembrane transport and protein kinetics in muscle. *JPEN J Parenter Enteral Nutr*, **4**, 305-315.
- Biolo, G.; Fleming, R.Y.; Maggi, S.P.; Wolfe, R.R. (1995). Transmembrane transport and intracellular kinetics of amino acids in human skeletal muscle. *Am J Physiol*, **268**, 75-84.
- Blaauw, B.; Schiaffino, S.; Reggiani, C. (2013). Mechanisms modulating skeletal muscle phenotype. *Compr. Physiol*, **3**, 1645–1687.
- Burniston, J.G.; McLean, L.; Beynon, R.J.; Goldspink, D.F. (2007). Anabolic effects of a non-myotoxic dose of the β_2 -adrenergic receptor agonist clenbuterol on the rat Plantaris muscle. *Muscle Nerve*, **35**, 217-223.
- Burniston, J.G. (2008). Changes in the rat skeletal muscle proteome induced by moderate-intensity endurance exercise. *Biochem. Biophys. Acta*, **178**, 1077-1086.
- Burniston, J.G. (2009). Adaptation of the rat cardiac proteome in response to intensity-controlled endurance exercise. *Proteomics*, **9**, 106-115.
- Burniston, J.G.; Hoffman, E.P. (2011). Proteomic responses of skeletal and cardiac muscle to exercise. *Proteomics*, **8**, 361-377.
- Burniston, J.G.; Connolly, J.; Kainulainen, H.; Britton, S.L.; Koch, L.G. (2014). Label-free profiling of skeletal muscle using high-definition mass spectrometry. *Proteomics*, **14**, 2339-2344.
- Burniston, J.G.; Chen, Y.W. (2019). Omics approaches to understanding muscle biology. Biomedical sciences, *Methods in Physiology*: Springer e-publishing.
- Busch, R.; Kim, Y.K.; Neese, R.A.; Schade-Serin, V.; Collins, M.; Awada, M.; Gardner, J.L.; Beysen, C.; Marino, M.E.; Misell, L.M.; Hellerstein, M.K. (2006). Measurement of protein turnover rates by heavy water labeling of nonessential amino acids. *Biochimica et Biophysica Acta*, **17**, 730-744.

Camera, D.; Burniston, J.; Pogson, M.; Smiles, W.; Hawley, J. (2017). Dynamic proteome profiling of individual proteins in human skeletal muscle after a high-fat diet and resistance exercise. *FASEB*, **31**, 1-17.

Chinkes DL. (2005). Methods for measuring tissue protein breakdown rate in vivo. *Curr Opin Clin Nutr Metab Care*, **8**, 534–537.

Coffey, V.G.; Hawley, J.A. (2007). The molecular basis of training adaptation. *Journal of Sports Medicine*, **37**, 737-763.

Commerford, S.L.; Carsten, A.L.; Cronkite, E.P. (1983). The distribution of tritium among the amino acids of proteins obtained from mice exposed to tritiated water. *Radiat. Res*, **94**, 151–155.

Dowling, P.; Zweyer, M.; Swandulla, D.; Ohlendieck, K. (2019). Characterization of Contractile Proteins from Skeletal Muscle Using Gel-Based Top-Down Proteomics. *Proteomes*, **7**, 1-23.

Elder, G.C.; Bradbury, K.; Roberts, R. (1982). Variability of fiber type distributions within human muscles. *J. Appl. Physiol*, **53**, 1473-1480.

Garlick, P.J.; McNurlan, M.A.; Essen, P.; Wernerman, J. (1994). Measurement of tissue protein synthesis rates in vivo: a critical analysis of contrasting methods. *Am J Physiol*, **266**, 287-297.

Gasier, H.G.; Fluckey, J.D.; Previs, S.F. (2010). The application of $^2\text{H}_2\text{O}$ to measure skeletal muscle protein synthesis. *Nutrition & Metabolism*, **7**, 31-35.

Gelfi, C.; Vigano, A.; Ripamonti, M.; Pontoglio, A.; Begum, S.; Pellegrino, A.M.; Grassi, B.; Bottinelli, R.; Wait, R.; Cerretelli, P. (2006). The Human Muscle Proteome in Aging. *Journal of proteome research*, **5**, 1344-1353.

Hellerstein, M.K.; Neese, R. (1992). Mass isotopomer distribution analysis: a technique for measuring biosynthesis and turnover of polymers. *Am. J. Physiol. Endocrinol. Metab*, **26**, 988–1001.

Hesketh, S.; Srisawat, K.; Sutherland, H.; Jarvis, J.; Burniston, J. (2016). On the rate of synthesis of individual proteins within and between different striated muscles of the rat. *Proteomes*, **4**, 1-12.

Holm, L.; Kjaer, M. (2010). Measuring protein breakdown rate in individual proteins in vivo. *Curr Opin Clin Nutr Metab Care*, **13**, 526–531.

Holm, L.; O'Rourke, B.; Ebenstein, D. (2013). Determination of steady state protein breakdown rate in vivo by the disappearance of protein-bound tracer-labeled amino acids: a method applicable in humans. *Am J Physiol*, **304**, 895–907.

Jaleel, A.; Short, K.R.; Asmann, Y.W.; Klaus, K.A.; Morse, D.M.; Ford, G.C.; Nair, K.S. (2008). In vivo measurement of synthesis rate of individual skeletal muscle mitochondrial proteins. *Am J Physiol Endocrinol Metab*, **295**, 1255-1268.

Jarvis, J.; Mokrusch, T.; Kwende, M.; Sutherland, H.; Salmons, S. (1996). Fast-to-slow transformation in stimulated rat muscle. *Muscle and Nerve*, **19**, 1469-1475.

Jones, P.J.; Leatherdale, S.T. (1991). Stable isotopes in clinical research: safety reaffirmed. *Clin Sci Lond*, **80**, 277-80.

Kasumov, T.; Dabkowski, E. R.; Shekar, K. C.; Li, L.; Ribeiro, R.; Walsh, K.; Previs, S.; Sadygov, R.; Willard, B.; Stanley, W. (2013). Assessment of cardiac proteome dynamics with heavy water: slower protein synthesis rates in interfibrillar than subsarcolemmal mitochondria. *Am J Physiol Heart Circ Physiol*, **304**, 201-214.

Kelleher, N.L.; Lin, H.Y.; Valaskovic, G.A.; Aaserud, D.J.; Fridriksson, E.K.; McLafferty, F.W. (1999). Top down versus bottom up protein characterization by tandem high-resolution mass spectrometry. *J. Am. Chem. Soc.*, **121**, 806–812.

Kelly, F.J.; Lewis, S.E.M.; Anderson, P.; Goldspink, D.F. (1984). Pre- and postnatal growth and protein turnover in four muscles of the rat. *Muscle Nerve*, **7**, 235–242.

Kim, S.T.Y.; Wang, D.; Kim, A.K.; Lau, E.; Lin, A.J.; Liem, D.A.; Zhang, J.; Zong, N.C.; Lam, M.P.Y.; Ping, P. (2012). Metabolic Labelling Reveals Proteome Dynamics of Mouse Mitochondria. *Molecular & Cellular Proteomics*, **11**, 1586– 1594.

Koizumi, (1974). Turnover rates of structural proteins of rabbit skeletal muscle. *J Biochem*, **2**, 431-439.

Lewis, S.E.M.; Kelly, F.J.; Goldspink, D.F. (1984). Pre- and post-natal growth and protein turnover in smooth muscle, heart and slow- and fast-twitch skeletal muscles of the rat. *Biochem. J*, **217**, 517-526.

MacInnis, M.J.; Gibala, M.J. (2017). Physiological adaptations to interval training and the role of exercise intensity. *J Physiol*, **9**, 2915-2930.

Malik, Z.A.; Colbey, J.N.; Morton, J.P.; Close, G.L.; Edwards, B.J.; Koch, L.G.; Britton, S.L.; Burniston, J.G. (2013). Label-free LC-MS profiling of skeletal muscle reveals heart-type fatty acid binding protein as a candidate biomarker of aerobic capacity. *Proteomes*, **1**, 290-308.

McCabe, B.J.; Bederman, I.R.; Croniger, C.M.; Millward, C.A.; Norment, C.J.; Previs, S.F. (2006). Reproducibility of gas chromatography-mass spectrometry measurements of ²H labelling of water: Application for measuring body composition in mice. *Analytical Biochemistry*, **350**, 171-176.

Miller, B.F.; Wolff, C.A.; Peelor, F.F.; Shipman, P.D.; Hamilton, K.L. (2015). Modeling the contribution of individual proteins to mixed skeletal muscle protein synthetic rates over increasing periods of label incorporation. *J Appl Physiol*, **118**, 655-661.

Murphy, S.; Dowling, P.; Ohlendieck, K. (2016). Comparative Skeletal Muscle Proteomics Using Two-Dimensional Gel Electrophoresis. *Proteomes*, **4**, 27-36.

Murphy, S.; Dowling, P.; Zweyer, M.; Swandulla, D.; Ohlendieck, K. (2019). Proteomic profiling of giant skeletal muscle proteins. *Expert Rev. Proteomics*, **16**, 241–256.

Nair, K.; Halliday, D.; Griggs, R. (1988). Leucine incorporation into mixed skeletal muscle protein in humans. *American Journal of Physiology*, **254**, 208-213.

Nishikawa, K.C.; Monroy, J.A.; Tahir, U. (2018). Muscle Function from Organisms to Molecules. *Integr. Comp. Biol*, **58**, 194–206.

Padula, M.P.; Berry, I.J.; O'Rourke, M.B.; Raymond, B.A.; Santos, J.; Djordjevic, S.P. (2017). A Comprehensive Guide for Performing Sample Preparation and Top-Down Protein Analysis. *Proteomes*, **5**, 11-31.

Price, J.; Khambatta, C.; Li, K.; Bruss, M.; Shankaran, M.; Dalidd, M.; Floreani, N.; Roberts, L.; Turner, S.; Holmes, W.; Hellerstein, M. (2012). The effect of long term calorie restriction on in vivo hepatic proteostasis: A novel combination of dynamic and quantitative proteomics. *Molecular and cellular proteomics*, **11**, 1801-1814.

Vesali, R.F.; Klaude, M.; Thunblad, L. (2004). Contractile protein breakdown in human leg skeletal muscle as estimated by [2H3]- 3-methylhistidine: a new method. *Metabolism*, **53**, 1076–1080.

Rennie, M.J.; Phillips, S.; Smith, K. (2008). Reliability of results and interpretation of measures of 3-methylhistidine in muscle interstitium as marker of muscle proteolysis. *J Appl Physiol*, **105**, 1380–1391.

Schoenheimer, R.; Rittenberg, D. (1935). Deuterium as an indicator in the study of intermediary metabolism. *Science*, **82**, 156–157.

Shankaran, M.; Shearer, T.; Stimpson, S.; Turner, S.; King, C.; Wong, P.; Shen, Y.; Turnbull, Kramer, F.; Clifton, L.; Russell, A.; Hellerstein, M.; Evans, W. (2016). Proteome-wide muscle protein fractional synthesis rates predict muscle mass gain in response to a selective androgen receptor modulator in rats. *Am J Physiol Endocrinol Metab*, **310**, 405-417.

Silva, J.C.; Gorenstein, M.V.; Li, G.Z.; Vissers, J.P.; Geromanos, S.J. (2006). Absolute Quantification of Proteins by LCMS. *Molecular & Cellular Proteomics*, **18**, 3696-3709.

Sollanek, K.J.; Burniston, J.G.; Kavazis, A.N.; Morton, A.B.; Wiggs, M.P.; Ahn, B.; Smuder, A.J.; Powers, S.K. (2017). Global proteome changes in the rat diaphragm induced by endurance exercise training. *PLoS One*, **12**, 375-388.

Soukup, T.; Zacharova, G.; Smerdu, V. (2002). Fibre type composition of soleus and extensor digitorum longus muscles in normal female inbred Lewis rats. *Acta Histochem*, **4**, 399-405.

Terjung, R.L. (1979). The turnover of cytochrome c in different skeletal-muscle fibre types of the rat. *Biochem. J*, **178**, 569–574.

Tuvdendorj, D.; Chinkes, D.L.; Herndon, D.N. (2013). A novel stable isotope tracer

method to measure muscle protein fractional breakdown rate during a physiological non-steady state condition. *Am J Physiol*, **304**, 623–630.

Wagenmakers, A. J. M. (1999). Tracers to investigate protein and amino acid metabolism in human subjects. *Proceedings of the Nutrition Society*, **58**, 987-1000.

Wisniewski, J.R.; Zougman, A.; Nagaraj, N.; Mann, M. (2009). Universal sample preparation method for proteome analysis. *Nature methods*, **6**, 359-363.

Wolfe, R.R.; Chinkes D.L. (2005). *Isotope Tracers in Metabolic Research: Principles and Practice of Kinetic Analysis* (2nd ed.), John Wiley & Sons, Inc., Hoboken, NJ.

Xiao, G.G.; Garg, M.; Lim, S.; Wong, D.; Go, V.L.; Lee, W.P. (2008). Determination of protein synthesis in vivo using labelling from deuterated water and analysis of MALDI-TOF spectrum. *J Appl Physiol*, **104**, 828-836.

Zhang, X.J.; Chinkes, D.L.; Sakurai, Y.; Wolfe, R.R. (1996). An isotopic method for measurement of muscle protein fractional breakdown rate in vivo. *Am J Physiol*, **270**, 759-767.

Zhang, X.J.; Chinkes, D.L.; Wolfe, R.R. (2002). Measurement of muscle protein fractional synthesis and breakdown rates from a pulse tracer injection. *Am J Physiol Endocrinol Metab*, **4**, 753-764.

Chapter 3. The role of protein turnover in skeletal muscle adaptation induced by chronic low-frequency stimulation.

3.1 Abstract

The health benefits of exercise training involve adaptations to the contractile and metabolic properties of muscle that are underpinned by changes in protein abundance. Exercise is also associated with a general increase in muscle protein turnover, but it is not yet known how the components of protein turnover (i.e. synthesis and degradation) are coordinated to bring about exercise-induced changes in protein abundance. We have used stable isotope labelling and chronic low-frequency stimulation (CLFS) *in vivo* to investigate how the synthesis, abundance and degradation of individual proteins change during exercise-induced muscle adaptation. Four independent groups of rats ($n = 3$ in each), received CLFS (10 Hz, 24 h/d) and deuterium oxide for either 0 d, 10 d, 20 d or 30 d. At each time point the extensor digitorum longus (EDL) muscle was harvested from the stimulated left hindlimb (Stim) and non-stimulated right hindlimb (Ctrl). Proteomic techniques were used to quantify changes in abundance of 30 myofibrillar proteins and 47 soluble proteins. Peptide mass spectrometry was used to calculate protein synthesis rates, protein degradation was calculated from the difference between the change in abundance and synthesis rate. Endurance activity tended ($P = 0.145$) to increase the average rate of synthesis in mixed myofibrillar proteins from Ctrl (8.63 ± 0.26 pg/d) to Stim (10.24 ± 1.63 pg/d). However, the synthesis rate of mixed soluble proteins increased ($P = 0.001$) from Ctrl (43.70 ± 0.07 pg/d) to Stim (60.17 ± 0.73 pg/d).

Protein turnover responses differ on a protein-by-protein basis regardless of protein function during the muscle transformation process. For example, Creatine kinase S-type, mitochondrial (KCRS), Sarcoplasmic/endoplasmic reticulum calcium ATPase 2 (AT2A2) and ATP synthase subunit beta, mitochondrial (ATPB) all increase ($P < 0.05$) in abundance but this is achieved in different ways. Independent responses; being partially accounted for by a greater synthesis rate (KCRS), without a detectable change in synthesis rate (AT2A2) or being entirely accounted for by an increase in the rate of synthesis in Stim compared to Ctrl muscle (ATPB). The abundance of Glycogen phosphorylase (PYGB), Beta-enolase (ENOB) and Troponin T, fast skeletal muscle (TNNT3) significantly ($P < 0.05$) decreased after CLFS. The decrease in abundance of ENOB was partially accounted for by a decreased synthesis rate in Stim compared to

Ctrl. The decrease in abundance of PYGB was entirely accounted for by a decrease in its rate of synthesis, whereas the abundance of TNNT3 decreased without a detectable change in synthesis rate.

To gain more detailed information, individual proteoforms of key myofibrillar proteins were investigated. Myosin regulatory light chain 2 (MLRS) was resolved as 2 separate proteoforms (spot 11 and spot 12). Spot 11 significantly ($P < 0.05$) decreased (62 %) in abundance and spot 12 increased (16 %) after 30 days of CLFS. There was no difference in synthesis rate between Stim and Ctrl muscle for either proteoform. Therefore, we attribute the changes in abundance to proteoform-specific changes to degradation rate.

In conclusion, we provide new evidence for selective degradation of individual proteins during muscle adaptation in response to CLFS. From this we can report, 50 proteins displayed a change in abundance in response to muscle adaptation. Of which 30 % of proteins were driven by synthesis, 38 % of proteins were driven by degradation and the remaining 32 % were driven by both synthesis and degradation. Our data suggest both protein synthesis and protein degradation regulate of changes in protein and proteoform abundance during muscle adaptation.

3.2 Introduction

A physically active lifestyle and/or participation in formal exercise training are fundamental to the prevention of chronic diseases, including metabolic disorders e.g. type 2 diabetes (Knowler et al, 2002) that affect skeletal muscle. Repeated bouts of muscle contraction that are associated with frequent exercise represent a potent stimulus for the physiological and biochemical adaptation of muscle. Skeletal muscle demonstrates a remarkable malleability in response to contractile activity (Salmons and Vrbova, 1969.; Fluck and Hoppeler, 2003.; Coffey and Hawley, 2007) and exercise training is associated with functional changes in the expression of contractile and metabolic proteins in muscle (Adams et al, 1993.; Widrick et al, 2002). As such, when cellular homeostasis is perturbed, for instance during muscular contraction, the metabolic demands of the tissue are altered significantly; leading to numerous structural, functional and biochemical changes that ultimately impact on tissue phenotype (Delp and Pette, 1994). This widely accepted molecular mechanism that governs the adaptation to exercise training, involves a gradual alteration in protein content and enzyme activities within skeletal muscle. However, exactly how this process is coordinated, e.g. through changes to the synthesis and degradation of proteins, is currently unknown. This is an important area to understand given the extensive catalogue of health benefits the adaptation to exercise initiates.

We have employed a robust model (Jarvis et al, 1996) of exercise adaptation (chronic low-frequency stimulation; CLFS) to study the complex mechanisms underpinning muscle adaptation. As a model, CLFS is an approach that enables the investigation of specific molecular events resulting in functional change of skeletal muscle. The artificial stimulation activates all motor units equally therefore abolishing the hierarchical order of motor unit recruitment associated with voluntary exercise (Pette and Vrbova, 1992). During CLFS, the largest, normally less active, motor units are activated in synchrony with the other normally more active motor units. Thus, the normally less active fibre types, i.e. the fast-twitch fatigable fibres, undergo profound adaptation when exposed to CLFS. The advantage of this method is that the unstimulated, contralateral muscle can be used as an intra-animal control, as unlike exercise, the activity is restricted to the stimulated muscle only. Therefore, the muscle is less influenced by other systemic factors that can occur in the body during more holistic methods of training.

Ultimately, CLFS challenges the adaptive potential of the target muscle to its limits by inducing transformations which exceed those promoted by any other form of increased contractile activity. CLFS is associated with well-established time-dependant changes in the molecular, structural and functional properties of fast-twitch muscle that can be followed from the beginning using the unstimulated, intra-animal control (Jarvis et al, 1996). Consequently, CLFS is well positioned to offer insight to the mechanism of muscle plasticity of which the use is well documented. The effects of CLFS were first reported (Salmons and Vrbova, 1969.; Pette et al, 1973) in the EDL and TA muscle of the rabbit and the FDL muscle of the cat (Eerbeek et al, 1984). These investigations showed that a transformation of a fast into a slow-twitch muscle can be brought about by a stimulation frequency pattern which is normally delivered to slow muscle. Continuous stimulation at 10 Hz is sufficient to convert fast-twitch muscles into slower contracting more fatigue resistant muscle that exhibits a greater time to peak twitch tension and half-relaxation time (Brown et al, 1976). Resistance to fatigue is one of the most pronounced changes in fast-twitch chronically stimulated muscle (Kwong and Vrbova, 1981.; Pette and Simoneau, 1990) and consistent with the changes in the velocity of muscle contraction, increases in the twitch to tetanus ratio of stimulated muscle are also observed (Salmons and Sreter, 1979.; Brown et al, 1989), indicating the duration of the active state of the muscle is prolonged.

Time course investigations of the response of rabbit fast-twitch muscle to CLFS (Froemming et al, 2000) report changes in the physiological properties of the muscle are detectable as early as 2 to 4 days after the onset of stimulation. The increase in time to peak tension induced by CLFS has two distinct phases. During the first two weeks of CLFS there is a rapid increase in time to peak tension, which reaches values approximately 1.8-fold greater than the unstimulated contralateral (control) muscle. More prolonged periods of stimulation (e.g. 20 weeks; Salmons and Sreter, 1976) lead to further increases in time to peak tension, but the rate of change is less. The early changes in time to peak tension and half-relaxation time are associated with changes in the release and sequestration of Ca^{2+} by the sarcoplasmic reticulum (Heilmann and Pette, 1979). Whereas, mechanisms other than Ca^{2+} handling seem responsible for the later changes in muscle contractile properties, including an increase in type I fibres (Pette et al, 1976). The appearance of type I fibres and the associated expression of slow myosin heavy chain isoforms affect the speed of contraction (Brown et al, 1983) and give the fast-twitch muscle physiological and morphological characteristics that

are more similar to a slow-twitch phenotype. In rabbit TA that is exposed to 12 h/d or continuous (24 h/d) CLFS (10 Hz) the predominant fast isoform MyHC IIx/d is down regulated and there is a concomitant up-regulation of the slower MyHC IIa that is latter replaced with MyHC I (Peucker et al, 1999). These transitions in MyHC expression are accompanied by a complementary fast-to-slow transition of myosin light chain isoforms (Leeuw and Pette, 1996), Troponin T (Hartner et al, 1989), Troponin I and C (Hartner et al, 1990). Coinciding with the changes in myofibrillar protein isoforms there is a transition from fast to slow isoforms of sarco-endoplasmic reticulum Ca^{2+} -ATPase (SERCA) and calsequestrin (Ohlendieck et al, 1999). Concomitant with the contractile changes there are increases in abundance of enzymes related to aerobic-oxidative metabolism (Pette and Simoneau, 1990). A linear correlation has been demonstrated (Reichmann et al, 1985) between citrate synthase activity and muscle aerobic-oxidative capacity. Therefore, elevations in citrate synthase have been used as a biomarker for the enhanced resistance to fatigue in the CLFS fast-twitch muscles of both the rat and rabbit (Green and Pette, 1997). The use of biomarkers like citrate synthase, permit certain strengths to analysis such as allowing for changes to be monitored easily and objectively. However, this is just one enzyme associated with the aerobic system, Burniston et al, (2014) reports a wide distribution of metabolic enzymes in muscle fibres that seemingly have the same fibre type and report protein abundance to span over four orders of magnitude. This alone suggests that reliance on a single biomarker is not going to enable us to pick apart complex proteomic changes to answers questions like how different proteins change in response to muscle adaptation.

Donoghue et al, (2005) reports proteomic analysis of CLFS rabbit fast-twitch TA and used techniques similar to our current work, including two dimensional-gel electrophoresis (2DGE) and mass spectrometry. Changes to more than 21 different proteins were reported (Donoghue et al, 2005), including isoform switches in Myosin heavy and light chains, troponin T and SERCA. The fast isoforms of troponin T and myosin light chain 2 were drastically down regulated (5-fold and 3-fold respectively) whilst their slow-twitch counterparts exhibited an increased expression (6-fold and 5-fold respectively) (Donoghue et al, 2005). However, the mechanisms underpinning these changes in abundance were not investigated. Mayne et al, (1993) established the CLFS model of muscle transformation *in vivo* in rat using 10 Hz of continuous stimulation of the TA and EDL muscles and demonstrated shifts from the fast to slow

myosin heavy chain isoforms. Jarvis et al, (1996) reported CLFS of rat EDL muscle *in vivo* and demonstrated that 10 Hz is optimal for muscle transformation, evidenced by a marked slowing of the isometric twitch and maximum shortening velocity. Accordingly, histochemical analysis of the stimulated muscles revealed a substantial increase in the type I fibre population at the expense of the type IIB/D fibres (Jarvis et al, 1996). Key to all of these findings is the consistent correlation with changes in muscle mass and the increased physiological properties of slow-twitch muscle. Chronic low-frequency stimulation induced changes are strongly correlated with a decline in muscle mass of the target muscle with a decrease of ~50 % typical of transformed muscle. Jarvis et al, (1996) recorded a 49 % decrease in TA muscle mass and a 58 % decrease in EDL muscle mass compared to unstimulated control muscles, in the rat over the 8 week stimulation period. Similar work has also demonstrated that fibre damage is not an inevitable consequence of electrical stimulation as it is closely related to the pattern and frequency of the stimulation (Lexell et al, 1992). Furthermore, degenerative processes have only been observed in the rabbit (Lexell et al, 1992.; Maier et al, 1986) and not in the rat (Delp and Pette, 1994.; Putman et al, 1999). Investigations into CLFS induced damage in rat EDL muscle has demonstrated that at frequencies of 10 and 20 Hz for periods up to 2 months of continuous stimulation there is no significant damage to the muscle (Jarvis et al, 1996). However, this decline in muscle mass correlates with a change to a smaller cross sectional area of the slow-twitch muscle fibres which subsequently decrease the peak force output and increase the contraction time of the muscle, all expected changes for the CLFS model, indicating the successful transformation of the target muscle. Thus, providing a robust link between the physiological and biochemical change of a muscle to measurable changes in muscle morphology. The CLFS model has been instrumental to the development of knowledge regarding the physiological and biochemical properties of skeletal muscle and the processes of muscle adaptation. It is well documented that CLFS induces overt changes in muscle function, with elevations in aerobic-oxidative capacity, decreased fibre calibre, switches in isoform expression patterns all established biochemical hallmarks of skeletal muscle transformation (Donoghue et al, 2007). However, it is the constituent proteins that are the functional component of the muscle and CLFS has been shown to induces changes in these muscle proteins accordingly (Donoghue 2005). Investigations that attempt to quantify individual proteins, primarily investigate solely protein abundance. However, the

abundance of a protein is the result of the net balance between its rate of synthesis versus its rate of degradation, but until very recently it was not possible to investigate the abundance, synthesis and degradation of proteins.

The processes underlying muscle adaptation centre on this balance of synthesis and degradation of individual proteins. Our current work is driven by an interest in the adaptive process of skeletal muscle and specifically by the contributions of synthesis and degradation to changes in the abundance of individual proteins in response to exercise. We employ CLFS to ensure robust changes in individual protein abundance occur over the experimental period. Proteome-wide technologies to investigate the rates of individual protein degradation in biological systems *in vivo* are lacking. The majority of the research in this field reports either protein abundance or protein synthesis in isolation and, therefore, misses part of this balance equation. Our lab has recently established a robust method for measuring the synthesis and abundance of individual proteins (Burniston and Chen, 2019). Our unique method nicknamed “Dynamic Proteome Profiling”, can give insight to protein degradation by calculating the contribution of synthesis to changes in protein abundance. The methodology gives us the power to calculate protein turnover on an individual protein scale, allowing access to new information on how muscle adaptation is orchestrated. It has been proposed that the net loss of protein abundance in response to CLFS is brought about by a wholesale increase in protein degradation, whilst observing a brake in protein synthesis (Loughna et al, 1986). Herein, we present a highly novel data set that challenges this paradigm, demonstrating that the mechanism of how protein abundance is regulated during the adaptive process differs on a protein-to-protein basis. Indicating that degradation not only has a regulatory role in skeletal muscle but also contributes to the pattern of change amongst proteoforms, which occur as part of the fast-to-slow transformation of skeletal muscle.

Objectives

Objective of chapter – To investigate how individual protein responses coordinate the adaptive response of the muscle to an endurance-type stimulus.

Specific Aim 1: To clarify quantitative changes of specific protein isoforms induced by CLFS to indicate the transformation from a fast-twitch phenotype to a more

oxidative phenotype.

Specific Aim 2: To investigate the time course of changes to individual protein turnover in both myofibrillar and soluble fraction proteins in response to CLFS.

Specific Aim 3: To identify proteoform-specific changes during muscle adaptation induced by CLFS and measure protein turnover to investigate how such changes are coordinated.

Specific Aim 4: To inform what is the dominant driver of change during CLFS induced skeletal muscle adaptation i.e. the percentage of individual proteins that where their changes in abundance is i) driven by synthesis, ii) driven by degradation, or iii) driven by a combination of both synthesis and degradation.

3.3 Methods

Experimental procedures were conducted under the British Home Office Animals (Scientific Procedures) Act 1986. Male Wistar rats aged 9 months old, 500 ± 69 g body weight and bred in-house in a conventional colony, housed in controlled conditions of 20 °C, 45 % relative humidity, and a 12 h light (0600–1800 hours) and 12 h dark cycle, with water and food available *ad libitum*. All aspects of animal husbandry were conducted by the LJMU animal facility staff.

Animals were assigned to four groups ($n = 3$ in each), including a sham-operated control group and three groups that received a programmed stimulation pattern (24 h at 10 Hz) of chronic low-frequency stimulation (CLFS) of the left hindlimb dorsiflexor muscles, as described previously by our group (Jarvis et al, 1996). Surgical procedures, anaesthetic protocol and the electrical stimulation model of CLFS were performed by Prof. Jonathan Jarvis and Dr. Hazel Sutherland as part of a wider project. Work conducted within this thesis focused solely on aspects associated with dynamic proteome profiling of muscle samples.

Surgery was performed in full aseptic precautions and the animals were anaesthetised using a gaseous mixture of isoflurane and O₂. An initial concentration of 4 % isoflurane was used for induction of anaesthesia and was then adjusted to levels of 1-2 % to maintain an adequate surgical plane of anaesthesia. Buprenorphine (Temgesic,

Indivior, Slough, UK) at a dose of 0.05 mg/kg^{-1} body mass, was administered pre-surgery for analgesia. Implantable stimulators were used according to Salmons & Jarvis, (1991) with minor modifications, fine multi-stranded stainless steel leads (Cooner Wire Assoc., Chatsworth, CA) were taken subcutaneously from the flank to just proximal to the knee on the left hind limb, the electrodes were fixed in close relationship to, but not in physical contact with, the common peroneal nerve. The body of the stimulator was situated in the abdominal cavity and held in place by suturing an integral dacron mesh tag into the closing of the abdominal wall. The post-operative recovery of the animals was monitored daily for 1 week prior to commencing the stimulation protocol. The 0-day experimental time point represents the sham-operated control group that were implanted with stimulators and then killed after the 1 week recovery period without being turned on. The remaining (10 d, 20 d and 30 d) experimental groups of animals had the device activated remotely via an optical link to a phototransistor in the device (Brown and Salmons, 1981). This initiated stimulation from day zero at a continuous 10 Hz of the fast dorsiflexor muscles of the anterior compartment of the hindlimb, including the Extensor digitorum longus (EDL). Simultaneously, deuterium oxide ($^2\text{H}_2\text{O}$; Sigma-Aldrich, St. Louis, MO) administration was initiated by an intraperitoneal loading injection of $10 \mu\text{L.g}$ 99 % $^2\text{H}_2\text{O}$ -saline, and then maintained by administration of 5 % (v/v) $^2\text{H}_2\text{O}$ in the drinking water available to the rats, which was refreshed daily.

At 10 d, 20 d and 30 d after the start of stimulation and deuterium oxide consumption, animals were killed humanely in a rising concentration of CO_2 followed by cervical dislocation. Plasma samples were obtained by cardiac puncture immediately after death to determine $^2\text{H}_2\text{O}$ enrichment and EDL muscles, from the left stimulated limb (Stim) and the right non-stimulated limb (Ctrl), were isolated. Each muscle was cleaned of fat and connective tissue then weighed before being frozen in liquid nitrogen and stored at $-80 \text{ }^\circ\text{C}$ pending further analysis.

Deuterium enrichment of the body water of each animal ($n = 12$) was determined by GC-MS analysis of ^2H enrichment in plasma samples against external standards. Full methods are described in Chapter 2, section 2.4.2. Muscle homogenates were fractionated into the myofibrillar, contractile proteins and soluble fraction proteins according to Chapter 2, section 2.4.3. The subsequent analysis of the myofibrillar proteins were analysed via top-down proteomic methods using the gel-based separation method, 2-dimensional gel electrophoresis (2DGE) to isolate individual

proteoforms and to quantify abundance changes. Individual proteins were identified from peptide mass fingerprinting and synthesis measurements were derived from MALDI mass spectrometry, detailed in its entirety in Chapter 2.5.

The analysis of the proteins in the soluble fraction was achieved by a bottom-up proteomic approach with full details described in Chapter 2.6. Here, protein samples underwent in-solution digest and were identified and abundance quantified via LC-MS/MS label free quantitation. MS data were normalised by an inter-sample abundance ratio, and the differences in relative protein abundance were quantified using nonconflicting peptides only. MS/MS spectra were exported into Mascot and individual proteins were identified, from which protein synthesis measurements were calculated based on the mass isotopomer distribution of specific peptides (Chapter 2.7).

Two spots (number 11 and 12) of similar M_r but different pI were identified as skeletal muscle myosin regulatory light chain (MLRS) and may indicate different post-translational states. To investigate post-translational modification of MLRS, tryptic peptides were analysed by LC-MS/MS. High-energy fragment mass spectra were created using a collision-induced dissociation with helium as the collision gas. MS/MS ions lists were searched against the Swiss-Prot database using error tolerant searches.

Fractional synthesis rates (FSR) were derived for all identified myofibrillar and soluble proteins using the methods detailed in Chapter 2.7. Synthesis rates were calculated in both control (right, non-stimulated) and stimulated (left) muscles in two primary ways. All proteins used the fitting of the mass isotopomer data collected at each of the 4 experimental time-points using a semi-log plot. In addition, data were fitted using a 2-point non-linear first-order equation in order to calculate FSR over intermediate time points e.g. 0 d – 10 d, 10 d – 20 d, 20 d – 30 d. These calculations are achieved by first calculating the rate of decay of the molar fraction of the m_0 mass isotopomer across 0 d, 10 d, 20 d and 30 d time points by using semi-log plots. The rate constant (k) is then divided by the number (n) of exchangeable hydrogen sites reported in standard tables (Commerford et al, 1983) and finally by the level of precursor enrichment (p) measured by GC-MS analysis of plasma samples. Protein FSR is then reported as the median of the peptide values assigned to each protein or proteoform. The individual rates for fractional degradation rate (FDR) were also calculated for each protein in the myofibrillar and soluble fractions. This was achieved by calculating the

difference between the rate of synthesis and the rate of change in protein abundance (Full details in Chapter 2, section 2.7.2).

From the FSR and FDR calculations absolute protein turnover was calculated for each individual protein in the myofibrillar and soluble fraction (Full calculation details in Chapter 2, section 2.7.3). Absolute synthesis rates were calculated by first multiplying the wet weight of the EDL by the total amount of protein extracted from the EDL and then multiplying by the rate of change in relative protein abundance for each individual protein.

Statistical analysis of myofibrillar protein abundance was conducted on normalised spot data from 2D-gels. Normalised protein abundance from LC-MS label-free quantitation were used for soluble protein abundance. Relative synthesis rates were analysed as percent per day (%/d) and absolute synthesis rates were analysed as pmol/d in the soluble fraction proteins and as mg/d in the myofibrillar fraction proteins, all values are the average of the analysed peptides for each protein and subsequent analysis is at the protein level. All statistical testing was performed on biological replicates (n = 3 in each group) conducted using SPSS (SPSS, v23, Chicago, USA) and the statistical significance level was set at $P < 0.05$. To assess the degree of consistency across control situations (right limb, non-stimulated muscle) for all time points (10 d, 20 d and 30 d) and sham operated animals (0 d) a one-way ANOVA was used to analyse protein abundance, synthesis and degradation data. To assess the differences between the non-stimulated control limb (right) and the stimulated limb (left), paired T-tests were conducted to compare stimulated and non-stimulated limbs at each experimental time point (0 d, 10 d, 20 d and 30 d) for protein abundance, synthesis and degradation rates at the individual protein level. To control the false-discovery rate, P-value distributions were used to calculate Q values and a criterion false-discovery rate of $< 1\%$ was set. This statistical approach considers the biological variation across each protein and, therefore, is more sophisticated than arbitrarily implementing a threshold on the basis of fold change.

3.4 Results

At the beginning of the experiment (0 days) the wet weight of extensor digitorum longus (EDL) was not different between the sham operated left limb (177.0 ± 12 mg) and the non-operated right limb (195.6 ± 4 mg). There was also no change in EDL mass of the non-stimulated right limb at any of the experimental time points encompassing the 30 days of unilateral chronic low-frequency stimulation (CLFS). In response to CLFS, EDL mass of the left, stimulated limb declined by 16 % after 10 days, 40 % after 20 days and 50 % after 30 days, consistent with our previous work (Jarvis, 1993). The difference in mass between the left, stimulated (Stim), and right contralateral non-stimulated (Ctrl) EDL was statistically significant ($P < 0.05$) after 20 days and 30 days of chronic endurance activity (Figure 3.1).

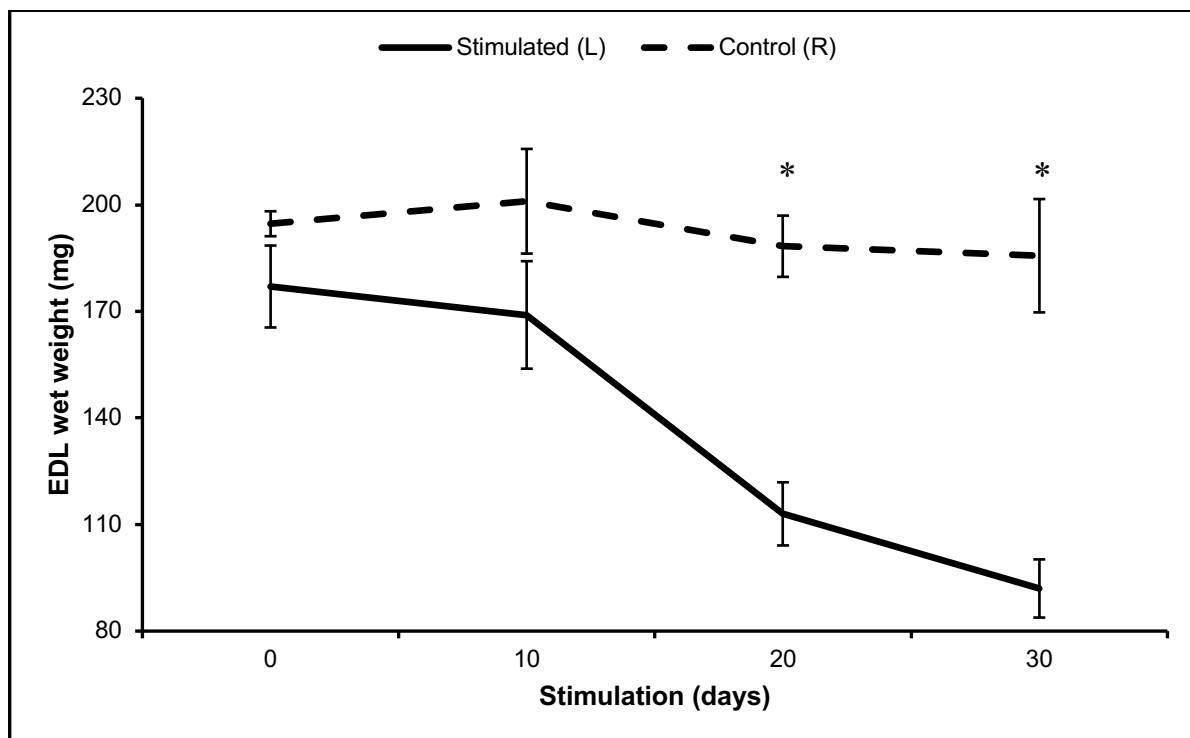


Figure 3.1. Time course of changes in muscle wet weight.

Wet weight (mg) of extensor digitorum longus (EDL) in non-stimulated right (broken line) and contralateral stimulated left (solid line) limbs after unilateral chronic low-frequency (10 Hz) stimulation *in vivo*. Data are presented as mean \pm SD from independent groups of $n = 3$ rats at each time point. * $P < 0.05$ statistically significant difference between the right and left limbs analysed by paired t-test at each time point. 2D Gel analysis of the myofibrillar fraction resolved 43 protein spots in each of the 24 biological samples. Mass spectra were recorded from in-gel digests of each spot in

each biological replicate (approximately 1000 gel spots analysed). After filtering based on quality control criteria, a total of 30 spots had complete data from 5 peptides per protein that were present in all samples. In addition, a further 8 spots were detected only in samples that had received CLFS for 20 days or greater. Figure 3.2, illustrates the gel position of the 38 spots that satisfied the requirements for protein synthesis calculations, the identity of each gel spot is reported in Table 3.1. The total number of non-redundant protein identifications was 23 and 10 proteins were present in multiple spots and therefore represent different proteoforms. The reproducibility of protein abundance measurements was good (coefficient of variation $2.7 \pm 0.06 \%$, $n = 3$ biological replicates) and the abundance of each proteoform in Ctrl and Stim muscles is reported in supplementary Table S3.

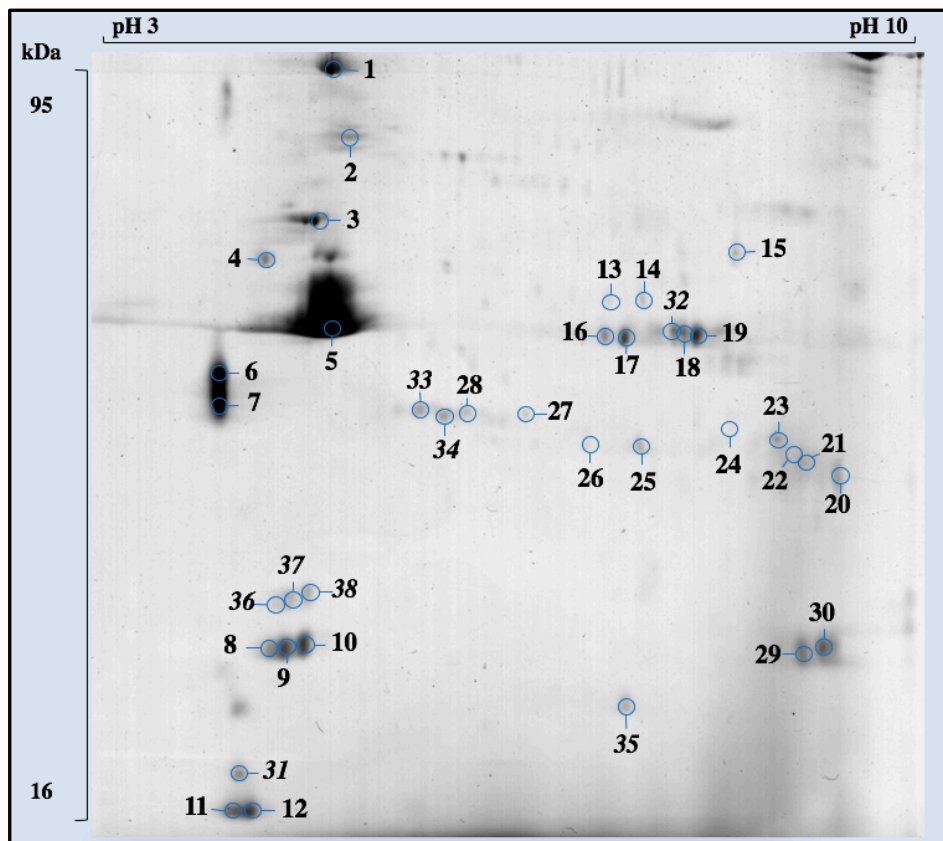


Figure 3.2. Separation of myofibrillar proteins by 2DGE.

Representative two-dimensional gel electrophoresis map of EDL myofibrillar proteins after 30 days of chronic low-frequency stimulation *in vivo*. The gel has been annotated with common spots across both conditions (stimulated and non-stimulated control) $n = 30$ (annotated 1-30) and spots unique to the stimulated samples only $n = 8$ (annotated 31-38). Spot annotations are consistent with the protein identities in Table

3.1.

Table 3.1. Myofibrillar protein identifications.

Spot number	Protein name/ Description	UniProt name	M_r	pI	Mows e score	Sequence coverage
1	Alpha-actinin-1	ACTN1	102960	5.23	133	15 %
2	Plectin	PLEC	533540	5.61	94	4 %
3	Desmin	DESM	53457	5.21	72	24 %
4	ATP synthase subunit beta	ATPB	56354	5.08	78	23 %
5	Actin, alpha skeletal muscle	ACTS/A CTC	42051	5.29	71	24 %
6	Tropomyosin alpha-4	TPM4	28510	4.71	119	37 %
7	Tropomyosin beta chain	TPM2	32837	4.71	93	34%
8	Myosin light chain 1	MYL1	20680	5.17	76	44 %
9	Myosin light chain 1	MYL1	20680	5.42	81	44 %
10	Myosin light chain 1	MYL1	20680	5.73	72	42 %
11	Myosin regulatory light chain 2	MLRS	18969	4.24	100	42 %
12	Myosin regulatory light chain 2	MLRS	18969	4.76	97	43 %
13	Beta-enolase	ENOB	47014	7.33	88	31 %
14	Beta-enolase	ENOB	47014	7.63	84	31 %
15	ATP synthase subunit alpha	ATPA	59754	8.66	113	30 %
16	Creatine kinase M-type	KCRM	43045	7.29	96	24 %
17	Creatine kinase M-type	KCRM	43045	7.74	98	26 %
18	Creatine kinase S-type	KCRS	47385	8.20	81	26 %
19	Creatine kinase S-type	KCRS	47385	8.22	76	28 %
20	Annexin A4	ANXA4	35849	9.43	61	22 %
21	Glyceraldehyde-3-phosphate dehydrogenase	G3P	35828	8.71	67	20 %
22	Glyceraldehyde-3-phosphate dehydrogenase	G3P	35828	8.70	63	18 %
23	Troponin I, fast	TNNI2	21328	9.05	93	36 %
24	Troponin I, slow	TNNI1	21724	7.87	117	34 %
25	Troponin T, fast	TNNT3	30750	7.79	78	21 %
26	Troponin T, fast	TNNT3	30750	7.11	84	22 %
27	Troponin T, slow	TNNT1	31215	6.19	70	24 %

28	Troponin T, fast	TNNT3	30750	5.97	79	23 %
29	Carbonic anhydrase 3	CAH3	29431	8.71	94	31 %
30	Carbonic anhydrase 3	CAH3	29431	8.74	89	30 %
31	Myosin regulatory light chain 2, ventricular/cardiac muscle isoform	MLRV	18880	4.92	103	27 %
32	Creatine kinase S-type	KCRS	47385	8.04	83	26 %
33	Troponin T, slow	TNNT1	31215	5.86	70	22 %
34	Troponin T, slow	TNNT1	31215	5.91	67	22 %
35	Alpha-crystallin B chain	CRYAB	20089	6.33	88	32 %
36	Myosin light chain 3	MYL3	22156	5.21	77	28 %
37	Myosin light chain 3	MYL3	22156	5.53	82	25 %
38	Myosin light chain 3	MYL3	22156	5.72	73	27 %

Spot number refers to the different proteoforms resolved by 2DGE and corresponds to the 2DGE image in Figure 3.2. Protein name relates to the Uni-Prot database, entries returned using the MASCOT search engine. A mowse score greater than 55 denotes a confident ($P < 0.05$) identification by peptide mass fingerprinting. Relative molecular mass (M_r) are from protein database entry, isoelectric point (pI) is observed from position on experimental 2DGE images. The amino acid sequence of peptides and residue positions (start and end) are available in supplementary information 'Table S1'.

At baseline (0-day time point) there was no difference in the abundance of myofibrillar proteins between Ctrl and Stim muscle. Accordingly, protein abundances were highly correlated ($R^2 = 0.97521$; Figure 3.3) between Ctrl and Stim muscle. Protein abundances in Ctrl muscles did not change during the 30-d experimental period (Fig. 3.3, upper panels). In contrast, the level of correlation (R^2) deteriorated from 0.67619 at day 10 to 0.50474 at day 30 (Figure 3.3) between baseline and Stim muscles. Protein abundances from each of the Ctrl were also assessed by one-way ANOVA of spot volumes in 0 d, 10 d, 20 d and 30 d and no differences ($P < 0.05$) were found. Relative fold-change in abundance, not taking into account the changing muscle mass, were calculated between the Ctrl and Stim EDL for each myofibrillar proteoform (Supplementary Table S3). Similar fold-change data were also calculated in absolute terms (Supplementary Table S3). Both methods of calculation gave similar rank orders

of change and equivalent outcomes in terms of the pattern of change for each myofibrillar proteoform (Supplementary Table S3). Twelve myofibrillar proteoforms exhibited significant ($P < 0.05$) differences in abundance after 10 days of stimulation. After 20 days of stimulation the abundance of a further 3 proteins became significantly different, and by the end of the experiment period (30 d) there were 16 significant differences in protein abundance between Ctrl and Stim EDL (Figure 3.4).

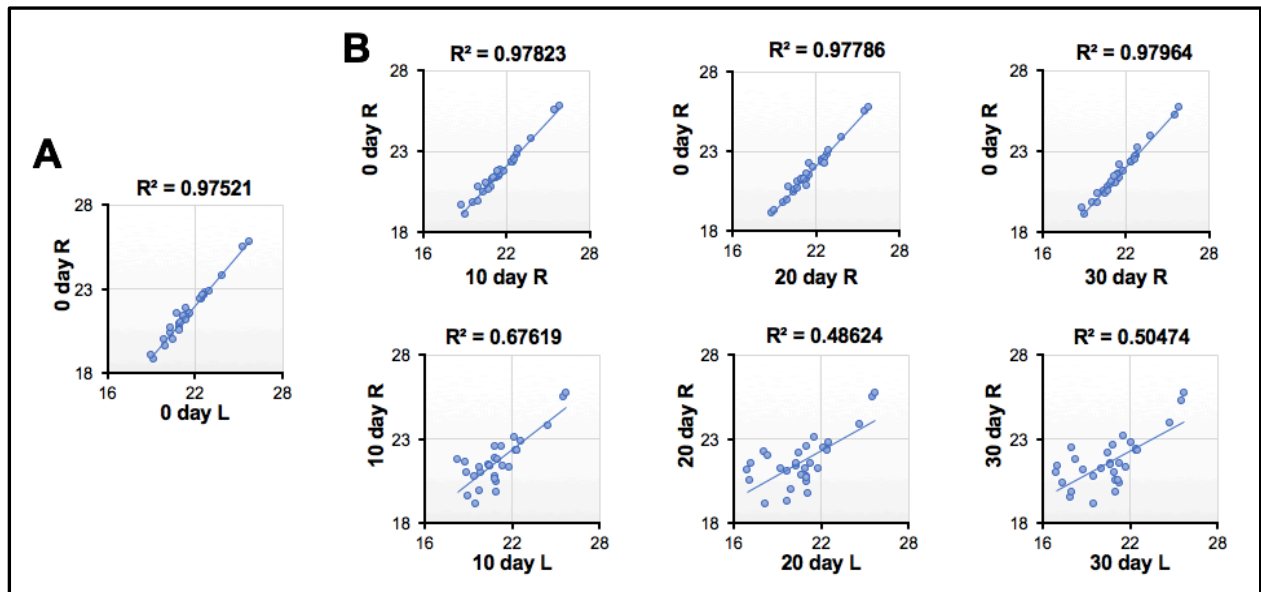


Figure 3.3. Correlation of relative myofibrillar protein abundance between stimulated and non-stimulated EDL.

Correlation matrix of normalised myofibrillar relative protein abundance (proteins 1-30 present in both stimulated and non-stimulated EDL at each time point). Correlation between (A) left and right limb of 0-day sham control. (B) Upper panels; 0-day sham control and either 10 d, 20 d or 30 d of right contralateral control limb. Lower panels; right contralateral control limb and chronic low-frequency stimulation in the left limb for either 10 d, 20 d or 30d.

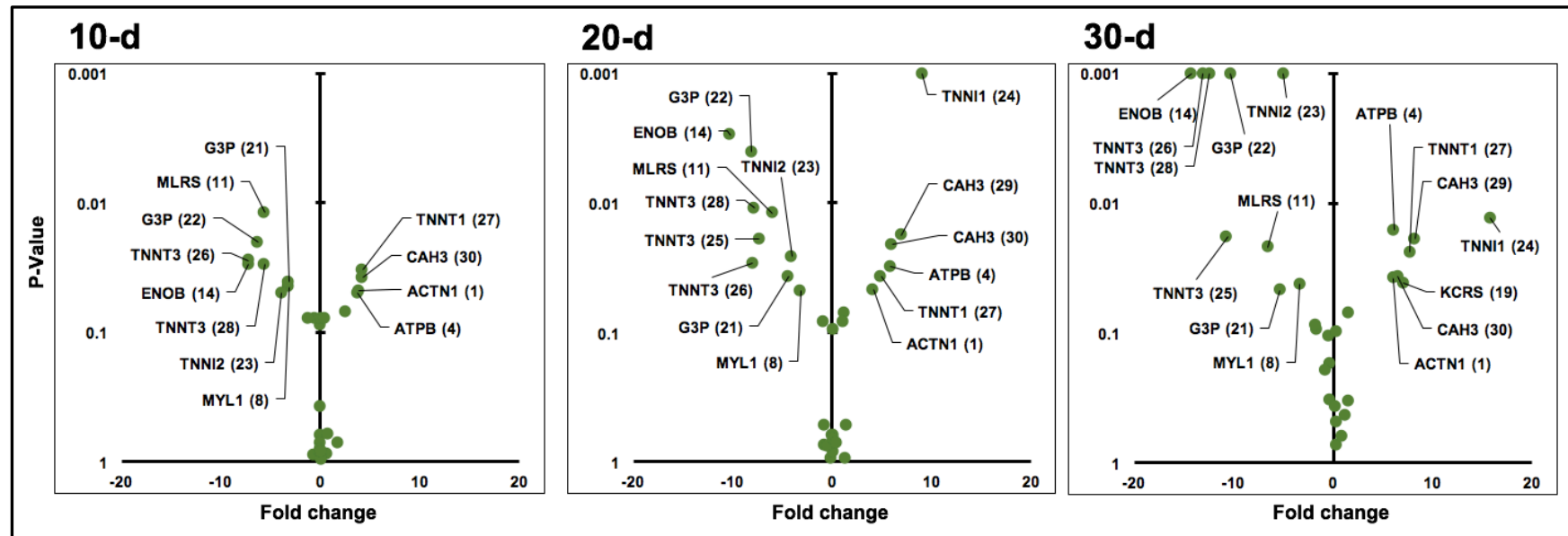


Figure 3.4. Changes in absolute abundance for the myofibrillar proteins between control and stimulated EDL muscle. Each data point represents an individual protein. Proteins that changed significantly ($P < 0.05$) determined via paired t-tests between control and stimulated muscle are labelled by their UniProt I.D. name returned using MASCOT search engine. Proteins are described as increasing, decreasing or not changing in absolute protein abundance calculated by the fold change from non-stimulated control muscle to stimulated muscle for the myofibrillar proteins only after 10 days, 20 days and 30 days of CLFS.

The changes in myofibrillar protein abundance are consistent with a shift toward a more slow-twitch phenotype in the stimulated EDL. The slow isoform of myosin essential light chain (MYL3) was absent in Ctrl EDL but was detected after 20 days of CLFS. The fast isoform of troponin T (TNNT3) was detected as three separate proteoforms (Table 3.1), these three proteoforms (spots 25, 26, 28) decreased by -12.1 ± 1.3 -fold after 30 days of CLFS. Conversely a single proteoform (spot 27) of the slow-twitch troponin T isoform (TNNT1) increased +7.7-fold in Stim muscle and two new proteoforms of troponin T slow (spots 33, 34) were detected after 20 days of CLFS.

There was no change in the absolute rate of synthesis in the non-stimulated right limb at any of the experimental time points encompassing the 30 days of CLFS. In response to CLFS, absolute rate of synthesis (ng/d) of the left, stimulated limb declined by 18 % after 10 days, 40 % after 20 days and 50 % after 30 days, consistent with the changes in muscle mass (Figure 3.1). The difference in absolute synthesis between Stim, and Ctrl EDL was statistically significant ($P < 0.05$) after 10 days, 20 days and 30 days of CLFS (Figure 3.5).

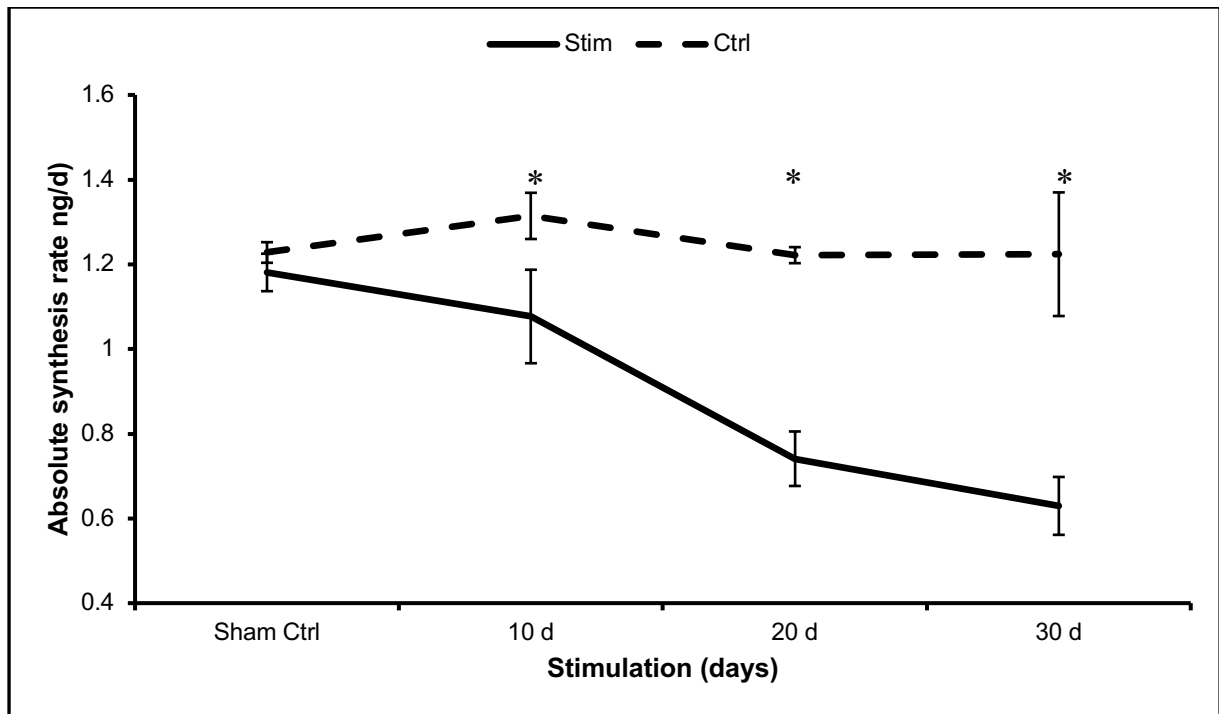


Figure 3.5. Absolute protein synthesis rates of stimulated and non-stimulated EDL. Synthesis data (ng/d) displayed as mean \pm SD (n = 3 per group) in 10-day intervals over 30 days of unilateral chronic stimulation (10 Hz) *in vivo*. Protein synthesis rates (ng/d) calculated from total protein content of the EDL in the non-stimulated control limb (broken line) and contralateral stimulated left (solid line). *P<0.05 statistically significant difference between the right and left limbs analysed by paired t-test at each time point.

In the Ctrl muscle, the 30 individual myofibrillar proteins spanned a 40-fold range in fractional synthesis rate (FSR), the protein with the highest FSR was spot 29 (CAH3) 17.02 ± 5.01 %/d and the protein with the lowest FSR was spot 2 (PLEC) 0.43 ± 0.15 %/d. This gave an average rate of mixed myofibrillar protein FSR of 4.70 ± 0.3 %/d in the Ctrl. CLFS did not increase FSR, with spot 29 (CAH3) the fastest 19.81 ± 6.88 %/d and spot 28 (TNNT3) with the slowest 0.72 ± 0.44 FSR. In the Stim muscle, the 30 myofibrillar proteins still covered a broad range (28-fold) in individual FSR with the average rate of relative protein synthesis in the Stim of mixed myofibrillar proteins of 4.97 ± 0.1 %/d. The average absolute synthesis rate (ASR) of mixed myofibrillar proteins in Ctrl muscle was 8.63 ± 0.26 pg/d and there was a broad distribution of synthesis rates (Table S4) amongst individual proteoforms, from 0.35 ± 1.06 pg/d (spot 20; ANXA4) to 76.08 ± 9.95 pg/d (spot 6; TPM4). Endurance activity tended (P =

0.145) to increase the average rate of synthesis (10.24 ± 1.63 pg/d) of mixed myofibrillar proteins, whilst the effect of stimulation on the absolute synthesis rate of individual proteoforms was statistically more robust. Twelve myofibrillar proteoforms exhibited significant ($P < 0.05$) differences in synthesis rate between Ctrl and Stim muscle. The greatest change in absolute synthesis rate was, spot 4: ATP synthase subunit beta (ATPB), which increased ($P = 0.001$) from 22.44 ± 1.55 pg/d to 40.02 ± 2.09 pg/d after 30 days of CLFS (Table S4). This increase in synthesis was also matched by a 6.2-fold increase ($P = 0.016$) in abundance between Ctrl to Stim muscle. In summary, top-down analysis of myofibrillar proteoforms revealed that a total of 16 proteins responded to CLFS by changing in abundance significantly ($P < 0.05$). In total, 7 increased in abundance and 9 decreased in abundance. These changes in abundance were associated with 6 different patterns of regulation in individual protein turnover that are summarised in Figure 3.6 and illustrated in further detail in Figures 3.7 and 3.8.

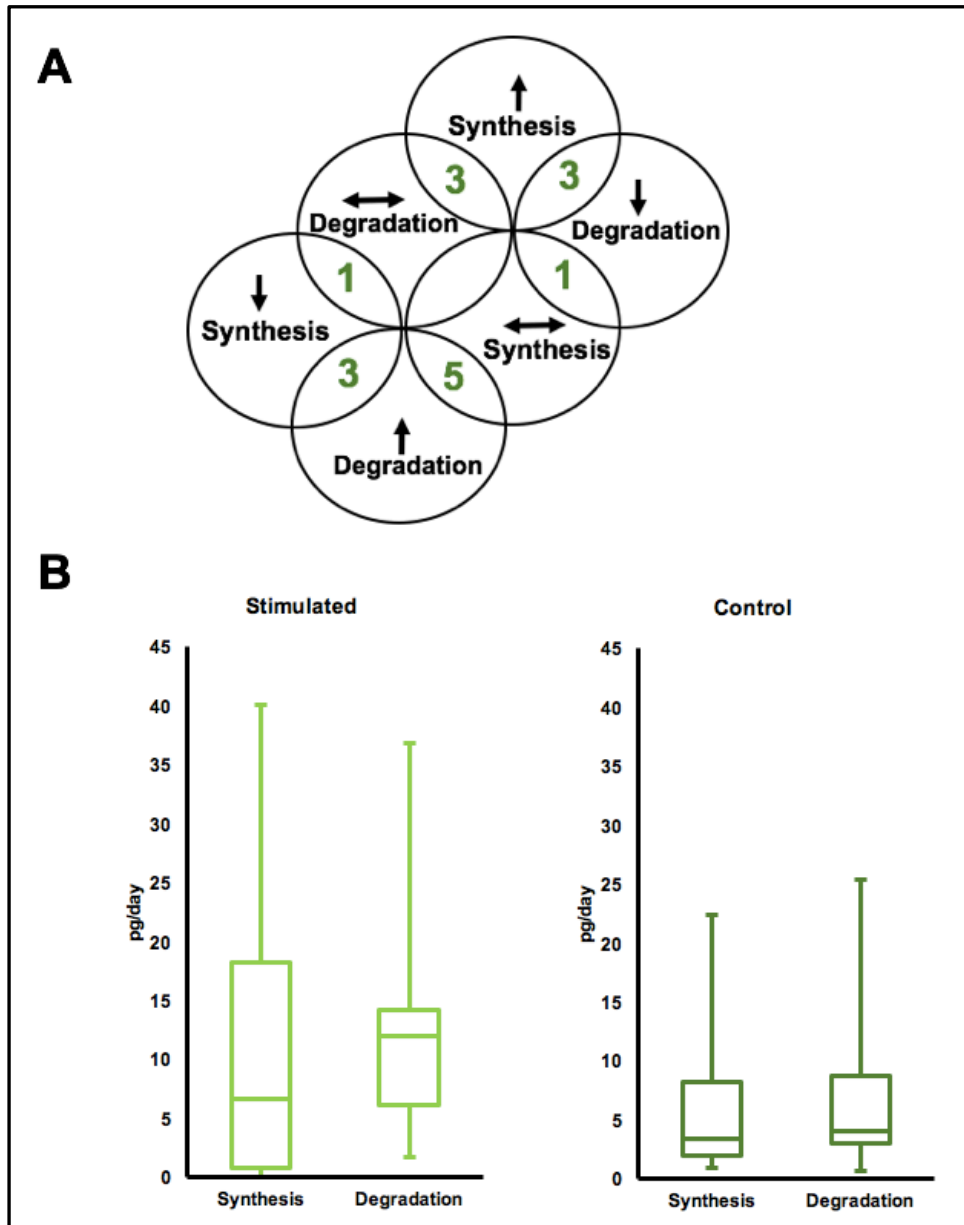


Figure 3.6. Contributions of synthesis and degradation to changes in abundance of myofibrillar proteins.

Mean protein turnover data is shown as absolute values for all myofibrillar proteins that exhibit a significant ($P < 0.05$) change in abundance from the control muscle to the 30-d stimulated muscle. (A) Venn diagram displays the number of myofibrillar proteins that show different responses in protein turnover: increases (\uparrow), decreases (\downarrow) or no change (\leftrightarrow) for synthesis and degradation in order to change their net abundance after 30 days of stimulation. (B) Box and whisker plot of data from proteins displayed panel A. The left panel shows the range of synthesis and degradation rates in picograms per day for the 30-d stimulated muscle only. The box and whisker plot on

the right shows the range of synthesis and degradation rates in picograms per day for the control muscle only.

In the myofibrillar fraction, 7 proteins increased, and 9 proteins decreased in abundance after CLFS. The increase in abundance of ATPB (spot 4), TNNT1 (spot 27) and CAH3 (spot 30) was entirely accounted for by the greater rate of synthesis in Stim compared to Ctrl muscle. The increase in abundance of KCRS (spot 19), TNNI1 (spot 24) and CAH3 (spot 29) was partially accounted for by the greater synthesis rate, whereas ACTN1 (spot 1) became more abundant in Stim muscle without a detectable change in synthesis (Figure 3.7). The decrease in abundance of TNNI2 (spot 23) was entirely accounted for by a decrease in the rate of synthesis in Stim compared to Ctrl muscle. The decrease in abundance of ENOB (spot 14) and TNNT3 (spot 26 and 28) was partially accounted for by a decreased synthesis rate, whereas MYL1 (spot 8), MLRS (spot 11), G3P (spot 21 and 22) and TNNT3 (spot 25) became less abundant in Stim muscle without a detectable change in synthesis (Figure 3.8).

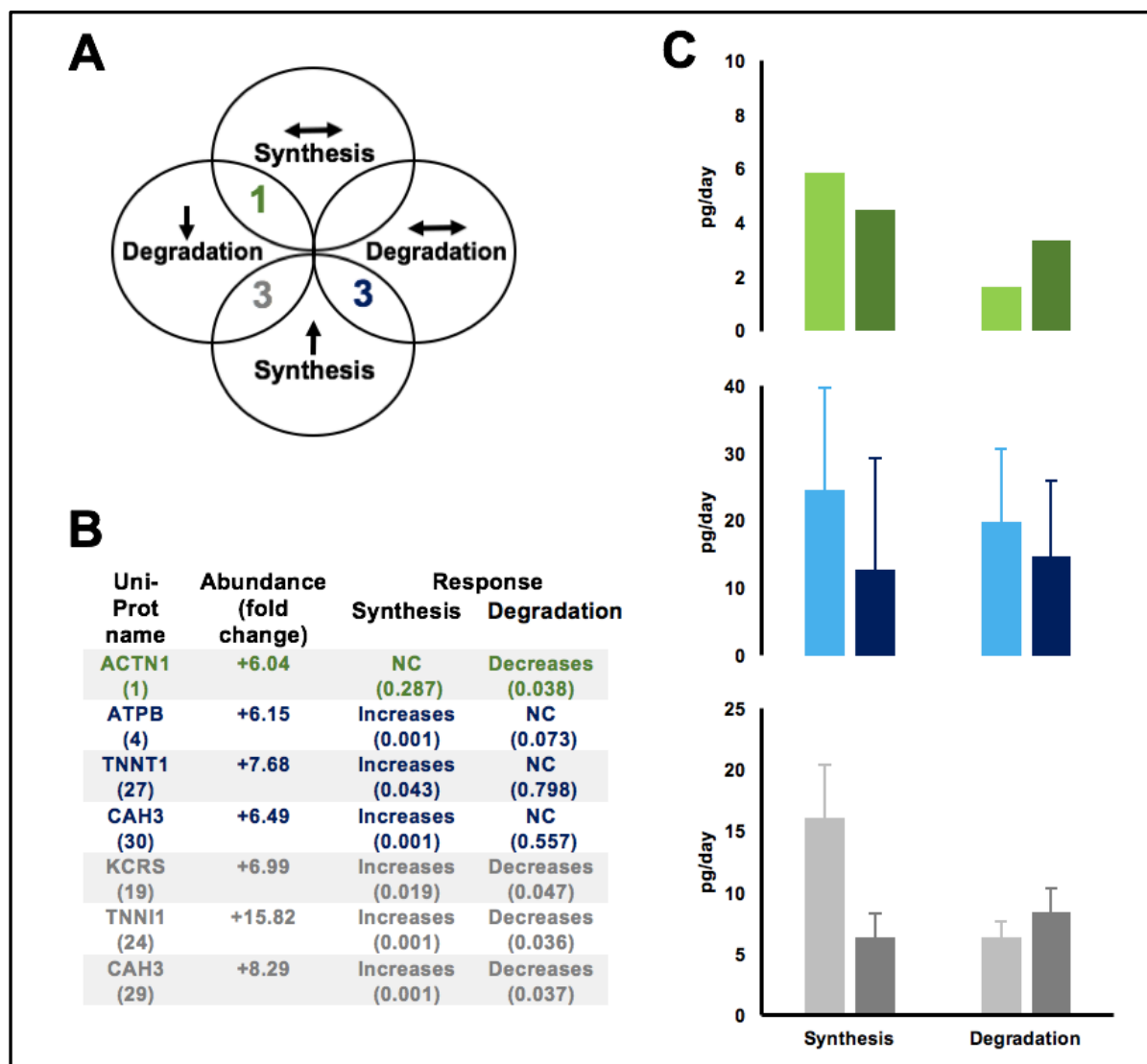


Figure 3.7. Protein turnover responses of myofibrillar proteins that increased in abundance.

Mean protein turnover data is shown in absolute terms (pg/d) for myofibrillar proteins that exhibit a significant ($P < 0.05$) increase in abundance between the control and stimulated muscle at the 30-d time point. (A) Venn diagram displays the number of myofibrillar proteins that show different responses in protein turnover: increases (\uparrow), decreases (\downarrow) or no change (\leftrightarrow) for synthesis and degradation in order to increase their net abundance after 30 days of stimulation. (B) Uni-Prot name relates to the protein I.D. using the Uni-Prot database, entries returned using the MASCOT search engine (number relates to the spot number in Figure 3.2). The response is described for both synthesis and degradation with significance level (P-value) for each protein which corresponds with the Venn diagram in panel A. (C) Summary of proteins identified in panel B, grouped and colour coded by their protein turnover responses.

Green text in panel B represent data in green in panel C etc. Data are displayed for absolute synthesis and degradation in picograms per day as mean \pm SD for each collective group (n = 3). The light-coloured bars represent the 30-d stimulated muscle and the darker coloured bars represent the control muscle.

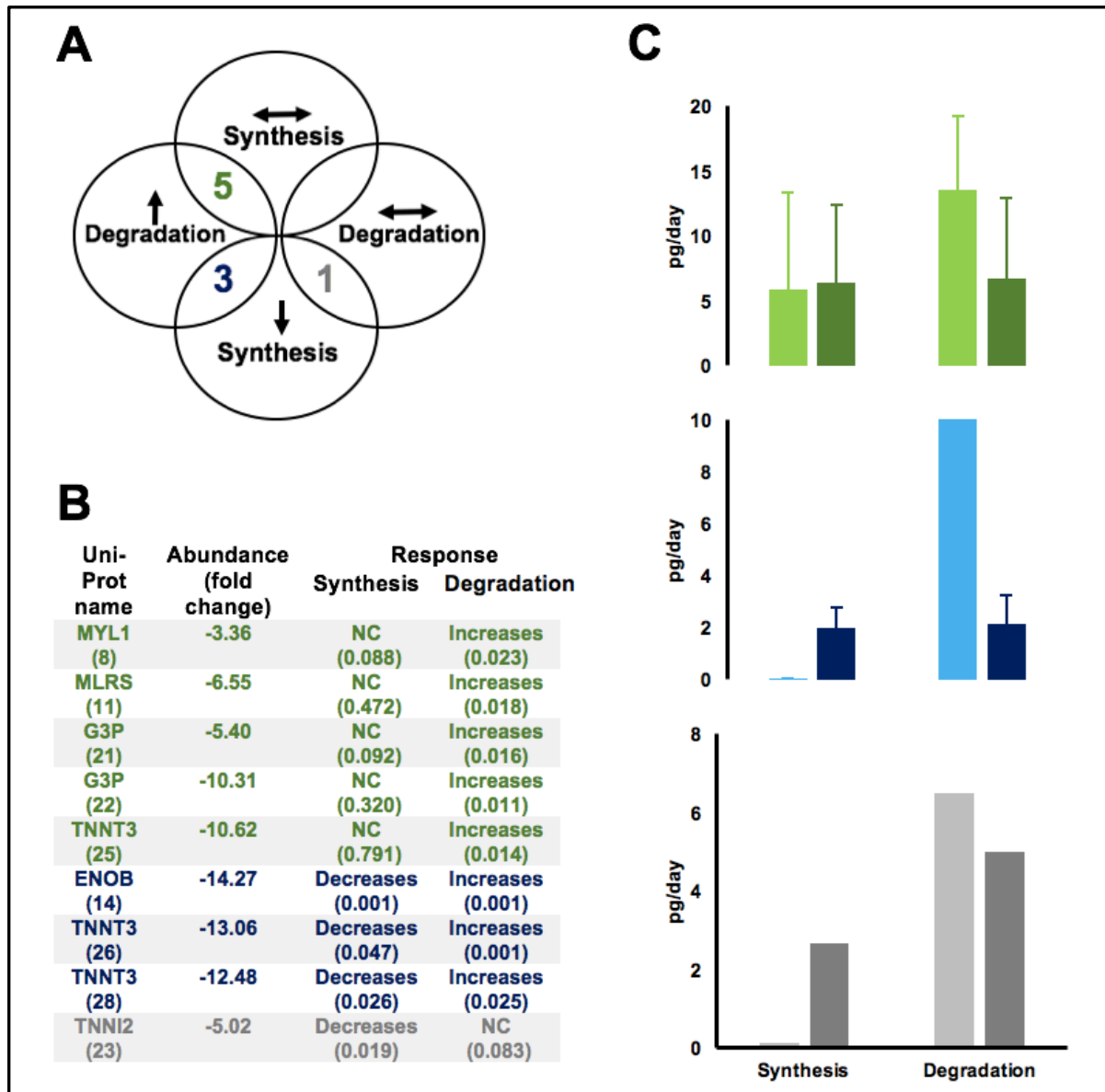


Figure 3.8. Protein turnover responses of myofibrillar proteins that decreased in abundance.

Mean protein turnover data is shown in absolute terms (pg/d) for myofibrillar proteins that exhibit a significant ($P < 0.05$) decrease in abundance between the control and stimulated muscle at the 30-d time point. (A) Venn diagram displays the number of myofibrillar proteins that show different responses in protein turnover: increases (\uparrow),

decreases (\downarrow) or no change (\leftrightarrow) for synthesis and degradation in order to decrease their net abundance after 30 days of stimulation. (B) Uni-Prot name relates to the protein I.D. using the Uni-Prot database, entries returned using the MASCOT search engine (number relates to the spot number in Figure 3.2). The response is described for both synthesis and degradation with significance level (P-value) for each protein which corresponds with the Venn diagram in panel A. (C) Summary of proteins identified in panel B, grouped and colour coded by their protein turnover responses. Green text in panel B represent data in green in panel C etc. Data is displayed for absolute synthesis and degradation in picograms per day as mean \pm SD for each collective group (n = 3). The light-coloured bars represent the 30-d stimulated muscle and the darker coloured bars represent the control muscle.

Figure 3.9 illustrates absolute synthesis and abundance data for myosin regulatory light chain (MLRS) proteoforms (spots 11 and 12) calculated in 10-day intervals. In Ctrl muscle, there was no significant change ($P = 0.69 \pm 0.02$) in abundance of either proteoform of MLRS (spot 11 and 12) at any of the experimental time points. In Stim muscle, the absolute abundance of spot 11 decreased (-5.5 ± 0.8 -fold change, $P = 0.001$) after 10 days, (-6.0 ± 1.3 -fold change, $P = 0.018$) after 20 days and (-6.6 ± 2.9 -fold change, $P = 0.022$) after 30 days of stimulation. However, the absolute synthesis of MLRS spot 11 did not change ($P = 0.472$) in response to stimulation, and was 7.52 ± 1.34 pg/d in Stim and 9.28 ± 3.06 pg/d in Ctrl (calculated using semi-log plot of all 4 data points). Absolute synthesis (Stim and Ctrl, respectively) calculated using the 2-point method was 6.11 ± 2.38 ; 5.93 ± 1.07 pg/d at 0-10 d, 4.76 ± 1.33 ; 4.33 ± 0.62 pg/d at 10-20 d and 5.58 ± 1.92 ; 4.41 ± 1.89 pg/d at 20-30 days.

This response was specific to the spot 11 proteoform. The proteoform of MLRS in spot 12 tended ($P = 0.100$) to exhibit the opposite response to stimulation and increased in abundance by 0.8 ± 1.6 -fold change over the 30-day stimulation period. The rate of synthesis (Ctrl: 15.1 ± 1.6 pg/d and Stim: 10.26 ± 5.3 pg/d) of MLRS proteoform 12 was not different ($P = 0.083$) between Ctrl and Stim muscles.

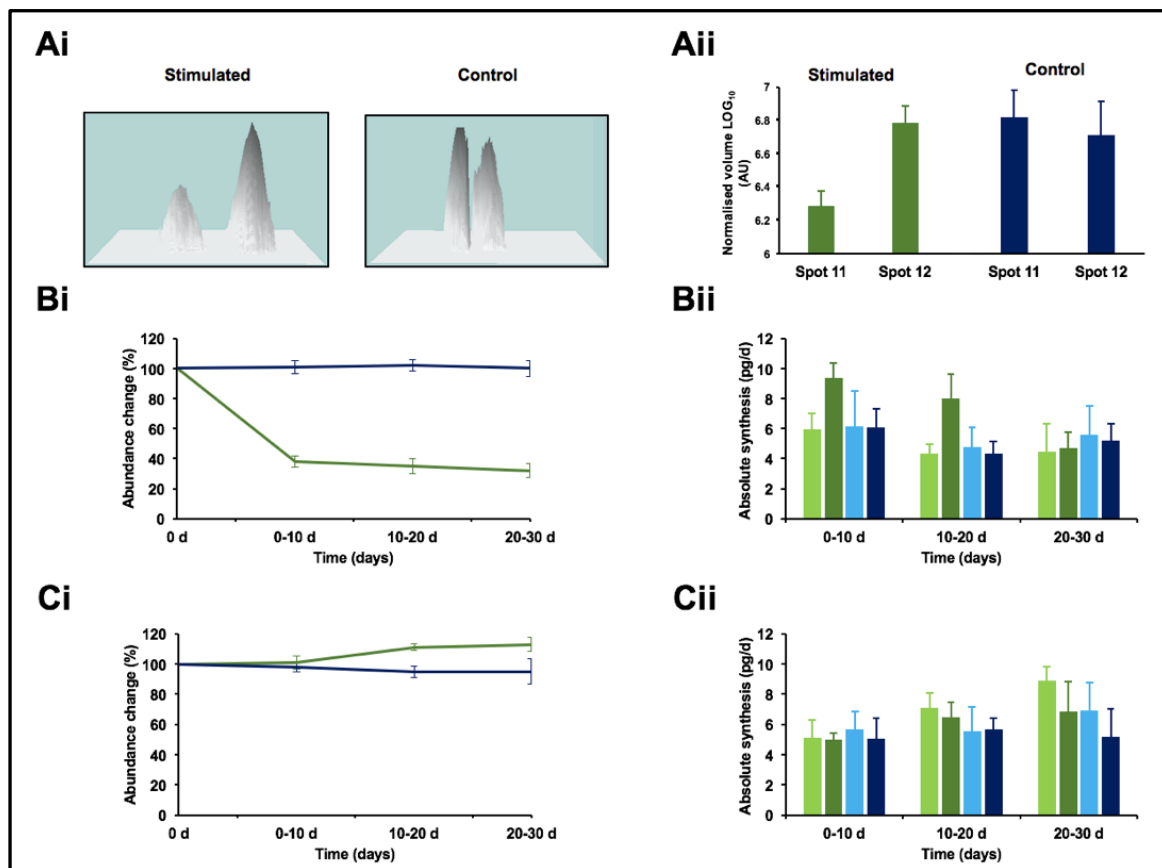


Figure 3.9. Changes in Myosin regulatory light chain (MLRS) proteoform distribution. Abundance and protein turnover of spots 11 and 12, in the stimulated (L) and non-stimulated control (R) limb over 30 days of chronic low-frequency (10 Hz) stimulation *in vivo*.

(Ai) 3D representations of spot volumes (abundance) presented for spot 11 and 12 in control and stimulated samples. Spot numbers correspond to Figure 3.2 and Table 3.1. (Aii) The normalised volume (AU) of spot 11 (M_r , ~19 kDa, pI ~4.2) was significantly ($P < 0.05$) less after 30 days of stimulation; whilst an increase (NS) was observed in the abundance of neighbouring spot 12 (M_r , ~19 kDa, pI ~4.7) in response to 30 days of stimulation. Data presented as mean \pm SD, dark green bars represent the stimulated muscle and dark blue bars represent the control muscle. (B, C) All data is displayed as mean \pm SD in 10-day intervals over 30 days of chronic stimulation. Each 10-day interval corresponds to an independent group of rats ($n = 3$). (Bi, Ci) The lines represent percent changes in abundance, the dark green lines represent the stimulated muscle and the dark blue lines represent non-stimulated control muscle. (Bii, Cii) Bars represent absolute protein synthesis and degradation rates in picograms per day. (B) Data for the most acidic proteoform of MLRS (spot 11). Protein synthesis

for the stimulated limb (light green bars) shows no change (NS) from 0 days – 30 days of stimulation when compared to the non-stimulated limb (light blue bars). Protein degradation shows a significant ($P < 0.05$) increase in the stimulated limb (dark green bars) at each 10-day interval compared to the non-stimulated limb (dark blue bars). (C) Data for the most basic proteoform of MLRS (spot 12). Protein synthesis for the stimulated limb (light green bars) shows no change (NS) from 0 days – 30 days of stimulation when compared to the non-stimulated limb (light blue bars). Protein degradation shows no change in the stimulated limb (dark green bars) at each 10-day interval compared to the non-stimulated limb (dark blue bars).

Site-specific post-translational modifications of MLRS were investigated by LC-MS/MS analysis of spots 11 and 12. A sequence coverage of 92 % (mowse score 1770) was achieved and error tolerant searches of the MS/MS spectra unambiguously identified serine 16 phosphorylation in both spot 11 and spot 12. Spot 11 also contained site-specific phosphorylation of serine 20 that was not detected in spot 12 (Figure 3.10).

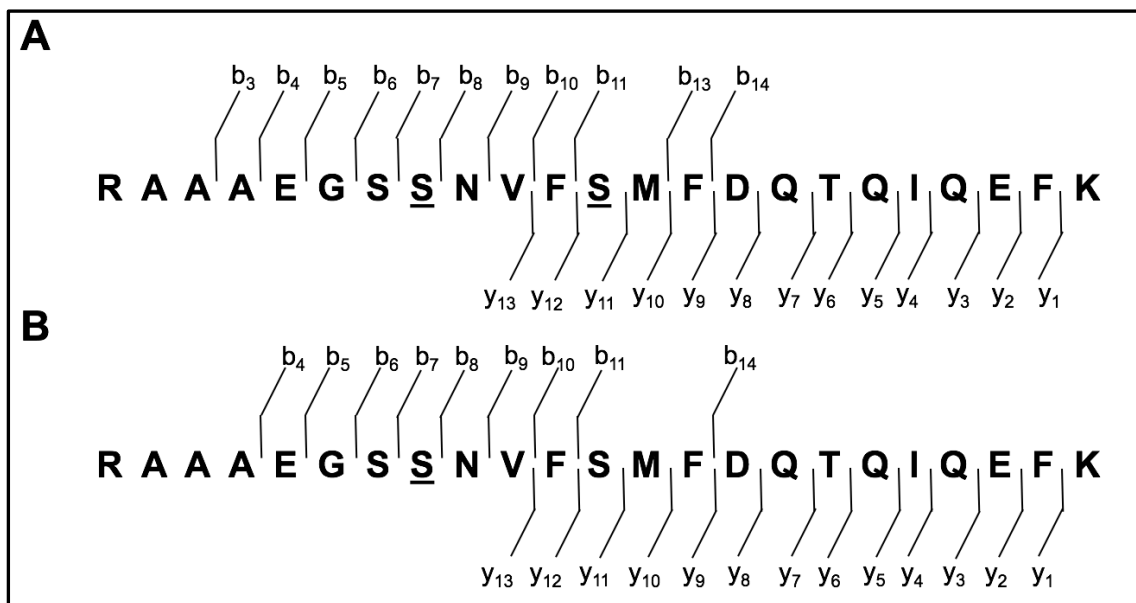


Figure 3.10. Myosin regulatory light chain site-specific phosphorylation.

(A) The amino acid sequence at residues 9-31 of spot 11 MLRS. The underlined amino acid highlight the phosphorylation at serine 16 and 20. In particular the b_7 and b_8 ions provide unambiguous evidence of serine 16 phosphorylation and b_{11} , y_{12} and b_{13} , y_{11} ions provide unambiguous evidence of serine 20 phosphorylation of spot 11 MLRS. (B) The amino acid sequence at residues 9-31 of spot 12 MLRS. The underlined amino

acid highlight the phosphorylation at serine 16. In particular, the b_7 and b_8 ions provide unambiguous evidence of serine 16 phosphorylation of spot 12 MLRS.

LC-MS/MS analysis of the soluble muscle proteins yielded a list of 47 proteins (Supplementary Table S2) that had at least one protein-specific peptide that could be detected in all ($n = 24$) Ctrl and Stim samples. The majority of proteins were enzymes of either mitochondrial/oxidative metabolism or glycolysis/anaerobic metabolism (Supplementary Table S2). The reproducibility of protein abundance measurements by label-free quantitation was good (coefficient of variation 2.9 ± 0.12 %, $n = 3$ biological replicates) and the abundance each protein in Ctrl and Stim muscles is reported in supplementary Table S5.

Similar to the analysis of myofibrillar proteoforms, there was a high correlation ($R^2 = 0.99024$; $P = 0.001$) in the abundance of soluble proteins between the Ctrl and the sham-operated muscle at the 0-day time point. There was also no significant difference ($P = 0.753$) in the abundance of soluble proteins in the Ctrl EDL (Figure 3.11, upper panels), assessed by one-way ANOVA of normalised peak abundances in 0 d, 10 d, 20 d and 30 d samples. Relative fold changes in abundance were calculated between the Ctrl and Stim EDL for each soluble protein (Supplementary Table S5). Similar fold change calculations for the soluble proteins were also used to calculate fold changes in abundance in absolute terms (Supplementary Table S5). Both calculations gave similar rank orders of change and equivalent patterns of change for each soluble protein (Supplementary Table S3). Figure 3.12 illustrates the changes in absolute abundance of the soluble muscle proteins induced by CLFS. From the 47 soluble proteins; 4 proteins exhibited significant ($P < 0.05$, $FDR < 0.1$ %) differences in abundance after 10 days of stimulation, and after 20 days of stimulation the abundance of a further 7 proteins became significantly different. By the end of the experiment period (30 d) there were 34 significant differences in protein abundance between the Stim and Ctrl EDL (Figure 3.12).

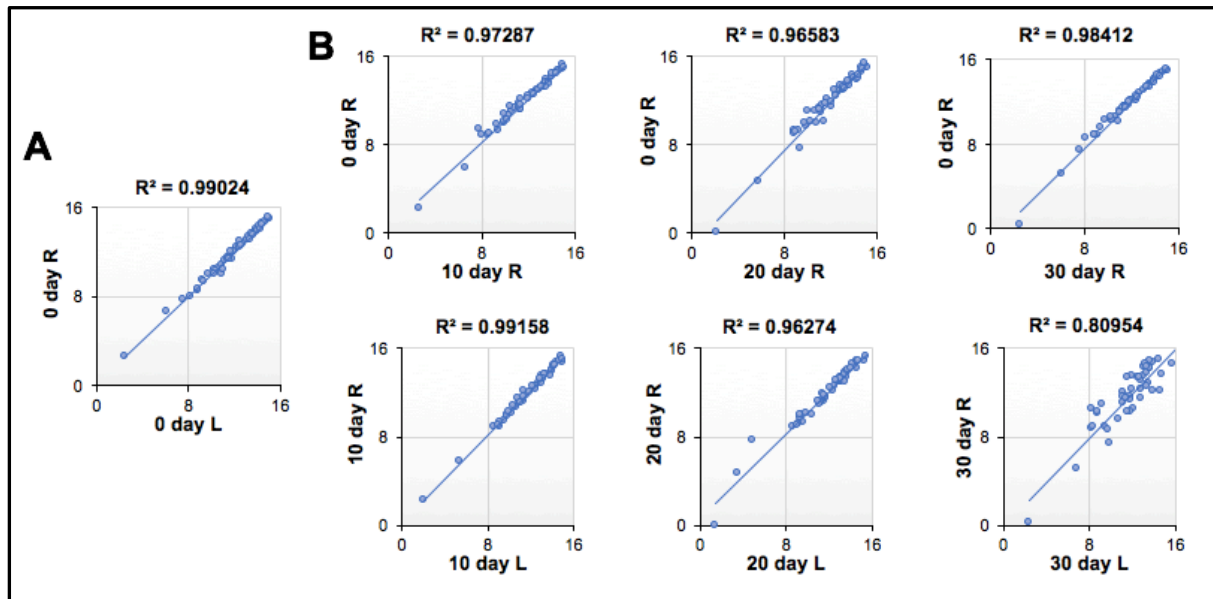


Figure 3.11. Correlation of relative soluble protein abundance between stimulated and non-stimulated EDL.

Correlation matrix of relative soluble protein abundance (proteins 1-47 present in both stimulated and non-stimulated EDL at each time point). Correlation between (A) left and right limb of 0-day sham control. (B) Upper panels; 0-day sham control and either 10 d, 20 d or 30 d of right contralateral control limb. Lower panels; right contralateral control limb and chronic low-frequency stimulation in the left limb for either 10 d, 20 d or 30d.

Data are presented as normalised peak abundances. Data was also assessed by one-way ANOVA of spot volumes in 0 d, 10 d, 20 d and 30 d samples.

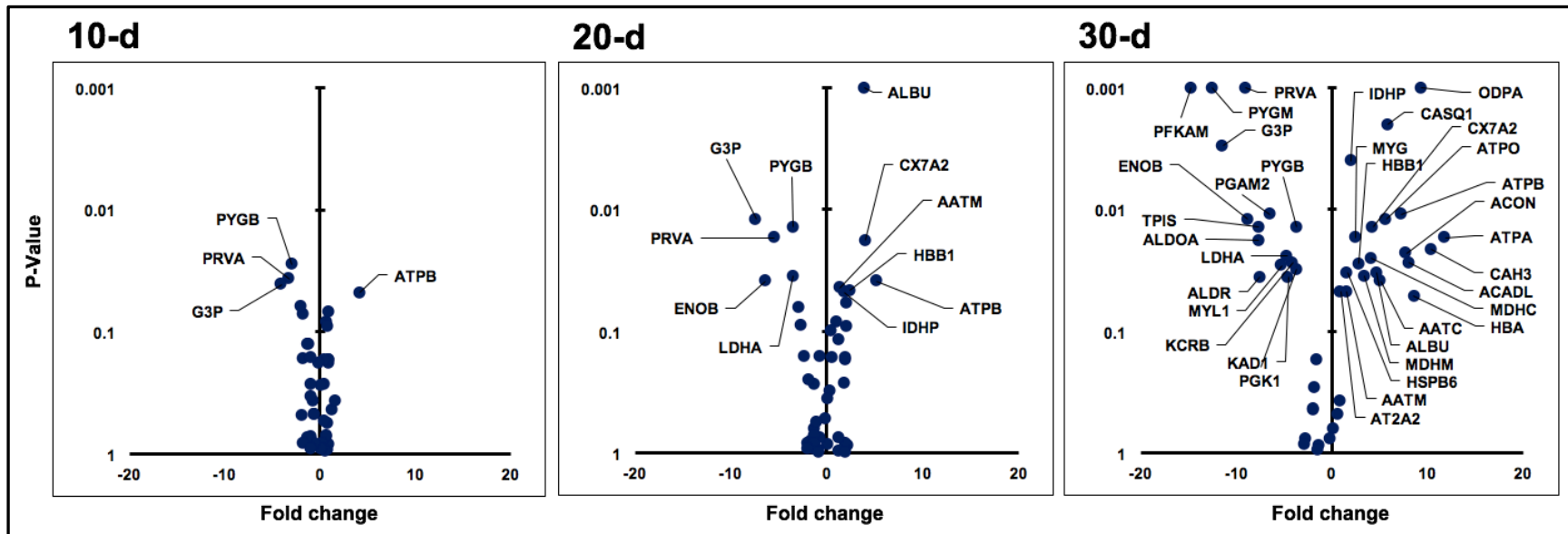


Figure 3.12. Changes in absolute abundance for the soluble proteins between control and stimulated EDL muscle. Each data point represents an individual protein. Proteins that changed significantly ($P < 0.05$) determined via paired t-tests between control and stimulated muscle are labelled by their UniProt I.D. name returned using MASCOT search engine. Proteins are described as increasing, decreasing or not changing in absolute protein abundance calculated by the fold change from non-stimulated control muscle to stimulated muscle for the soluble proteins only after 10 days, 20 days and 30 days of CLFS.

After 30 days of CLFS, of the 12 mitochondrial proteins identified, 11 became more ($P < 0.05$ abundant ($+5.91 \pm 3.21$ -fold) and of the 12 proteins identified that are associated with glycolysis, 10 became less ($P < 0.05$) abundant (-8.14 ± 3.79 -fold). In addition, CLFS increased ($P = 0.017$) the abundance ($+2.49 \pm 1.1$ -fold) of the oxygen transport protein myoglobin (MYG) from Ctrl to Stim muscle (Supplementary Figure S1). Whereas, proteins of high-energy phosphate metabolism, including muscle creatine kinase B-type (KCRB) and adenylate kinase isoenzyme 1 (KAD1), became less abundant (-4.10 ± 1.9 -fold, $P = 0.027$; -4.51 ± 1.2 -fold, $P = 0.036$) in Stim EDL, respectively (Supplementary Figure S3). The calcium binding protein parvalbumin alpha (PRVA) decreased in abundance (-9.10 ± 2.5 -fold, $P = 0.001$) and the slow-twitch isoform of sarcoplasmic/endoplasmic reticulum calcium ATPase (AT2A2) increased in abundance ($+0.93 \pm 0.8$ -fold, $P = 0.047$) in response to CLFS (Supplementary Figure S2).

In the Ctrl muscle, the 47 individual soluble proteins spanned a 18-fold range in fractional synthesis rate (FSR), the protein with the highest FSR was CAH3 14.83 ± 4.01 %/d and the protein with the lowest FSR was AATC 0.81 ± 0.16 %/d. This gave an average rate of mixed soluble protein FSR of 5.17 ± 0.04 %/d in the Ctrl. CLFS did not change FSR with CAH3 the fastest 17.20 ± 6.80 %/d and G3P with the slowest 0.74 ± 0.47 FSR. In the Stim muscle, the 47 soluble proteins still covered a broad range (23-fold) in individual FSR with the average rate of relative protein synthesis in the Stim of mixed soluble proteins of 5.43 ± 0.39 %/d. The average rate of absolute protein synthesis (ASR) in the Ctrl of mixed soluble proteins was 43.70 ± 0.07 pg/d, based on $n = 3$ biological replicates. The distribution of individual proteins in the control muscle spanned from 0.82 ± 0.29 pg/d (G3P) to 112.65 ± 8.91 pg/d (ALDOA). Chronic low-frequency stimulation increased ($P = 0.001$) the average (60.17 ± 0.73 pg/d) synthesis rate of mixed soluble proteins. The range of synthesis rates (Table S6) was also broader in Stim compared Ctrl muscle. The lowest synthesis rate in Stim muscle was 0.04 ± 0.03 pg/d (G3P) and the greatest was 173.69 ± 5.21 pg/d (ATPB). Proteins that exhibited the greatest synthesis responses to endurance activity include ATPA which increased ($P = 0.001$) from 33.89 ± 6.46 pg/d to 136.51 ± 4.12 pg/d and TPIS which decreased ($P = 0.014$) from 50.13 ± 11.53 pg/d to 3.21 ± 2.49 pg/d after 30 days of CLFS.

In summary, bottom-up analysis of soluble proteins detected protein-specific responses to endurance activity that were consistent with the changes found by top-

down analysis of myofibrillar proteoforms. A total of 34 proteins exhibited a statistically significant change in protein abundance (Table S5) in response to chronic endurance activity. Twenty proteins increased and 14 proteins decreased in abundance. These changes in protein abundance were associated with 7 different patterns of regulation in protein turnover (Figure 3.13).

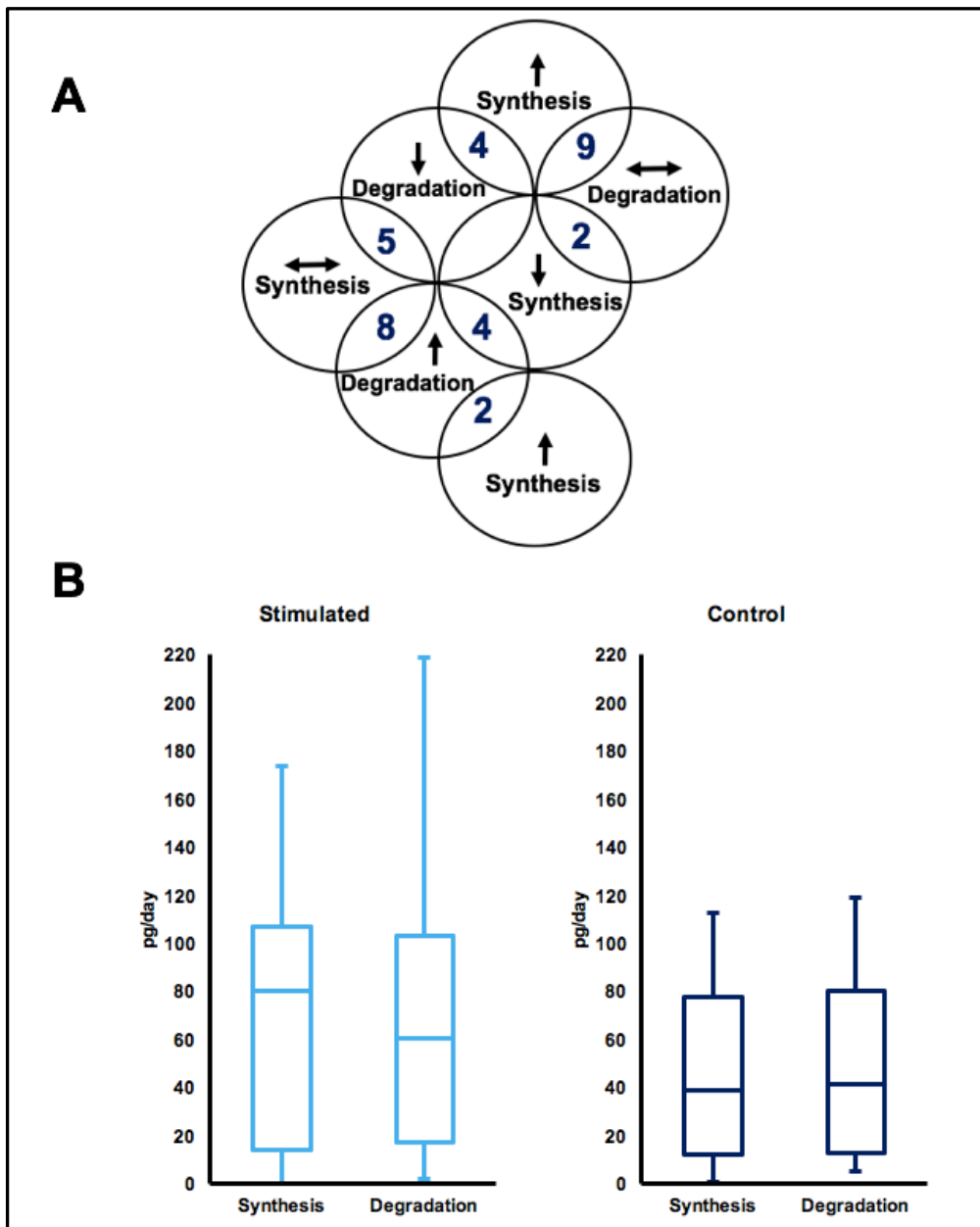


Figure 3.13. Different patterns in protein turnover response of soluble muscle proteins.

Mean protein turnover data is shown as absolute values for all soluble proteins that

exhibit a significant ($P < 0.05$) change in abundance from the control muscle to the 30-d stimulated muscle. (A) Venn diagram displaying the number of soluble proteins that exhibit different responses in protein turnover, including: increases (\uparrow), decrease (\downarrow) or no change (\leftrightarrow) in synthesis and degradation in order to change their net abundance after 30 days of stimulation. (B) The data displayed here are all the proteins from panel A. The box and whisker plot on the left shows the range of synthesis and degradation rates in picograms per day for the 30-d stimulated muscle only for all soluble proteins that have significantly different abundance from control to stimulated muscle. The box and whisker plot on the right shows the range of synthesis and degradation rates in picograms per day for the control muscle only for all soluble proteins that have significantly different abundance from control to stimulated muscle.

Figure 3.14 illustrates four separate responses amongst the 11 mitochondrial proteins that increased ($P < 0.05$) in abundance in Stim muscle. The increase in abundance of AATM, ACADL, ATPA and ATPB was entirely accounted for by the greater rate of synthesis in Stim compared to Ctrl muscle. The increase in abundance of ACON, ATPO, ODPA and MDHC was partially accounted for by the greater synthesis rate, whereas CX7A2, IDHP and MDHM became more abundant in Stim muscle without a detectable change in synthesis rate (Figure 3.14).

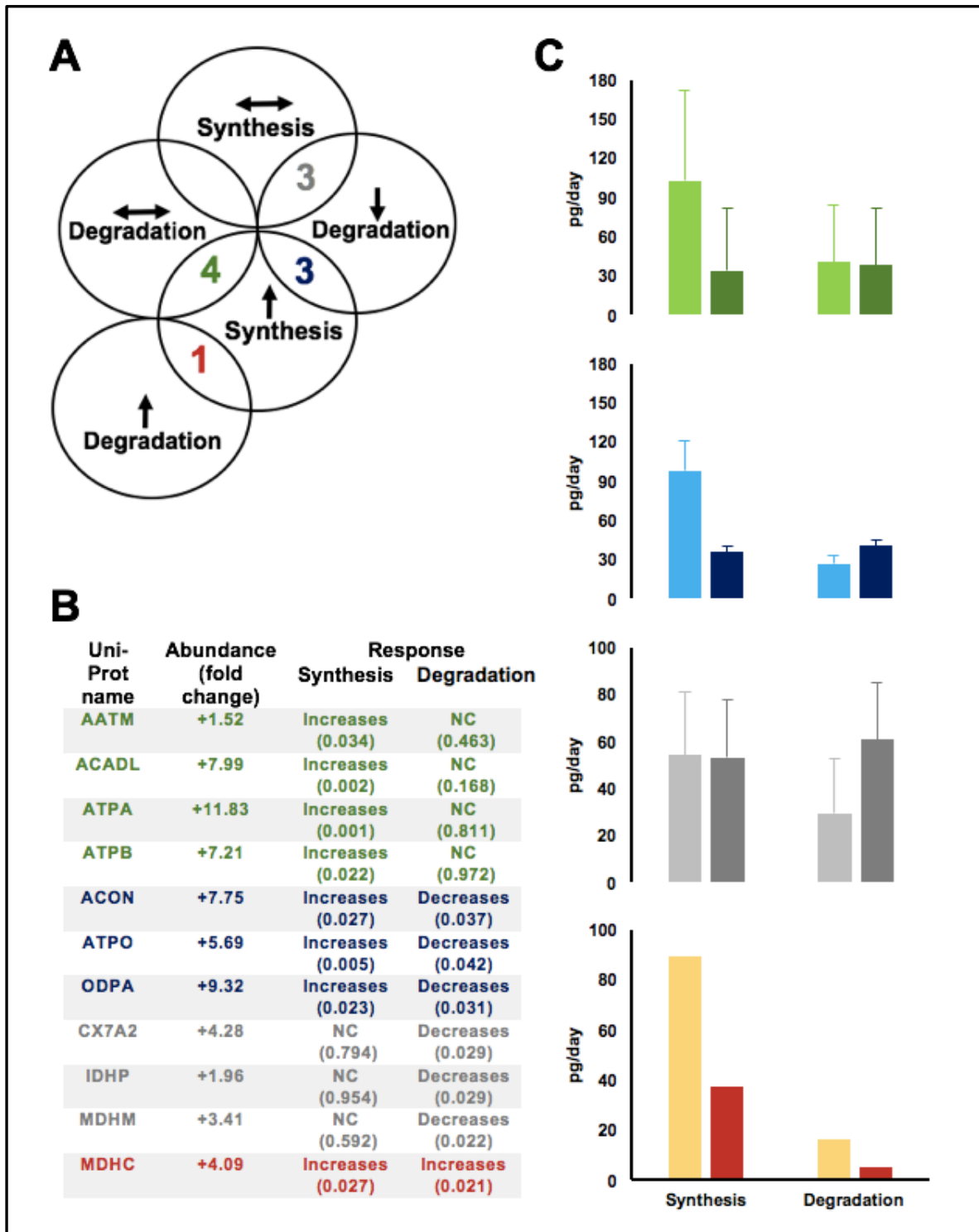


Figure 3.14. Protein turnover responses of mitochondrial proteins that increased in abundance.

Mean protein turnover data is shown in absolute terms (pg/d) for mitochondrial proteins that exhibit a significant ($P < 0.05$) increase in abundance between the control and stimulated muscle at the 30-d time point. (A) Venn diagram displays the number of mitochondrial proteins that show different responses in protein turnover: increases

(↑), decreases (↓) or no change (↔) for synthesis and degradation in order to increase their net abundance after 30 days of stimulation. (B) Uni-Prot name relates to the protein I.D. using the Uni-Prot database, entries returned using the MASCOT search engine (number relates to the spot number in Figure 3.2). The response is described for both synthesis and degradation with significance level (P-value) for each protein which corresponds with the Venn diagram in panel A. (C) Summary of proteins identified in panel B, grouped and colour coded by their protein turnover responses. Green text in panel B represent data in green in panel C etc. Data is displayed for absolute synthesis and degradation in picograms per day as mean ± SD for each collective group (n = 3). The light-coloured bars represent the 30-d stimulated muscle and the darker coloured bars represent the control muscle.

Figure 3.15 details the patterns of change amongst proteins of glycolysis that decreased ($P < 0.05$) in abundance in response to CLFS. The decrease in abundance of PYGB was entirely accounted for by a decrease in the rate of synthesis in Stim compared to Ctrl muscle. The decrease in abundance of ENOB, G3P, PFKAM and TPIS was partially accounted for by a decreased synthesis rate, whereas ALDOA, LDHA, PGAM2, PGK1 and PYGM became less abundant in Stim muscle without a detectable change in synthesis (Figure 3.15).

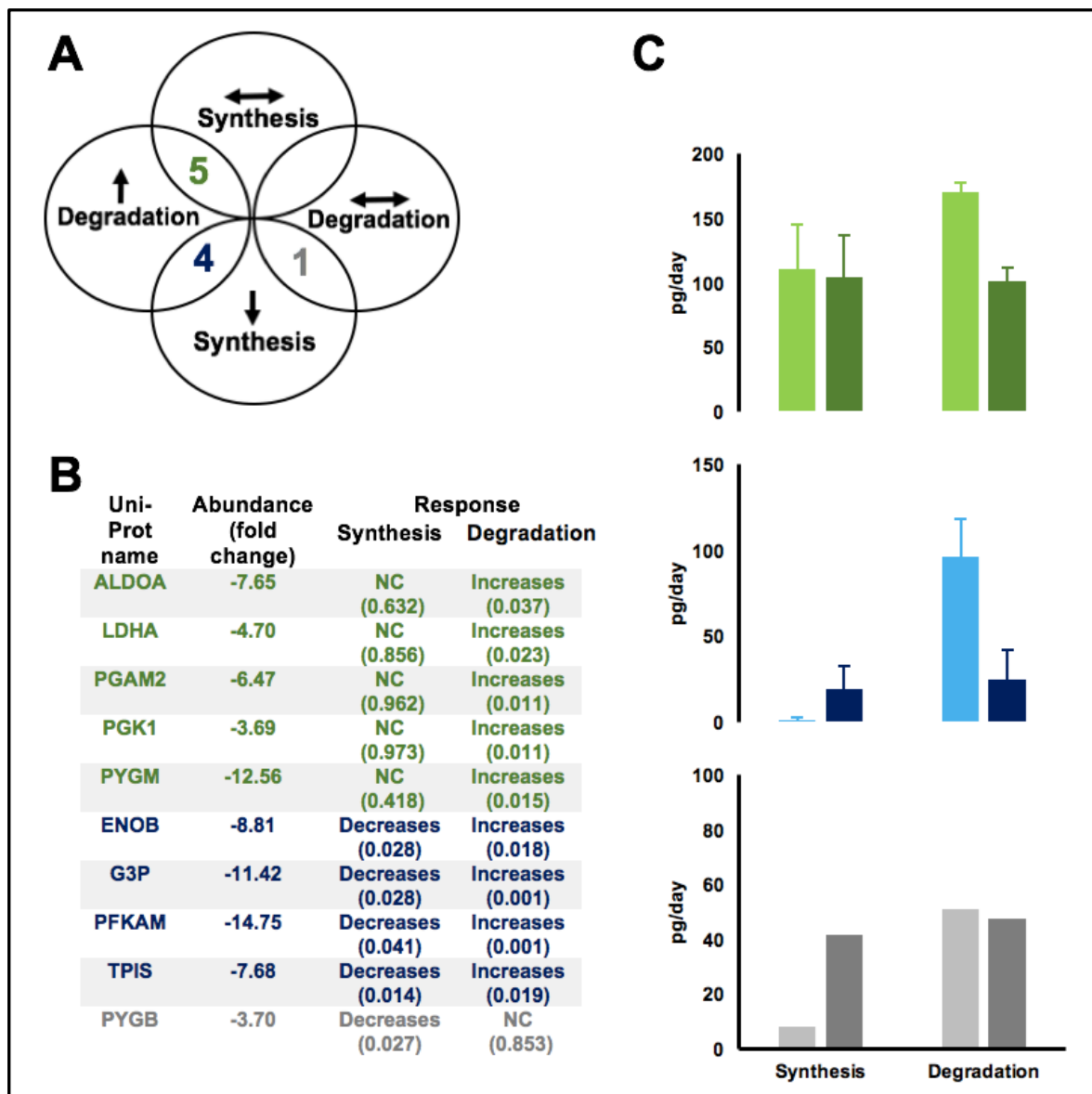


Figure 3.15. Protein turnover responses of glycolysis proteins that decreased in abundance.

Mean protein turnover data is shown in absolute terms (pg/d) for glycolysis proteins that exhibit a significant ($P < 0.05$) decrease in abundance between the control and stimulated muscle at the 30-d time point. (A) Venn diagram displays the number of glycolysis proteins that show different responses in protein turnover: increases (\uparrow), decreases (\downarrow) or no change (\leftrightarrow) for synthesis and degradation in order to decrease their net abundance after 30 days of stimulation. (B) Uni-Prot name relates to the protein I.D. using the Uni-Prot database, entries returned using the MASCOT search engine (number relates to the spot number in Figure 3.2). The response is described for both synthesis and degradation with significance level (P-value) for each protein which corresponds with the Venn diagram in panel A. (C) Summary of proteins

identified in panel B, grouped and colour coded by their protein turnover responses. Green text in panel B represent data in green in panel C etc. Data is displayed for absolute synthesis and degradation in picograms per day as mean \pm SD for each collective group (n = 3). The light-coloured bars represent the 30-d stimulated muscle and the darker coloured bars represent the control muscle.

3.5 Discussion

Skeletal muscle is renowned for its malleability, particularly in response to changes in activity pattern associated with exercise training. Adaptations of the muscle proteome, including an increase in mitochondrial proteins induced by endurance exercise, are well-established and contribute to the health benefits of a physically active lifestyle (Coffey and Hawley, 2007). Nevertheless, the dynamic processes that govern changes in protein abundance have seldom been reported. We have brought together techniques of stable isotope labelling and muscle transformation *in vivo*, with advanced peptide mass spectrometry analysis to generate new insight to the dynamic response of muscle to endurance activity. Specifically, we report the first data in rat EDL on the contributions that synthesis and degradation make to changes in the abundance of individual muscle proteins. Our data include a variety of patterns of response (Fig. 3.6 and 3.12), including proteins that both increase and decrease in abundance without exhibiting a change in synthesis rate. In addition, we show (Figure 3.9) that different proteoforms of a protein can respond independently to an endurance exercise stimulus.

Changes in protein abundance occur principally because of a difference between the rate of synthesis and degradation of a protein. We used a robust and well-established model of muscle transformation to investigate protein-specific changes in abundance as well as synthesis rate. Consistent with earlier work (Jarvis et al, 1993) we report chronic endurance activity is associated with a decrease in muscle mass and a shift toward a slower-twitch oxidative profile. The mass of EDL muscle decreases by 50 % after 30 days of CLFS, we are confident to report that this decrease in muscle mass is not reflective of muscle damage, as the muscles showed no signs of degeneration upon extraction and we report decreases amongst glycolytic enzymes with concomitant increases in oxidative metabolism proteins, suggesting that this is more likely to do with the change in phenotype induced by the stimulation. In addition, Jarvis et al, (1996) document continuous stimulation of rat EDL at 10 and 20 Hz, showing that CLFS does not cause significant damage to this muscle in the rat. Furthermore, the average rate of relative protein synthesis in the Ctrl of mixed soluble proteins (5.17 ± 0.04 %/d) and mixed myofibrillar proteins (4.69 ± 0.33 %/d) was no different than for the Stim (5.43 ± 0.39 %/d, 4.97 ± 0.1 %/d, respectively). This suggests that after 30 days of stimulation, the smaller muscle (Stim) is making a similar amount of protein as

the larger one (Ctrl). However, the absolute rate of synthesis was calculated for whole EDL muscle at each experimental time point (Figure 3.5) and can account for the 50 % change in muscle mass at 30 days (Figure 3.1). The absolute synthesis of Ctrl muscle did not change throughout the experimental period, consistent with the unchanging mass of Ctrl muscle. Yet, similar to the changes in the mass of Stim muscle, the absolute rate of synthesis in Stim muscle significantly ($P < 0.05$) declines compared to Ctrl by 18 %, 40 % and 50 % after 10, 20 and 30 d. This means that as the muscle gets smaller, the average relative synthesis rate of mixed proteins does not change and at the whole muscle level, the absolute rate of newly synthesised protein declines in-line with muscle mass. Therefore, we can be confident that any changes in the abundance of an individual protein not accompanied by a change in synthesis can be attributed to protein degradation.

The individual proteins analysed were quantified for their changes in abundance at each of the time points during the experimental period. It is generally expected that increased mixed muscle protein synthesis following an endurance-type stimulus is predominantly driven by increases in sarcoplasmic and mitochondrial protein synthesis, rather than myofibrillar protein synthesis (Wilkinson et al, 2008.; Donges et al, 2012). This is logical from a physiological standpoint as increases in mitochondrial protein synthesis potentially reflect the adaptations to endurance-type exercise e.g. mitochondrial biogenesis. Furthermore, the myofibrillar fraction of the muscle contain much larger structural and contractile proteins that are thought to turn over much more slowly when compared to proteins found in the soluble fraction, that is predominately composed of metabolic enzymes (Balagopal et al, 2007a). However, the comparison between Figure 3.4 and 3.12 highlights a very different pattern of response. Initially (0-20 d) a greater number of myofibrillar proteins exhibit a significantly altered abundance compared to proteins in the soluble fraction. For example, the majority of the changes in myofibrillar protein abundance seem to be complete after 20 days, but in the soluble fraction, less than one-half of the proteins that exhibit significant changes in abundance after 30 days have changed at the 20-day time point. There have been suggestions in the literature that there may be an effect present in myofibrillar protein synthesis following acute bouts of endurance exercise in humans, with significant increases in myofibrillar protein synthesis measured between 30 min and 4.5 h post-exercise which can be maintained for periods up to 24 h depending on intensity (Di Donato et al, 2014). However, the changes that we measure in the current work are

more likely due to the fact that the proteins included in the myofibrillar fraction are resolved from 2DGE and therefore do not include larger structural proteins that are documented to have slower turnover rates like titin (Isaacs et al, 1989) and myosin heavy chain (Balagopal et al, 2007b). The fractionation process also must be considered as there are proteins normally expected to be seen in the soluble fraction included in the myofibrillar fraction; for example, ATPB. Furthermore, from the 30 common spots (Figure 3.2) there are 20 individual protein identifications of which, 18 are expressed as multiple proteoforms (Table 3.1). This information is routinely overlooked in literature from more comprehensive 'bottom-up' proteomic methods. That is, while LC-MS/MS profiling often provides more extensive coverage (i.e. total number of proteins) the level of detail is less because proteins are grouped in to the sum of all of their proteoforms. Herein, we provided evidence that proteoform-level changes may be the earliest to show response during the fast-to-slow adaptive process (Figure 3.9). Importantly, we report absolute data (Fig. 3.4 and 3.12) that reflects changes at the whole muscle level. This is an important consideration when investigating muscle adaptation associated with significant changes in muscle mass. Moreover, we do not adopt the same assumptions made within the wider literature, attributing increases in synthesis to increases in abundance, but, instead, we measure each of these processes and report the turnover of individual proteins (Fig. 3.6 and 3.13). Based on our detailed analysis, changes in abundance are highly individualised and differ on a protein-by-protein basis. Changes in synthesis do not always equate to changes in abundance when degradation is driving the adaptive change and could potentially explain why, in contrast to the mainstream literature, we report that abundance changes in the myofibrillar fraction proteins are the first that respond to CLFS in comparison to the soluble fraction.

CLFS was associated with a prominent shift in protein from a fast to slow-twitch muscle phenotype. Our data are in agreement with Mayne et al, (2003) who observed the appearance of slow twitch myosin light chain isoform expression using 1DGE in chronically stimulated rat EDL muscle after 61 days. However, we are able to show that the decrease in the protein abundance of the TNNT3 spots ($n = 3$ spots, Table 3.1) is conducted by a combination of two different responses (Figure 3.8). Spot 26 and 28 both decrease in synthesis rate in Ctrl (1.91 ± 0.51 pg/d) compared to Stim (0.02 ± 0.01 pg/d). However, the synthesis rate of spot 25 is maintained and the rate

of degradation is increased in Ctrl (3.99 ± 4.20 pg/d) compared to Stim (1.21 ± 3.06 pg/d) after 30 d of CLFS.

Chronic low-frequency stimulation not only alters the contractile elements of the muscle but creates a robust shift from anaerobic to aerobic energy metabolism. Qualitatively, the effects of CLFS on muscle metabolism are similar to that of endurance training, although the effects induced by CLFS greatly surmount the changes caused by exercise. For example, Donoghue et al, (2007) reports proteins such as Glycerol-3-phosphate dehydrogenase to decrease (-4.7-fold) in abundance, whereas Cytochrome-c oxidase increases (+6.3-fold) in protein abundance in response to a 60-day period of CLFS. Findings from the current study support these data, reporting an increase ($+5.91 \pm 3.21$ -fold) in the abundance of proteins that are associated with the mitochondria (Figure 3.14) and a decrease (-8.14 ± 3.79 -fold) in the abundance of proteins associated with glycolysis (Figure 3.15) following 30 days of CLFS. For the first time in rat muscle, we report the mechanisms underlying these changes in abundance that clearly differ on a protein-to-protein basis during muscle transformation. The increases in abundance of the mitochondrial proteins were achieved by four different patterns of response in protein turnover (Figure 3.14). Importantly, these data suggest degradation is capable of driving adaptation just as much as synthesis. Furthermore, we also report different patterns of response to CLFS from proteins that decrease in abundance. For example, the glycolysis proteins, such as LDHA, G3P and PYGB each decrease in abundance after 30 days of stimulation, but this decrease is orchestrated through three different patterns of response in protein turnover (Figure 3.15). The synthesis rate of LDHA does not change from Ctrl to Stim but the rate of degradation is increased from Ctrl (100.53 ± 13.18 pg/d) to Stim (218.90 ± 15.55 pg/d). In contrast, G3P and PYGB both decrease the rate of synthesis from Ctrl to Stim, but G3P simultaneously increases the rate of degradation from Ctrl (11.82 ± 9.44 pg/d) to Stim (105.21 ± 8.29 pg/d) to lower its abundance, whereas PYGB does not change the rate of degradation from Ctrl to Stim to achieve a similar decrease in abundance.

One of the primary stimuli for muscle adaptation is neuromuscular activity. Under conditions such as CLFS where a fast-to-slow transformation of the skeletal muscle is induced, robust changes in the isoform expression pattern of calcium handling proteins occur, including the ryanodine receptor Ca^{2+} release channel of the junctional sarcoplasmic reticulum and the relaxation-inducing Ca^{2+} -ATPases (Harmon et al,

2001). Chronic stimulation has also been shown to lead to elevations in free sarcoplasmic Ca^{2+} (Everts et al, 1993) which affects Ca^{2+} homeostasis of the muscle and is associated with a pronounced decrease in parvalbumin (PRVA; Leberer et al, 1986), which is a cytosolic Ca^{2+} binding protein present at high concentrations in fast-twitch muscle fibres (Heizmann et al, 1982). Furthermore, these changes in Ca^{2+} regulation induced by CLFS involve a switch in isoform expression of sarco/endoplasmic reticulum Ca^{2+} -ATPase (SERCA) from fast (SERCA 1a) to slow (SERCA 2a) isoform (Leberer et al, 1989.; Ohlendieck et al, 1991). Our data are entirely consistent with these earlier observations. We report a -9.1-fold decrease in PRVA abundance and a +0.93-fold increase in SERCA 2a (Uniprot ID: AT2A2) abundance. Furthermore, our work adds new insight by demonstrating the synthesis rate for the two calcium handling proteins, PRVA and AT2A2 does not change from Ctrl to Stim muscle despite changes in abundance, meaning that the entire regulation of these proteins is done so by degradation. Parvalbumin consequently increases its rate of degradation in Stim (97.15 ± 2.38 pg/d) compared to Ctrl (5.59 ± 1.48 pg/d) in order to decrease protein abundance. Whereas, AT2A2 increases in abundance but achieves this result by decreasing its rate of degradation in Stim (2.00 ± 1.80 pg/d) compared to Ctrl (8.53 ± 0.61 pg/d). It is clear that skeletal muscle adapts by expressing different quantities of functional proteins dependent on the needs of the muscle, achieved by changing the abundance of individual proteins via protein turnover. Here we have not only investigated the mechanisms used by muscle to execute this process by measuring the individual protein turnover of each protein, illustrating that both synthesis and degradation play a unique and complementary role during the adaptive process in skeletal muscle; but have gone one step further to identify proteoform-specific changes that complement the adaptive process.

During muscle transformation, there are also some proteins that do not change in abundance. For instance, it is known that both fast and slow isoforms of myosin light chain can exist in the same muscle fibre after chronic stimulation (Donoghue, 2007). Although both fast and slow isoforms maybe present and unchanging in absolute levels, the relative quantities of each isoform may be different (Brown et al, 1983). The current study has quantified skeletal myosin light chain (MLRS) as an absolute value of protein abundance and has additionally resolved MLRS as two separate proteoforms (Table 3.1). In response to CLFS, the total amount of MLRS protein abundance does not change in absolute terms. However, when analysed at the

proteoform level, one MLRS proteoform (spot 11) decreases significantly and the other (spot 12) increases (Figure 3.9). This has meaningful implications when investigating muscle transformation, as it appears the process of muscle adaptation from a fast-to-slow-twitch muscle is brought about by proteoform-specific changes in abundance. The spot 11 proteoform of MLRS (Figure 3.9), exhibited a significant decrease in abundance (-6.55 ± 2.9 -fold) after 30 days of stimulation but the synthesis rate of MLRS spot 11 was not significantly different in the Ctrl over the 30 days of stimulation than the Stim. Therefore, we interpret a net loss in abundance of the more acidic proteoform of MLRS (spot 11) without a decrease in synthesis rate to mean a greater contribution of protein degradation. Furthermore, the decrease in MLRS spot 11 abundance after 30 days (62 %) coincides with the 50 % decrease in the overall decrease in mass of the EDL (50 %). However, during the 0-10 day period, the EDL only reduces in mass by 16 % and MLRS spot 11 decreases the most over this period (55 %), we therefore interpret the decrease in spot 11 to be, at least in part due to be proteoform-specific degradation that occurs before any major changes to gross EDL mass and is amongst the earliest indicator of the change in muscle phenotype. Compared to spot 11, spot 12 tended to exhibit the opposite response to stimulation (Figure 3.9). Although the abundance of spot 12 increased by 16 % over the 30-day period of stimulation, the decrease in the abundance of spot 11 was proportionally greater than the increase in the abundance of spot 12 and so the change in abundance is not entirely due to a change in post-translational state. For the MLRS spot 12 proteoform the rate of protein synthesis did not change from Ctrl to Stim. However, synthesis tended to be greater than degradation in the Stim muscle, which possibly explains why there is a trend for the abundance MLRS spot 12 to rise (Figure 3.9). These data from MLRS indicate that chronic stimulation affects the EDL muscle proteome by changing the protein turnover kinetics of not just a whole protein but of individual proteoforms within it. Moreover, it is degradation that appears to regulate this process, which is at least true for MLRS. More specifically, from the multiple proteoforms resolved (spot 11 and 12) we have identified two site-specific phosphorylations (Figure 3.10). Serine 16 phosphorylation is present in both spot 11 and 12 proteoforms but there is an additional serine 20 phosphorylation in spot 11 only. This indicates that selective degradation of individual proteins maybe regulated by site-specific post translational modifications. Serine 16 and 20 phosphorylation of MLRS have previously been documented in human phospho-proteomic mapping

studies such as Hojlund et al, (2009). Furthermore, proteomic analysis of the ventricular/slow twitch isoform of myosin light chain (MLRV) in rat cardiac muscle revealed endurance training to decrease phosphorylated (serine 15) myosin light chain (Burniston, 2011), which may in turn relate to the improved myocardial Ca^{2+} handling associated with endurance training (Kemi et al, 2008). However, it is known that during muscle contraction MLRS is phosphorylated by an increase in Ca^{2+} -calmodulin-dependant myosin light chain kinase which is activated by a rise in free calcium ions (Sweeney et al, 1993). In skeletal muscle, phosphorylation of this kind correlates with potentiation of the rate of force development and maximal isometric twitch tension (Szczesna et al, 2002) and a significant increase in the level of MLRS phosphorylation has also been reported after a repetitive low-frequency stimulus (Sweeney et al, 1993). However, this work lacks information about site-specific phosphorylation meaning we cannot know if there are multiple sites of phosphorylation that are specific to each of these situations. The physiological function of MLRS phosphorylation is still somewhat unclear but it is thought to increase calcium sensitivity of the myofibrils and enhance basic mechanical properties affecting the dynamic aspects of muscle force and power (Sweeney et al, 1993), as well as modulating alterations in cross bridge function and muscle activation during muscle fatigue (Grange et al, 1993).

Here, we have not only presented two site-specific phosphorylations of MLRS (Figure 3.10) that maybe responsible for selective degradation but have also reported the individual protein turnover data for MLRS in each of these phosphorylated states. This type of information is highly unprecedented and could prove to be of paramount importance when studying the sequence of events that occur during muscle adaptation. Thus, providing a level of detail that gives an explanation of exactly how the adaptation process is orchestrated, in this case through proteoform-specific protein degradation. These data also suggest that this level of change occurs early on in the fast-to-slow adaptation process (55 % decrease after 10 days, Figure 3.9) suggesting that proteoform-specific changes in MLRS abundance largely precede structural or metabolic changes in not only gross muscle but also at the level of the individual protein, therefore suggesting that proteoform-specific changes may be the best early indicators currently available to recognise changes in muscle phenotype.

3.6 Conclusions

We report fully integrated dynamic proteomic profiling (DPP) to simultaneously measure the rate of synthesis and net abundance, allowing accurate calculation of the rate of degradation in muscle proteins and proteoforms during muscle adaptation. We have shown that additional proteins are introduced and others increase or are removed from the muscle proteome in both the functional and metabolic sense during muscle transformation. It is generally regarded that such changes are attributed to differences in synthetic processes only. However, by using DPP, we provide novel data to show that changes in muscle proteins during adaptation occur via several different patterns of response that involve the modulation of both synthetic and degradative processes. Such profusion of different adaptive responses in the muscle proteome has only recently been captured in human resistance training (Camera et al, 2017). Together, with our current data, a mechanistic insight into the regulation of protein abundance within the muscle cell and protein metabolism is provided. Moreover, results from this study add to the now growing list of evidence demonstrating whole mixed-muscle protein synthesis rates give less than adequate information compared to synthesis rates at the individual protein level. We also provide new evidence for selective degradation of individual proteins at varying rates to decrease and/or to maintain the same relative abundance of protein in the muscle. From this we can report, 50 proteins displayed a change in abundance in response to muscle adaptation from the 77 proteins that were measured. Of which 30 % of proteins were driven by synthesis, 38 % of proteins were driven by degradation and the remaining 32 % were driven by both synthesis and degradation. In addition, we document proteoform-specific degradation appearing to drive fast-to-slow muscle adaptation.

Our work is the first of its kind to show the response of proteoform-specific turnover during muscle adaptation and provides further evidence that protein turnover is increased and decreased by increasing and/or decreasing the relative contributions of synthesis and degradation to marshal the abundance of individual proteins that are required to control the physiological demands of the muscle.

3.7 Bibliography

References

Adams, G.R.; Hather, B.M.; Baldwin, K.M.; Dudley, G.A. (1993). Skeletal muscle myosin heavy chain composition and resistance training. *Journal of Applied Physiol*, **74**, 911-915.

Balagopal, P.; Rooyackers, O.E.; Adey, D.B.; Ades, P.A.; Nair, K.S. (1997a). Effects of aging on in vivo synthesis of skeletal muscle myosin heavy chain and sarcoplasmic proteins in humans. *Am J Physiol*, **4**, 273-280.

Balagopal, P.; Ljungqvist, O.; Nair, K.S. (1997b). Skeletal muscle myosin heavy-chain synthesis rate in healthy humans. *Am J of Physiol Endocrinol and Metabolism*, **45**, 272-281.

Brown, MD.; Cotter, MA.; Hudlicka, O.; Vrbova, G. (1976). The effects of different patterns of muscle activity on capillary density, mechanical properties and structure of slow and fast rabbit muscles. *Pflugers Arch*, **361**, 241-250.

Brown, J.; Salmons, S. (1981). Percutaneous control of an implantable muscle stimulator via optical link. *J. Biomed. Eng*, **3**, 206-208.

Brown, W.; Salmons, S.; Whalen, G. (1983). The sequential replacement of myosin subunit isoforms during muscle type transformation induced by long term electrical stimulation. *J Bio Chem*, **23**, 14686-14692.

Brown, M.C.; Henriksson, J.; Salmons, S. (1989). Restoration of fast muscle characteristics following cessation of chronic stimulation in the rabbit: physiological, histochemical and metabolic changes during slow-to fast transformation. *Proc R Soc*, **235**, 321 346.

Burniston, J.G.; Hoffman, E.P. (2011). Proteomic responses of skeletal and cardiac muscle to exercise. *Proteomics*, **8**, 361-377.

Burniston. J.G; Chen, Y.W. (2019). Omics approaches to understanding muscle biology. Biomedical sciences, *Methods in Physiology: Springer e-publishing*.

Camera, D.; Burniston, J.; Pogson, M.; Smiles, W.; Hawley, J. (2017). Dynamic proteome profiling of individual proteins in human skeletal muscle after a high-fat diet and resistance exercise. *FASEB*, **31**, 1-17.

Coffey, V.G.; Hawley, J.A. (2007). The molecular basis of training adaptation. *Journal of Sports Medicine*, **37**, 737-763.

Commerford, S.L.; Carsten, A.L.; Cronkite, E.P. (1983). The distribution of tritium among the amino acids of proteins obtained from mice exposed to tritiated water. *Radiat. Res*, **94**, 151–155.

Delp, M.; Pette, D. (1994). Morphological changes during fiber type transitions in low-frequency stimulated rat fast-twitch muscle. *Cell Tissue Res*, **277**, 363-371.

Di Donato, D.M.; West, D.W.; Churchward-Venne, T.A.; Breen, L.; Baker, S.K.; Phillips, S.M. (2014). Influence of aerobic exercise intensity on myofibrillar and mitochondrial protein synthesis in young men during early and late post exercise recovery. *Am J Physiol Endocrinol Metab*, **9**, 1025-1032.

Donges, C.E.; Burd, N.A.; Duffield, R. (2012). Concurrent resistance and aerobic exercise stimulates both myofibrillar and mitochondrial protein synthesis in sedentary middle-aged men. *J Appl Physiol*, **12**, 1992-2001.

Donoghue, P.; Doran, P.; Dowling, P.; Ohlendieck, K. (2005). Differential expression of the fast-skeletal muscle proteome following chronic low-frequency stimulation. *Biochimica et Biophysica Acta*, **1752**, 166-176.

Donoghue, P.; Doran, P.; Wynee, K.; Pedersen, K.; Dunn, M.; Ohlendieck, K. (2007). Proteomic profiling of chronic low-frequency stimulated fast muscle. *Proteomics*, **7**, 3417-3430.

EerBeek, O.; Kernell, D.; Verhey, BA. (1984). Effects of fast and slow patterns of tonic long-term stimulation on contractile properties of fast muscle in the cat. *J Physiol*, **352**, 73-90.

Everts, M.; Lomo, T.; Clausen, T. (1993). Changes in K⁺, Na⁺ and calcium contents during in vivo stimulation of rat skeletal muscle. *Acta Physiol Scand*, **147**, 357-368.

Fluck, M.; Hoppler, H. (2003). Molecular basis of skeletal muscle plasticity--from gene to form and function. *Rev Physiol Biochem Pharmacol*, **146**, 159-216.

Gorg, A.; Weiss, W.; Dunn, M. (2004). Current two-dimensional electrophoresis technology for proteomics. *Proteomics*, **4**, 3665-3685.

Grange, R.; Vandenboom, R.; Houston, M. (1993). Physiological significance of myosin phosphorylation in skeletal muscle. *Can J Appl Physiol*, **18**, 229-242.

Harmon, S.; Froemming, G, R.; Leisner, E.; Pette, D.; Ohlendieck, K. (2001). Low-frequency stimulation of fast muscle affects the abundance of Ca²⁺-ATPase but not its oligomeric status. *J Appl Physiol*, **90**, 371-379.

Hartner, KT.; Kirschbaum, BJ.; Pette, D. (1989). The multiplicity of troponin T Isoforms Distribution in normal rabbit muscles and effects of chronic stimulation. *Eur. J. Biochem*, **179**, 32 -38.

Hartner, KT.; Pette, D. (1990). Fast and slow isoforms of troponin I and troponin C Distribution in normal rabbit muscles and effects of chronic stimulation. *Eur. J. Biochem*, **188**, 261 -267.

Heilmann, C.; Pette, D. (1979). Molecular transformations in sarcoplasmic reticulum of fast- twitch muscle by electrostimulation. *Eur. J. Biochem*, **93**, 437-446.

Heizmann, C.; Berhtold, M.; Rowlerson, A. (1982). Correlation of Parvalbumin concentration with relaxation speed in mammalian muscles. *Proc Natl Acad Sci USA*, **79**, 7243-7247.

Hojlund, K.; Bowen, B.; Hwang, H.; Flynn, C.; Madireddy, L.; Geetha, T.; Langlais, P.; Meyer, C.; Mandarino, L.; Yi, Z. (2009). In vivo phosphoproteome of human skeletal muscle revealed by phosphopeptide enrichment and HPLC-ESI-MS/MS. *J Proteome Res*, **11**, 4954-4965.

Isaacs, W.B.; Kim, I.S.; Struve, A.; Fulton, A.B. (1989). Biosynthesis of Titin in Cultured Skeletal Muscle Cells. *The Journal of Cell Biology*, **109**, 2189-2195.

Jarvis, J.C. (1993). Power production and working capacity of rabbit tibialis anterior muscles after chronic electrical stimulation at 10 Hz. *Journal of Physiology*, **470**, 157-169.

Jarvis, J.; Mokrusch, T.; Kwende, M.; Sutherland, H.; Salmons, S. (1996). Fast-to-slow transformation in stimulated rat muscle. *Muscle and Nerve*, **19**, 1469-1475.

Kemi, O.J.; Ellingsen, O.; Smith, G.; Wisloff, U. (2008). Exercise-induced changes in calcium handling in left ventricular cardiomyocytes. *Front Biosci*, **13**, 356-368.

Knowler, W.C.; Barrett-Connor, E.; Fowler, S.E.; Hamman, R.F.; Lachin, J.M.; Walker, E.A.; Nathan, D.M. (2002). Reduction in the incidence of type 2 diabetes with lifestyle intervention or metformin. *N. Engl. J. Med*, **346**, 393-403.

Kwong, W.H.; Vrbova, G. (1981). Effects of low-frequency electrical stimulation on fast and slow muscle of the rat. *Pflugers Arch*, **3**, 200-7.

Leberer, E.; Seedorf, U.; Pette, D. (1986). Neural control of gene expression in skeletal muscle Ca-sequestering proteins in developing and chronically stimulated rabbit skeletal muscles. *Biochem J*, **239**, 295-300.

Leberer, E.; Hartner, K.; Brandl, C.; Fujii, J.; Tada, M.; MacLennan, D.; Pette, D. (1989). Slow/cardiac sarcoplasmic reticulum Ca-ATPase and phospholamban mRNAs are expressed in chronically stimulated rabbit fast-twitch muscle. *Eur J Biochem*, **185**, 51-54.

Leeuw, T., Pette, D. (1996). Coordinate changes of myosin light and heavy chain isoforms during forced fiber type transitions in rabbit muscle. *Dev. Genet*, **19**, 163-168.

Lexell, J., Jarvis, J., Downham, D., and Salmons, S. (1992). Quantitative morphology of stimulation-induced damage in rabbit fast-twitch skeletal muscles. *Cell Tissue Res*, **269**, 195-204.

Loughna, P.; Goldspink, G.; Goldspink, D. (1986). Effect of inactivity and passive stretch on protein turnover in phasic and postural rat muscles. *J Appl Physiol*, **61**, 173-179.

Maier, A., Gambke, B., and Pette, D. (1986). Degeneration-regeneration as a mechanism contributing to the fast to slow conversion of chronically simulated fast-twitch rabbit muscle. *Cell Tissue Res*, **244**, 635-643.

Malik, Z.A.; Colbey, J.N.; Morton, J.P.; Close, G.L.; Edwards, B.J.; Koch, L.G.; Britton, S.L.; Burniston, J.G. (2013). Label-free LC-MS profiling of skeletal muscle reveals heart-type fatty acid binding protein as a candidate biomarker of aerobic capacity. *Proteomes*, **1**, 290-308.

Mayne, C.; Mokrusch, T.; Jarvis, J.; Gilroy, S.; Salmons, S. (1993). Stimulation-induced expression of slow muscle myosin in a fast muscle of the rat. *FEBS*, **327**, 297-300.

Ohlendieck, K.; Briggs, F.; Lee, K.; Wechsler, A.; Campbell, K. (1991). Analysis of excitation-contraction-coupling components in chronically stimulated canine skeletal muscle. *Eur J Biochem*, **202**, 739-747.

Ohlendieck, K., Murray, B.E., Froemming, G.R., Maguire, P.B., Leisner, E., Traub, I., Pette, D. (1999). Effects of chronic low-frequency stimulation on Ca²⁺ regulatory membrane proteins in rabbit fast muscle. *Pflugers Arch*, **438**, 700-708.

Pette, D.; Smith, M.E.; Staudte, H.W.; Vrbova, G. (1973). Effects of long-term electrical stimulation on some contractile and metabolic characteristics of fast rabbit muscles. *Pflugers Arch*, **338**, 257-272.

Pette, D.; Muller, W.; Leisner, E.; Vrbova, G. (1976). Time dependant effects on contractile properties, fiber population, myosin light chains and enzymes of energy metabolism in intermittently a continuously stimulated fast twitch muscles of the rabbit. *Pflugers Arch*, **364**, 103-112.

Pette, D.; Simoneau, J.A. (1990). Species specific responses of muscle lactate dehydrogenase isozymes to increased contractile activity. *Pflugers Arch*, **413**, 679-81.

Pete, D.; Vrbova, G. (1992). Adaptation of mammalian skeletal muscle fibres to chronic electrical stimulation. *Reviews of physiology, biochemistry and pharmacology*, **120**, 115-202.

Peuker, H.; Conjard, A.; Putman, C.T.; Pette, D. (1999). Transient expression of myosin heavy chain MHC1a in rabbit muscle during fast-to-slow transition. *J. Muscle Res. Cell Motil*, **20**, 147-154.

Putman, C.T.; Dusterhoff, S.; Pette, D. (1999). Changes in satellite cell content and myosin isoforms in low-frequency simulated fast muscle of hypothyroid rat. *J. Appl. Physiol*, **86**, 40-51.

Reichmann, H.; Hoppeler, H.; Mathieu-Costello, O.; von Bergen, R.; Pette, D. (1985). Biochemical and ultrastructural changes of skeletal muscle mitochondria after chronic electrical stimulation in rabbits. *Pflugers Arch*, **404**, 1-9.

Salmons, S.; Sreter, F.A. (1979). Significance of impulse activity in the transformation

of skeletal muscle type. *Nature*, **263**, 30-34.

Salmons, S.; Jarvis, J.C. (1991). Simple optical switch for implantable devices. *Med. & Biol. Eng. Compute*, **29**, 554-556.

Salmons, S.; Vrbova, G. (1969). The influence of activity on some contractile characteristics of mammalian fast and slow muscles. *J Physiol*, **201**, 535-549.

Sweeney, H.L.; Bowman, B.F.; Stull, J.T. (1993). Myosin light chain phosphorylation in vertebrate striated muscle: regulation and function. *Am J Physiol Cell Physiol*, **264**, 1085-1095.

Szczesna, D.; Zhao, J.; Jones, M.; Zhi, G.; Stull, J.; Potter, J. (2002). Phosphorylation of the regulatory light chains of myosin affects Ca^{2+} sensitivity of skeletal muscle contraction. *J Appl Physiol*, **92**, 1661-1670.

Widrick, J.J.; Stelzer, J.E.; Shoepe, T.C.; Garner, D.P. (2002). Functional properties of human muscle fibers after short-term resistance exercise training. *Am. J. Physiol. Regul. Integr. Comp. Physiol*, **283**, 408–416.

Wilkinson, S.B.; Phillips, S.M.; Atherton, P.J. (2008). Differential effects of resistance and endurance exercise in the fed state on signalling molecule phosphorylation and protein synthesis in human muscle. *J Physiol*, **15**, 3701-3717.

Supplementary tables

Table S1. Myofibrillar protein identifications and peptide information.

Myofibrillar fraction					
Spot Number	Protein	Score	Coverage	Peptide sequence	Residue
1	ACTN1	133	15 %	ASLHEAWTR	417-425
				ATLPEADRER	570-579
				DGLALCALIHR	189-199
				VGEPSMSAMQRK	315-326
				LSHRPAFMPSEGK	361-373
2	PLEC	94	4 %	QAQEEAER	1631-1638
				LSVAAQEAAR	2423-2432
				VPVDVAYQR	3292-3300
				LPVDVAYQR	3623-3631
				HRELAEEAAR	1956-1966
3	DESM	72	24 %	TSGGAGGLGSLR	59-70
				LEEEIRHLK	369-377
				RQVEVLTNQR	163-172
				HLREYQDLLNVK	383-394
				FLEQQNAALAAEVNR	127-141
4	ATPB	78	23 %	IPVGPETLGR	134-143
				IMNVIGEPIDER	144-155
				FTQAGSEVSALLGR	311-324
				TIAMDGTEGLVRGQK	110-124
				VALVYGQMNEPPGAR	265-279
5	ACTS/ ACTC	71	24 %	HQGVMVGMGQK	42-52
				DSYVGDEAQSK	53-63
				QEYDEAGPSIVHR	362-274
				IWHHTFYNELR	87-97
				MQKEITALAPSTMK	315-328
6	TPM4	119	37 %	HIAEEADRK	117-125
				ELDGERERR	34-42
				MEIQEMQLK	105-113
				RIQLVEEELDR	55-65
				AGLNSLEAVK	2-11
7	TMP2	93	34 %	KMQMLKLDK	7-15
				LVILEGELER	169-178
				EDKYEEEIK	218-226
				AQERLATALQK	102-112
				LEEAEKAADESER	113-125
8, 9, 10	MYL1	76	44 %	HVLATLGEK	149-157
				EAFLLFDR	52-59

				ITLSQVGDVLR	65-75
				DQGGYEDFVEGLR	120-132
				KPAAAAPAPAPAPAPAK	9-29
				PK	
11, 12	MLRS	100	42 %	DGIIDKEDLR	42-51
				EAFVIDQNR	32-41
				LKGADPEDVITGAFK	91-112
				KQFLEELLTTQCDR	117-130
				AAAEGSSNVFSMFDQTQIQ	10-31
				EFK	
13, 14	ENOB	88	31 %	IGAEVYHHLK	184-193
				GVLKAVEHINK	61-71
				IFAREILDSR	6-15
				GNPTVEVDLHTAK	16-28
				LAQSNWGWVMVSHR	359-372
15	ATPA	113	30 %	AVDSLVPGR	195-204
				VGSAQTR	417-424
				RFNDGTDEK	231-239
				GIRPAINVGLSVSR	403-416
				TGAIVDVPVGDELLGR	134-149
16, 17	KCRM	96	24 %	LMVEMEKK	359-366
				GYTLPPHCSR	139-148
				DLFDPIIQDR	87-96
				GGDDLDPNYVLSSR	117-130
				GTGGVDTAAVGAVFDISNA	321-341
				DR	
18, 19, 32	KCRS	81	26 %	GIWHNYDK	250-257
				GLSLPPACSR	173-182
				ITHGQFDER	150-158
				VPPPLPQFGR	409-418
				LFPPSADYPDLR	47-58
20	ANXA4	61	22 %	TAYKSTIGR	54-62
				NKPAYFAER	245-253
				SMKGLGTDDSTLIR	257-270
				GLGTDEDAIIGVLACR	29-44
				GAGTDEGCLIEILASR	101-116
21, 22	G3P	67	20 %	LVTRAAFSCDK	15-25
				VTPNVSVVDLTCR	233-246
				GAAQNIIPASTGAAK	199-213
				IVSNASCTTNCLAPLAK	144-160
				VIHDNFGIVEGLMTTVHAIT	161-184
				ATQK	
23	TNNI2	93	36 %	VRMSADAMLK	115-124
				SSKELEDMNQK	89-99
				MSADAMLKALLGSK	117-130
				YDMEVKVQK	80-88
				QHLKSVMLQIAATELEK	16-32
24	TNNI1	117	34 %	VEVVDEER	73-80
				VSMDLRANLK	134-143
				NVEAMSGMEGR	164-174

				YLSERIPTLQTR	44-55
				AKECWEQEHEER	26-37
25	TNNT3	78	21 %	QKYDITTLR	225-233
				KPLNIDHLSDDKLR	185-198
				IPEGEKVFDDIQK	49-62
				SRIDQAQK	234-241
				LTAPKIPEGEK	44-54
26	TNNT3	84	22 %	LTAPKIPEGEK	44-54
				QKYDITTLR	225-233
				KPLNIDHLSDDKLR	185-198
				IPEGEKVFDDIQK	49-62
				IDQAQKHSK	236-244
28	TNNT3 (fTnT2)	79	23 %	KEEEELIALK	85-94
				YDIMNVR	227-233
				LTAPKIPEGEK	44-54
				QNRLAEEK	118-126
				QNKDLMELQALIDSHFEAR	65-83
27	TNNT1 (sTnT1 or sTnTx)	70	24 %	AEDDAK	143-148
				YEINVLYR	232-240
				IPEGERVDFDDIHR	54-67
				DLLELQTLIDVHFEQR	73-88
				EEERP KPSRPVVPPLIPPK	35-53
33	TNNT1 (sTnT1 or sTnTx)	70	22 %	VDFDDIHRK	60-68
				YEINVLYR	232-240
				EEEEELIALKDR	91-101
				EEERP KPSRPVVPPLIPPK	35-53
				MEKDLLELQTLIDVHFEQR	70-88
34	TNNT1 (sTnT2 or sTnT3)	67	22 %	VDFDDIHRK	60-68
				YEINVLYR	232-240
				IPEGERVDFDDIHR	54-67
				EERP KPSRPVVPPLIPPK	36-53
				MEKDLLELQTLIDVHFEQR	70-88
29, 30	CAH3	94	31 %	DGIAIGIFLK	138-148
				TILNNGKTCR	58-67
				GGPLPGPYRLR	81-91
				GENQSPVELHTK	25-36
				FDPSCLPACR	178-188
31	MLRV	103	27 %	VFDPEGKGLK	105-115
				DGFIDKNDLR	41-50
				EAFIMDQNR	31-40
				NLVHIITHGEEKD	154-166
				LKGADPEETILNAFK	92-104
35	CRYAB	88	32 %	QDEHGFISR	108-116
				EEKPAVTAAPK	164-174
				VLGDVIEVHGK	93-103
				DRFSVNLVVK	73-82
				RPFFPFHSPSR	12-22
36, 37, 38	MYL3	77	28 %	HVLATLGER	160-168
				EAFQLFDR	61-68
				ITYGQCQGDVLR	76-86

ALGQNPTQAEVLR	87-99
AAPAPAAAPAAAPERPK	19-38

Spot number refers to the different proteoforms resolved by 2DGE and corresponds to the 2DGE image in Figure 3.2. Protein name relates to the Uni-Prot database, entries returned using the MASCOT search engine. A mowse score greater than 55 denotes a confident ($P < 0.05$) identification by peptide mass fingerprinting. Coverage is the amount of sequence covered of the protein for identification. Peptide sequence refers to the amino acid sequence of each peptide used for peptide mass spectrometry and the residues are where each peptide occurs in the protein sequence.

Table S2. Soluble proteins identification.

Soluble fraction			
Protein I.D.	Protein name	GO function	Peptide #
AATC	Aspartate aminotransferase , cytoplasmic	Unassigned	2
AATM	Aspartate aminotransferase, mitochondrial	Mitochondrial	4
ACADL	Long-chain specific acyl-CoA dehydrogenase, mitochondrial	Mitochondrial	1
ACON	Aconitate hydratase, mitochondrial	Mitochondrial	2
ACTC	Actin, alpha cardiac muscle 1	Unassigned	3
ALBU	Serum albumin	Unassigned	23
ALDOA	Fructose-bisphosphate aldolase A	Glycolysis	7
ALDR	Aldose reductase	High-energy phosphate	3
AT2A2	Sarcoplasmic/endoplasmic reticulum calcium ATPase 2	Ca ²⁺ Handling	8
ATPA	ATP synthase subunit alpha, mitochondrial	Mitochondrial	3
ATPB	ATP synthase subunit beta, mitochondrial	Mitochondrial	2
ATPO	ATP synthase subunit O, mitochondrial	Mitochondrial	1
CAH3	Carbonic anhydrase 3	Unassigned	4
CASQ1	Calsequestrin-1	Ca ²⁺ Handling	5
CX7A2	Cytochrome c oxidase subunit 7A2, mitochondrial	Mitochondrial	2
ENOB	Beta-enolase	Glycolysis	4
FHL1	Four and a half LIM domains protein 1	Unassigned	2
G3P	Glyceraldehyde-3-phosphate dehydrogenase	Glycolysis	4
HBA	Hemoglobin subunit alpha-1/2	O ₂ Transport	2
HBB1	Hemoglobin subunit beta-1	O ₂ Transport	2
HBB2	Hemoglobin subunit beta-2	O ₂ Transport	1
HINT1	Histidine triad nucleotide-binding protein 1	Unassigned	3
HSPB6	Heat shock protein beta-6	Unassigned	4

IDH3A	Isocitrate dehydrogenase [NAD] subunit alpha, mitochondrial	Mitochondrial	2
IDHP	Isocitrate dehydrogenase [NADP], mitochondrial	Mitochondrial	2
KAD1	Adenylate kinase isoenzyme 1	High-energy phosphate	4
KCRB	Creatine kinase B-type	High-energy phosphate	1
KCRM	Creatine kinase M-type	High-energy phosphate	7
KPYM	Pyruvate kinase PKM	Glycolysis	12
LDHA	L-lactate dehydrogenase A chain	Glycolysis	5
MDHC	Malate dehydrogenase, cytoplasmic	Mitochondrial	1
MDHM	Malate dehydrogenase, mitochondrial	Mitochondrial	6
MYG	Myoglobin	O ₂ Transport	2
MYL1	Myosin light chain 1/3, skeletal muscle isoform	Unassigned	2
ODPA	Pyruvate dehydrogenase E1 component subunit alpha, somatic form, mitochondrial	Mitochondrial	1
PARK7	Protein/nucleic acid deglycase DJ-1	Unassigned	2
PFKAM	ATP-dependent 6-phosphofructokinase, muscle type	Glycolysis	1
PGAM2	Phosphoglycerate mutase 2	Glycolysis	3
PGK1	Phosphoglycerate kinase 1	Glycolysis	6
PGM1	Phosphoglucomutase-1	Glycolysis	2
PRVA	Parvalbumin alpha	Ca ²⁺ Handling	2
PYGB	Glycogen phosphorylase, brain form	Glycolysis	1
PYGM	Glycogen phosphorylase, muscle form	Glycolysis	2
SAFB1	Scaffold attachment factor B1	Unassigned	1
TPIS	Triosephosphate isomerase	Glycolysis	6
TRY1	Anionic trypsin-1	Unassigned	1
VDAC1	Voltage-dependent anion-selective channel protein 1	Unassigned	2

Protein I.D. relates to the Uni-Prot database, entries returned using the MASCOT search engine. Full protein name is given with assigned gene ontology function. The peptide number refers to the number of unique peptides used for each protein to gain a positive identification.

Table S3. Rank order for abundance changes in myofibrillar proteins after 30-d of stimulation in EDL muscle.

Protein I.D.	Relative ABD	P-Value	Protein I.D.	Absolute ABD	P-Value
TNNI1 (24)	+4.82 ± 1.1	0.021	TNNI1 (24)	+15.82 ± 3.8	0.013
CAH3 (29)	+4.19 ± 2.0	0.011	CAH3 (29)	+8.29 ± 3.2	0.019
CAH3 (30)	+3.57 ± 0.9	0.016	TNNT1 (27)	+7.68 ± 2.8	0.024
TNNT1 (27)	+3.19 ± 1.2	0.022	KCRS (19)	+6.99 ± 1.5	0.041
ACTN1 (1)	+2.70 ± 0.8	0.048	CAH3 (30)	+6.49 ± 2.2	0.037
KCRS (19)	+2.63 ± 0.9	0.032	ATPB (4)	+6.15 ± 0.1	0.016
ATPB (4)	+2.43 ± 1.3	0.044	ACTN1 (1)	+6.04 ± 1.0	0.038
KCRM (17)	+2.32 ± 1.8	0.057	KCRM (17)	+1.61 ± 3.5	0.338
KCRS (18)	+1.94 ± 1.4	0.069	MYL1 (10)	+1.55 ± 2.7	0.071
MYL1 (10)	+1.85 ± 1.3	0.067	KCRM (16)	+1.12 ± 2.4	0.439
ANXA4 (20)	+1.48 ± 2.1	0.089	ANXA4 (20)	+0.88 ± 2.8	0.629
KCRM (16)	+1.47 ± 1.7	0.087	MLRS (12)	+0.81 ± 1.6	0.100
ATPA (15)	+1.32 ± 1.8	0.093	ATPA (15)	+0.39 ± 2.2	0.732
TPM2 (7)	+0.92 ± 1.1	0.088	KCRS (18)	+0.36 ± 3.2	0.489
ACTS (5)	+0.81 ± 0.6	0.094	TPM2 (7)	+0.28 ± 0.2	0.372
MLRS (12)	+0.38 ± 0.7	0.083	DESM (3)	-0.35 ± 2.0	0.331
DESM (3)	+0.26 ± 1.3	0.224	ACTS (5)	-0.36 ± 0.4	0.174
PLEC (2)	-0.40 ± 1.8	0.157	PLEC (2)	-0.47 ± 4.9	0.106
ENOB (13)	-0.42 ± 2.0	0.274	ENOB (13)	-0.77 ± 2.9	0.194
MYL1 (9)	-0.71 ± 1.5	0.079	TPM4 (6)	-1.66 ± 2.3	0.094
TPM4 (6)	-0.79 ± 1.9	0.267	MYL1 (9)	-1.71 ± 2.1	0.088
TNNI2 (23)	-2.64 ± 0.9	0.045	MLY1 (8)	-3.36 ± 2.5	0.042
MLY1 (8)	-2.66 ± 0.7	0.018	TNNI2 (23)	-5.02 ± 0.8	0.001

MLRS (11)	-3.05 ± 1.0	0.001	G3P (21)	-5.40 ± 2.7	0.047
TNNT3 (25)	-3.13 ± 0.9	0.001	MLRS (11)	-6.55 ± 2.9	0.022
G3P (21)	-3.23 ± 1.1	0.001	G3P (22)	-10.31 ± 1.7	0.001
G3P (22)	-3.31 ± 0.7	0.001	TNNT3 (25)	-10.62 ± 2.5	0.018
TNNT3 (26)	-4.27 ± 1.1	0.001	TNNT3 (28)	-12.48 ± 1.9	0.001
ENOB (14)	-4.88 ± 1.3	0.001	TNNT3 (26)	-13.06 ± 2.1	0.001
TNNT3 (28)	-4.94 ± 2.1	0.014	ENOB (14)	-14.27 ± 1.8	0.001

Protein I.D. relates to the Uni-Prot database, entries returned using the MASCOT search engine. Spot numbers are in brackets which refers to the different proteoforms resolved by 2DGE and corresponds to the 2DGE image in Figure 3.2. Relative abundance (ABD) represents data normalised to spot density from the 2D-gels only. Absolute abundance (ABD) represents data normalised to spot density and total EDL mass. All data is represented as MEAN ± SD for biological replicates (n = 3) and is displayed as the positive (+) or negative (-) fold change from non-stimulated control muscle to 30 days chronically stimulated muscle, in rank order of largest positive change to largest negative change. P-Values are generated from paired t-tests between control and 30-d stimulated muscle.

Table S4. Rank order for synthesis rates in myofibrillar proteins after 30-d of stimulation in EDL muscle.

Protein I.D.	Relative (Stim)	Relative (Ctrl)	P-Value	Protein I.D.	Absolute (Stim)	Absolute (Ctrl)	P-Value
CAH3 (29)	19.81 ± 6.88	17.02 ± 5.01	0.048	ATPB (4)	40.02 ± 2.09	22.44 ± 1.55	0.001
KCRS (19)	4.80 ± 1.40	2.14 ± 0.75	0.047	TNNI1 (24)	18.88 ± 2.61	5.53 ± 3.34	0.001
ATPB (4)	11.07 ± 2.42	9.10 ± 1.48	0.021	CAH3 (29)	18.23 ± 2.10	7.79 ± 2.42	0.001
CAH3 (30)	22.21 ± 7.99	20.69 ± 7.17	0.049	CAH3 (30)	24.12 ± 2.71	14.92 ± 1.61	0.001
TNNT1 (27)	2.04 ± 0.27	0.94 ± 0.84	0.028	TNNT1 (27)	9.71 ± 1.10	0.99 ± 2.52	0.043
TNNI1 (24)	4.23 ± 0.32	3.31 ± 1.36	0.037	KCRS (19)	11.05 ± 2.94	5.70 ± 1.77	0.019
ACTN1 (1)	5.00 ± 1.28	4.10 ± 0.91	0.432	ACTN1 (1)	5.85 ± 4.27	1.49 ± 3.65	0.287
KCRS (18)	4.56 ± 2.24	3.70 ± 0.40	0.051	MYL1 (8)	18.34 ± 3.60	14.86 ± 5.65	0.088
ATPA (15)	3.18 ± 0.86	2.52 ± 0.48	0.049	TPM2 (7)	27.86 ± 3.84	24.66 ± 6.02	0.739
PLEC (2)	0.89 ± 0.10	0.43 ± 0.15	0.115	MYL1 (10)	12.82 ± 3.88	10.08 ± 4.47	0.114
KCRM (17)	3.61 ± 0.72	3.22 ± 0.28	0.057	KCRS (18)	7.55 ± 2.27	5.79 ± 5.89	0.073
MYL1 (10)	3.33 ± 0.95	3.04 ± 3.45	0.832	KCRM (17)	3.45 ± 1.09	1.96 ± 2.95	0.063
TPM2 (7)	1.47 ± 0.21	1.22 ± 0.85	0.548	KCRM (16)	5.14 ± 2.33	3.69 ± 3.38	0.254
ACTS (5)	1.84 ± 0.81	1.66 ± 1.35	0.194	ATPA (15)	0.96 ± 1.21	0.62 ± 0.98	0.361

KCRM (16)	5.22 ± 0.58	5.12 ± 2.43	0.594	ANXA4 (20)	0.51 ± 2.56	0.35 ± 1.06	0.337
DESM (3)	4.80 ± 1.72	4.71 ± 0.74	0.853	G3P (21)	1.07 ± 2.76	0.93 ± 1.68	0.092
MLRS (12)	1.69 ± 0.41	1.60 ± 0.30	0.071	ACTS (5)	1.60 ± 1.15	1.66 ± 0.63	0.842
ANXA4 (20)	1.19 ± 1.26	1.12 ± 0.99	0.965	PLEC (2)	0.46 ± 1.59	0.60 ± 1.63	0.973
G3P (22)	7.32 ± 5.03	7.43 ± 4.21	0.472	ENOB (13)	8.81 ± 3.51	10.24 ± 3.77	0.117
MYL1 (8)	4.67 ± 0.94	4.81 ± 0.27	0.624	G3P (22)	1.13 ± 1.13	2.61 ± 1.30	0.320
MLRS (11)	2.74 ± 0.57	2.92 ± 0.89	0.346	TNNT3 (26)	0.02 ± 0.22	1.55 ± 0.68	0.047
G3P (21)	1.13 ± 1.13	1.32 ± 0.05	0.743	MLRS (11)	7.52 ± 1.34	9.28 ± 3.06	0.472
ENOB (13)	6.79 ± 0.32	7.01 ± 1.60	0.071	ENOB (14)	0.03 ± 0.33	2.08 ± 0.34	0.001
TNNT3 (25)	2.50 ± 0.30	2.73 ± 0.63	0.854	DESM (3)	3.41 ± 2.24	5.63 ± 2.49	0.357
MYL1 (9)	3.02 ± 1.20	3.27 ± 0.66	0.733	TNNT3 (28)	0.02 ± 0.16	2.27 ± 1.18	0.026
TPM4 (6)	9.21 ± 1.70	9.61 ± 2.99	0.964	MYL1 (9)	0.97 ± 1.96	3.45 ± 1.02	0.087
TNNT3 (28)	0.72 ± 0.44	1.49 ± 0.11	0.052	TNNI2 (23)	0.13 ± 0.10	2.65 ± 0.90	0.019
TNNT3 (26)	0.74 ± 0.43	1.94 ± 0.86	0.046	TNNT3 (25)	1.21 ± 3.06	3.99 ± 4.20	0.791
TNNI2 (23)	2.75 ± 0.10	4.31 ± 0.57	0.042	MLRS (12)	10.26 ± 5.27	15.09 ± 1.63	0.083
ENOB (14)	6.48 ± 2.26	8.12 ± 1.62	0.042	TPM4 (6)	66.07 ± 5.11	76.08 ± 9.95	0.762

Protein I.D. relates to the Uni-Prot database, entries returned using the MASCOT search engine. Spot numbers are in brackets which refers to the different proteoforms resolved by 2DGE and corresponds to the 2DGE image in Figure 3.2. Synthesis rates are presented in relative format which relates to fractional synthesis rate in percent per day and in absolute terms which is reflective of whole EDL synthesis with rates expressed in picograms per day. All data is represented as MEAN \pm SD for biological replicates (n = 3) in the 30 days stimulated muscle (Stim) and the non-stimulated control muscle (Ctrl). The proteins are ranked in order of largest increase in synthesis rate from Ctrl to Stim through to largest decrease in synthesis rate from Ctrl to Stim. P-Values are generated from paired t-tests between control and 30-d stimulated muscle.

Table S5. Rank order for abundance changes in soluble proteins after 30-d of stimulation in EDL muscle.

Protein I.D.	Relative ABD	P-Value	Protein I.D.	Absolute ABD	P-Value
ALBU	+3.27 ± 0.8	0.001	ATPA	+11.83 ± 1.2	0.017
CX7A2	+3.06 ± 0.9	0.004	CAH3	+10.34 ± 2.4	0.021
IDHP	+3.01 ± 1.1	0.014	ODPA	+9.32 ± 2.9	0.001
HBB1	+2.93 ± 0.7	0.036	HBA	+8.53 ± 5.6	0.051
AATM	+2.84 ± 0.5	0.001	ACADL	+7.99 ± 1.3	0.027
ATPB	+2.76 ± 1.2	0.019	ACON	+7.75 ± 1.6	0.023
CASQ1	+2.38 ± 1.0	0.028	ATPB	+7.21 ± 2.2	0.011
ATPO	+2.35 ± 1.4	0.015	CASQ1	+5.80 ± 1.7	0.002
MYG	+2.05 ± 0.8	0.039	ATPO	+5.69 ± 2.0	0.012
HBA	+2.02 ± 0.6	0.036	AATC	+5.10 ± 0.3	0.039
CAH3	+1.95 ± 0.4	0.037	ALBU	+4.60 ± 1.8	0.033
ACON	+1.92 ± 0.7	0.041	CX7A2	+4.28 ± 1.3	0.014
HSPB6	+1.88 ± 1.0	0.042	MDHC	+4.09 ± 0.4	0.025
ATPA	+1.71 ± 0.3	0.026	MDHM	+3.41 ± 1.4	0.035
AT2A2	+1.69 ± 0.4	0.039	HBB1	+2.78 ± 0.6	0.028
ACADL	+1.66 ± 0.6	0.028	MYG	+2.49 ± 1.1	0.017
ODPA	+1.32 ± 1.1	0.041	IDHP	+1.96 ± 0.8	0.004
MDHC	+1.31 ± 0.9	0.045	HSPB6	+1.63 ± 0.2	0.033
MDHM	+1.24 ± 0.9	0.049	AATM	+1.52 ± 0.7	0.047
AATC	+1.18 ± 0.7	0.031	AT2A2	+0.93 ± 0.8	0.047
HBB2	+0.94 ± 1.2	0.611	IDH3A	+0.86 ± 0.7	0.371
IDH3A	+0.94 ± 0.9	0.108	HBB2	+0.65 ± 0.5	0.482
SAFB1	+0.90 ± 0.7	0.821	ACTA	+0.26 ± 0.9	0.625

HINT1	+0.52 ± 0.6	0.893	VDAC	-0.17 ± 0.1	0.763
ACTA	+0.21 ± 0.4	0.673	SAFB1	-1.41 ± 0.8	0.884
VDAC	-0.20 ± 0.3	0.934	HINT1	-1.47 ± 3.1	0.942
TRY1	-0.35 ± 0.2	0.68	FHL1	-1.58 ± 1.0	0.174
KCRM	-0.48 ± 0.8	0.942	KPYM	-1.75 ± 1.4	0.290
KPYM	-0.49 ± 1.2	0.773	KCRM	-1.92 ± 0.2	0.439
FHL1	-0.56 ± 0.9	0.167	PARK7	-1.92 ± 1.7	0.431
PARK7	-0.60 ± 0.8	0.122	TRY1	-2.70 ± 2.2	0.771
PGM1	-0.66 ± 1.2	0.199	PGM1	-2.95 ± 2.8	0.847
ALDR	-0.71 ± 0.7	0.784	PGK1	-3.69 ± 1.3	0.031
KCRB	-1.03 ± 0.4	0.042	PYGB	-3.70 ± 1.4	0.014
MYL1	-1.31 ± 0.7	0.048	KCRB	-4.10 ± 1.9	0.027
PFKAM	-1.39 ± 0.8	0.045	KAD1	-4.51 ± 1.2	0.036
KAD1	-1.65 ± 1.0	0.037	LDHA	-4.70 ± 2.1	0.024
PGAM2	-2.03 ± 1.1	0.013	MYL1	-5.20 ± 1.3	0.029
PGK1	-2.04 ± 0.8	0.028	PGAM2	-6.47 ± 1.2	0.011
TPIS	-2.06 ± 1.3	0.037	ALDR	-7.53 ± 1.3	0.036
PYGM	-2.25 ± 0.7	0.022	ALDOA	-7.65 ± 1.4	0.018
ALDOA	-2.53 ± 0.6	0.023	TPIS	-7.68 ± 1.9	0.014
LDHA	-2.96 ± 1.3	0.028	ENOB	-8.81 ± 2.7	0.012
PRVA	-3.22 ± 1.1	0.001	PRVA	-9.10 ± 2.5	0.001
ENOB	-3.63 ± 0.9	0.033	G3P	-11.42 ± 1.4	0.003
PYGB	-4.01 ± 1.2	0.001	PYGM	-12.56 ± 2.3	0.001
G3P	-4.46 ± 1.2	0.001	PFKAM	-14.75 ± 1.8	0.001

Protein I.D. relates to the Uni-Prot database, entries returned using the MASCOT search engine. Relative abundance (ABD) represents Log-transformed MS data normalised by inter-sample abundance ratio using nonconflicting peptides only. Absolute abundance (ABD) represents Log-transformed MS data normalised by inter-sample abundance ratio using nonconflicting peptides and total EDL mass. All data is represented as MEAN \pm SD for biological replicates (n = 3) and is displayed as the positive (+) or negative (-) fold change from non-stimulated control muscle to 30 days chronically stimulated muscle, in rank order of largest positive change to largest negative change. P-Values are generated from paired t-tests between control and 30-d stimulated muscle.

Table S6. Rank order for synthesis rates in soluble proteins after 30-d of stimulation in EDL muscle.

Protein I.D.	Relative (Stim)	Relative (Ctrl)	P-Value	Protein I.D.	Absolute (Stim)	Absolute (Ctrl)	P-Value
CAH3	17.20 ± 6.80	14.83 ± 4.01	0.019	ATPA	136.51 ± 4.12	33.89 ± 6.46	0.001
ACON	7.39 ± 3.07	5.10 ± 1.23	0.024	CAH3	157.36 ± 15.51	60.37 ± 8.98	0.019
ATPA	3.19 ± 2.45	1.21 ± 0.47	0.028	HBA	167.32 ± 19.90	71.78 ± 21.37	0.042
HSPB6	4.00 ± 2.00	2.23 ± 0.51	0.027	ODPA	122.80 ± 5.68	40.21 ± 8.01	0.023
ATPO	8.36 ± 0.03	6.64 ± 0.02	0.015	ACADL	85.95 ± 9.58	3.95 ± 0.70	0.002
CASQ1	11.17 ± 4.28	9.64 ± 0.73	0.025	ATPB	173.69 ± 5.21	95.66 ± 8.57	0.022
ACADL	4.18 ± 1.58	2.65 ± 0.12	0.041	CASQ1	74.21 ± 10.25	11.30 ± 8.06	0.011
MDHC	4.89 ± 0.96	3.39 ± 0.94	0.033	LDHA	171.41 ± 25.69	110.05 ± 5.20	0.856
MYG	3.77 ± 0.71	2.30 ± 0.02	0.013	ACON	94.27 ± 12.81	37.92 ± 9.23	0.027
ATPB	10.76 ± 2.72	9.42 ± 1.77	0.044	MYG	141.20 ± 5.94	85.83 ± 11.68	0.021
AATM	2.09 ± 0.11	0.84 ± 0.13	0.037	MDHC	89.31 ± 3.82	37.27 ± 2.14	0.027
HBA	8.36 ± 0.62	7.11 ± 0.13	0.014	AATC	108.48 ± 4.93	58.46 ± 3.03	0.016
ODPA	9.29 ± 1.16	8.11 ± 0.80	0.047	ATPO	76.47 ± 9.40	28.37 ± 4.20	0.005
HBB1	6.97 ± 1.48	5.86 ± 0.91	0.046	HBB1	37.34 ± 1.28	8.58 ± 1.06	0.001

IDH3A	4.00 ± 0.79	3.01 ± 0.79	0.052	HSPB6	29.65 ± 2.81	11.41 ± 3.15	0.036
AATC	1.78 ± 0.17	0.81 ± 0.16	0.048	AATM	14.98 ± 6.39	3.34 ± 1.21	0.034
CX7A2	7.68 ± 3.45	7.32 ± 0.23	0.754	ACTA	14.85 ± 8.75	10.00 ± 5.35	0.775
ACTA	1.26 ± 0.23	1.00 ± 0.23	0.775	MDHM	83.70 ± 8.35	79.42 ± 6.76	0.592
IDHP	5.69 ± 1.17	5.46 ± 1.11	0.173	PGM1	34.98 ± 2.97	31.08 ± 5.51	0.852
MDHM	10.93 ± 1.66	10.73 ± 1.52	0.964	IDH3A	7.18 ± 3.32	3.96 ± 2.05	0.271
HBB2	7.54 ± 0.07	7.35 ± 0.17	0.427	HBB2	9.62 ± 7.16	6.62 ± 3.10	0.095
AT2A2	1.18 ± 0.09	1.04 ± 0.12	0.976	CX7A2	46.85 ± 5.86	44.68 ± 3.46	0.794
SAFB1	1.03 ± 0.88	0.98 ± 0.22	0.463	AT2A2	13.99 ± 2.45	12.22 ± 2.24	0.864
ALBU	7.23 ± 0.24	7.19 ± 0.18	0.954	SAFB1	7.78 ± 8.31	6.32 ± 4.02	0.857
KCRM	4.78 ± 1.03	4.85 ± 1.53	0.958	VDAC	9.20 ± 8.00	7.88 ± 2.56	0.739
HINT1	1.15 ± 0.14	1.29 ± 0.19	0.904	PRVA	13.25 ± 6.56	12.71 ± 2.35	0.947
PYGM	9.65 ± 0.94	9.80 ± 1.04	0.342	KAD1	19.29 ± 6.34	18.90 ± 8.83	0.492
PGAM2	5.57 ± 1.28	5.74 ± 0.92	0.875	MYL1	1.58 ± 2.36	2.24 ± 1.66	0.906
FHL1	0.80 ± 0.21	0.99 ± 0.16	0.729	G3P	0.04 ± 0.03	0.82 ± 0.29	0.028
LDHA	11.24 ± 1.43	11.47 ± 0.23	0.996	ALBU	111.36 ± 1.09	112.59 ± 4.53	0.375

PARK7	1.14 ± 0.45	1.37 ± 0.28	0.663	ALDR	60.15 ± 5.98	61.47 ± 4.14	0.821
ALDR	8.54 ± 0.34	8.79 ± 0.31	0.655	KCRM	82.19 ± 4.42	84.21 ± 2.44	0.841
PGK1	5.95 ± 0.2	6.19 ± 1.07	0.722	FHL1	5.49 ± 4.10	7.59 ± 3.15	0.885
MYL1	1.53 ± 0.38	1.78 ± 0.69	0.504	PARK7	3.17 ± 2.55	5.91 ± 3.57	0.336
TRY1	1.06 ± 0.08	1.37 ± 0.18	0.933	PGAM2	90.96 ± 6.29	94.01 ± 7.20	0.962
VDAC	1.26 ± 0.02	1.58 ± 0.13	0.411	PGK1	101.81 ± 7.95	104.89 ± 5.43	0.973
KAD1	1.43 ± 0.55	1.78 ± 0.14	0.195	IDHP	31.04 ± 4.01	34.62 ± 6.55	0.954
ALDOA	8.11 ± 0.79	8.50 ± 2.80	0.785	TRY1	20.10 ± 3.59	23.72 ± 2.14	0.944
PRVA	4.38 ± 3.34	4.79 ± 0.96	0.182	HINT1	3.12 ± 4.20	7.30 ± 2.17	0.625
KPYM	2.25 ± 0.22	2.69 ± 0.13	0.885	PFKAM	0.13 ± 0.43	4.64 ± 1.45	0.041
G3P	0.74 ± 0.47	1.79 ± 0.16	0.048	KPYM	35.12 ± 10.19	40.55 ± 1.44	0.798
TPIS	0.91 ± 0.20	2.00 ± 0.14	0.047	PYGM	89.70 ± 7.81	98.22 ± 12.08	0.418
PGM1	2.12 ± 2.17	3.30 ± 1.29	0.163	ALDOA	98.22 ± 7.82	112.65 ± 8.91	0.632
KCRB	5.12 ± 0.14	6.35 ± 0.51	0.031	ENOB	1.80 ± 1.44	21.42 ± 4.59	0.028
PFKAM	9.22 ± 0.84	10.48 ± 0.82	0.029	KCRB	8.98 ± 1.68	41.89 ± 4.89	0.015
ENOB	7.31 ± 1.64	8.97 ± 1.71	0.029	PYGB	7.80 ± 1.50	41.31 ± 8.25	0.027

PYGB	10.81 ± 2.55	12.69 ± 2.95	0.031	TPIS	3.21 ± 2.49	50.13 ± 11.53	0.014
------	--------------	--------------	-------	------	-------------	---------------	-------

Protein I.D. relates to the Uni-Prot database, entries returned using the MASCOT search engine. Synthesis rates are presented in relative format which relates to fractional synthesis rate in percent per day and in absolute terms which is reflective of whole EDL synthesis with rates expressed in picograms per day. All data is represented as MEAN ± SD for biological replicates (n = 3) in the 30 days stimulated muscle (Stim) and the non-stimulated control muscle (Ctrl). The proteins are ranked in order of largest increase in synthesis rate from Ctrl to Stim through to largest decrease in synthesis rate from Ctrl to Stim. P-Values are generated from paired t-tests between control and 30-d stimulated muscle.

Supplementary figures

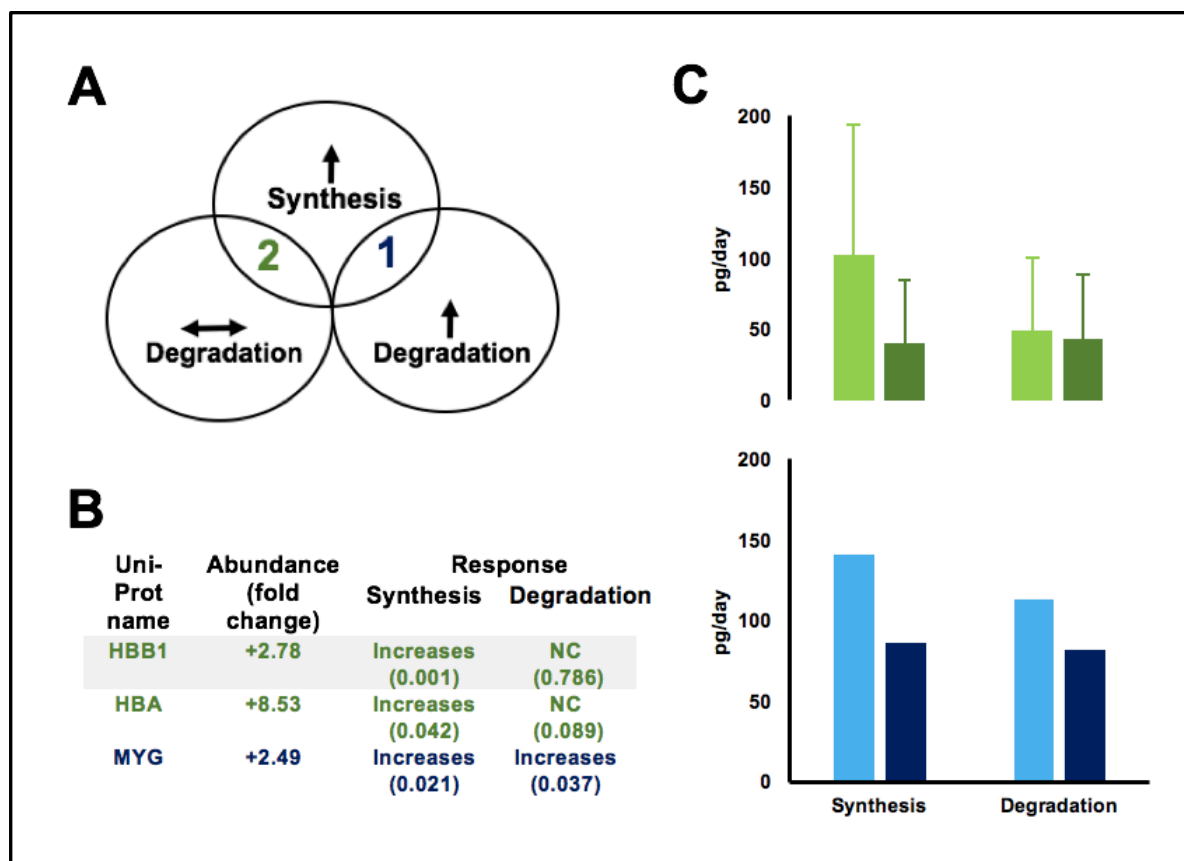


Figure S1. Protein turnover responses of oxygen transport proteins.

Mean protein turnover data is shown in absolute terms (pg/d) for oxygen transport proteins that exhibit a significant ($P < 0.05$) difference in abundance between the control and stimulated muscle at the 30-d time point. (A) Venn diagram displays the number of oxygen transport proteins that show different responses in protein turnover: increases (\uparrow), decreases (\downarrow) or no change (\leftrightarrow) for synthesis and degradation in order to change their net abundance after 30 days of stimulation. (B) Uni-Prot name relates to the protein I.D. using the Uni-Prot database, entries returned using the MASCOT search engine (number relates to the spot number in Figure 3.2). The response is described for both synthesis and degradation with significance level (P-value) for each protein which corresponds with the Venn diagram in panel A. (C) Summary of proteins identified in panel B, grouped and colour coded by their protein turnover responses. Green text in panel B represent data in green in panel C etc. Data is displayed for absolute synthesis and degradation in picograms per day as mean \pm SD for each collective group ($n = 3$). The light-coloured bars represent the 30-d stimulated muscle and the darker coloured bars represent the control muscle.

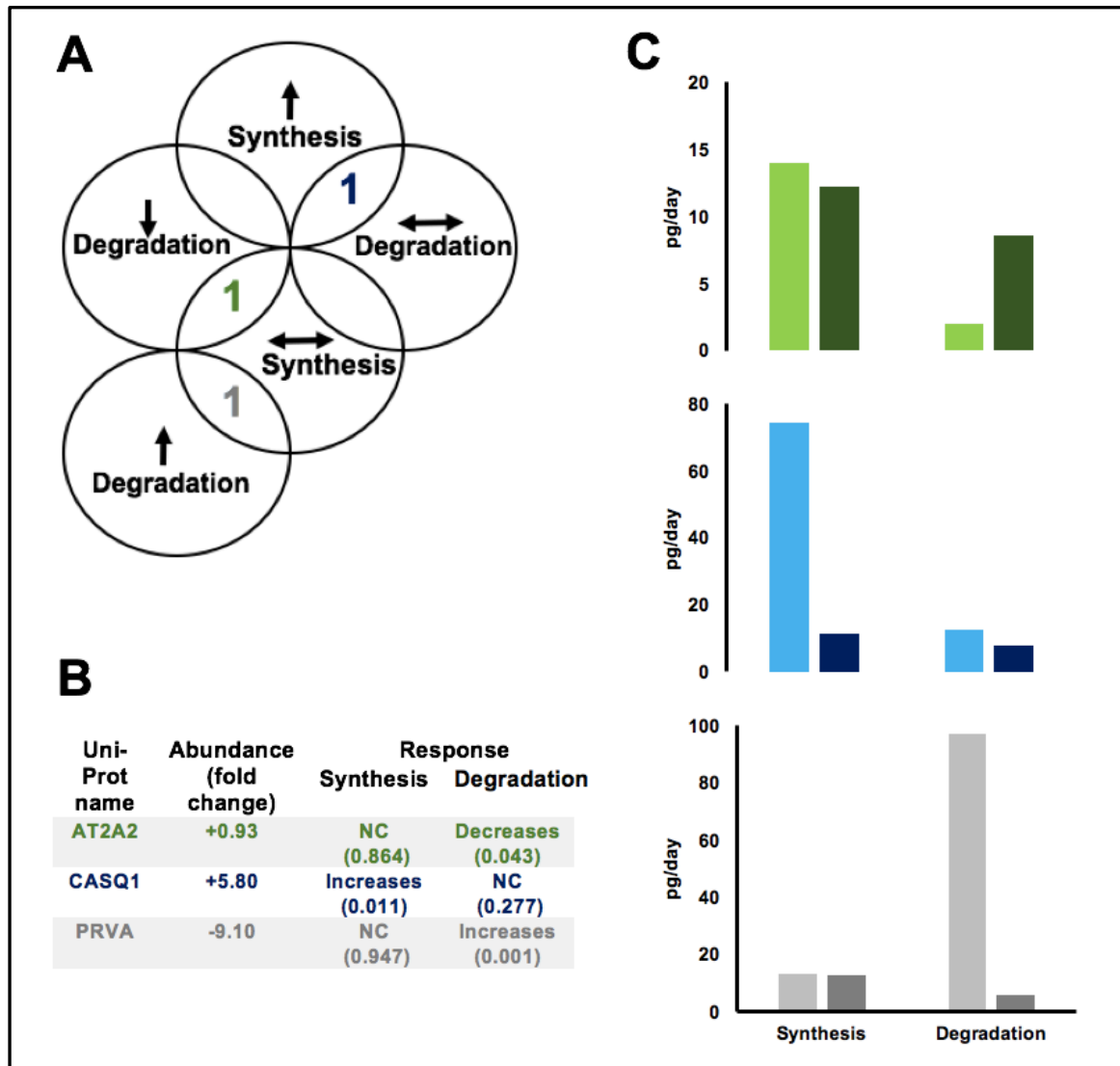


Figure S2. Protein turnover responses of calcium handling proteins.

Mean protein turnover data is shown in absolute terms (pg/d) for calcium handling proteins that exhibit a significant ($P < 0.05$) difference in abundance between the control and stimulated muscle at the 30-d time point. (A) Venn diagram displays the number of calcium handling proteins that show different responses in protein turnover: increases (\uparrow), decreases (\downarrow) or no change (\leftrightarrow) for synthesis and degradation in order to change their net abundance after 30 days of stimulation. (B) Uni-Prot name relates to the protein I.D. using the Uni-Prot database, entries returned using the MASCOT search engine (number relates to the spot number in Figure 3.2). The response is described for both synthesis and degradation with significance level (P-value) for each protein which corresponds with the Venn diagram in panel A. (C) Summary of proteins identified in panel B, grouped and colour coded by their protein turnover responses. Green text in panel B represent data in green in panel C etc. Data is displayed for

absolute synthesis and degradation in picograms per day as mean \pm SD for each collective group (n = 3). The light-coloured bars represent the 30-d stimulated muscle and the darker coloured bars represent the control muscle.

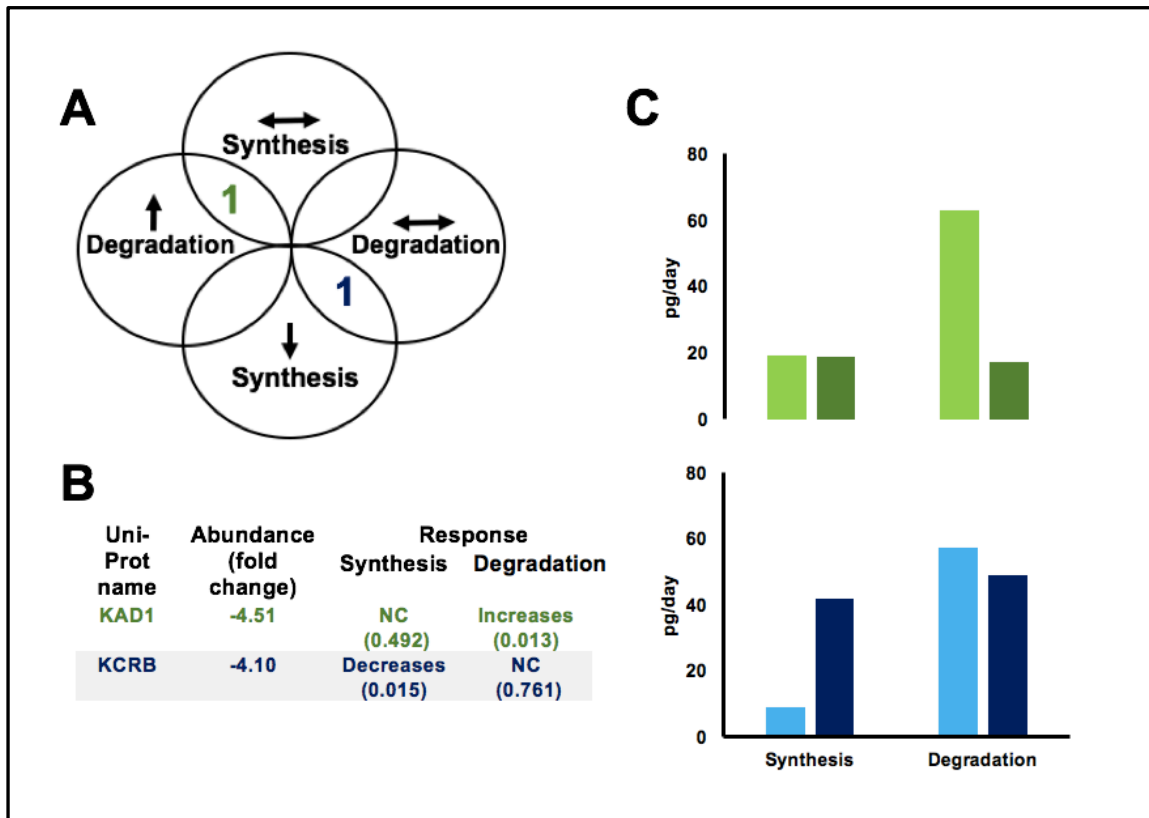


Figure S3. Protein turnover responses of high-energy phosphate proteins.

Mean protein turnover data is shown in absolute terms (pg/d) for high-energy phosphate proteins that exhibit a significant ($P < 0.05$) difference in abundance between the control and stimulated muscle at the 30-d time point. (A) Venn diagram displays the number of high-energy phosphate proteins that show different responses in protein turnover: increases (\uparrow), decreases (\downarrow) or no change (\leftrightarrow) for synthesis and degradation in order to change their net abundance after 30 days of stimulation. (B) Uni-Prot name relates to the protein I.D. using the Uni-Prot database, entries returned using the MASCOT search engine (number relates to the spot number in Figure 3.2). The response is described for both synthesis and degradation with significance level (P-value) for each protein which corresponds with the Venn diagram in panel A. (C) Summary of proteins identified in panel B, grouped and colour coded by their protein turnover responses. Green text in panel B represent data in green in panel C etc. Data is displayed for absolute synthesis and degradation in picograms per day as mean \pm SD for each collective group ($n = 3$). The light-coloured bars represent the 30-d stimulated muscle and the darker coloured bars represent the control muscle.

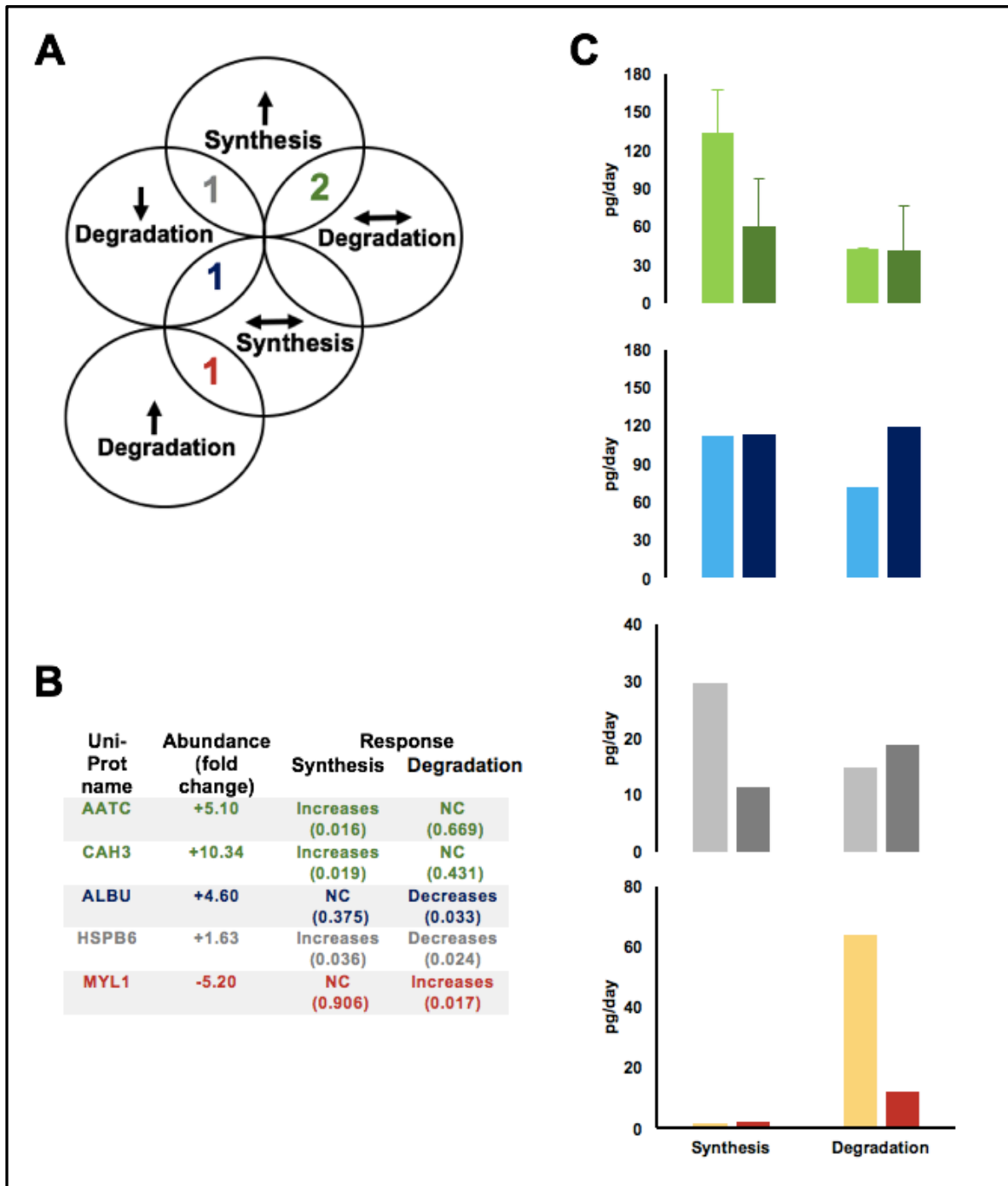


Figure S4. Protein turnover responses of unassigned proteins.

Mean protein turnover data is shown in absolute terms (pg/d) for unassigned proteins that exhibit a significant ($P < 0.05$) difference in abundance between the control and stimulated muscle at the 30-d time point. (A) Venn diagram displays the number of unassigned proteins that show different responses in protein turnover: increases (\uparrow), decreases (\downarrow) or no change (\leftrightarrow) for synthesis and degradation in order to change their net abundance after 30 days of stimulation. (B) Uni-Prot name relates to the protein I.D. using the Uni-Prot database, entries returned using the MASCOT search engine

(number relates to the spot number in Figure 3.2). The response is described for both synthesis and degradation with significance level (P-value) for each protein which corresponds with the Venn diagram in panel A. (C) Summary of proteins identified in panel B, grouped and colour coded by their protein turnover responses. Green text in panel B represent data in green in panel C etc. Data is displayed for absolute synthesis and degradation in picograms per day as mean \pm SD for each collective group (n = 3). The light-coloured bars represent the 30-d stimulated muscle and the darker coloured bars represent the control muscle.

Chapter 4. The role of protein turnover in skeletal muscle adaptation induced by co-contraction high-frequency stimulation.

4.1 Abstract

Adaptations to resistance exercise training can support improvements in athletic performance but also improve health-related musculoskeletal function and offset the loss of muscle mass and strength in pathological states. Resistance exercise is also associated with a general increase in muscle protein turnover, but it is not yet known how the components of protein turnover (i.e. synthesis and degradation) are coordinated to bring about exercise-induced changes in protein abundance. We have used stable isotope labelling and co-contraction high-frequency stimulation (CHFS) *in vivo* to investigate how the synthesis, abundance and degradation of individual proteins change during resistance exercise-induced muscle hypertrophy.

Four independent groups of rats ($n = 4$ in each), received CHFS (5 sets of 10 repetitions at 100 Hz, daily) and deuterium oxide for either 0 d, 10 d, 20 d or 30 d. At each time point the tibialis anterior (TA) muscle was harvested from the stimulated left hindlimb (Stim) and non-stimulated right hindlimb (Ctrl). Proteomic techniques were used to quantify changes in abundance of 35 myofibrillar proteins and 57 soluble proteins. Peptide mass spectrometry was used to calculate protein synthesis rates, protein degradation was calculated from the difference between the change in abundance and synthesis rate. Resistance exercise training increased ($P = 0.002$) the average rate of synthesis in mixed myofibrillar proteins from Ctrl (34.71 ± 1.07 pg/d) to Stim (40.18 ± 0.96 pg/d). However, the synthesis rate of mixed soluble proteins did not change ($P = 0.639$) from Ctrl (49.66 ± 0.82 pg/d) to Stim (52.04 ± 1.07 pg/d). However, there was a large range 2.71 ± 0.55 pg/d (PFKAM) to 140.53 ± 0.24 pg/d (KCRM) of individual protein synthesis rates. Protein turnover responses differ on a protein-by-protein basis during muscle adaptation. For example, ALBU and ACTS both increase ($P = 0.014$, 0.003 respectively) in abundance in response to CHFS, but ALBU does not change ($P = 0.831$) its synthesis in Stim compared to Ctrl, whereas ACTS increases ($P = 0.016$) the rate of synthesis in Stim. In contrast, CAH3 and G3P both do not change ($P = 0.271$, 0.113 respectively) in abundance in response to CHFS, but CAH3 increases ($P = 0.001$) and G3P decreases ($P = 0.013$) the rate of synthesis in Stim compared to Ctrl. In conclusion, muscle adaptation in response to CHFS is

underpinned by protein-specific changes in synthesis and degradation. Our data suggest both protein synthesis and protein degradation contribute to changes in protein abundance during muscle adaptation to resistance exercise training.

4.2 Introduction

Resistance exercise training elicits a range of morphological and neurological adaptations, including increases in muscle mass and strength that contribute towards whole-body changes in physiological function (Booth and Thomason, 1991.; Folland and Williams, 2007). Strength directly refers to the capacity of the muscle to exert force against an external load, whereas hypertrophy is defined as an increase in muscle mass (Folland and Williams, 2007). Muscle adaptations to resistance exercise include changes to the metabolic properties of a muscle as well as the contractile elements of the muscle, and these gross changes in muscle phenotype are underpinned by complex changes in the abundance or modification status of numerous proteins (Roux et al, 2013). Such changes in protein abundance are brought about through differences in synthesis and degradation. Exercise is generally associated with a universal increase in muscle protein turnover, especially following resistance activity (Chesley et al, 1992; MacDougall et al, 1995). Biolo et al, (1995) reported protein turnover to increase compared to resting values post resistance exercise, but fractional synthesis rate (FSR) to be higher (~133 %) than the degradation (~40 %) rate (FDR) of mixed muscle proteins in untrained humans, even for up to 3 hours after exercise cessation. Thus, demonstrating an increase in whole muscle protein turnover in response to resistance exercise and a likely shift towards a more positive net protein balance (i.e. synthesis increased more than degradation). However, these data are the average synthesis and degradation rates of mixtures of thousands of different proteins and it is not yet known how the individual components of protein turnover (i.e. synthesis and degradation) are coordinated on an individual level to bring about changes in protein abundance that underpin phenotypic changes associated with resistance exercise. Changes in protein abundance and the subsequent increases in protein content of the muscle leading to hypertrophy can result in improvements in strength, muscular endurance, power and neuromuscular control (Kraemer et al, 1988; Folland and Williams, 2007). These adaptations can support improvements in athletic performance as well as improve health-related musculoskeletal function in general populations, e.g. by offsetting the loss of muscle mass and strength in pathological states such as sarcopenia (Macaluso and De Vito, 2004). This ability of skeletal muscle to adapt to external stimuli i.e. resistance training can be used to access the range of benefits associated with a greater muscle

hypertrophy. Muscle has been shown to elicit an increase in size in response to resistance exercise at an intensity of 65-80 % 3 times per week ~40 %, based on myofibre size and ~4 %, based on fat free mass increases in humans (Bamman et al, 2003.; Rennie et al, 2004) and ~7 % to ~30 % in rats (Alway et al, 2005). Furthermore, progressive resistance training can alter the individual abundance of key muscle proteins, which in turn increases the protein content of the muscle (up to 24 % in rat over 8 weeks of training; Hornberger and Farrar, 2004) to induce adaptations to the physiology, cell biology and neuromuscular control of a muscle in order to efficiently fulfil the demands of a particular locomotion task. There are well developed guidelines for resistance training that produce muscular characteristics such as strength, hypertrophy, power and endurance that are extensively documented (ACSM, 2009). There are also many advantages to long-term health that resistance exercise training affords, such as the maintenance of strength and lean muscle tissue to prevent the onset of conditions such as sarcopenia (Marzetti et al, 2017). However, with the advent of exercise proteomics, there is now room to refine our understanding regarding such adaptations, permitting investigation of how the synthesis and degradation of individual proteins contribute to changes in protein turnover. Employing the use of exercise proteomics will provide a more explicit understanding to the mechanism of how this adaptation to resistance exercise occurs addressing issues that previous literature has failed to. Whilst at the same time providing insight in to how pathophysiological conditions (e.g. sarcopenia) are manifested in skeletal muscle. To maintain or increase the volume of skeletal muscle mass is of clear benefit to health (Landi et al, 2014). Exercise induced gains in muscle mass are commonly attributed to a greater protein synthetic response, Brook et al, (2015) recently reported an ~20 % increase in the synthesis rate of mixed myofibrillar proteins during the first 3 weeks of a resistance exercise intervention that accounted for most of the observed increase in muscle mass. However, their study did not measure individual protein responses to exercise, so the relationship between an average increase in synthesis across mixed myofibrillar proteins and selective changes in myofibrillar protein abundance was not clear. Furthermore, Phillips et al, (1997) also demonstrate that muscle is often in a catabolic state unless exercise is undertaken or protein is consumed, underlining the importance of exercise training to maintain muscle mass. Here, FSR and FDR was determined using primed constant infusions of amino acid tracer to study subjects in a fasted state at rest and up to 48 hours after a resistance exercise bout. Resistance

exercise resulted in significant increases in FSR and FDR, ~113 % and ~31 % respectively. However, in the resting state only, FDR exceeded FSR by ~83% resulting in the net loss of muscle protein. This work highlights the importance of muscle protein degradation in the adaptive response and suggests that degradation may have a fundamental role in the remodelling of skeletal muscle in response to resistance exercise. Furthermore, reports (Mitchell et al, 2014) that acute (~6 h) elevations in muscle protein synthesis rates tend to over-estimate the longer-term hypertrophy responses which also indicate that protein degradation is an important component of the response to chronic resistance training.

Exercise proteomic techniques, such as dynamic proteome profiling (DPP), enables the time course of adaptation to be investigated over longer periods. Compared to the traditional amino acid tracer methods that can be sustained for approximately <12 h, DPP relies on oral consumption of stable isotope and investigation can occur over days or weeks. Currently, it is not known how resistance exercise training influences protein turnover in this manner i.e. over weeks, and little is known about the modulation of synthetic and degradative processes over longer time courses of adaptation, that this would encompass. Camera et al, (2017) attempts to fill this gap by using dynamic proteome profiling in humans and reports key findings in that shows resistance exercise-induced changes in muscle protein abundance occurred via several different patterns of response that involved the modulation of both synthetic and degradative processes proteins. However, this was only a 9-day intervention and lacked absolute data to inform how individual protein responses are informing adaptation at the whole muscle level. Furthermore, human subjects have a larger body mass and subsequently have a slower uptake of deuterium (used in DPP) making curve fitting calculations more complex. These issues can be overcome with use of small laboratory animals, the precursor enrichment is rapid and stable making the calculation of synthesis rates more robust allowing the calculation of both individual protein turnover rates in both relative and absolute terms. Animal models also allow for whole muscle mass and protein abundance to be measured accurately, consequently overcoming the limitations of using DPP in human populations. However, models of resistance training in rats have been difficult to implement.

Research in this area has utilised several different animal models, that attempt to induce muscular hypertrophy in order to investigate the mechanisms associated with muscle growth. Compensatory overload is one of the longest established approaches

to producing muscle hypertrophy in rodents (Tomanek et al, 1970.; Timson, 1990) currently, several models of application exist, including: tenotomy (Goldberg et al, 1975), surgical removal (Iannuzzo et al, 1976.; Gollnick et al, 1981) or denervation (Degens et al, 2003) of synergistic muscles. Primarily, compensatory overload models are implemented unilaterally so the contralateral limb can serve as an intra-animal control. Hypertrophy is then achieved by inactivating or removing the synergists in the target limb, so that the remaining muscle is overloaded during movement by the animal (Armstrong et al, 1979; Roy et al, 1982). This is an attractive experimental approach and has been widely adopted because it provides a large (65-97 %) and rapid (hours after surgery) hypertrophic response with relatively little stress for the animal. Synergist ablation of gastrocnemius and soleus muscles is perhaps the most common, overloading the plantaris muscle (Armstrong et al, 1979; Baldwin et al, 1982). There are two distinct phases, a short-term inflammatory response of the muscle ranging from 1 hour to 10 days after the surgical removal of the synergist (Armstrong et al, 1979). As a result, there is a significant increase in the overloaded plantaris wet weight as early as 1 hour following surgery, but 96 % of this increase is accounted for by oedema. Muscle oedema appears to peak between 1–5 days post-surgery. However, the mass increases of the muscle appear to be due to surgical trauma rather than the increased stretch imposed on the muscle (Armstrong et al, 1979). The second phase is a slower long-term response, which can take as long as two-weeks, whereby the muscle responds to the increased functional demands imposed on it due to the removal of synergistic muscles. Tenotomy, the process of severing the distal tendon of synergist muscles has also been used to study hypertrophy of rat plantaris and soleus muscles (Goldberg et al, 1975; Timson, 1990). Tenotomy of the gastrocnemius results in rapid compensatory growth (~30-40 %) of the plantaris and soleus during the first week after surgery (Castle and Reyman, 1984.; Goldberg et al, 1975). However, Gollnick et al, (1981) report muscle mass then reduces (to ~10 % greater than control) after 2–3 weeks. Moreover, it seems compensatory hypertrophy is not a good model for studying the initial adaptations to skeletal muscle as the first stages of adaptation are largely missed due to the massive response of muscle oedema masking the hypertrophic response during the early part of compensatory overload. Armstrong et al, (1979) have illustrated that even with sham operations used as controls in surgical ablation models, the first initial increase in muscle size is due surgery related trauma evidenced by significant (~91 %) oedema of the muscle.

Furthermore, a potential complication with tenotomy is that the distal tendon may reattach to the remaining musculature, thus reducing the overload stimulus (Castle and Reyman, 1984.; Lowe and Alway, 2002). However, the degree of muscle hypertrophy is variable and seems to be due, at least in part, to the activity of the animal, with more active animals, such as mice showing greater hypertrophy than less active animals, for example cats (Roy and Edgerton, 1995).

Rodent models of either voluntary and involuntary resistance exercise have been developed and are reviewed in (Timson, 1990). These models attempt to establish weight-lifting strategies that mimic human resistance training. Wong and Booth, (1988) reported a unilateral model for resistance training in anaesthetised rats using bespoke apparatus to give mechanical resistance against plantar flexion of the foot in response to electrical stimulation. Resistance exercise was performed twice per week for 16 weeks and resulted in a 13-18 % increase wet muscle. However, a potential drawback of this design is that rats were also exposed to multiple rounds of anaesthesia which may have interfered with the hypertrophic response. Wong and Booth, (1990) used the same experimental setup again to study the differences between unloaded and high resistance concentric contractions of the gastrocnemius in anaesthetised rats during a high-frequency (20 bouts of 192 repetitions) training protocol. They reported an increase in muscle wet weight of the stimulated TA of 16 % for the unloaded group and 30 % for the high resistance group, in comparison to a sedentary control group. However, these values need to be interpreted with care, as the non-stimulated muscles of the trained animals also showed significant growth. Comparing the average muscle mass of the stimulated versus non-stimulated muscles within each group, gives a relative increase of 6 % for the unloaded group and 13 % for the high resistance group. The model described by Wong and Booth, (1988; 1990) led to the development of a much-improved model by Baar and Esser, (1999) here the use of stimulation to the sciatic nerve results in a simultaneous contraction of all innervated hind limb muscles. Thus, creating a model of co-contraction which has the benefit of working the target muscles antagonistically to produce a model of resistance exercise training that is highly comparable to human resistance exercise.

The strategy developed by Baar and Esser, (1999) utilised the fact that the plantar-flexors (gastrocnemius, GAS; soleus, SOL; plantaris, PLN) produce more force (~800 g maximal output, Wong and Booth, 1988) than the dorsi-flexors (extensor digitorum longus, EDL; tibialis anterior, TA) resulting in net plantar-flexion of the ankle. Thus,

producing a concentric contraction of the plantar-flexors, and an eccentric contraction of the dorsi-flexors. However, training sessions were again, performed in anaesthetised animals, twice a week for a total of 6 weeks resulting in a significant increase of wet muscle mass of ~14 % and in both the EDL and TA, but no comparable changes were observed within any of the plantar-flexor muscles. Unfortunately, these stimulation models (Wong and Booth, 1988; Baar and Esser, 1999) still require a lot of manual interaction and multiple periods of repeat anaesthesia to conduct an experiment which leads to increased stress for the animals and may subsequently affect the hypertrophic response. To address concerns regarding repeated periods of anaesthesia, Hornberger and Farrar, (2004) developed a model of resistance training in conscious rats. Animals were trained to climb a 1.1 metre ladder (80° incline) and resistance was added by attaching weights to the animals' tails. Hornberger and Farrar, (2004) report a 23 % increase in flexor hallucis longus (FHL) mass after 8 weeks of training (every 3 days per week, 4-9 climbs per session). Hindlimb training of the plantar-flexor muscles to mimic squat exercise in humans is effective and results in 20-30 % hypertrophy of the plantaris after 15 training sessions over a 3-week period (Wirth et al, 2003). Voluntary models may reflect physiological adaptation of muscle to resistance exercise more faithfully than the aforementioned surgical interventions. For example, Hornberger and Farrar, (2004) report muscle growth is underpinned by accretion of muscle protein, rather than oedema. Similarly, Duncan et al, (1998) report muscle growth after ladder climbing is associated with 50 % increase in fibre cross sectional area (i.e. true hypertrophy rather than damage response). These findings make voluntary models attractive, particularly because training parameters such as exercise type and intensity as well as rest intervals can be prescribed in a manner analogous to human training (Nader and Esser, 2001.; Haddad and Adams, 2002). However, operant conditioning strategies e.g. light or shock (Ho et al, 1980.; Tamaki et al, 1992) and are rewarded with food when they complete a lifting task (Gonyea and Ericson, 1976.; Wirth et al, 2003) are often required to ensure the animals will perform resistance exercise training, and can be challenging to achieve complete and reproducible execution of each task. This likely adds to inter-subject variability compared to involuntary protocols. Furthermore, food deprivation and reward or the use of an electrical shock stimulus to promote a lifting activity may interfere with intended outcome of the training programme (Des Neves et al, 2017). Lastly, voluntary

hindlimb training models are bilateral and thus the experimental muscles must be compared to muscles from control, sedentary animals.

The hypertrophic response to electrical stimulation models appear to be the least variable in terms of outcome (e.g. range of 13-18 % hypertrophy compared to 7-30 % seen in voluntary resistance training models and 30-97 % produced by compensatory overload models). Furthermore, models requiring surgical intervention, in comparison to more voluntary models, could be considered more ethical due to the animals being unaware of the surgery. Whereas operant conditioning involves a lot of interaction with the animals resulting in an increased amount of stress. Surgical intervention also allows for a better controlled model meaning less animals are required but with a greater statistical power due to the unilateral model permitting pair-sample analysis. Electrical stimulation differs from the natural ordered recruitment of motor units (Henneman et al, 1965), which may be regarded as non-physiological, but this also benefits the experiment design when the aim is to study the mechanisms of proteome adaptation. Electrical motor nerve stimulation has been used to activate muscles and induce muscular hypertrophy in anaesthetised animals to establish models of resistance exercise training (Wong and Booth, 1988; Baar and Esser, 1999). These animal models that incorporate electrical stimulation provide a robust means of studying both the acute and chronic responses of various contraction types in skeletal muscle, and are well positioned to offer an improved understanding of the mechanisms that contribute towards muscle hypertrophy (Wong and Booth, 1988; Baar and Esser, 1999).

Herein, we have used a relatively new model, developed within our group (Schmoll et al, 2018), involving electrically stimulated co-contraction of plantar flexors and dorsi flexors *in vivo*. Our model replicates the co-contraction design reported in Baar and Esser, (1999) but uses an implanted programmable stimulator and therefore does not involve repeat bouts of anaesthesia. Stimulation can be adjusted to optimise the load on the dorsi-flexors by moderating the activation of the plantar-flexors to result in isometric contraction. The model is unilateral and muscles of the non-stimulated limb provide a contralateral, internal control. In recent work (Schmoll et al, 2018), this model has produced comparable increases in muscle mass (14 % in TA and 11 % in EDL achieved over 4 weeks) with published in the literature (Baar and Esser, 1999).

Increases in muscle wet weight and protein content are common responses of skeletal muscle to mechanical loading (Timson, 1990). Wong and Booth, (1990) report both

shortening and lengthening contractions increase muscle size through increasing protein synthesis rates by ~50 % above baseline during the 12–17 h period after resistance stimulation. Furthermore, Baar and Esser, (1999) report p70S6k phosphorylation correlates with the increases EDL and TA size and therefore provides a mechanistic link to the processes underpinning protein translation. These data agree well with mixed muscle fractional synthesis data in humans. Phillips et al, (1997) reports resistance exercise results in significant increases above rest that is at its highest point 3 h post exercise (112 %) but is still elevated for up to 48 h (24 h, 65 %; 48 h, 34 %). Jacobs et al, (2013) report mTORC1 as a downstream target of p70S6k and a known mediator of protein synthesis. (Song et al, 2017) report higher levels of phosphorylation of p70S6k and subsequent mTORC1 activation in response to resistance exercise training in humans.

Exercise proteomics is a rapidly growing area of research, but to date there has been little work that has focused on resistance training or hypertrophy. Isfort et al, (2002) reports proteomic analysis of rat soleus muscle involving two dimensional gel electrophoresis (2DGE) to identify individual proteins. Isfort et al, (2002) implement a unilateral model of hindlimb suspension to induce atrophy for 14 days, subsequently the soleus is then reweighted to induce hypertrophy. Proteomic 2DGE separation was then performed on the samples after undergoing 7 days of reweighting induced hypertrophy. During the hypertrophic response, there were significant changes to the abundance of 15 muscle proteins that encompassed both contractile and metabolic proteins such as troponin T (increased) and beta enolase (decreased). Although we do not learn if these changes are brought about due to changes in synthesis or degradation, Isfort et al, (2002) provides evidence that both contractile and metabolic proteins are selectively gained or lost during muscle hypertrophy. Shankaran et al, (2016) reports growth in rat triceps muscle in response to selective androgen receptor (SAR) stimulation. The mass of the triceps increased ~10 % after 28 days of SAR administration and several metabolic and structural proteins such as, ATPB and MYL1/3 increased in fractional synthesis rates. However, in this case the authors did not measure protein abundance, and so these data do not distinguish between changes in synthesis rate that result in protein accumulation rather than elevated protein turnover. Therefore, it is necessary to measure synthesis, degradation and abundance simultaneously to gain an accurate representation of how protein turnover and ultimately muscle adaptation is organised. More recently, our lab reported

(Camera et al, 2017) dynamic proteome profiling of the human muscle response to a 9-day period of resistance exercise and high-fat diet. Dynamic proteome profiling combines traditional proteomic methods for measuring protein abundance with the new stable isotope incorporation methods recently reported in Shankaran et al, (2016) for measuring protein synthesis. Camera et al, (2017) reported synthesis and abundance measurements for almost 100 muscle proteins and used these data to also calculate protein specific degradation rates. These data (Camera et al, 2017) provide crucial evidence to demonstrate the processes of protein synthesis and degradation in response to resistance training are probably more complex than has been previously recognised. For example, there were at least 6 different patterns of response, including (i) proteins that increased in turnover rate with no change in abundance, (ii) proteins that increased in abundance with no increase in synthesis rate or (iii) proteins that decreased in abundance despite increasing in synthesis rate. Based on these data it will be of interest to investigate longer term responses to more prolonged training regimens that result in measurable increases in muscle mass. However, a limitation of dynamic proteome profiling using human participants is that accurate measurements of whole muscle mass are not easily obtainable. Comparison of fractional synthesis rate data from muscle at baseline and after a period of growth induced by exercise could be confounded by changes in overall muscle mass. For example, the fractional synthesis rate could be identical prior to and after training, and the relative abundance of the protein may be unchanged, but if overall the muscle has increased in size then the absolute amount of protein being synthesised will be greater. Without the ability to provide information at the whole muscle level i.e. absolute values, we cannot gain an entirely clear picture of how individual muscle protein turnover is orchestrated during resistance exercise adaptation. This limitation is circumvented by using an animal model where the mass of the isolated muscle can be measured. Moreover, calculation of protein synthesis using deuterium incorporation is more robust in small laboratory animals and our unilateral model provides internal control, which further enhances the robustness of the technique. Herein, we report a proteomic analysis, utilising our unique DPP method, whilst employing an *in vivo* animal model of co-contraction high-frequency stimulation (CHFS). A resistance training stimulus was delivered over a 30-day period and samples were taken at 10-day intervals in order to capture time-dependent changes in individual protein turnover.

Objectives

Objective of chapter - To investigate how individual protein responses coordinate the adaptive response of the muscle in response to hypertrophy.

Specific Aim 1: To measure increases in protein content to confirm a hypertrophic response from the model.

Specific Aim 2: To investigate the time course of changes to individual protein turnover in both myofibrillar and soluble fraction proteins in response to muscle hypertrophy.

Specific Aim 3: To identify proteoform-specific changes during muscle adaptation induced by CHFS and measure protein turnover to investigate how such changes are coordinated.

4.3 Methodology

All experimental procedures were conducted under the British Home Office Animals (Scientific Procedures) Act 1986. Male Wistar rats aged 3 months, 412 ± 69 g body weight were bred in-house in a conventional colony, housed in controlled conditions of 20 °C, 45 % relative humidity, and a 12 h light (0600–1800 hours) and 12 h dark cycle, with water and food available *ad libitum*. All aspects of animal husbandry were conducted by the LJMU animal facility staff. Surgery procedures and the electrical stimulation model of co-contraction were performed by Prof. Jonathan Jarvis and Dr. Hazel Sutherland as part of a wider project. Work conducted within this thesis focused solely on aspects associated with dynamic proteome profiling of muscle samples.

Animals were assigned to four groups ($n = 4$ in each), including a sham-operated control group and three groups (10, 20 and 30 days) that received deuterium oxide ($^2\text{H}_2\text{O}$; Sigma-Aldrich, St. Louis, MO) administration that was initiated by an intraperitoneal loading injection of 10 $\mu\text{L.g}$ 99 % $^2\text{H}_2\text{O}$ -saline, and was then maintained by administration of 5 % (v/v) $^2\text{H}_2\text{O}$ in the drinking water available to the rats, which was refreshed daily. Animals also received a programmed stimulation pattern that simulated high intensity resistance training from an implanted device, by means of

electrical nerve stimulation intended to induce hypertrophy of the Tibialis anterior (TA) muscle, described previously by our group (Schmoll et al, 2018). All surgical procedures and anaesthetic protocol were conducted according to Schmoll et al, (2018). Surgery was performed with full aseptic precautions and the animals were anaesthetised using a gaseous mixture of isoflurane and O₂. An initial concentration of 4 % isoflurane was used for induction of anaesthesia and was then adjusted to levels of 1-2 % to maintain an adequate surgical plane of anaesthesia. Buprenorphine (Temgesic, Indivior, Slough, UK) at a dose of 0.05 mg/kg⁻¹ body mass, was administered pre-surgery for analgesia. The animals received stimulation via the cathode electrode placed underneath the common peroneal nerve while the anode was positioned underneath the tibial nerve. This configuration takes advantage of the different stimulation thresholds for anodic and cathodic stimulation. The lower stimulation threshold at the cathode results in an initial recruitment of all the axons of the peroneal nerve followed by additional depolarization of some motor neurones within the tibial nerve at higher stimulation amplitudes. An amplitude was set that provided enough activation of the plantar-flexors to resist the action of the dorsi-flexors so that the ankle angle did not decrease. The forces produced by the much stronger plantar-flexor muscles were transmitted via the ankle joint and caused additional loading in auxotonic contractions of the TA muscle. The 0-day time point represents the sham-operated control group that were implanted with inactive stimulators and then killed after the 1-week recovery period. The remaining animals had the stimulation patterns implemented remotely using the Mini-VStim-App installed on a standard Android driven tablet computer (Xperia Tablet Z, Sony Corporation, Tokyo, Japan). The tablet computer maintained an active Bluetooth connection to a Mini-VStim programming device which served as bridge to communicate with the pulse generator via an additional radio frequency link to adjust the stimulation amplitude on day zero (all stimulation was initiated, monitored and controlled by researchers Mark Viggars and Steffen Eickhoff). Thereafter the stimulator operated autonomously and the animals were maintained in their normal cages. The stimulation pattern consisted of a daily 'warm-up' phase of 40 twitches at 4 Hz for a duration of 10 seconds immediately before the main daily training session. The main training stimulus entailed the animals receiving 5 sets of 10 repetitions. Each repetition was a 2 second contraction at a stimulation frequency of 100 Hz producing a fused, near maximal tetanic contraction of the recruited motor units. The devices were programmed to give

2 seconds of rest between repetitions and 2.5 minutes of rest between the sets. After 10 d, 20 d and 30 d of stimulation and deuterium oxide consumption, animals were euthanised humanely in a rising concentration of CO₂ followed by cervical dislocation. Plasma samples were obtained by cardiac puncture immediately after death and TA muscles, from the left stimulated limb (Stim) and the right non-stimulated limb (Ctrl), were isolated. Each muscle was cleaned of fat and connective tissue, weighed before being frozen in liquid nitrogen and stored at -80 °C pending further analysis.

Deuterium enrichment of the body water of each animal (n = 16) was determined by GC-MS analysis of ²H enrichment in plasma samples against external standards. Full methods are described in Chapter 2, section 2.4.2. Muscle homogenates were fractionated into the myofibrillar, contractile proteins and soluble fraction proteins according to Chapter 2, section 2.4.3. The subsequent analysis of the myofibrillar proteins were analysed via top-down proteomic methods using the gel-based separation method, 2-dimensional gel electrophoresis (2DGE) to isolate individual proteoforms and to quantify abundance changes. Individual proteins were identified from peptide mass fingerprinting and synthesis measurements were derived from MALDI mass spectrometry, detailed in its entirety in Chapter 2.5.

The analysis of the proteins in the soluble fraction was achieved by a bottom-up proteomic approach with full details described in Chapter 2.6. Here, protein samples underwent in-solution digest and were identified and abundance quantified via LC-MS/MS label free quantitation. MS data was normalised by an inter-sample abundance ratio, and the differences in relative protein abundance were quantified using nonconflicting peptides only. MS/MS spectra were exported into Mascot and individual proteins were identified, from which protein synthesis measurements were calculated based on the mass isotopomer distribution of specific peptides (Chapter 2.7).

Fractional synthesis rates (FSR) were derived for all identified myofibrillar and soluble proteins using the methods detailed in Chapter 2.7. Synthesis rates were calculated in both control (right, non-stimulated) and stimulated (left) muscles in two primary ways. All proteins used the fitting of the mass isotopomer data collected at each of the 4 experimental time-points using a semi-log plots. In addition, data were fitted using a 2-point non-linear first-order equation in order to calculate FSR over intermediate time points e.g. 0 d – 10 d, 10 d – 20 d, 20 d – 30 d. These calculations are achieved by first calculating the rate of decay of the molar fraction of the m₀ mass isotopomer

across 0 d, 10 d, 20 d and 30 d time points by using semi-log plots. The rate constant (k) is then divided by the number (n) of exchangeable hydrogen sites reported in standard tables (Commerford et al, 1983) and finally by the level of precursor enrichment (p) measured by GC-MS analysis of plasma samples. Protein FSR is then reported as the median of the peptide values assigned to each protein or proteoform. The individual rates for fractional degradation rate (FDR) were also calculated for each protein in the myofibrillar and soluble fractions. This was achieved by calculating the difference between the rate of synthesis and the rate of change in protein abundance (Full details in Chapter 2, section 2.7.2).

From the FSR and FDR calculations absolute protein turnover was calculated for each individual protein in the myofibrillar and soluble fraction (Full calculation details in Chapter 2, section 2.7.3). Absolute synthesis rates were calculated by first multiplying the wet weight of the TA by the total amount of protein extracted from the TA and then multiplying by the rate of change in relative protein abundance for each individual protein.

Statistical analysis of myofibrillar protein abundance was conducted on normalised spot data from 2D-gels. Normalised protein abundance from LC-MS label-free quantitation were used for soluble protein abundance. Relative synthesis rates were analysed as percent per day (%/d) and absolute synthesis rates were analysed as pmol/d in the soluble fraction proteins and as mg/d in the myofibrillar fraction proteins, all values are the average of the analysed peptides for each protein and subsequent analysis is at the protein level. All statistical testing was performed on biological replicates ($n = 4$ in each group) conducted using SPSS (SPSS, v23, Chicago, USA) and the statistical significance level was set at $P < 0.05$. To assess the degree of consistency across control situations (right limb, non-stimulated muscle) for all time points (10 d, 20 d and 30 d) and sham operated animals (0 d) a one-way ANOVA was used to analyse protein abundance, synthesis and degradation data. To assess the differences between the non-stimulated control limb (right) and the stimulated limb (left), paired T-tests were conducted to compare stimulated and non-stimulated limbs at each experimental time point (0 d, 10 d, 20 d and 30 d) for protein abundance, synthesis and degradation rates at the individual protein level. To control the false-discovery rate, P-value distributions were used to calculate Q values and a criterion false-discovery rate of $< 1\%$ was set. This statistical approach considers the biological

variation across each protein and, therefore, is more sophisticated than arbitrarily implementing a threshold on the basis of fold change.

4.4 Results

At the beginning of the experiment (0 days) the wet weight of the tibialis anterior (TA) was not different between the sham operated left limb (580.0 ± 46.6 mg) and the non-operated right limb (617.0 ± 46.8 mg). There was also no significant change in TA mass of the non-stimulated right limb at any of the experimental time points encompassing the 30 days of unilateral co-contraction high-frequency stimulation (CHFS). In response to CHFS, TA mass of the left, stimulated limb increased by 16 % after 10 days, and a further 4 % after 20 and 30 days. The difference in mass between the left, stimulated (Stim), and right contralateral non-stimulated (Ctrl) TA was statistically significant ($P < 0.05$) after 10, 20 days and 30 days of CHFS (Figure 4.1).

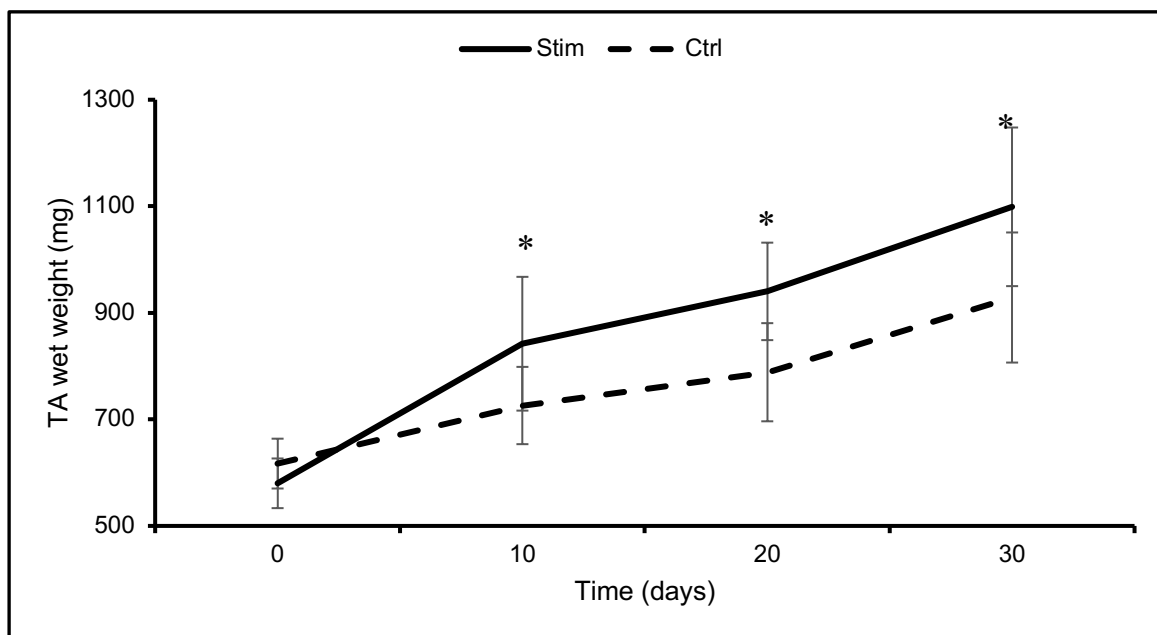


Figure 4.1. Time course of changes in muscle wet weight.

Wet weight (mg) of tibialis anterior (TA) in non-stimulated right (broken line) and contralateral stimulated left (solid line) limbs after unilateral high-frequency (100 Hz) stimulation *in vivo*. Data are presented as mean \pm SD from independent groups of $n = 4$ rats at each time point. * $P < 0.05$ statistically significant difference between the right and left limbs analysed by paired t-test at each time point.

The changes in protein content in the TA over the experimental time course at 10-day intervals for the Stim and Ctrl TA is shown in Figure 4.2. At the start of the experiment period (0 days) the total protein content of the TA was no different between the sham operated left limb (89.36 ± 19.9 mg) and the non-operated right limb (88.08 ± 9.5 mg). There was also no change in TA protein content of the non-stimulated right limb at any of the experimental time points during the 30 days of unilateral CHFS. However, the protein content of the TA in the Stim increased by 65 % after the first 10 days of CHFS. A further 19 % in total protein content of the TA occurred by the end of the experiment (30 days). The difference in mass between Stim, and Ctrl TA was statistically significant ($P < 0.05$) after 10, 20 days and 30 days of CHFS (Figure 4.2).

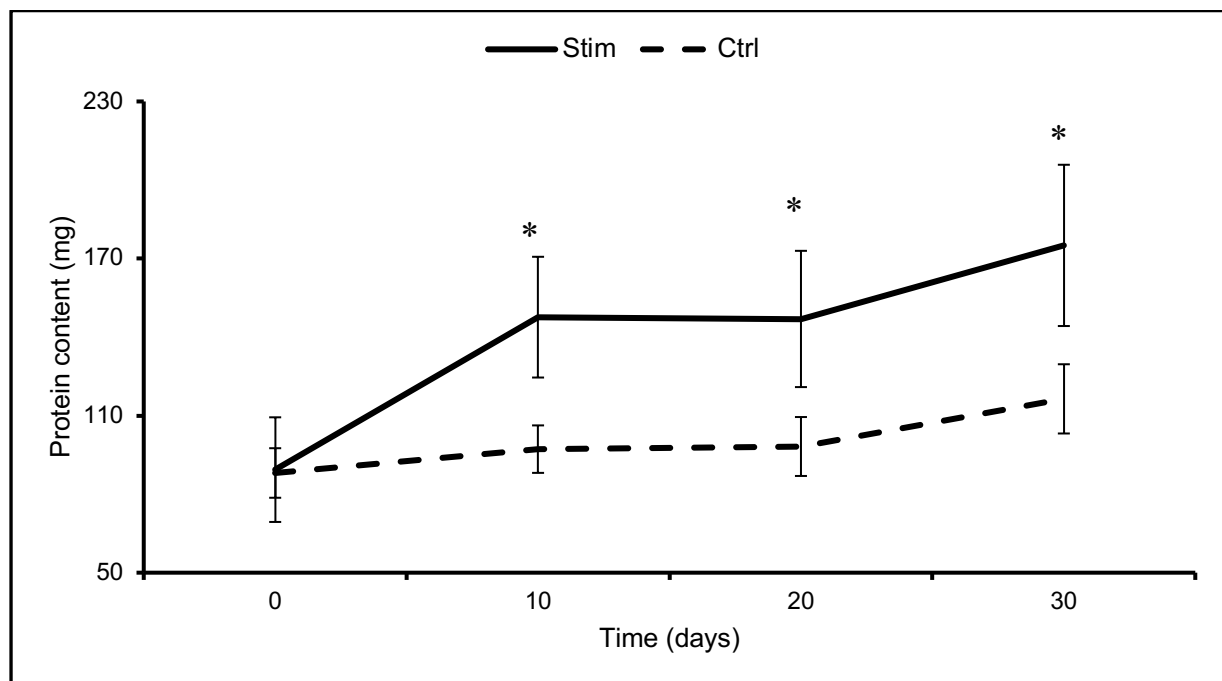


Figure 4.2. Time course of changes in muscle protein content.

Protein content (mg) of the tibialis anterior (TA) in non-stimulated right (broken line) and contralateral stimulated left (solid line) limbs after unilateral high-frequency (100 Hz) stimulation *in vivo*. Data are presented as mean \pm SD from independent groups of $n = 4$ rats at each time point. * $P < 0.05$ statistically significant difference between the right and left limbs analysed by paired t-test at each time point.

2D Gel analysis of the myofibrillar fraction resolved 50 protein spots in each of the 32 biological samples. Mass spectra were recorded from in-gel digests of each spot in

each biological replicate (approximately 1600 gel spots analysed). After filtering based on quality control criteria, a total of 35 spots had complete data from 5 peptides per protein that were present in all samples. Figure 4.3, illustrates the gel position of the 35 spots that satisfied the requirements for protein synthesis calculations, the identity of each gel spot is reported in Table 4.1. The total number of non-redundant protein identifications was 18 and 10 proteins were present in multiple spots and therefore represent different proteoforms. The reproducibility of protein abundance measurements was good (coefficient of variation 3.1 ± 0.05 %, $n = 4$ biological replicates) and both the relative and absolute abundance of each proteoform in Ctrl and Stim muscles is reported in supplementary Table S3.

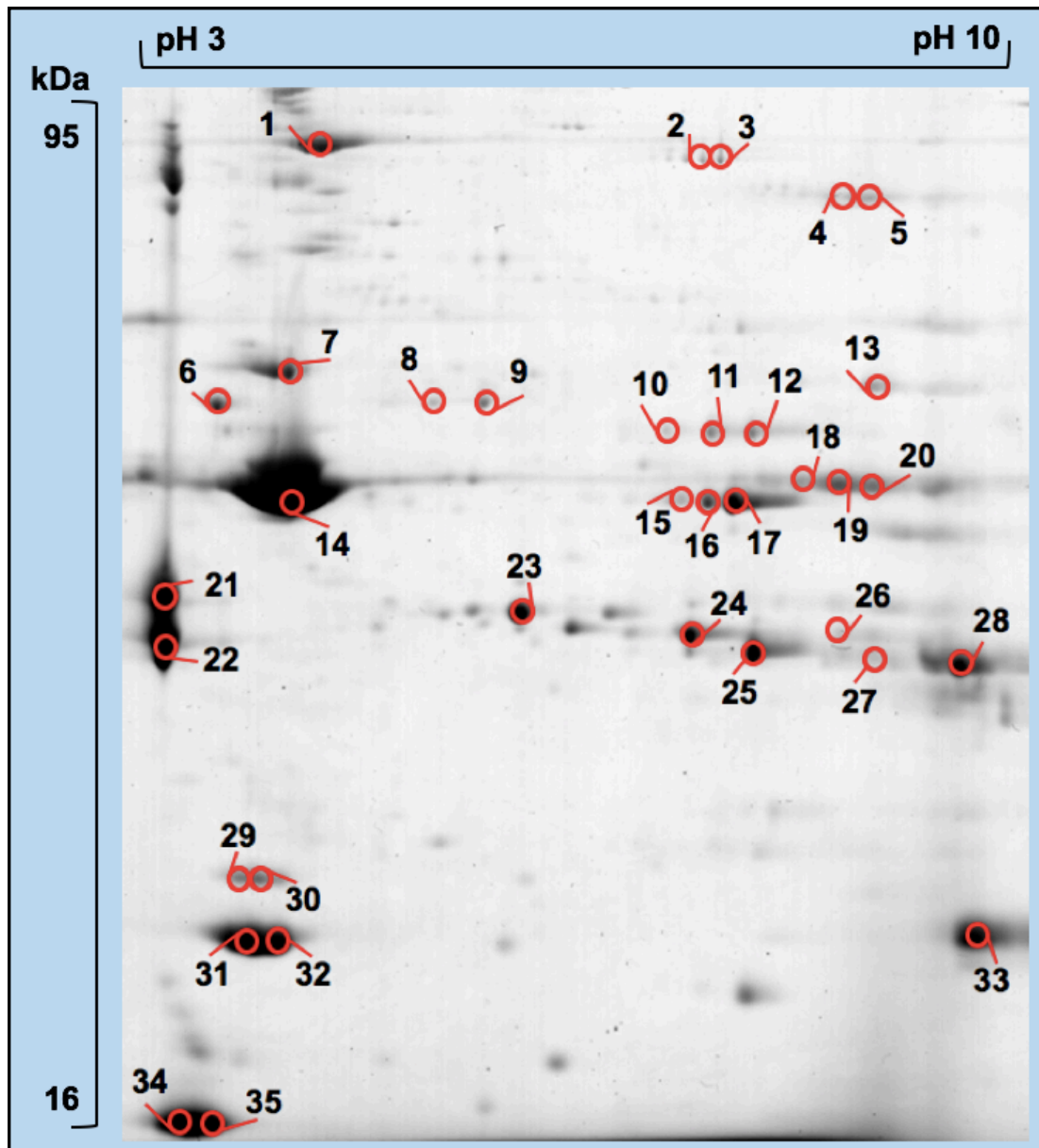


Figure 4.3. Separation of myofibrillar proteins by 2DGE.

Representative two-dimensional gel electrophoresis map of TA myofibrillar proteins after 30 days of co-contraction high-frequency stimulation *in vivo*. The gel has been annotated with common spots across both conditions (stimulated and non-stimulated control) $n = 35$ (annotated 1-35). Spot annotations are consistent with the protein identities in Table 4.1.

Table 4.1. Myofibrillar protein identifications.

Spot number	Protein name/Description	UniProt name	M_r	pI	Mowse score	Sequence coverage
-------------	--------------------------	--------------	-------	----	-------------	-------------------

1	Plectin	PLEC	533540	5.61	88	4 %
2	Glycogen phosphorylase, brain form	PYGB	96174	7.27	93	18%
3	Glycogen phosphorylase, brain form	PYGB	96174	7.30	96	18 %
4	ATP-dependant 6-phosphofructokinase, muscle type	PFKAM	85560	8.41	92	12 %
5	ATP-dependant 6-phosphofructokinase, muscle type	PFKAM	85560	8.60	84	12%
6	ATP synthase subunit beta	ATPB	56354	5.08	128	22 %
7	Desmin	DESM	53457	5.21	115	25 %
8	Alpha-enolase	ENOA	47128	5.48	109	26 %
9	Alpha-enolase	ENOA	47128	5.72	98	26 %
10	Beta-enolase	ENOB	47014	7.03	114	30 %
11	Beta-enolase	ENOB	47014	7.33	93	30 %
12	Beta-enolase	ENOB	47014	7.63	97	30 %
13	ATP synthase subunit alpha	ATPA	59754	8.66	102	30 %
14	Actin, alpha skeletal muscle	ACTS	42051	5.29	126	26 %
15	Creatine kinase M-type	KCRM	43045	7.19	98	24 %
16	Creatine kinase M-type	KCRM	43045	7.29	91	24 %
17	Creatine kinase M-type	KCRM	43045	7.74	91	24 %
18	Creatine kinase S-type	KCRS	47385	8.20	86	28 %
19	Creatine kinase S-type	KCRS	47385	8.22	92	28 %
20	Creatine kinase S-type	KCRS	47385	8.48	84	28 %
21	Tropomyosin alpha-1 chain	TPM1	28510	4.71	98	37 %
22	Tropomyosin beta chain	TPM2	32837	4.71	107	34 %
23	Troponin T, fast	TNNT3	30750	5.97	97	24 %
24	Troponin T, fast	TNNT3	30750	7.23	91	24 %
25	Troponin T, fast	TNNT3	30750	7.79	93	21 %
26	Troponin I, fast	TNNI2	21328	8.21	94	34 %
27	Troponin I, fast	TNNI2	21328	8.55	96	34 %
28	Troponin T, fast	TNNT3	30750	8.80	89	24 %
29	Myosin light chain 1/3	MYL1/3	22156	5.21	112	28 %
30	Myosin light chain 1/3	MYL1/3	22156	5.53	92	28 %
31	Myosin light chain 1/3	MYL1/3	20680	5.42	82	28 %

32	Myosin light chain 1/3	MYL1/3	20680	5.73	85	28 %
33	Carbonic anhydrase 3	CAH3	29431	8.74	96	30 %
34	Myosin regulatory light chain 2	MLRS	18969	4.24	92	42 %
35	Myosin regulatory light chain 2	MLRS	18969	4.76	98	43 %

Spot number refers to the different proteoforms resolved by 2DGE and corresponds to the 2DGE image in Figure 4.3. Protein name relates to the Uni-Prot database, entries returned using the MASCOT search engine. A mowse score greater than 55 denotes a confident ($P < 0.05$) identification by peptide mass fingerprinting. Relative molecular mass (M_r) are from protein database entry, isoelectric point (pI) is observed from position on experimental 2DGE images. The amino acid sequence of peptides and residue positions (start and end) are available in supplementary information 'Table S1'.

At baseline (0-day time point) there was no difference in the abundance of myofibrillar proteins between Ctrl and Stim muscle. Accordingly, protein abundances were highly correlated ($R^2 = 0.98878$; Figure 4.4) between Ctrl and Stim muscle at the beginning of the experiment. Protein abundances in Ctrl muscles did not change during the 30-d experimental period (Fig. 4.4, upper panels). Protein abundances from the Ctrl limb were also assessed by one-way ANOVA of spot volumes in 0 d, 10 d, 20 d and 30 d and no differences ($P < 0.05$) were found. In contrast, the level of correlation (R^2) between baseline and Stim muscles deteriorated from 0.97882 at day 10 to 0.81623 at day 30 (Figure 4.4). Relative fold-change in abundance were calculated between the Ctrl and Stim TA for each myofibrillar proteoform (Supplementary Table S3). Similar fold-change data were also calculated in absolute terms, taking into account the changing muscle mass (Supplementary Table S3). Both relative and absolute methods of calculation gave similar rank orders of change and equivalent outcomes in terms of the pattern of change for each myofibrillar proteoform (Supplementary Table S3). Two myofibrillar proteoforms (spot 8, ENOA and spot 2, PYGM exhibited significant ($P < 0.05$) decreases in abundance after 10 days of stimulation. After 20 days of stimulation the abundance of 16 proteins was significantly increased and by the end of the experimental period (30 d) there were 19 significant differences in protein abundance between Ctrl and Stim TA (Figure 4.5).

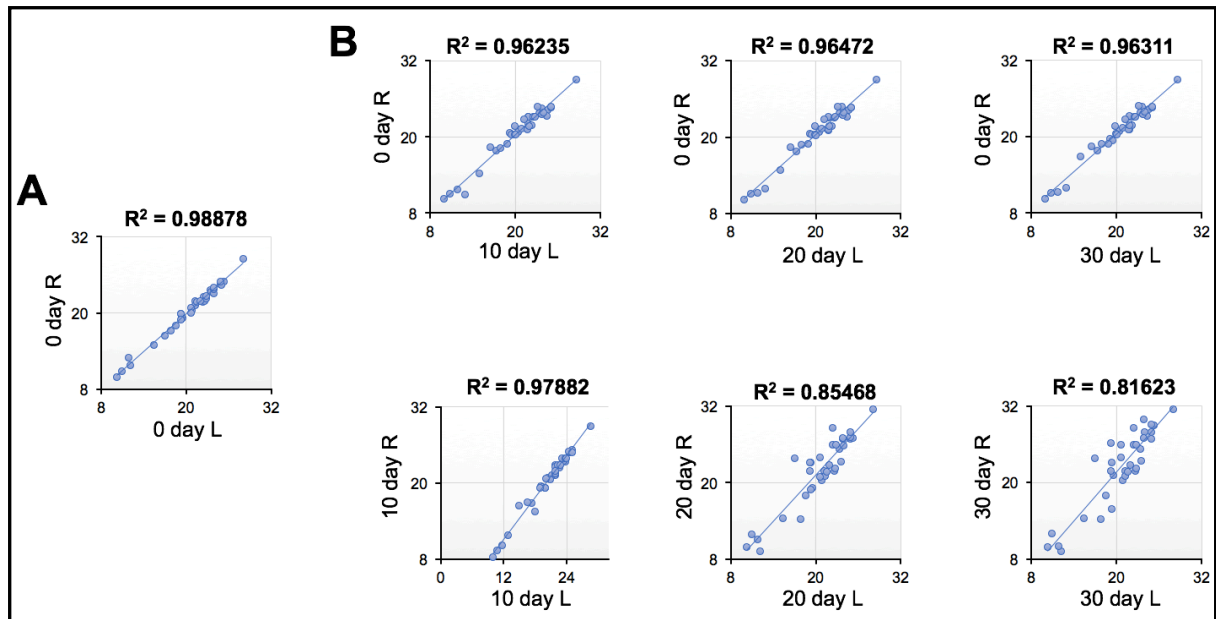


Figure 4.4. Correlation of relative myofibrillar protein abundance between stimulated and non-stimulated TA.

Correlation matrix of normalised myofibrillar relative protein abundance (proteins 1-35 present in both stimulated and non-stimulated TA at each time point). Correlation between (A) left and right limb of 0-day sham control. (B) Upper panels; 0-day sham control and either 10 d, 20 d or 30 d of right contralateral control limb. Lower panels; right contralateral control limb and co-contraction high-frequency stimulation in the left limb for either 10 d, 20 d or 30d.

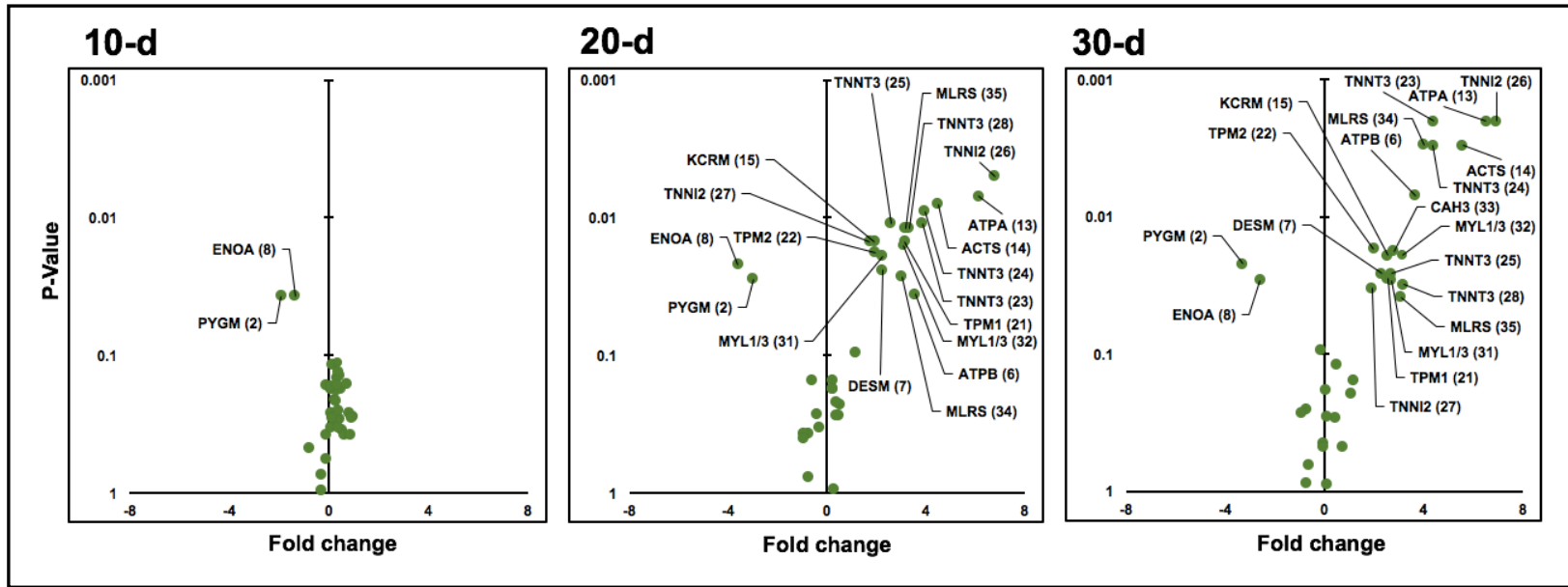


Figure 4.5. Changes in absolute abundance for the myofibrillar proteins between control and stimulated TA muscle. Each data point represents an individual protein. Proteins that changed significantly ($P < 0.05$) determined via paired t-tests between control and stimulated muscle are labelled by their UniProt I.D. name returned using MASCOT search engine. Proteins are described as increasing, decreasing or not changing in absolute protein abundance calculated by log-transformed fold change from non-stimulated control muscle to stimulated muscle for the myofibrillar proteins only after 10 days, 20 days and 30 days of CHFS.

The changes in myofibrillar protein abundance are consistent with an increase in the contractile machinery of the muscle in the stimulated TA. Of the 19 proteins that changed significantly in abundance only 2 proteins (spot 2 glycogen phosphorylase, PYGM; spot 8 alpha-enolase, ENOA) decreased in abundance whilst the remaining 17 proteins all responded to CHFS by gaining in abundance. The most significant period of change in response to CHFS was after 20 days, where 18 of the 19 proteins that exhibit significant changes in abundance were altered. The protein with greatest change was spot 26, TNNI2 ($+6.8 \pm 0.8$ -fold; $P = 0.022$; $+6.9 \pm 0.3$ -fold; $P = 0.002$) after 20 and 30 days of stimulation respectively. Proteins detected as multiple proteoforms (see Table 4.1) tended to exhibit a similar response to CHFS. Troponin T (TNNT3) was detected as four separate proteoforms (spots 23, 24, 25, 28) which each increased in abundance after both 20 ($+3.43 \pm 0.62$ -fold) and 30 days ($+3.66 \pm 0.86$ -fold) of CHFS. Creatine kinase S-type (KCRS) was resolved as three separate proteoforms (spots 18, 19, 20) and none of these spots changed ($P = 0.489 \pm 0.3$) in abundance in response to stimulation. However, myosin light chain 1/3 (MLY1/3) which was also detected as four separate proteoforms (spots 29, 30, 31, 32) had a mixed response. Spots 29 and 30 did not change ($P = 0.119$ and 0.184 , respectively) in abundance but spots 31 and 32 each increased ($+2.56 \pm 0.02$ -fold; $+3.17 \pm 0.83$ -fold; $P = 0.019$; 0.031 respectively) in abundance in response to stimulation.

The average FSR of the myofibrillar proteins in the TA over 30 days was 5.33 ± 0.03 %/d ($n = 4$ biological replicates) in Ctrl. Carbonic anhydrase 3 (spot 33, CAH3) as the most rapidly (15.38 ± 0.8 %/d) synthesised protein and plectin (spot 1, PLEC) as the slowest (1.06 ± 0.3 %/d). Thirty days of CHFS increased ($P = 0.001$) the average FSR to 9.85 ± 0.08 %/d in Stim TA. The protein with the fastest FSR in Stim was again spot 33, CAH3 (26.84 ± 0.4 %/d) and the slowest was spot 29, MYL1/3 (2.15 ± 0.4 %/d). Figure 4.6 reports the absolute synthesis rate of the whole TA at each of the 10-day experimental time series. There was no change in the absolute rate of synthesis in the non-stimulated right limb at any of the experimental time points encompassing the 30 days of CHFS. In response to CHFS, absolute rate of synthesis (pg/d) of the left, stimulated limb increased by 12 % after 10 days, 17 % after 20 days and 14 % after 30 days, consistent with the changes in muscle mass (Figure 4.1). The difference in absolute synthesis between Stim, and Ctrl TA was statistically significant ($P < 0.05$) after 10 days, 20 days and 30 days of CHFS (Figure 4.6).

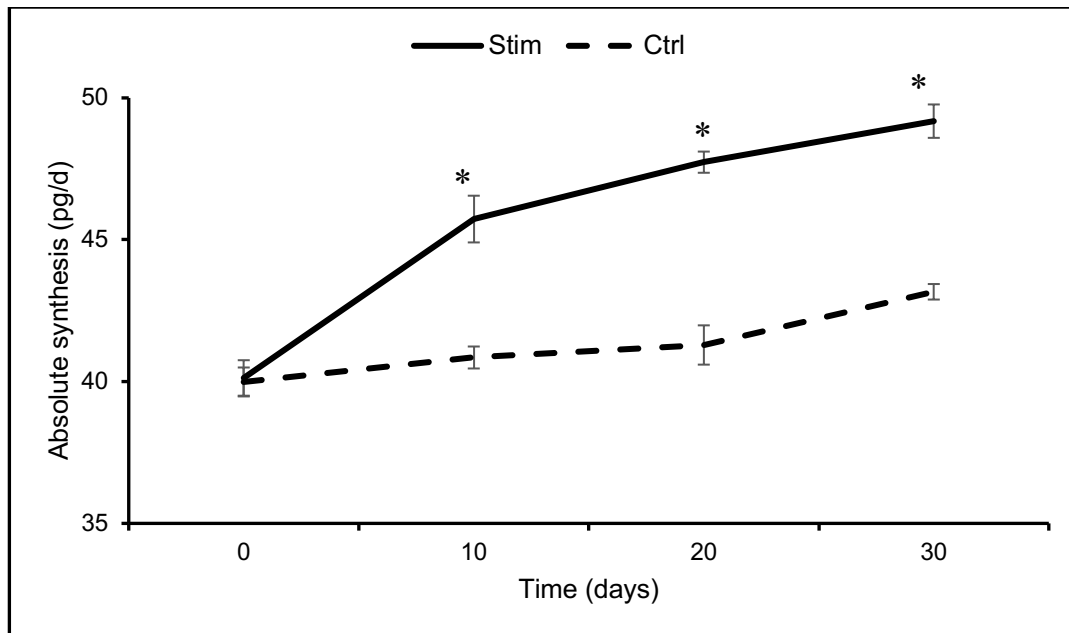


Figure 4.6. Absolute protein synthesis rates of stimulated and non-stimulated TA.

Synthesis data (pg/d) displayed as mean \pm SD ($n = 4$ per group) in 10-day intervals over 30 days of unilateral high-frequency stimulation (100 Hz) *in vivo*. Protein synthesis rates (pg/d) calculated from total protein content of the TA in the non-stimulated control limb (broken line) and contralateral stimulated left (solid line). * $P < 0.05$ statistically significant difference between the right and left limbs analysed by paired t-test at each time point.

The average absolute synthesis rate of mixed myofibrillar proteins in Ctrl muscle was 34.71 ± 1.07 pg/d and there was a broad distribution of synthesis rates (Table S4) amongst individual proteoforms, from 2.84 ± 0.73 pg/d (spot 1; PLEC) to 72.12 ± 0.85 pg/d (spot 5; PFKAM). Furthermore, the rank order of protein synthesis rates were different for FSR values versus the absolute data (supplementary Table S4) Stimulation increased ($P = 0.002$) the average rate of synthesis (40.18 ± 0.96 pg/d) of mixed myofibrillar proteins (Figure 4.7) and 23 individual proteoforms exhibited significant ($P < 0.05$) differences in synthesis rate between Ctrl and Stim muscle after 10 days, 20 days and 30 days of stimulation (Figure 4.8). The greatest change in absolute synthesis rate was, spot 28: Creatine kinase M-type (KCRM), which increased ($P = 0.012$) from 42.14 ± 0.86 pg/d to 58.26 ± 0.85 pg/d after 30 days of CHFS (Table S4). This increase in synthesis was also matched by a 3.17-fold increase ($P = 0.031$) in abundance between Ctrl to Stim muscle.

In summary, top-down analysis of myofibrillar proteoforms revealed that a total of 20 proteins responded to CHFS by changing in abundance significantly ($P < 0.05$). In total, 18 increased in abundance and 2 decreased in abundance. These changes in abundance were associated with 2 different patterns of regulation in individual protein turnover that are summarised in Figure 4.7. Whereas the other 15 proteins that did not change in abundance achieved this maintenance by a further 2 different patterns of regulation (Figure 4.7).

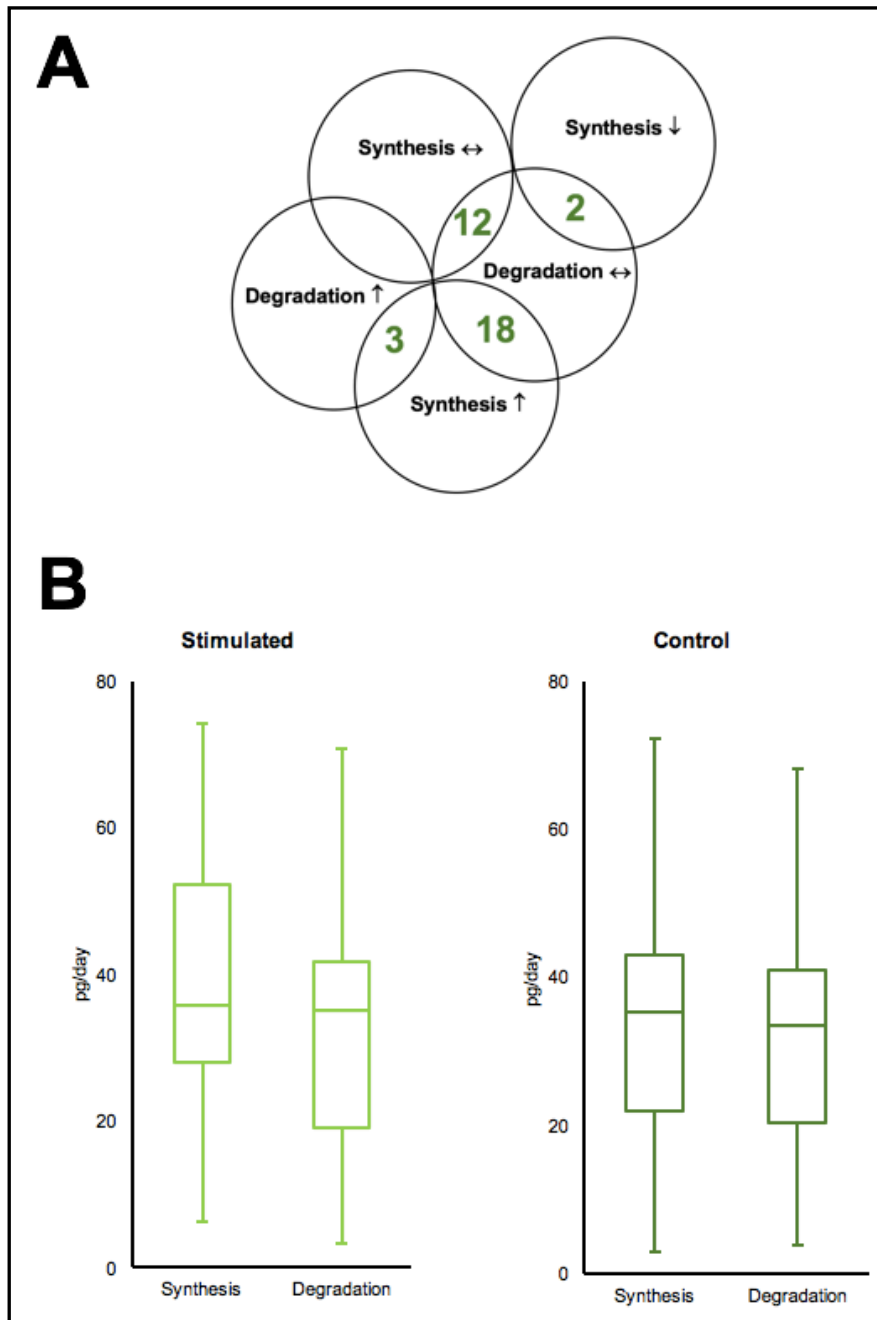


Figure 4.7. Contributions of synthesis and degradation to changes in the protein turnover of myofibrillar proteins.

Mean protein turnover data is shown as absolute values for all 35 identified myofibrillar proteoforms. (A) Venn diagram displays the number of myofibrillar proteins that show different responses in protein turnover: increases (\uparrow), decreases (\downarrow) or no change (\leftrightarrow) for synthesis and degradation in response to 30 days of stimulation. (B) box and whisker plot of data from proteins displayed panel A. The left panel shows the range of synthesis and degradation rates in picograms per day for the 30-d stimulate muscle

only. The box and whisker plot on the right shows the range of synthesis and degradation rates in picograms per day for the control muscle only.

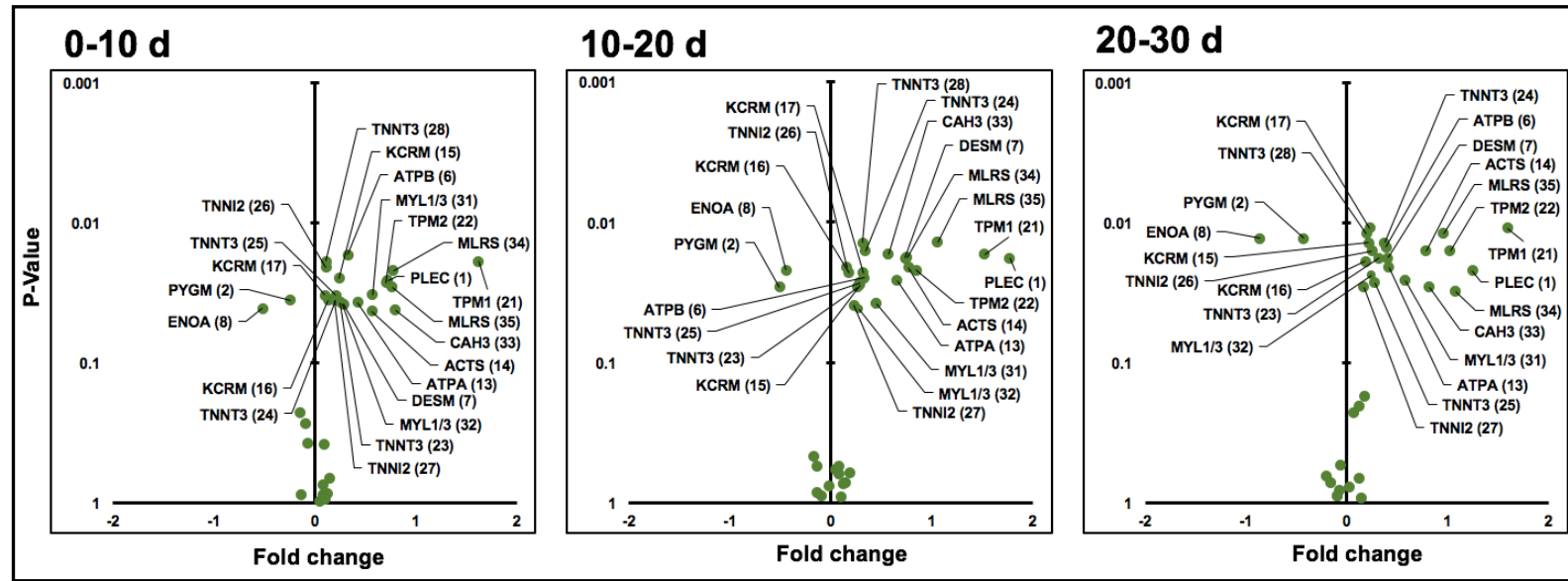


Figure 4.8. Changes in absolute synthesis rates for the myofibrillar proteins between control and stimulated TA muscle. Each data point represents an individual protein. Proteins that changed significantly ($P < 0.05$) determined via paired t-tests between control and stimulated muscle are labelled by their UniProt I.D. name returned using MASCOT search engine. Proteins are described as increasing, decreasing or not changing in absolute protein synthesis rate calculated by log-transformed fold change from non-stimulated control muscle to stimulated muscle for the myofibrillar proteins only during 0-10 days, 10-20 days and 20-30 days of CHFS.

In the myofibrillar fraction, the 18 proteins that increased in abundance after 30 days of CHFS did so by increasing the rate of synthesis in Stim compared to Ctrl muscle (Figure 4.9). The two proteins in the myofibrillar fraction that decreased in abundance after 30 days of CHFS, did so by decreasing the rate of synthesis in Stim compared to Ctrl muscle (Figure 4.9). For the remaining 15 myofibrillar proteins that did not change in abundance, 12 of these were unaffected by CHFS, whereas the other 3 increased (spot 1 PLEC, $P = 0.027$; spot 16 KCRM, $P = 0.028$; spot 17 KCRM, $P = 0.031$) their rate of protein turnover to maintain abundance levels within Stim TA after 30 days of CHFS.

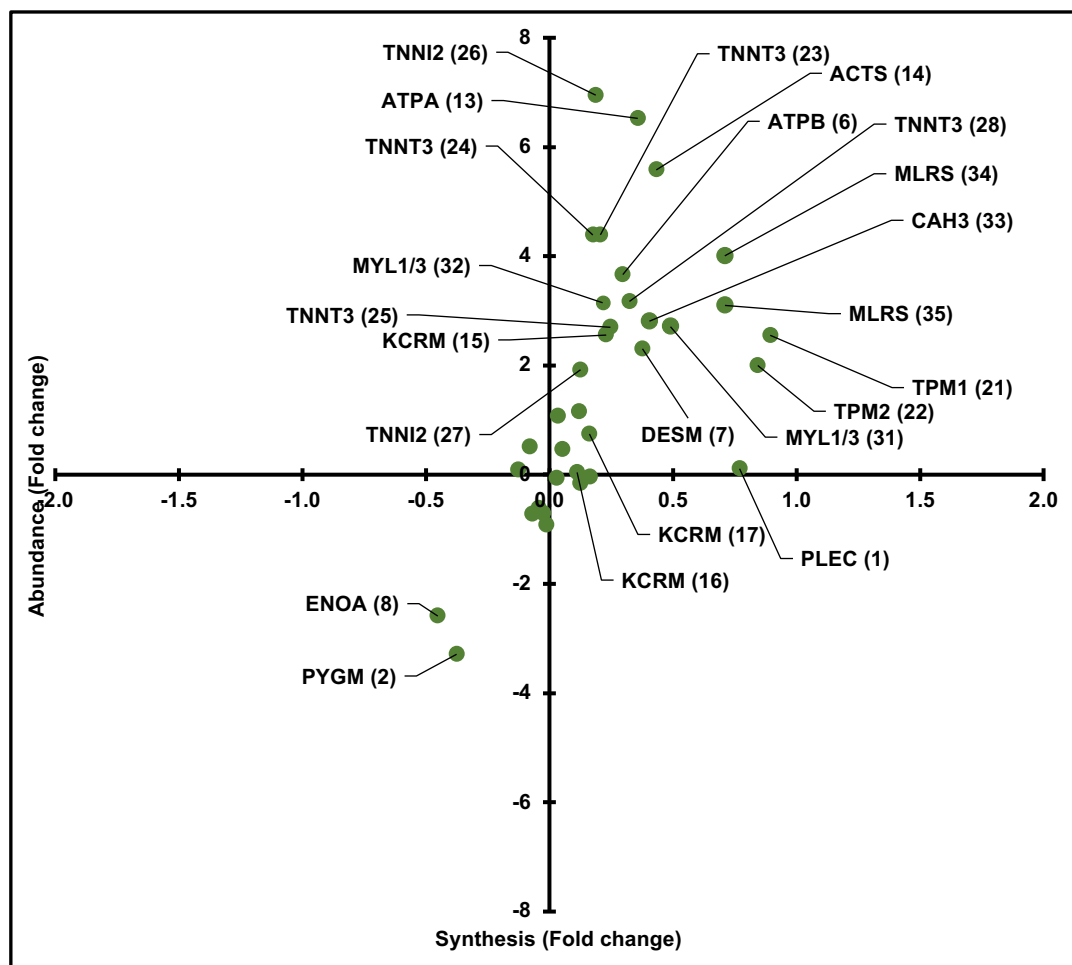


Figure 4.9. Dynamic proteome responses to CHFS of the myofibrillar proteins. Data is presented for the 35 myofibrillar proteins as log-transformed fold change from the non-stimulated control muscle to 30 days of co-contraction high-frequency stimulation in the TA for absolute synthesis against absolute changes in abundance. Each data point represents an individual protein and proteins that exhibit a significant ($P < 0.05$) change in synthesis from control to stimulated muscle are labelled by their

UniProt I.D. name returned using MASCOT search engine. The upper left quadrant represents an increase in abundance over the 30 days of stimulation but a greater rate of synthesis in control muscle compared with CHFS muscle. Proteins that increase in abundance in the stimulated muscle, where the protein synthesis rate is also greater in stimulated muscle compared with control are displayed in the upper right quadrant. The lower right quadrant represents proteins that have decreased in abundance in response to 30 days of stimulation and increased in protein synthesis in the stimulated muscle compared to the non-stimulated control. Proteins that decrease in abundance after stimulation and have a synthesis rate that is also less than that in the control muscle are displayed in the lower left quadrant.

LC-MS/MS analysis of the soluble muscle proteins yielded a list of 56 proteins (Supplementary Table S2) that had at least one protein-specific peptide that could be detected in all ($n = 32$) Ctrl and Stim samples. The majority of proteins were enzymes of either mitochondrial/oxidative metabolism or glycolysis/anaerobic metabolism (Supplementary Table S2). The reproducibility of protein abundance measurements by label-free quantitation was good (coefficient of variation 4.9 ± 0.07 %, $n = 4$ biological replicates) and the abundance each protein in Ctrl and Stim muscles is reported in supplementary Table S5.

Similar to the analysis of myofibrillar proteoforms, there was a high correlation ($R^2 = 0.99502$; $P = 0.001$) in the abundance of soluble proteins between the Ctrl and the sham-operated muscle at the 0-day time point. There was also no significant difference ($P = 0.863$) in the abundance of soluble proteins in the Ctrl TA (Figure 4.10, upper panels), assessed by one-way ANOVA of normalised peak abundances in 0 d, 10 d, 20 d and 30 d samples. Relative fold changes in abundance were calculated between the Ctrl and Stim TA for each soluble protein (Supplementary Table S5). Similar fold change calculations were also used to calculate changes in soluble protein abundance in absolute terms (Supplementary Table S5). Both relative and absolute calculations gave similar rank orders of change and equivalent patterns of change for each soluble protein (Supplementary Table S3). Figure 4.11 illustrates the changes in absolute abundance of the soluble muscle proteins induced by CHFS. From the 56 soluble proteins; 5 proteins exhibited significant ($P < 0.05$) differences in abundance after 10 days of stimulation, after 20 days of stimulation the abundance of a further 2 proteins became significantly different. By the end of the experiment period (30 d)

there were a total of 7 significant differences in protein abundance between the Stim and Ctrl TA (Figure 4.11).

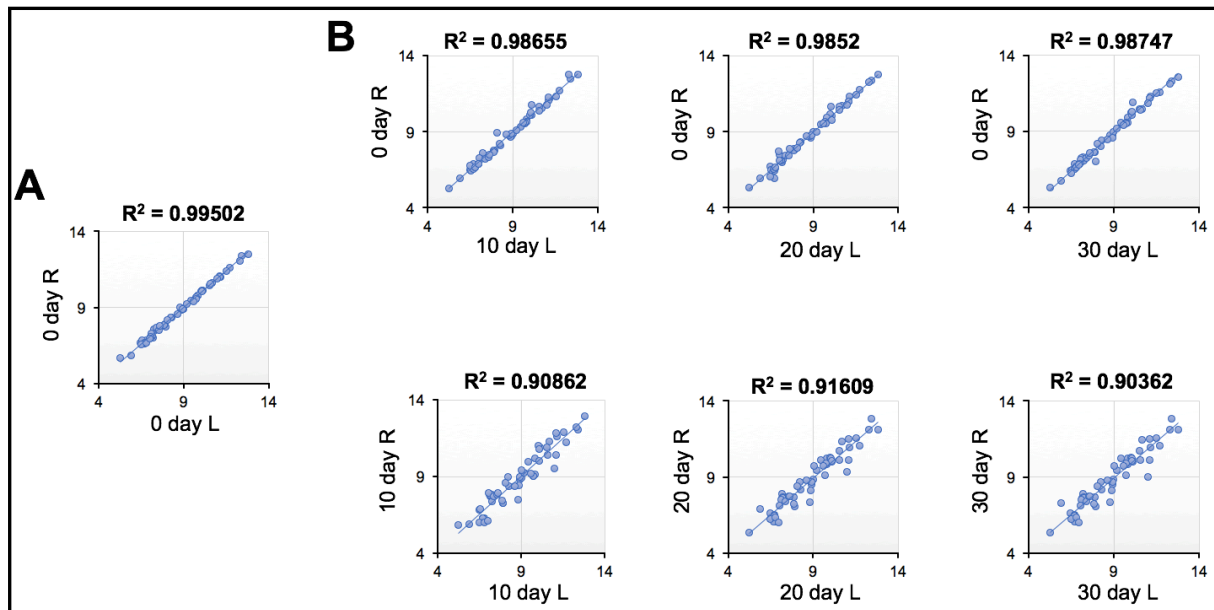


Figure 4.10. Correlation of relative soluble protein abundance between stimulated and non-stimulated TA.

Correlation matrix of normalised soluble relative protein abundance (proteins 1-56 present in both stimulated and non-stimulated TA at each time point). Correlation between (A) left and right limb of 0-day sham control. (B) Upper panels; 0-day sham control and either 10 d, 20 d or 30 d of right contralateral control limb. Lower panels; right contralateral control limb and co-contraction high-frequency stimulation in the left limb for either 10 d, 20 d or 30d.

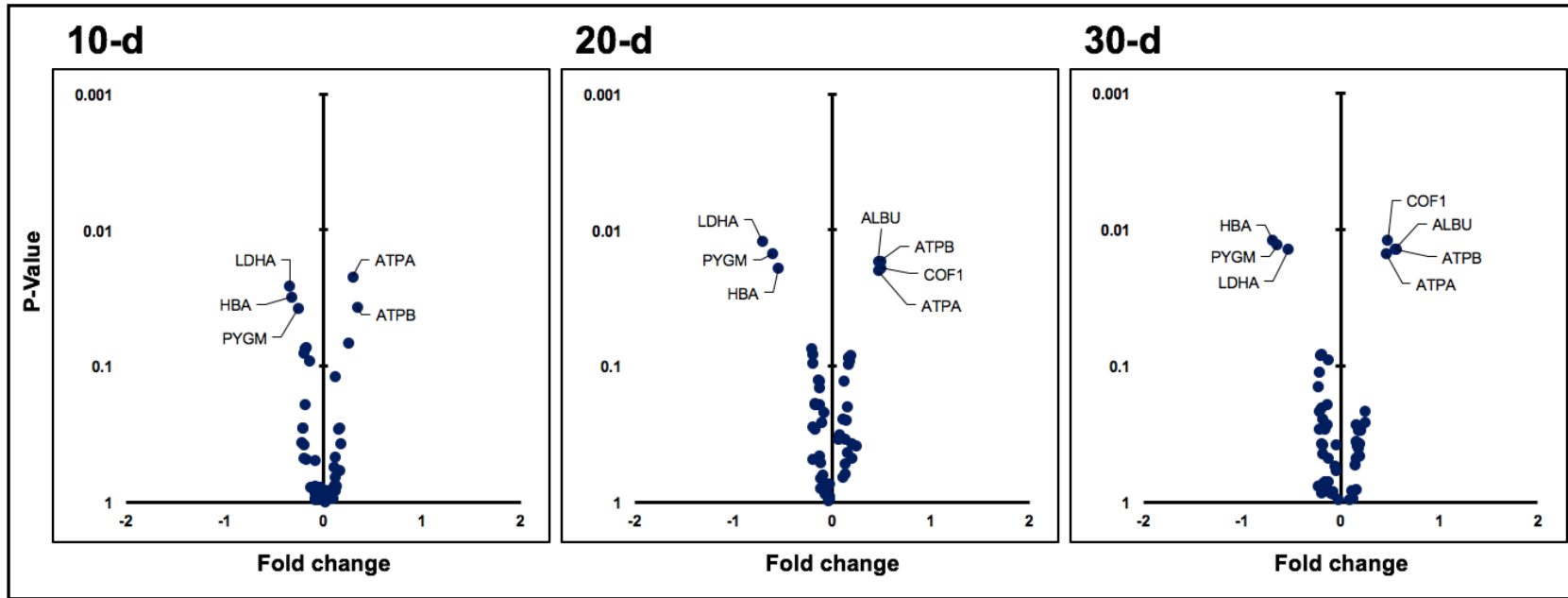


Figure 4.11. Changes in absolute abundance for the soluble proteins between control and stimulated TA muscle. Each data point represents an individual protein. Proteins that changed significantly ($P < 0.05$) determined via paired t-tests between control and stimulated muscle are labelled by their UniProt I.D. name returned using MASCOT search engine. Proteins are described as increasing, decreasing or not changing in absolute protein abundance calculated by log-transformed fold change from non-stimulated control muscle to stimulated muscle for the soluble proteins only after 10 days, 20 days and 30 days of CHFS.

After 30 days of CHFS, of the 7 soluble proteins that significantly changed in abundance, 3 decreased (-0.62 ± 0.08 -fold) in abundance and 4 increased ($+0.61 \pm 0.13$ -fold) in abundance. Lactate dehydrogenase (LDHA) and glycogen phosphorylase (PYGM) are two proteins associated with glycolysis that decreased (-0.53 ± 0.08 -fold; -0.64 ± 0.07 -fold; $P = 0.014$; 0.013 , respectively) in abundance in response to 30 days of CHFS. The blood protein haemoglobin (HBA) also decreased (-0.69 ± 0.05 -fold; $P = 0.012$) in abundance after 30 days of stimulation. Of the remaining 4 proteins that increased in abundance after 30 days of CHFS, 2 were mitochondrial proteins (ATPA, $+0.66 \pm 0.03$ -fold; ATPB, $+0.77 \pm 0.06$ -fold), 1 was serum albumin (ALBU, $+0.55 \pm 0.04$ -fold) and the other was actin-binding protein (COF1, $+0.48 \pm 0.01$ -fold). The average rate of protein synthesis in the Ctrl of mixed soluble proteins was 4.28 ± 0.63 %/d in relative terms (FSR) and 49.66 ± 0.82 pg/d as an absolute (ASR) value (Figure 4.12). The distribution of individual proteins in the control muscle spanned from 8.44 ± 0.47 pg/d (PARK7) to 142.73 ± 0.17 pg/d (PYGM). Co-contraction High-frequency stimulation did not change ($P = 0.639$) the average (FSR = 4.74 ± 0.84 %/d; ASR = 52.04 ± 1.07 pg/d) synthesis rate of mixed soluble proteins (Figure 4.12). However, the range of synthesis rates (Table S6) was broader in Stim compared Ctrl muscle (Figure 4.14).

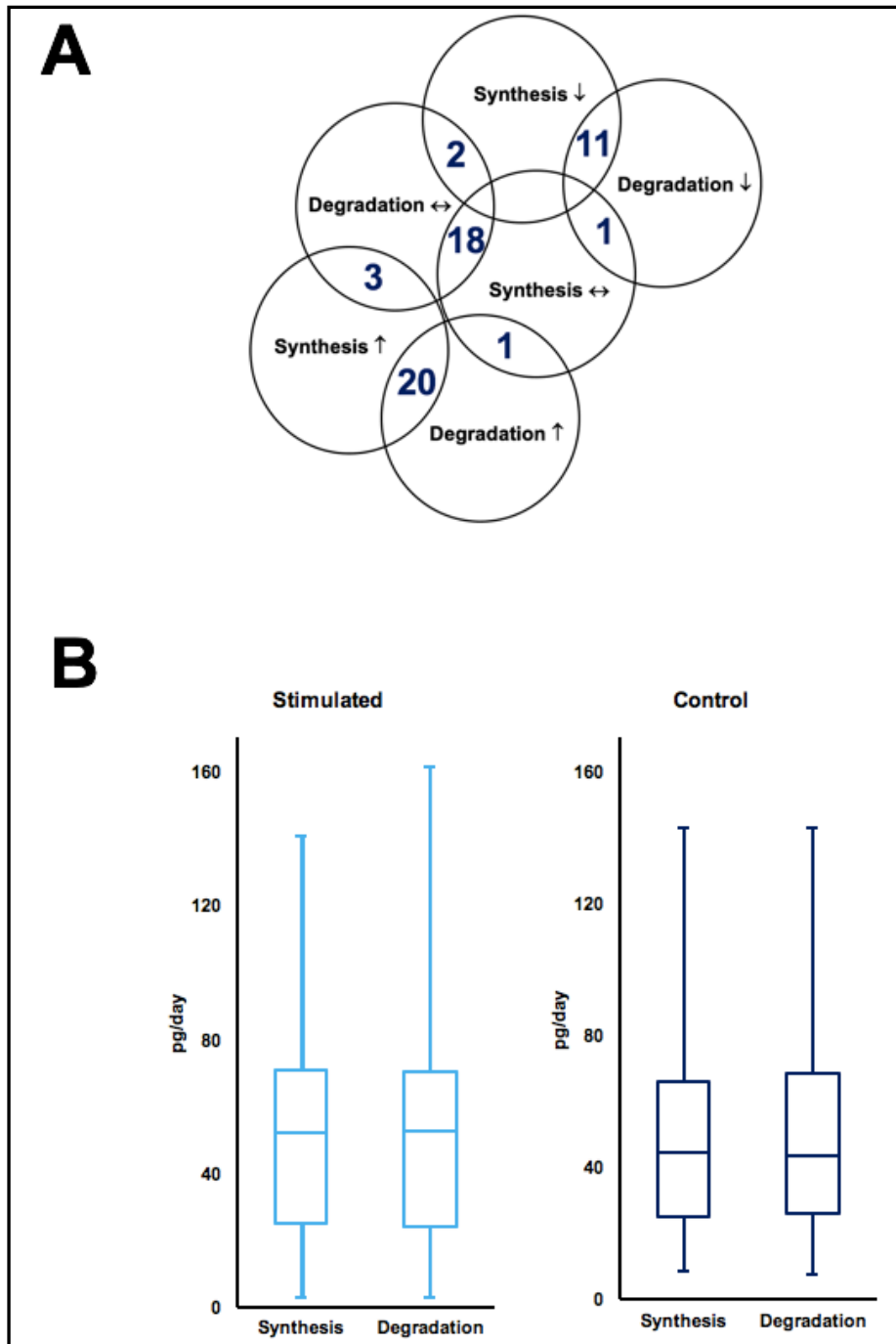


Figure 4.12. Contributions of synthesis and degradation to changes in the protein turnover of soluble proteins.

Mean protein turnover data is shown as absolute values for all 56 identified soluble proteoforms. (A) Venn diagram displays the number of soluble proteins that show different responses in protein turnover: increases (↑), decreases (↓) or no change (↔) for synthesis and degradation in response to 30 days of stimulation. (B) box and whisker plot of data from proteins displayed panel A. The left panel shows the range of synthesis and degradation rates in picograms per day for the 30-d stimulated

muscle only. The box and whisker plot on the right shows the range of synthesis and degradation rates in picograms per day for the control muscle only.

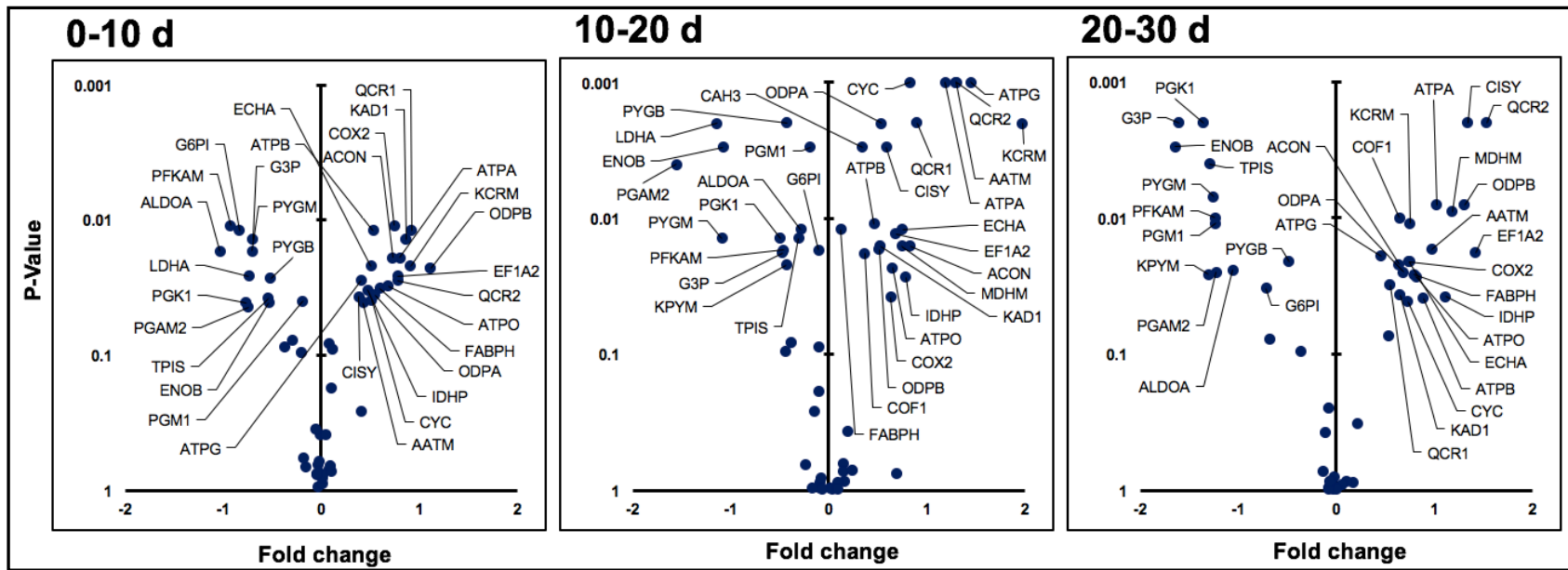


Figure 4.13. Changes in absolute synthesis rates for the soluble proteins between control and stimulated TA muscle. Each data point represents an individual protein. Proteins that changed significantly ($P < 0.05$) determined via paired t-tests between control and stimulated muscle are labelled by their UniProt I.D. name returned using MASCOT search engine. Proteins are described as increasing, decreasing or not changing in absolute protein synthesis rate calculated by log-transformed fold change from non-stimulated control muscle to stimulated muscle for the soluble proteins only during 0-10 days, 10-20 days and 20-30 days of CHFS.

The lowest synthesis rate in Stim muscle was 2.71 ± 0.55 pg/d (PFKAM) and the greatest was 140.53 ± 0.24 pg/d (KCRM). Proteins that exhibited the greatest synthesis responses to resistance exercise training include CAH3 which increased ($P = 0.001$) from 73.19 ± 0.36 pg/d to 98.55 ± 0.40 pg/d and PYGM which decreased ($P = 0.001$) from 142.73 ± 0.17 pg/d to 100.33 ± 0.44 pg/d after 30 days of CHFS. In summary, bottom-up analysis of soluble proteins detected protein-specific responses to resistance exercise training that were similar to the changes found by the top-down analysis of myofibrillar proteoforms. Only 7 proteins from 56 exhibited a statistically significant change in protein abundance (Table S5) in response to CHFS. However, 36 proteins changed the rate of protein synthesis in Stim TA compared to Ctrl after 30 days of stimulation (Fig. 4.12 and 4.13). Of the 36 proteins that changed in rate of synthesis, 20 proteins increased the rate of synthesis but did not change in abundance, 11 decreased the rate of synthesis but did not change in abundance. Two proteins decreased the rate of synthesis subsequently decreasing their abundance levels and the remaining 3, increased in both synthesis and abundance (Fig. 4.12 and 4.14). Two more proteins had no change in protein synthesis and displayed opposite responses, 1 increased in abundance and the other decreased in abundance. The remaining 18 proteins displayed no effect after 30 days of CHFS (Fig. 4.12 and 4.14).

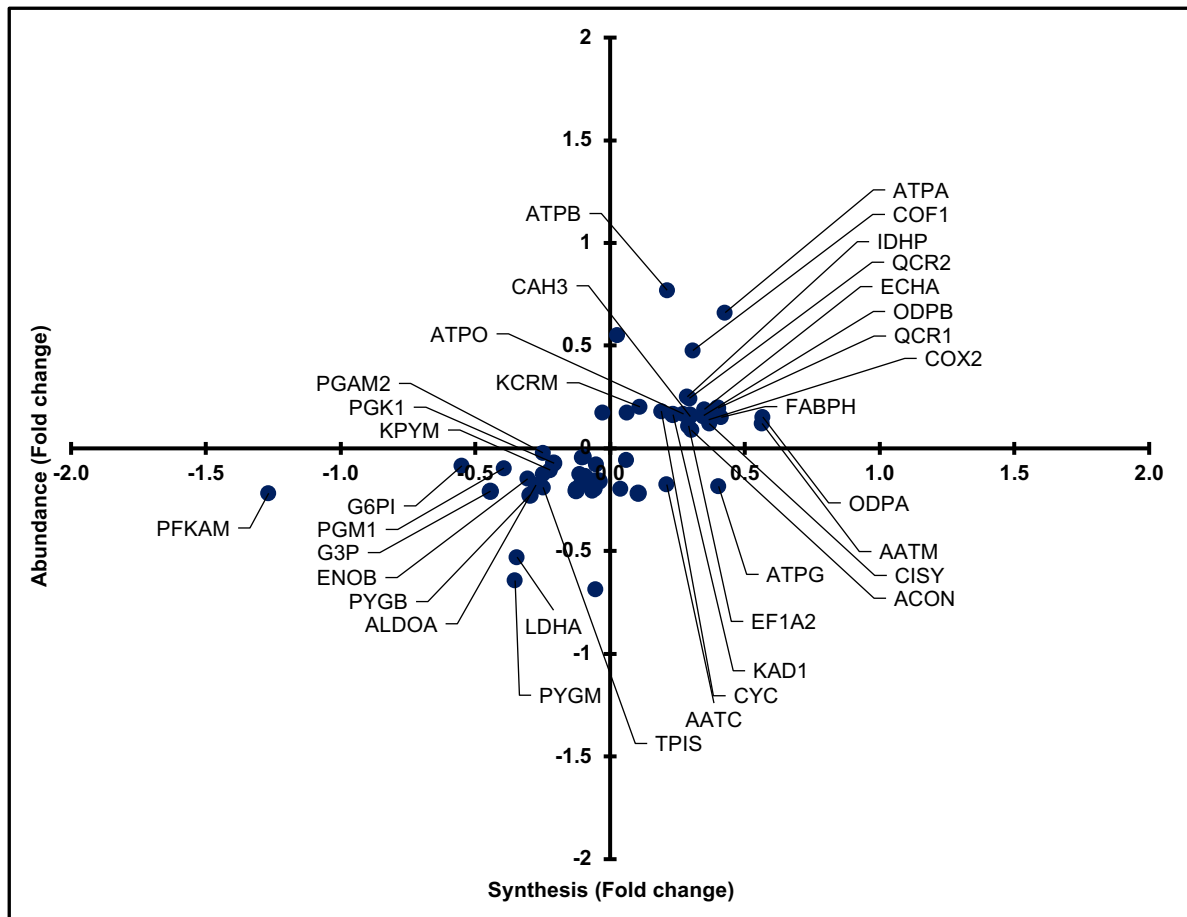


Figure 4.14. Dynamic proteome responses to CHFS of the soluble proteins.

Data is presented for the 56 soluble proteins as log-transformed fold change from the non-stimulated control muscle to 30 days of co-contraction high-frequency stimulation in the TA for absolute synthesis against absolute changes in abundance. Each data point represents an individual protein and proteins that exhibit a significant ($P < 0.05$) change in synthesis from control to stimulated muscle are labelled by their UniProt I.D. name returned using MASCOT search engine. The upper left quadrant represents an increase in abundance over the 30 days of stimulation but a greater rate of synthesis in control muscle compared with CHFS muscle. Proteins that increase in abundance in the stimulated muscle, where the protein synthesis rate is also greater in stimulated muscle compared with control are displayed in the upper right quadrant. The lower right quadrant represents proteins that have decreased in abundance in response to 30 days of stimulation and increased in protein synthesis in the stimulated muscle compared to the non-stimulated control. Proteins that decrease in abundance after stimulation and have a synthesis rate that is also less than that in the control muscle are displayed in the lower left quadrant.

4.5 Discussion

Skeletal muscle is well-known for its plasticity, eliciting biochemical, metabolic and contractile adaptations in response to environmental changes to the muscle cell i.e. contractile stress (Coffey and Hawley, 2007). These functional adaptations manifest through discrete alterations of the muscle proteome which include increases in total protein content that are underpinned by the abundance changes of individual muscle proteins. Resistance exercise is known to induce hypertrophy and can preserve lean muscle mass in various pathophysiological conditions such as sarcopenia (Walston, 2012). However, data on the dynamic processes (i.e. synthesis and degradation) that contribute towards these changes in individual protein abundance are not widely available. In an attempt to inform this knowledge gap, we report the dynamic response of skeletal muscle to resistance exercise training. We achieve this by the marriage of stable isotope labelling and mass spectrometry analysis during an *in vivo* model of muscle growth. This is the first data to report how the contributions of both synthesis and degradation produce changes to individual protein abundance in rat TA muscle during resistance exercise training. Our data report several different patterns of response to individual protein turnover (Fig. 4.7 and 4.12), including proteins that exhibit both increases and decreases in protein synthesis but do not change in protein abundance.

Changes in protein abundance primarily occur because of a difference between the rate of synthesis and degradation of a protein. The results from this study demonstrate whole mixed-muscle protein synthesis rates give less than adequate information compared to synthesis rates at the individual protein level. We also provide new evidence to demonstrate that in response to resistance exercise training individual proteins increase the rates of protein turnover and can be selectively degraded at varying rates to decrease and/or to maintain the same relative abundance of protein in the muscle. As a result, we can report, 27 proteins displayed a change in abundance in response to muscle adaptation from the 91 proteins that were measured. Of which 96 % of proteins were driven by synthesis, 4 % of proteins were driven by degradation. For the remaining 64 proteins that did not change in abundance, 36 % increased both the contributions of synthesis and degradation to increase protein turnover, 17 % decreased in protein turnover and 47 % of proteins were unaffected by CHFS. Our work is the first of its kind in CHFS to document the response of protein-specific

turnover during muscle adaptation that provides further evidence to show protein turnover is increased and decreased by increasing and/or decreasing the relative contributions of synthesis and degradation to coordinate the adaptive response. Suggesting that protein degradation is equally as important as synthesis in skeletal muscle during adaptation to resistance exercise training.

The co-contraction high-frequency stimulation (CHFS) model we have implemented to simulate resistance exercise training was developed by our group (Schmoll et al, 2018) and has subsequently been applied to investigate protein-specific changes in abundance as well as synthesis rate. Consistent with our earlier work (Schmoll et al, 2018) we report resistance exercise training is associated with an increase in muscle mass and a greater turnover of muscle protein (Phillips et al, 1999). The mass of the TA muscle increased by 16 % after the first 10 days of CHFS and subsequently rises to ~20 % greater than Ctrl after 30 days of stimulation (Figure 4.1). Several other animal models that attempt to simulate resistance training e.g. compensatory overload, also see large increases in muscle mass that constitute to ~34 % increase compared to intra-animal control muscles. However, in a compensatory overload model of the rat PLN Armstrong et al, (1979) reports almost all (~91 %) of this gain in muscle weight is due to oedema. We are confident that our changes in muscle mass are a result of resistance exercise-induced protein accretion, as we measure a concomitant increase in total protein content (Figure 4.2). In addition, Baar and Esser, (1999) used a similar model of muscle co-contraction and report elevated levels of p70S6k phosphorylation, as a proxy of increased protein synthesis. They document phosphorylation levels to peak just 12 h after resistance exercise training, with sustained effects up to 36 h post exercise. Although we did not measure phosphorylation of p70S6k, we can report the absolute protein synthesis of the TA (Figure 4.6). Our data describes an increase from Ctrl to Stim muscle of ~20 % after 30 days of CHFS, aligning closely with the muscle mass increase illustrated in Figure 4.1. Furthermore, relative data generated from our study reports mixed muscle FSR values increase by ~85 % from Ctrl to Stim similar to previous work in trained humans reporting ~50 % increases in mixed protein FSR in response to resistance exercise training (Phillips et al, 1999). We can further report a large range of individual protein responses (2-27 %/d), underlining issues with gross or mixed muscle data on muscle adaptation.

To investigate individual muscle proteins further, proteomic separation techniques such as 2DGE enable individual proteins to be isolated based on their molecular mass and isoelectric point, which allows proteoform-specific responses during muscle transformation to be investigated (Burniston, 2008). Two dimensional-gel electrophoresis is well known for its ability to resolve proteoforms of the myofibrillar fraction (Dowling et al, 2019) and by using this method we can report protein turnover data for the identified myofibrillar proteoforms (Table 4.1) during adaptation to resistance exercise training. This is vital information that would be otherwise missed by more common 'bottom-up' proteomic techniques. The majority of the data from resistance exercise concerning mixed muscle or the myofibrillar fraction generally report an increase in protein turnover (Biolo et al, 1995.; Phillips et al, 1997). Whilst this is true for the first 10 days of stimulation in the myofibrillar fraction (Fig. 4.5 and 4.8) where we observe an increase in the synthesis rates of 23 proteins (Figure 4.8) from Ctrl to Stim, resulting in a change of abundance in only 2 proteins (PYGM and ENOA; Figure 4.5), the remaining 20-day period show a different response. Similar to the data presented in Shankaran et al, (2016) who reported increases in muscle mass after 28 days of SAR administration to correlate with increases in protein synthesis of individual proteins. We too see increases in muscle mass, but in response to CHFS, and also measure increases in protein synthesis rates of individual proteins. We measured 11 of the same myofibrillar proteins as Shankaran et al, (2016) and our data agree with the exception of ENOB where we detect no changes in synthesis from Ctrl to Stim, and ENOA were we found synthesis to decrease in response to resistance training. We have (Hesketh et al, 2016) previously reported tissue-specific regulation of synthesis rates of individual proteins and since Shankaran et al, (2016) data report synthesis rates from rat triceps and our data is from rat TA this may provide an explanation as to why ENOB and ENOA response may be different. Furthermore, Shankaran et al, (2016) did not measure protein abundances to indicate if these increases in proteins synthesis are a protein turnover response or a synthesis-specific anabolic response. However, we can report that after 30 days of CHFS of the 35 myofibrillar proteoforms identified in this study (Table 4.1), 20 proteoforms significantly change their abundance (2 decrease and 18 increase) despite measuring 23 proteoforms that significantly alter their synthesis rates. Figure 4.9 highlights the proteins that exhibit these changes in abundance, from which the remaining 15 proteoforms maintain abundance via increasing the rate of protein turnover (n = 3) i.e.

increases in synthesis that is matched by degradation or by no response to CHFS (n = 12). Furthermore, myofibrillar proteins detected as multiple proteoforms (n = 10, Table 4.1) tended to respond in a similar manner to each other in response to CHFS. For example, the four spots identified as TNNT3 all increased in response to hypertrophy, consistent with previous findings (Isfort et al, 2002). In addition, other proteoforms like KCRS (spots 18, 19, 20) did not change in abundance but all increased in synthesis, consistent with an increased turnover response of the muscle proteome to resistance exercise training (Phillips et al, 1997). However, most of the myofibrillar proteoforms increased in abundance in response to CHFS. For example, the two MLRS proteoforms (spot 34 and spot 35) increased ($+3.6 \pm 0.6$ -fold) in abundance, as did TNNI2 (spot 26, +7-fold; spot 27 +1.9-fold), ACTS (spot 14, +5.6-fold), tropomyosin (spot 21 TPM1, +2.6-fold; spot 22 TPM4, +2-fold) and DESM (spot 7, +2.3-fold). These increases in protein abundance, could be explained by the assembly of striated myofibrils in the development of premyofibril complexes (Sanger et al, 2017). Not only are premyofibrils known to contain thin protein filaments (e.g. actin, tropomyosin, and troponin) and cosameric proteins (e.g. DESM), but proteins that are involved in the early phase of premyofibril assembly are documented to be highly dynamic (Sanger et al, 2017). Specifically, DESM has been associated with lateral force transmission from contracting sarcomeres to the muscle exterior (Bloch and Gonzalez-Serratos, 2003) and is known to increase in the muscle, post resistance exercise (Woolstenhulme et al, 2006). Given that the protein content of the muscle is significantly increased (Figure 4.2) in response to CHFS and there are greater contractile demands placed on the muscle, this may explain why we document these significant increases in key contractile proteins, in response to resistance exercise training. However, not all contractile proteoforms follow this pattern. Myosin light chain 1/3 (MLY1/3) was resolved as four separate proteoforms (spots 29, 30, 31, 32; Figure 4.3). MYL1 and MLY3 are two proteins with almost identical amino acid sequences. Due to the nature of peptide mass fingerprinting if the unique peptide sequence is not identified then we cannot distinguish between the two and the protein is identified as MYL1/3. On this occasion peptide mass fingerprinting did not identify the unique peptide to differentiate these proteoforms (supplementary Table S1). This could provide reasoning as to why we observe 2 MYL1/3 proteoforms to increase ($+2.93 \pm 0.3$ -fold) in abundance (spots 31 and 32), where the other 2 (spots 29 and 30) exhibit no change ($P = 0.220 \pm 0.09$) to the stimulation. Furthermore, spot 29 and 30 share

the same molecular mass consistent with MLY3, as spot 31 and 32 are consistent with MLY1.

The absolute synthesis rate for the average mixed soluble fraction did not change ($P = 0.639$) from Ctrl (49.66 ± 0.82 pg/d) to Stim (52.04 ± 1.07). This is inconsistent with previous work that report relative data (Phillips et al, 2007) but increases in muscle mass (Wong and Booth, 1990.; Shankaran et al, 2016). Largely, this is due to the fact previous literature reported mixed muscle synthesis and/or turnover data, failing to differentiate the highly abundant myofibrillar proteins from the soluble proteins. Furthermore, here we report the average across 56 soluble proteins that encompass a range of synthesis rates that spans 2 orders of magnitude. This equates to 36 out of 56 proteins significantly changing (23 increase, 13 decrease) the rate of synthesis from Ctrl to Stim after 30 days of CHFS. Further highlighting the problem of working with whole muscle data; thus, demonstrating that clearly some proteins increase and others decrease accordingly, in response to resistance exercise training, information that is otherwise missed when not measuring individual proteins. Camera et al, (2017) applied DPP methods similar to that in this thesis to quantify protein turnover of 91 muscle proteins (31 myofibrillar and 60 of soluble fraction) in response to resistance exercise training in humans. Similarly, they reported different patterns of response that differ on a protein-by-protein basis involving changes to both the synthesis and degradation of individual proteins. Furthermore, consistent with our findings Camera et al, (2017) reported an increase in myofibrillar protein synthesis and no significant change in protein synthesis for the soluble fraction. However, when analysed at the individual protein level, 7 proteins from the soluble fraction increased in response to resistance exercise training, were we showed 36 soluble proteins to change significantly in synthesis but only 7 change in abundance. An explanation for reporting this difference between relative and absolute data is that the proteins in the soluble fraction are being turned over more rapidly due to quality control within the muscle as a result of resistance training. Furthermore, the changes we see in the soluble fraction between our data and Camera et al, (2017) are less than consistent, with only one protein agreeing with our findings. ALDOA shows a significant decrease in protein synthesis in response to exercise training which is apparent in both data sets. Whereas we report the abundance of glycolytic enzymes LDHA and PYGM to decrease in response to CHFS, Camera et al, (2017) reported LDHA to not change in abundance but to increase in turnover. Although we report contrasting findings to

some of the previous literature that has observed increases in glycolytic metabolism to correlate with resistance exercise (Tesch et al, 1986.; Camera et al, 2017). We report 15 other proteins associated with oxidative metabolism that increase their turnover rates which may be associated with maintaining enzyme pool efficiency (Lam et al, 2014). Amongst the proteins that increase in abundance is COF1 the response observed for this protein may be necessary to stabilise the cytoskeleton and myofibril structures to prevent protein denaturation during periods of increased contractile activity (Benndorf et al, 1994). There are potentially several explanations why our data do not exactly align with Camera et al, (2017). Firstly, part of the Camera et al, (2017) intervention includes a high fat diet and the study did not include a healthy control diet so we cannot compare even our Ctrl TA data to their control group (which was fed a high fat diet only). Furthermore, our intervention is over a 30-day period of resistance training with significant hypertrophic gains compared to an intra-subject control, in comparison to just 9 days of resistance training with a separate control group and no muscle growth shown. Finally, although overall trends are similar, changes on a protein-by-protein basis, and specifically in protein synthesis (i.e. increases in mixed myofibrillar fraction and no change in mixed soluble fraction in response to resistance exercise) there may be species dependent responses that does not translate to protein specific differences.

4.6 Conclusions

We have used deuterium labelling and peptide mass spectrometry to establish fully integrated DPP in order to measure the rate of synthesis and net abundance, allowing accurate calculation of the rate of degradation for muscle proteins in both the myofibrillar and soluble fractions in response to resistance exercise training. We have demonstrated that proteins increase, decrease and are more rapidly or slowly turned over in response to resistance exercise. Previously, it has been largely assumed that such changes are due to alterations of protein synthesis only. However, by using DPP, we present highly novel data to show that changes in muscle proteins during muscle hypertrophy occur via several different patterns of response that involve the modulation of both synthetic and degradative processes. This level of detail has only previously been detected in human resistance training over a 9-day period (Camera et al, 2017). We present measurement of rat TA using DPP over 30 days of resistance exercise training, resulting in significant hypertrophy to provide a mechanistic insight into the regulation of protein abundance during adaptation within the muscle cell and protein metabolism.

4.7 Bibliography

References

Alway, S.E.; Siu, P.M.; Murlasits, Z.; Butler, D.C. (2005). Muscle hypertrophy models: Applications for research on aging. *Can. J. Appl. Physiol*, **5**, 591-624.

American College of Sports Medicine ACSM. (2009). American College of Sports Medicine position stand. Progression models in resistance training for healthy adults. *Med Sci Sports Exerc*, **41**, 687–708.

Armstrong, R.B.; Marum, P.; Tullson, P.; Saubert, C.W. (1979). Acute hypertrophic response of skeletal muscle to removal of synergists. *J. Appl. Physiol*, **46**, 835-842.

Baldwin, K.M.; Valdez, V.; Herrick, R.E.; Macintosh, A.M.; Roy, R.R. (1982). Biochemical properties of overloaded fast-twitch skeletal muscle. *J. Appl. Physiol*, **52**, 467-472.

Bamman, M.; Hill, V.; Adams, G.; Haddad, F.; Wetzstein, C.; Gower, B.; Ahmed, A.; Hunter, G. (2003). Gender Differences in Resistance-Training-Induced Myofiber Hypertrophy Among Older Adults. *Journal of Gerontology: Biological Sciences*, **2**, 108–116.

Baar, K.; Esser, K. (1999). Phosphorylation of p70(s6k) correlates with increased skeletal muscle mass following resistance exercise. *Am. J. Physiol*, **276**, 120-127.

Benndorf, R.; Hayess, K.; Ryazantsev, S.; Wieske, M.; Behlke, J.; Lutsch, G. (1994). Phosphorylation and supramolecular organization of murine small heat shock protein HSP25 abolish its actin polymerization-inhibiting activity. *J. Biol. Chem*, **269**, 20780–20784.

Biolo, G.; Maggi, S. P.; Williams, B. D.; Tipton, K. D.; Wolfe, R. R. (1995). Increased rates of muscle protein turnover and amino acid transport after resistance exercise in humans. *Am. J. Physiol*, **268**, 514–520.

Bloch, R. J.; Gonzalez-Serratos, H. (2003). Lateral force transmission across costameres in skeletal muscle. *Exerc. Sport Sci. Rev*, **31**, 73–78.

Booth, F.W.; Thomason, D.B. (1991). Molecular and cellular adaptation of muscle in response to exercise: perspectives of various models. *Physiol. Rev*, **71**, 541–585.

Brook, M. S.; Wilkinson, D. J.; Mitchell, W. K.; Lund, J. N.; Szewczyk, N. J.; Greenhaff, P. L.; Smith, K.; Atherton, P. J. (2015). Skeletal muscle hypertrophy adaptations predominate in the early stages of resistance exercise training, matching deuterium oxide-derived measures of muscle protein synthesis and mechanistic target of rapamycin complex 1 signaling. *FASEB J*, **29**, 4485–4496.

Burniston, J.G. (2008). Changes in the rat skeletal muscle proteome induced by moderate-intensity endurance exercise. *Biochem. Biophys. Acta*, **178**, 1077-1086.

Camera, D.; Burniston, J.; Pogson, M.; Smiles, W.; Hawley, J. (2017). Dynamic proteome profiling of individual proteins in human skeletal muscle after a high-fat diet and resistance exercise. *FASEB*, **31**, 1-17.

Castle, M.E.; Reyman, T.A. (1984). The effect of tenotomy and tendon transfers on muscle fiber types in the dog. *Clin. Orthop*, **186**, 302-310.

Chesley, A.; macDougall, J.D.; Tarnopolsky, M.A.; Atkinson, S.A.; Smith, K. (1992). Changes in human muscle protein synthesis after resistance exercise. *J. Appl. Physiol*, **73**, 1383–1388.

Coffey, V.G.; Hawley, J.A. (2007). The molecular basis of training adaptation. *Journal of Sports Medicine*, **37**, 737-763.

Commerford, S. L.; Carsten, A. L.; Cronkite, E. P. (1983). The distribution of tritium among the amino acids of proteins obtained from mice exposed to tritiated water. *Radiat. Res*, **94**, 151–155.

Degens, H.; Turek, Z.; Binkhorst, R.A. (1993). Compensatory hypertrophy and training effects on the functioning of aging rat m. Plantaris. *Mech Ageing Dev*, **66**, 299–311.

Des Neves, W.; de Oliveira, L.F.; da Silva, R.P.; Alves, C.R.R.; Lancha, A.H. (2017). Fasting: a major limitation for resistance exercise training effects in rodents. *Braz J Med Biol Res*, **51**, 5755-5763.

Dowling, P.; Zweyer, M.; Swandulla, D.; Ohlendieck, K. (2019). Characterization of Contractile Proteins from Skeletal Muscle Using Gel-Based Top-Down Proteomics. *Proteomes*, **7**, 1-23.

Duncan, N.D.; Williams, D.A.; and Lynch, G.S. (1998). Adaptations in rat skeletal muscle following long-term resistance exercise training. *Eur. J. Appl. Physiol. Occup. Physiol*, **77**, 372-378.

Folland, J.P.; Williams, A.G. (2007). The adaptations to strength training: morphological and neurological contributions to increased strength. *Sports Med*, **37**, 145–168.

Gollnick, P.D.; Timson, B.F.; Moore, R.L.; Riedy, M. (1981). Muscular enlargement and number of fibers in skeletal muscles of rats. *J Appl Physiol*, **50**, 936–943.

Goldberg, A.L.; Etlinger, J.D.; Goldspink, D.F.; Jablecki, C. (1975). Mechanism of work-induced hypertrophy of skeletal muscle. *Med Sci Sports*, **7**, 185–198.

Gonyea, W.J.; Ericson, G.C. (1976). An experimental model for the study of exercise-induced skeletal muscle hypertrophy. *J. Appl. Physiol*, **40**, 630-633.

Haddad, F.; Adams, G.R. (2002). Selected contribution: Acute cellular and molecular responses to resistance exercise. *J. Appl. Physiol*, **93**, 394-403.

Henneman, E.; Somjen, G.; Carpenter, DO. (1965). Excitability and Inhibitibility of Motoneurons of Different Sizes. *J Neurophysiol*, **28**, 599–620.

Hesketh, S.; Srisawat, K.; Sutherland, H.; Jarvis, J.; Burniston, J. (2016). On the rate of synthesis of individual proteins within and between different striated muscles of the rat. *Proteomes*, **4**, 1-12.

Ho, K-W.; Roy, RR.; Tweedle, CD.; Heusner, WW.; van Huss, WD.; Carrow, RE. (1980). Skeletal muscle fiber splitting with weight-lifting exercise in rats. *Am J Anat*, **157**, 433–440.

Hornberger, T.A.; Farrar, R.P. (2004). Physiological hypertrophy of the FHL muscle following 8 weeks of progressive resistance exercise in the rat. *Can. J. Appl. Physiol*, **29**, 16-31.

Ianuzzo, CD.; Gollnick, PD.; Armstrong RB. (1976). Compensatory adaptations of skeletal muscle fiber types to a long-term functional overload. *Life Sci*, **19**, 1517–1523.

Isfort, R.; Wang, F.; Greis, K.; Sun, Y.; Keough, T.; Farrar, R.; Bodine, S.; Anderson, L. (2002). Proteomic analysis of rat soleus muscle undergoing hindlimb suspension-induced atrophy and reweighting hypertrophy. *Proteomics*, **2**, 543–550.

Jacobs, BL.; You, JS.; Frey, JW.; Goodman, CA.; Gundermann, DM.; Hornberger, TA. (2013). Eccentric contractions increase the phosphorylation of tuberous sclerosis complex-2 (TSC2) and alter the targeting of TSC2 and the mechanistic target of rapamycin to the lysosome. *J Physiol*, **18**, 4611-20.

Kraemer, WJ.; Deschenes, MR.; Fleck, SJ. (1988). Physiological adaptations to resistance exercise. Implications for athletic conditioning. *Sports Med*, **4**, 246-256.

Lam, M. P.; Wang, D.; Lau, E.; Liem, D. A.; Kim, A.K.; Liang, X.; Bleakley, B. J.; Liu, C.; Tabaraki, J.D.; Cadeiras, M.; Wang, Y.; Deng, M. C.; Ping, P. (2014). Protein kinetic signatures of the remodeling heart following isoproterenol stimulation. *J. Clin. Invest*, **124**, 1734–1744.

Landi, F.; Marzetti, E.; Martone, AM.; Bernabei, R.; Onder, G. (2014). Exercise as a remedy for sarcopenia. *Curr Opin Clin Nutr Metab Care*, **1**, 25-31.

Lowe, D.A.; Alway, S.E. (2002). Animal models for inducing muscle hypertrophy: Are they relevant for clinical applications in humans? *J. Orthop. Sports Phys. Ther*, **32**, 36-43.

MacDougall, JD.; Gibala, MJ.; Tarnopolsky, MA.; MacDonald, JR.; Interisano, SA.; Yarasheski, KE. (1995). The time course for elevated muscle protein synthesis following heavy resistance exercise. *Can J App Physiol*, **4**, 480-486.

Marzetti, E.; Calvani, R.; Tosato, M.; Cesari, M.; Di Bari, M.; Cherubini, A.; Collamati, A.; D'Angelo, E.; Pahor, M.; Bernabei, R.; Landi, F. (2017). Sarcopenia: an overview *Aging Clin Exp Res*, **29**, 11–17.

Mitchell, C. J.; Churchward-Venne, T. A.; Parise, G., Bellamy, L.; Baker, S.K.; Smith, K.; Atherton, P. J.; Phillips, S.M. (2014). Acute post-exercise myofibrillar protein synthesis is not correlated with resistance training-induced muscle hypertrophy in young men. *PlosOne*, **9**, 824-31.

Nader, G.A.; Esser, K.A. (2001). Intracellular signaling specificity in skeletal muscle in response to different modes of exercise. *J. Appl. Physiol*, **90**, 1936-1942.

Phillips, S.M.; Tipton, K. D.; Aarsland, A.; Wolf, S. E.; Wolfe, R. R. (1997). Mixed muscle protein synthesis and breakdown after resistance exercise in humans. *Am. J. Physiol*, **273**, 99–107.

Rennie, M.; Wackerhage, H.; Spangenburg, E.; Booth, F. (2004). Control of the size of the human muscle mass. *Annu. Rev. Physiol*, **66**, 799–828.

Roux, PP.; Thibault, P. (2013). The coming of age of phosphoproteomics-from large data sets to inference of protein functions. *Mol Cell Proteomics*, **12**, 3453-64.

Roy, R.R.; Meadows, I.D.; Baldwin, K.M.; Edgerton, V.R. (1982). Functional significance of compensatory overloaded rat fast muscle. *J. Appl. Physiol*, **52**, 473-478.

Roy, R.R.; Edgerton, V.R. (1995). Response of mouse plantaris muscle to functional over- load: Comparison with rat and cat. *Comp. Biochem. Physiol. A Physiol*, **111**, 569-575.

Sanger, J. W.; Wang, J.; Fan, Y.; White, J.; Mi-Mi, L.; Dube, D. K.; Sanger, J. M.; Pruyne, D. (2017). Assembly and maintenance of myofibrils in striated muscle. *Handb. Exp. Pharmacol*, **235**, 39–75.

Schmoll, M.; Unger, E.; Sutherland, H.; Haller, M.; Bijak, M.; Lanmuller, H. (2018). Spillover stimulation: A novel hypertrophy model using co-contraction of the plantarflexors to load the tibial anterior muscle in rats. *PlosONE*, **11**, 207-216.

Shankaran, M.; Shearer, T.; Stimpson, S.; Turner, S.; King, C.; Wong, P.; Shen, Y.; Turnbull, Kramer, F.; Clifton, L.; Russell, A.; Hellerstein, M.; Evans, W. (2016). Proteome-wide muscle protein fractional synthesis rates predict muscle mass gain in response to a selective androgen receptor modulator in rats. *Am J Physiol Endocrinol Metab*, **310**, 405-417.

Song, Z.; Moore, DR.; Hodson, N.; Ward, C.; Dent, JR.; O'Leary, MF.; Shaw, AM.; Hamilton, DL.; Sarkar, S.; Gangloff, YG.; Hornberger, TA.; Spriet, LL.; Heigenhauser, GJ.; Philp, A. (2017). Resistance exercise initiates mechanistic target of rapamycin (mTOR) translocation and protein complex co-localisation in human skeletal muscle. *Sci Rep*, **1**, 502-508.

Tamaki, T.; Uchiyama, S.; Nakano, S. (1992). A weight-lifting exercise model for inducing hypertrophy in the hindlimb muscles of rats. *Med. Sci. Sports Exerc*, **24**, 881-886.

Tesch, P. A.; Colliander, E. B.; Kaiser, P. (1986). Muscle metabolism during intense, heavy-resistance exercise. *Eur. J. Appl. Physiol. Occup. Physiol*, **55**, 362–366.

Timson, B. F. (1990). Evaluation of animal models for the study of exercise-induced muscle enlargement. *J. Appl. Physiol*, **69**, 1935– 1945.

Tomanek, R.J.; Woo, Y.K. (1970). Compensatory hypertrophy of the plantaris muscle in relation to age. *J. Gerontol*, **25**, 23-29.

Walston JD. (2012). Sarcopenia in older adults. *Curr Opin Rheumatol*, **24**, 623–627.

Wirth, O.; Gregory, E.W.; Cutlip, R.G.; Miller, G.R. (2003). Control and quantitation of voluntary weight-lifting performance of rats. *J. Appl. Physiol*, **95**, 402-412.

Woolstenhulme, M. T.; Conlee, R. K.; Drummond, M. J.; Stites, A. W.; Parcell, A. C. (2006). Temporal response of desmin and dystrophin proteins to progressive resistance exercise in human skeletal muscle. *J. Appl. Physiol*, **100**, 1876–1882.

Wong, T.S.; Booth, F.W. (1988). Skeletal muscle enlargement with weight-lifting exercise by rats. *J. Appl. Physiol*, **65**, 950-954.

Wong, T.S.; Booth, F.W. (1990). Protein metabolism in rat gastrocnemius muscle after stimulated chronic concentric exercise. *J. Appl. Physiol*, **69**, 1709-1717.

Supplementary tables

Table S1. Myofibrillar protein identifications and peptide information.

Myofibrillar fraction					
Spot Number	Protein	Score	Coverage	Peptide sequence	Residue
1	PLEC	88	4 %	QAQEEAER	1631-1638
				LSVAAQEAAR	2423-2432
				VPVDVAYQR	3292-3300
				LPVDVAYQR	3623-3631
				HRELAEEAAR	1956-1966
2, 3	PYGM	96	18 %	DHLVDR	62-67
				YFEGIFNQK	162-170
				IGEEYISDLQQLR	508-520
				QEYFVVAATLQDIIR	296-310
				LITAIGDVVNHDPVAVGDR	623-640
4, 5	PFKAM	92	12 %	ITAEER	145-150
				FDEAIK	367-372
				DLQVNVEHLVQK	604-615
				VLVVDHGFEGFLAK	433-445
				LNITIVAEGAIDKNGK	257-272
6	ATPB	128	22 %	IPVGPETLGR	134-143
				IMNVIGEPIDER	144-155
				FTQAGSEVSALLGR	311-324
				TIAMDGTEGLVRGQK	110-124
				VALVYQGMNEPPGAR	265-279
7	DESM	115	25 %	TSGGAGGLGSLR	59-70
				LEEEIRHLK	369-377
				RQVEVLTNQR	163-172
				HLREYQDLLNVK	383-394
				FLEQQNAALAAEVNR	127-141
8, 9	ENOA	109	26 %	GVPLYR	127-132
				SPDDASR	263-269
				LNVVEQEK	82-89
				GNPTVEVDLYTAK	16-28
				FGANAILGVSLAVCK	106-120
10, 11, 12	ENOB	114	30 %	IGAENVYHHLK	184-193
				GVLKAVEHINK	61-71
				IFAREILDSR	6-15
				GNPTVEVDLHTAK	16-28
				LAQSNWGWVMVSHR	359-372
13	ATPA	102	30 %	AVDSLVPPIGR	195-204
				VGSAAQTR	417-424

				RFNDGTDEK	231-239
				GIRPAINVGLSVSR	403-416
				TGAIVDVPVGDPELLGR	134-149
14	ACTS	126	26 %	HQGVMVGMGQK	42-52
				DSYVGDEAQSK	53-63
				QEYDEAGPSIVHR	362-274
				IWHHTFYNELR	87-97
				MQKEITALAPSTMK	315-328
15, 16, 17	KCRM	91	24 %	LMVEMEKK	359-366
				GYTLPPHCSR	139-148
				DLFDPIIQDR	87-96
				GGDDLDPNYVLSSR	117-130
				GTGGVDTAAVGAVFDISNA	321-341
				DR	
18, 19, 20	KCRS	92	28 %	GIWHNYDK	250-257
				GLSLPPACSR	173-182
				ITHGQFDER	150-158
				VPPPLPQFGR	409-418
				LFPPSADYPDLR	47-58
21	TPM1	98	37 %	LEEAEK	113-118
				YEEVARK	162-168
				KMQMLKLD	7-14
				GTEDELDK	52-59
				SLEAQAEK	206-213
				KATDAEADVASLNR	77-90
22	TMP2	107	34 %	KMQMLKLDK	7-15
				LVILEGELER	169-178
				EDKYEEEIK	218-226
				AQERLATALQK	102-112
				LEEAEKAADESER	113-125
23, 24, 25, 28	TNNT3	97	24 %	LTAPKIPEGEK	44-54
				QKYDITTLR	225-233
				QNRLAEEK	118-126
				IPEGEKVDFDDIQK	49-62
				QNKDLMELQALIDSHFEAR	65-83
26, 27	TNNI2	96	34 %	VRMSADAMLK	115-124
				SSKELEDMNQK	89-99
				MSADAMLKALLGSK	117-130
				YDMEVKVQK	80-88
				QHLKSVMLQIAATELEK	16-32
29, 30, 31, 32	MYL1/3	112	28 %	HVLATLGEK	149-157
				EAFLLFDR	52-59
				ITLSQVGDVLR	65-75
				DQGGYEDFVEGLR	120-132
				ALGQNPTQAEVLR	87-99
33	CAH3	96	30 %	DGIAIGIFLK	138-148
				TILNNGKTCR	58-67
				GGPLPGPYRLR	81-91
				GENQSPVELHTK	25-36
				FDPSCLFPACR	178-188

34, 35	MLRS	98	42 %	DGIIDKEDLR	42-51
				EAFVIDQNR	32-41
				LKGADPEDVITGAFK	91-112
				KQFLEELLTTQCDR	117-130
				AAAEGSSNVFSMFDQTQIQ	10-31
				EFK	

Spot number refers to the different proteoforms resolved by 2DGE and corresponds to the 2DGE image in Figure 4.3. Protein name relates to the Uni-Prot database, entries returned using the MASCOT search engine. A mowse score greater than 55 denotes a confident ($P < 0.05$) identification by peptide mass fingerprinting. Coverage is the amount of sequence covered of the protein for identification. Peptide sequence refers to the amino acid sequence of each peptide used for peptide mass spectrometry and the residues are where each peptide occurs in the protein sequence.

Table S2. Soluble proteins identification.

Protein I.D.	Soluble fraction		Peptide #
	Protein name	GO function	
AATC	Aspartate aminotransferase , cytoplasmic	Unassigned	8
AATM	Aspartate aminotransferase, mitochondrial	Mitochondrial	6
ACON	Aconitate hydratase, mitochondrial	Mitochondrial	11
ADT1	ADP/ATP translocase 1	Mitochondrial	7
ALBU	Serum albumin	Unassigned	14
ALDOA	Fructose-bisphosphate aldolase A	Glycolysis	22
AT2A1	Sarcoplasmic/endoplasmic reticulum calcium ATPase 1	Ca ²⁺ Handling	34
ATP5H	ATP synthase subunit d, mitochondrial	Mitochondrial	2
ATPA	ATP synthase subunit alpha, mitochondrial	Mitochondrial	13
ATPB	ATP synthase subunit beta, mitochondrial	Mitochondrial	20
ATPG	ATP synthase subunit gamma, mitochondrial	Mitochondrial	4
ATPO	ATP synthase subunit O, mitochondrial	Mitochondrial	2
CAH3	Carbonic anhydrase 3	Unassigned	11
CASQ1	Calsequestrin-1	Ca ²⁺ Handling	3
CISY	Citrate synthase	Mitochondrial	7
COF1	Cofilin-1	Unassigned	1
COX2	Cytochrome c oxidase subunit 2	Mitochondrial	3
CYC	Cytochrome c	Mitochondrial	4
ECHA	Trifunctional enzyme subunit alpha	Mitochondrial	4
EF1A2	Elongation factor 1-alpha 2	Unassigned	2
ENOB	Beta-enolase	Glycolysis	14
FABPH	Fatty acid-binding protein, heart	Unassigned	12
G3P	Glyceraldehyde-3-phosphate dehydrogenase	Glycolysis	5
G6PI	Glucose-6-phosphate isomerase	Glycolysis	6
GPDA	Glycerol-3-phosphate dehydrogenase [NAD(+)], cytoplasmic	High-energy phosphate	2

HBA	Hemoglobin subunit alpha-1/2	O ₂ Transport	2
HBB1	Hemoglobin subunit beta-1	O ₂ Transport	2
HBB2	Hemoglobin subunit beta-2	O ₂ Transport	2
HS90B	Heat shock protein HSP 90-beta	Unassigned	2
HSP7C	Heat shock cognate 71 kDa protein	Unassigned	7
IDHP	Isocitrate dehydrogenase [NADP], mitochondrial	Mitochondrial	4
KAD1	Adenylate kinase isoenzyme 1	High-energy phosphate	16
KCRM	Creatine kinase M-type	High-energy phosphate	24
KPYM	Pyruvate kinase PKM	Glycolysis	19
LDHA	L-lactate dehydrogenase A chain	Glycolysis	7
MDHC	Malate dehydrogenase, cytoplasmic	Mitochondrial	14
MDHM	Malate dehydrogenase, mitochondrial	Mitochondrial	2
MPCP	Phosphate carrier protein	Mitochondrial	8
MYG	Myoglobin	O ₂ Transport	1
MYL1	Myosin light chain 1/3, skeletal muscle isoform	Unassigned	3
ODPA	Pyruvate dehydrogenase E1 component subunit alpha, somatic form, mitochondrial	Mitochondrial	1
ODPB	Pyruvate dehydrogenase E1 component subunit alpha, somatic form	Mitochondrial	2
PARK7	Protein/nucleic acid deglycase DJ-1	Unassigned	3
PFKAM	ATP-dependent 6-phosphofructokinase, muscle type	Glycolysis	4
PGAM2	Phosphoglycerate mutase 2	Glycolysis	13
PGK1	Phosphoglycerate kinase 1	Glycolysis	14
PGM1	Phosphoglucomutase-1	Glycolysis	18
PRDX5	Peroxiredoxin-5	Mitochondrial	2
PRVA	Parvalbumin alpha	Ca ²⁺ Handling	9
PYGB	Glycogen phosphorylase, brain form	Glycolysis	2
PYGM	Glycogen phosphorylase, muscle form	Glycolysis	21

QCR1	Cytochrome b-c1 complex subunit 1	Mitochondrial	2
QCR2	Cytochrome b-c1 complex subunit 2	Mitochondrial	1
TPIS	Triosephosphate isomerase	Glycolysis	12
TRY1	Anionic trypsin-1	Unassigned	1
VDAC1	Voltage-dependent anion-selective channel protein 1	Unassigned	5

Protein I.D. relates to the Uni-Prot database, entries returned using the MASCOT search engine. Full protein name is given with assigned gene ontology function. The peptide number refers to the number of unique peptides used for each protein to gain a positive identification.

Table S3. Rank order for abundance changes in myofibrillar proteins after 30-d of stimulation in TA muscle.

Protein I.D.	Relative ABD	P-Value	Protein I.D.	Absolute ABD	P-Value
ATPB (6)	1.48 ± 0.06	0.024	TNNI2 (26)	6.95 ± 0.3	0.002
TNNI2 (26)	1.34 ± 0.03	0.012	ATPA (13)	6.52 ± 0.52	0.002
TNNT3 (23)	1.18 ± 0.09	0.033	ACTS (14)	5.58 ± 0.44	0.003
TNNT3 (28)	1.15 ± 0.72	0.024	TNNT3 (23)	4.39 ± 0.18	0.002
TNNT3 (25)	1.13 ± 0.32	0.026	TNNT3 (24)	4.39 ± 0.26	0.003
MLRS (34)	1.12 ± 0.17	0.021	MLRS (34)	4.01 ± 0.83	0.003
ACTS (14)	1.12 ± 0.08	0.012	ATPB (6)	3.66 ± 1.02	0.007
MYL1/3 (32)	1.12 ± 0.04	0.021	TNNT3 (28)	3.17 ± 0.91	0.031
DESM (7)	1.08 ± 0.07	0.025	MYL1/3 (32)	3.15 ± 0.83	0.019
MLRS (35)	0.99 ± 0.06	0.025	MLRS (35)	3.10 ± 1.20	0.039
ATPA (13)	0.92 ± 0.05	0.015	CAH3 (33)	2.81 ± 0.96	0.018
TNNT3 (24)	0.92 ± 0.05	0.042	MYL1/3 (31)	2.71 ± 0.92	0.029
CAH3 (33)	0.86 ± 0.09	0.039	TNNT3 (25)	2.70 ± 0.93	0.026
MYL1/3 (31)	0.86 ± 0.04	0.023	KCRM (15)	2.56 ± 0.95	0.019
TPM1 (21)	0.81 ± 0.01	0.041	TPM1 (21)	2.55 ± 0.96	0.028
KCRM (15)	0.79 ± 0.06	0.021	DESM (7)	2.30 ± 0.97	0.026
TPM2 (22)	0.79 ± 0.05	0.028	TPM2 (22)	2.00 ± 0.93	0.017
TNNI2 (27)	0.66 ± 0.08	0.038	TNNI2 (27)	1.92 ± 0.95	0.033
KCRM (17)	0.08 ± 0.05	0.156	MYL1/3 (30)	1.16 ± 0.96	0.155
PLEC (1)	0.07 ± 0.04	0.866	KCRS (20)	1.07 ± 0.97	0.195
KCRM (16)	0.02 ± 0.09	0.263	KCRM (17)	0.75 ± 0.37	0.477
MYL1/3 (29)	0.02 ± 0.00	0.731	KCRS (19)	0.51 ± 0.36	0.119
KCRS (18)	0.02 ± 0.00	0.332	KCRS (18)	0.46 ± 0.22	0.291
KCRS (20)	0.01 ± 0.00	0.195	PLEC (1)	0.11 ± 0.04	0.887
KCRS (19)	0.01 ± 0.00	0.174	MYL1/3 (29)	0.09 ± 0.01	0.288
MYL1/3 (30)	0.01 ± 0.00	0.832	KCRM (16)	0.04 ± 0.00	0.184
ENOB (12)	-0.02 ± 0.00	0.429	ENOB (12)	-0.04 ± 0.00	0.471
ENOB (11)	-0.03 ± 0.00	0.885	PFKAM (4)	-0.07 ± 0.01	0.446
PFKAM (4)	-0.03 ± 0.02	0.431	ENOA (9)	-0.16 ± 0.05	0.094
ENOB (10)	-0.03 ± 0.00	0.732	PYGM (3)	-0.61 ± 0.42	0.642
PYGM (3)	-0.07 ± 0.06	0.177	PFKAM (5)	-0.71 ± 0.35	0.251
PFKAM (5)	-0.08 ± 0.01	0.323	ENOB (10)	-0.72 ± 0.63	0.874
ENOA (9)	-0.53 ± 0.21	0.116	ENOB (11)	-0.92 ± 0.61	0.266
ENOA (8)	-0.92 ± 0.02	0.027	ENOA (8)	-2.59 ± 0.19	0.029
PYGM (2)	-1.28 ± 0.71	0.033	PYGM (2)	-3.29 ± 0.20	0.022

Protein I.D. relates to the Uni-Prot database, entries returned using the MASCOT search engine. Spot numbers are in brackets which refers to the different proteoforms resolved by 2DGE and corresponds to the 2DGE image in Figure 4.3. Relative

abundance (ABD) represents data normalised to spot density from the 2D-gels only. Absolute abundance (ABD) represents data normalised to spot density and total TA mass. All data is represented as MEAN \pm SD for biological replicates (n = 4) and is displayed as the positive (+) or negative (-) fold change from non-stimulated control muscle to 30 days co-contraction high-frequency stimulated muscle, in rank order of largest positive change to largest negative change. P-Values are generated from paired t-tests between control and 30-d stimulated muscle.

Table S4. Rank order for synthesis rates in myofibrillar proteins after 30-d of stimulation in TA muscle.

Protein I.D.	Relative (Sim)	Relative (Ctrl)	P-Value	Protein I.D.	Absolute (Stim)	Absolute (Ctrl)	P-Value
TNNI2 (27)	20.33 ± 0.45	6.78 ± 0.88	0.029	TNNT3 (28)	58.26 ± 0.85	42.14 ± 0.86	0.012
TNNT3 (25)	14.86 ± 0.46	2.75 ± 0.76	0.041	MLRS (35)	29.05 ± 1.08	14.28 ± 0.74	0.014
CAH3 (33)	26.84 ± 0.42	15.38 ± 0.84	0.026	KCRM (15)	70.82 ± 0.48	56.28 ± 1.27	0.019
TPM1 (21)	15.29 ± 0.52	4.73 ± 0.78	0.013	MYL1/3 (31)	33.73 ± 0.70	20.66 ± 0.86	0.011
MYL1/3 (32)	12.42 ± 0.43	2.03 ± 0.97	0.018	TNNI2 (26)	74.24 ± 0.69	61.55 ± 1.21	0.029
ATPB (6)	21.45 ± 0.75	11.74 ± 0.73	0.019	ATPB (6)	48.27 ± 0.37	35.86 ± 1.74	0.018
MYL1/3 (31)	11.52 ± 0.44	1.93 ± 1.03	0.033	TNNT3 (25)	56.24 ± 0.21	43.94 ± 0.83	0.016
TNNT3 (23)	12.03 ± 0.48	2.79 ± 0.84	0.026	MLRS (34)	23.44 ± 0.24	11.53 ± 0.93	0.017
TNNI2 (26)	11.81 ± 0.45	4.99 ± 1.28	0.019	TPM2 (22)	19.26 ± 0.72	8.28 ± 0.84	0.016
TNNT3 (24)	8.68 ± 0.48	1.94 ± 1.17	0.034	KCRM (17)	68.20 ± 0.51	58.01 ± 3.92	0.031
TPM2 (22)	9.49 ± 0.50	2.82 ± 0.62	0.011	ATPA (13)	33.27 ± 0.31	23.27 ± 0.98	0.021
KCRM (16)	11.64 ± 0.55	5.18 ± 0.56	0.021	TNNT3 (23)	46.93 ± 0.52	38.18 ± 0.93	0.011
KCRM (15)	12.17 ± 0.56	5.74 ± 0.94	0.031	TPM1 (21)	14.27 ± 0.24	5.84 ± 0.61	0.028
MLRS (34)	8.34 ± 0.41	1.94 ± 0.94	0.029	DESM (7)	26.73 ± 0.36	18.34 ± 0.61	0.012
PLEC (1)	7.44 ± 1.10	1.06 ± 0.37	0.017	MYL1/3 (32)	41.17 ± 0.55	33.20 ± 0.91	0.023
DESM (7)	11.52 ± 0.72	5.26 ± 0.63	0.024	TNNI2 (27)	66.03 ± 0.24	58.23 ± 0.93	0.013
MLRS (35)	7.83 ± 0.41	1.88 ± 0.88	0.021	CAH3 (33)	22.74 ± 0.32	15.17 ± 0.93	0.011
ATPA (13)	11.21 ± 0.67	5.27 ± 0.84	0.027	ACTS (14)	19.37 ± 0.30	12.57 ± 1.75	0.016
ACTS (14)	7.93 ± 0.59	1.98 ± 0.88	0.019	TNNT3 (24)	42.18 ± 0.21	35.39 ± 0.58	0.027
TNNT3 (28)	9.55 ± 0.44	3.63 ± 0.93	0.023	KCRM (16)	61.34 ± 0.39	54.84 ± 3.62	0.028
KCRM (17)	9.54 ± 0.54	4.72 ± 0.84	0.017	ENOB (12)	42.74 ± 0.31	36.28 ± 0.96	0.109
PFKAM (5)	9.97 ± 0.77	8.03 ± 1.18	0.162	ENOA (9)	38.24 ± 0.35	33.74 ± 0.85	0.755
ENOB (11)	7.35 ± 0.69	5.43 ± 0.64	0.183	MYL1/3 (30)	31.83 ± 0.27	28.20 ± 0.93	0.838
ENOB (12)	7.26 ± 0.68	5.38 ± 0.78	0.116	PLEC (1)	6.13 ± 0.39	2.84 ± 0.73	0.027
KCRS (20)	5.12 ± 0.52	3.58 ± 0.91	0.553	KCRS (19)	38.19 ± 0.41	35.28 ± 0.83	0.643

PFKAM (4)	10.27 ± 0.82	8.95 ± 0.86	0.291	MYL1/3 (29)	23.54 ± 0.98	20.73 ± 0.97	0.375
KCRS (18)	4.28 ± 0.53	3.27 ± 0.47	0.742	PFKAM (4)	70.22 ± 0.38	68.27 ± 0.89	0.188
PYGM (3)	8.24 ± 0.99	7.26 ± 0.93	0.744	KCRS (18)	35.02 ± 0.58	33.26 ± 0.74	0.911
MYL1/3 (30)	3.13 ± 0.44	2.20 ± 0.88	0.227	KCRS (20)	31.19 ± 0.70	30.12 ± 1.17	0.228
ENOA (9)	9.46 ± 0.71	8.74 ± 0.81	0.416	ENOB (11)	40.82 ± 0.33	41.37 ± 1.02	0.277
ENOB (10)	7.34 ± 0.70	7.24 ± 0.83	0.229	PYGM (3)	39.24 ± 0.39	40.98 ± 0.81	0.743
KCRS (19)	3.28 ± 0.52	3.73 ± 0.73	0.618	PFKAM (5)	70.26 ± 0.38	72.12 ± 0.85	0.277
MYL1/3 (29)	2.15 ± 0.44	2.72 ± 0.73	0.174	ENOB (10)	35.82 ± 0.34	38.37 ± 0.92	0.561
ENOA (8)	3.01 ± 0.71	9.10 ± 1.04	0.023	ENOA (8)	20.20 ± 0.35	31.74 ± 1.05	0.033
PYGM (2)	2.18 ± 1.35	9.46 ± 0.77	0.023	PYGM (2)	33.13 ± 0.39	48.24 ± 0.93	0.018

Protein I.D. relates to the Uni-Prot database, entries returned using the MASCOT search engine. Spot numbers are in brackets which refers to the different proteoforms resolved by 2DGE and corresponds to the 2DGE image in Figure 4.3. Synthesis rates are presented in relative format which relates to fractional synthesis rate in percent per day and in absolute terms which is reflective of whole TA synthesis with rates expressed in picograms per day. All data is represented as MEAN ± SD for biological replicates (n = 4) in the 30 days stimulated muscle (Stim) and the non-stimulated control muscle (Ctrl). The proteins are ranked in order of largest increase in synthesis rate from Ctrl to Stim through to largest decrease in synthesis rate from Ctrl to Stim. P-Values are generated from paired t-tests between control and 30-d stimulated muscle.

Table S5. Rank order for abundance changes in soluble proteins after 30-d of stimulation in TA muscle.

Protein I.D.	Relative ABD	P-Value	Protein I.D.	Absolute ABD	P-Value
ALBU	0.52 ± 0.34	0.014	ATPB	0.77 ± 0.06	0.014
ATPB	0.52 ± 0.46	0.013	ATPA	0.66 ± 0.03	0.015
COF1	0.45 ± 0.69	0.012	ALBU	0.55 ± 0.04	0.014
ATPA	0.42 ± 0.56	0.012	COF1	0.48 ± 0.01	0.012
QCR2	0.20 ± 0.21	0.079	IDHP	0.25 ± 0.23	0.218
IDHP	0.20 ± 0.69	0.075	QCR2	0.24 ± 0.27	0.263
ECHA	0.16 ± 0.49	0.151	KCRM	0.20 ± 0.27	0.298
KCRM	0.15 ± 0.74	0.164	QCR1	0.20 ± 0.28	0.377
CAH3	0.15 ± 0.23	0.092	ECHA	0.19 ± 0.28	0.457
QCR1	0.15 ± 0.26	0.147	CYC	0.18 ± 0.29	0.296
CYC	0.14 ± 0.46	0.153	MDHC	0.18 ± 0.30	0.402
ODPA	0.14 ± 0.48	0.169	ATP5H	0.17 ± 0.30	0.462
ATPO	0.12 ± 0.50	0.174	ATPO	0.17 ± 0.31	0.385
MDHM	0.12 ± 0.38	0.268	MDHM	0.17 ± 0.31	0.368
KAD1	0.10 ± 0.71	0.118	KAD1	0.16 ± 0.31	0.362
ATP5H	0.10 ± 0.31	0.263	ODPB	0.16 ± 0.35	0.815
COX2	0.10 ± 0.49	0.119	CAH3	0.16 ± 0.35	0.271
ODPB	0.09 ± 0.51	0.464	ODPA	0.15 ± 0.35	0.477
AATM	0.09 ± 0.86	0.374	FABPH	0.15 ± 0.37	0.538
EF1A2	0.08 ± 0.24	0.422	COX2	0.14 ± 0.37	0.271
MDHC	0.08 ± 0.45	0.317	AATM	0.12 ± 0.39	0.482
FABPH	0.07 ± 0.53	0.482	CISY	0.12 ± 0.42	0.942
ACON	0.05 ± 0.47	0.637	EF1A2	0.11 ± 0.43	0.826
CISY	0.05 ± 0.19	0.536	ACON	0.09 ± 0.44	0.961
PRDX5	-0.03 ± 0.17	0.728	PGAM2	-0.02 ± 0.45	0.957
G6PI	-0.05 ± 0.18	0.635	GPDA	-0.04 ± 0.59	0.593
PARK7	-0.06 ± 0.26	0.512	VDAC1	-0.04 ± 0.69	0.381
PGK1	-0.06 ± 0.27	0.611	PRDX5	-0.06 ± 0.33	0.542
PGAM2	-0.06 ± 0.11	0.758	PGK1	-0.07 ± 0.43	0.846
PGM1	-0.07 ± 0.31	0.599	PARK7	-0.08 ± 0.43	0.842
VDAC1	-0.07 ± 0.52	0.433	G6PI	-0.09 ± 0.44	0.871
GPDA	-0.08 ± 0.94	0.306	PGM1	-0.10 ± 0.44	0.866
MYG	-0.09 ± 0.96	0.338	KPYM	-0.11 ± 0.45	0.852
KPYM	-0.09 ± 0.45	0.417	AT2A1	-0.12 ± 0.46	0.091
TRY1	-0.10 ± 0.09	0.336	TRY1	-0.13 ± 0.47	0.710
MPCP	-0.11 ± 0.40	0.272	CASQ1	-0.13 ± 0.47	0.192
TPIS	-0.11 ± 2.38	0.364	ENOB	-0.15 ± 0.48	0.773
CASQ1	-0.11 ± 0.46	0.171	HBB2	-0.16 ± 0.49	0.294
ENOB	-0.11 ± 0.43	0.266	MYG	-0.16 ± 0.49	0.716
AATC	-0.13 ± 0.53	0.106	AATC	-0.18 ± 0.50	0.247

HSP7C	-0.14 ± 0.19	0.158	MPCP	-0.18 ± 0.51	0.381
G3P	-0.14 ± 0.68	0.148	ALDOA	-0.18 ± 0.51	0.744
ALDOA	-0.14 ± 0.37	0.293	ATPG	-0.18 ± 0.52	0.443
HBB2	-0.14 ± 0.72	0.184	TPIS	-0.19 ± 0.53	0.852
MYL1	-0.15 ± 0.15	0.195	HSP7C	-0.20 ± 0.56	0.375
ATPG	-0.15 ± 0.08	0.288	PRVA	-0.20 ± 0.58	0.204
ADT1	-0.16 ± 0.78	0.103	HS90B	-0.20 ± 0.60	0.082
PRVA	-0.16 ± 0.42	0.088	ADT1	-0.21 ± 0.61	0.295
HS90B	-0.16 ± 0.27	0.097	HBB1	-0.21 ± 0.62	0.084
PYGB	-0.17 ± 0.15	0.087	G3P	-0.21 ± 0.64	0.113
AT2A1	-0.17 ± 0.28	0.084	MYL1	-0.22 ± 0.79	0.774
PFKAM	-0.17 ± 0.31	0.085	PFKAM	-0.22 ± 0.83	0.217
HBB1	-0.18 ± 0.64	0.096	PYGB	-0.23 ± 0.83	0.143
LDHA	-0.45 ± 0.39	0.014	LDHA	-0.53 ± 0.08	0.014
PYGM	-0.54 ± 0.34	0.011	PYGM	-0.64 ± 0.07	0.013
HBA	-0.56 ± 0.18	0.015	HBA	-0.69 ± 0.05	0.012

Protein I.D. relates to the Uni-Prot database, entries returned using the MASCOT search engine. Relative abundance (ABD) represents Log-transformed MS data normalised by inter-sample abundance ratio using nonconflicting peptides only. Absolute abundance (ABD) represents Log-transformed MS data normalised by inter-sample abundance ratio using nonconflicting peptides and total TA mass. All data is represented as MEAN ± SD for biological replicates (n = 4) and is displayed as the positive (+) or negative (-) fold change from non-stimulated control muscle to 30 days of co-contraction high-frequency stimulated muscle, in rank order of largest positive change to largest negative change. P-Values are generated from paired t-tests between control and 30-d stimulated muscle.

Table S6. Rank order for synthesis rates in soluble proteins after 30-d of stimulation in TA muscle.

Protein I.D.	Relative (Sim)	Relative (Ctrl)	P-Value	Protein I.D.	Absolute (Stim)	Absolute (Ctrl)	P-Value
CAH3	17.64 ± 0.25	11.12 ± 0.16	0.003	CAH3	98.55 ± 0.40	73.19 ± 0.36	0.001
EF1A2	8.20 ± 0.41	2.52 ± 0.39	0.001	COF1	92.27 ± 0.44	67.86 ± 0.48	0.014
ATPO	13.67 ± 0.63	8.12 ± 0.31	0.003	ODPA	56.26 ± 0.39	31.92 ± 0.71	0.013
KCRM	10.42 ± 0.43	6.26 ± 0.36	0.012	ECHA	81.34 ± 0.48	57.33 ± 0.58	0.018
ATPB	11.58 ± 0.65	7.46 ± 0.13	0.002	QCR1	69.01 ± 0.63	46.23 ± 0.24	0.025
IDHP	12.57 ± 0.40	8.57 ± 2.10	0.019	ATPG	68.41 ± 0.58	45.74 ± 0.72	0.018
QCR2	5.41 ± 0.29	1.63 ± 0.70	0.001	EF1A2	84.47 ± 0.51	63.12 ± 0.52	0.028
FABPH	6.51 ± 0.45	2.76 ± 0.60	0.003	ATPB	107.39 ± 0.32	86.92 ± 0.76	0.024
QCR1	4.46 ± 0.33	1.22 ± 0.21	0.012	ATPA	58.44 ± 0.24	38.13 ± 0.26	0.019
CYC	4.49 ± 0.36	1.36 ± 0.18	0.002	MDHM	71.73 ± 0.26	53.33 ± 0.29	0.027
ATPG	5.35 ± 0.61	2.23 ± 0.95	0.022	CISY	55.27 ± 0.46	38.26 ± 0.48	0.022
CISY	4.34 ± 0.37	1.43 ± 0.14	0.001	IDHP	68.24 ± 0.27	51.24 ± 0.51	0.011
ATPA	4.76 ± 0.15	1.92 ± 0.53	0.003	AATC	81.37 ± 0.32	65.93 ± 0.53	0.024
KAD1	3.72 ± 0.98	1.13 ± 0.05	0.018	QCR2	59.44 ± 0.28	44.28 ± 0.40	0.018
ECHA	4.15 ± 0.47	1.57 ± 0.41	0.011	ATPO	63.34 ± 0.28	48.24 ± 0.73	0.026
MDHM	8.71 ± 0.18	6.32 ± 0.44	0.011	COX2	49.04 ± 0.51	34.02 ± 0.34	0.024
ODPA	11.71 ± 0.61	9.39 ± 0.59	0.018	ACON	57.62 ± 0.49	42.63 ± 0.51	0.013
AATM	2.62 ± 0.38	1.01 ± 0.43	0.026	KCRM	140.53 ± 0.24	125.84 ± 0.53	0.016
COF1	1.81 ± 0.58	0.35 ± 0.62	0.002	KAD1	70.27 ± 0.65	55.63 ± 0.89	0.021
ODPB	2.09 ± 0.36	0.66 ± 0.91	0.001	ODPB	43.48 ± 0.81	30.72 ± 0.26	0.016
ALBU	14.57 ± 0.11	13.72 ± 0.29	0.189	CYC	71.27 ± 0.34	58.94 ± 0.47	0.031
ATP5H	1.17 ± 0.60	0.52 ± 0.33	0.072	FABPH	28.62 ± 0.19	18.94 ± 0.56	0.025
COX2	1.71 ± 0.43	1.19 ± 0.37	0.013	AATM	16.91 ± 0.14	9.62 ± 0.49	0.014
MYL1	1.96 ± 0.74	1.49 ± 0.15	0.166	ALBU	139.79 ± 0.34	136.24 ± 0.21	0.831
GPDA	2.27 ± 0.83	1.86 ± 0.23	0.081	PRDX5	30.22 ± 0.42	28.47 ± 0.33	0.866

MDHC	5.61 ± 0.13	5.22 ± 0.17	0.726	MDHC	25.66 ± 0.26	24.13 ± 0.24	0.261
AATC	2.19 ± 0.42	1.82 ± 0.13	0.097	MYL1	14.37 ± 0.85	12.94 ± 0.65	0.085
AT2A1	1.29 ± 0.24	0.98 ± 0.24	0.082	HSP7C	22.36 ± 0.42	21.53 ± 0.30	0.227
MYG	1.67 ± 0.26	1.46 ± 0.35	0.266	PARK7	8.01 ± 0.48	8.44 ± 0.47	0.811
HBB2	4.42 ± 0.27	4.27 ± 0.08	0.971	TRY1	9.97 ± 0.47	11.17 ± 0.29	0.634
PRVA	7.03 ± 2.25	6.89 ± 0.47	0.862	ATP5H	42.96 ± 0.61	44.19 ± 0.50	0.558
PRDX5	2.50 ± 0.22	2.36 ± 0.21	0.931	HS90B	9.83 ± 0.20	11.13 ± 0.92	0.736
HSP7C	1.58 ± 0.19	1.49 ± 0.74	0.885	GPDA	14.27 ± 0.27	15.74 ± 0.94	0.855
ADT1	2.05 ± 0.51	1.96 ± 0.40	0.883	VDAC1	13.27 ± 0.33	14.74 ± 0.44	0.373
HBB1	4.77 ± 0.33	4.68 ± 0.35	0.973	CASQ1	16.27 ± 0.55	17.82 ± 0.08	0.437
MPCP	1.41 ± 0.55	1.43 ± 0.73	0.844	HBB2	27.77 ± 0.36	29.47 ± 0.38	0.853
VDAC1	2.30 ± 0.33	2.35 ± 0.31	0.936	PRVA	35.27 ± 0.28	37.27 ± 2.36	0.914
PARK7	1.09 ± 0.36	1.14 ± 0.35	0.947	HBB1	32.74 ± 0.46	34.94 ± 0.44	0.852
HS90B	11.48 ± 0.81	11.54 ± 0.52	0.874	ADT1	19.27 ± 0.86	21.83 ± 0.41	0.092
TRY1	0.32 ± 0.18	0.66 ± 1.05	0.082	HBA	46.24 ± 0.21	48.84 ± 0.51	0.682
HBA	5.95 ± 0.40	6.36 ± 0.29	0.715	MYG	70.45 ± 0.67	73.24 ± 0.17	0.912
CASQ1	11.73 ± 0.17	12.25 ± 0.64	0.973	MPCP	30.24 ± 0.25	33.73 ± 0.66	0.725
G3P	1.31 ± 0.23	2.06 ± 0.76	0.031	AT2A1	15.24 ± 0.16	19.53 ± 0.35	0.426
KPYM	0.86 ± 0.16	1.63 ± 0.09	0.017	PFKAM	2.71 ± 0.55	9.63 ± 0.70	0.011
G6PI	1.03 ± 0.65	2.04 ± 0.98	0.019	G3P	16.21 ± 0.96	25.27 ± 0.13	0.013
TPIS	1.44 ± 0.14	3.15 ± 0.25	0.007	KPYM	40.38 ± 0.49	50.42 ± 0.07	0.025
PGAM2	2.36 ± 0.18	4.22 ± 0.10	0.027	G6PI	18.37 ± 0.63	31.83 ± 0.76	0.019
PGM1	2.25 ± 0.29	4.26 ± 0.03	0.023	PGM1	32.55 ± 0.44	48.27 ± 0.40	0.027
ACON	2.23 ± 0.41	4.40 ± 0.22	0.019	TPIS	56.45 ± 0.54	72.36 ± 0.25	0.026
PGK1	1.59 ± 0.35	3.87 ± 0.16	0.014	PYGB	49.23 ± 0.88	66.24 ± 0.13	0.028
ALDOA	2.21 ± 0.51	5.15 ± 0.42	0.019	PGK1	91.27 ± 2.00	112.33 ± 0.26	0.019
PFKAM	2.02 ± 0.59	5.54 ± 0.95	0.016	PGAM2	79.05 ± 0.51	101.44 ± 0.29	0.011
PYGB	2.43 ± 0.22	6.41 ± 0.15	0.002	ALDOA	70.84 ± 0.53	93.28 ± 0.62	0.019

ENOB	6.51 ± 0.26	11.30 ± 0.37	0.001	ENOB	64.33 ± 0.46	87.37 ± 0.37	0.019
PYGM	1.41 ± 0.26	7.87 ± 0.53	0.001	LDHA	75.23 ± 0.53	106.24 ± 0.32	0.019
LDHA	4.63 ± 0.41	15.17 ± 0.17	0.001	PYGM	100.33 ± 0.44	142.73 ± 0.17	0.001

Protein I.D. relates to the Uni-Prot database, entries returned using the MASCOT search engine. Synthesis rates are presented in relative format which relates to fractional synthesis rate in percent per day and in absolute terms which is reflective of whole TA synthesis with rates expressed in picograms per day. All data is represented as MEAN ± SD for biological replicates (n = 4) in the 30 days stimulated muscle (Stim) and the non-stimulated control muscle (Ctrl). The proteins are ranked in order of largest increase in synthesis rate from Ctrl to Stim through to largest decrease in synthesis rate from Ctrl to Stim. P-Values are generated from paired t-tests between control and 30-d stimulated muscle.

Chapter 5. General discussion

5.1 Abstract

Skeletal muscle is a diverse tissue that has a remarkable ability to adapt to physiological, biochemical and metabolic stresses. Exercise training elicits changes in muscle phenotype through alterations in the abundance of individual proteins. However, there is a paucity of data reporting how changes in protein abundance are coordinated through relative contributions of synthesis and degradation. Preservation or increases in skeletal muscle mass through exercise training can ameliorate metabolic dysfunction and contribute to the prevention of chronic diseases. These benefits are facilitated, at least in part, by extensive metabolic and contractile remodelling of skeletal muscle in response to exercise. Endurance and resistance exercise training represent two extremes on the continuum and elicit markedly different training responses that are each underpinned by complex changes to the muscle proteome. We, for the first time in rat muscle, report individual protein responses in response to both endurance and resistance exercise training. Using novel techniques, we present evidence of two contrasting sequences of adaptation, including 8 different protein-specific patterns of protein turnover in the myofibrillar fraction, 4 which were unique to the endurance stimulus and 2 that were unique to resistance exercise. Similarly, we report 9 different patterns in protein turnover from proteins of the soluble fraction, with 2 unique to endurance stimulation and 1 unique to resistance exercise training. Consequently, our work provides new evidence documenting the mechanisms underpinning muscle adaptation. These data are evidence of highly individualised responses on a protein-by-protein basis to coordinate muscle adaptation, including selective degradation of individual proteins at varying rates to decrease and/or to maintain the relative abundance of proteins in muscle.

5.2 General commentary

Skeletal muscle is a heterogeneous tissue composed of functionally diverse fibre types (Staron, 1997). The heterogeneous nature of muscle is what permits its broad application to fulfil a variety of functional demands. It is also well established that skeletal muscle demonstrates a high degree of plasticity in regard to its physiological, biochemical and metabolic characteristics in order to meet the functional demands placed upon it (Pette and Staron, 2001). Such changes ultimately result in exchanges of muscle phenotype involving the gradual alteration of protein content and enzyme activity, manifested through overt changes to individual protein abundance. For resistance exercise training, these alterations usually contribute to significant increases in muscle hypertrophy (Kraemer et al, 2004). Conversely, in endurance exercise the metabolic status of the cell is significantly modified, often with no notable increases in cross-sectional area of the muscle fibre. However, currently there are little data on the exact processes that coordinate changes in protein abundance i.e. it is not clear to what extent synthesis and degradation contribute to individual protein turnover, during muscle adaptation. More detailed understanding of the mechanisms of muscle adaptation may help to support public health recommendations and data showing that regular exercise participation can be effectively used in the prevention, management, and the treatment of chronic conditions, including hypertension, heart disease, obesity, type 2 diabetes, and age-related muscle wasting (Haskell et al, 2007; Colberg et al, 2010). Understanding how exercise causes muscles to adapt is fundamental to improving our knowledge towards improving health, quality of life and longevity. Exercise capacity is strongly and inversely related with all-cause mortality and offsetting the age-associated loss of muscle mass is a key component of this protective effect. In adults, muscle is the most abundant tissue in the body, it is the largest reservoir of amino acids that can be used to support metabolism and repair other tissues, and in healthy individuals it is the primary site of postprandial glucose disposal (Theibaud et al, 1982). Clearly there is an intimate and reciprocal relationship between exercise and muscle; without muscle we could not exercise and without exercise our muscles deteriorate and become dysfunctional. Despite the clear importance of skeletal muscle and the key role of both resistance and endurance exercise to human health we know surprisingly little about the molecular events that link muscle contraction to muscle adaptation. Now, with the arrival of exercise

proteomics as a rapidly emerging field, there is scope to enhance this understanding of how skeletal muscle adaptation occurs in response to exercise. Since proteins are the functional components of the cell, a comprehensive analysis of the protein complement of muscle can give an unprecedented and detailed insight to changes in muscle phenotype. The focus of this thesis has been to extend traditional proteomic analysis in to include the dynamic aspects of protein turnover to muscle adaptation. Mixed muscle protein turnover is widely acknowledged to increase in response to resistance exercise (Chesley et al 1992; Biolo et al, 1995), with mixed protein fractional synthetic rates (FSR) maintaining elevation above mixed protein fractional degradation (FDR) 48 h post resistance exercise, to increase the net protein content of the muscle (Phillips et al, 1997). However, Burniston et al, (2014) reported a wide distribution of metabolic enzymes in muscle fibres that seemingly have the same fibre type and reports protein abundances span more than four orders of magnitude. This, in itself suggests that reliance on averaged mixed protein data is insufficient to pick apart complex proteomic changes. With regard endurance exercise, Burniston, (2008) documented 15 significant changes in the abundance of individual proteins in response to endurance training using intensity-controlled treadmill running. However, despite such work quantifying changes in the muscle proteome in response to endurance exercise, this leaves us with no information on whether these protein changes are a result of increases in synthesis rate, a decrease in degradation rate or a combination of the two. Taken together, this largely stations the evidence from whole mixed-muscle protein turnover in a redundant position to inform us how the mechanism of muscle adaptation is coordinated. It also suggests that general proteomics data is inadequate to provide information on the dynamic changes involved in muscle adaptation, exposing the requirement for protein turnover to be measured on the individual level during muscular perturbation events.

We have successfully refined a unique method, coined dynamic proteome profiling (DPP; Chapter 2) to allow the dynamic muscle proteome to be captured during programmed exercise. We have employed DPP and combined it with two robust models of exercise adaptation *in vivo* that simulate endurance activity (chronic low-frequency stimulation, CLFS; Chapter 3) and resistance exercise training (co-contraction high-frequency stimulation, CHFS; Chapter 4) in order to study the complex mechanisms underpinning muscle adaptation. This work has quantified two very different responses of the muscle proteome in two contrasting modes of

programmed exercise in the rat. Demonstrating that the mechanism for skeletal muscle adaptation is organised through two distinct ways that seems dependent on the given exercise stimulus. Using animal models to investigate these processes holds several advantages over studies in human participants. Firstly, models such as CLFS have a long history of robust and effective change to induce the desired outcome (Salmons and Vrbova, 1969.; Pette et al, 1973). Furthermore, models like this can administer a much larger degree of change to the muscle that controlled human exercise studies could ever achieve, allowing us to study the full extent of muscle adaptation. This is primarily achieved through the specific regulation of the stimulation parameters that can be more readily controlled in animal models than in humans. Moreover, environmental conditions and nutritional intake can be accurately standardised in laboratory animals, while activity level is manipulated and/or monitored. Furthermore, animals used in laboratory studies have a much more homogenous gene pool than human subjects, and the studies can be completely randomised whereas this is difficult to do in humans. These factors increase the sensitivity and reproducibility of the experimental outcomes. Another invaluable benefit of animal models is the accessibility of analytical sample. For instance, the amount of muscle tissue that can be harvested compared to human biopsies. At the end of an exercise training period, whole muscles can be dissected and studied extensively in animal models. In contrast, biopsies in humans are often limited to the most accessible muscles such as the vastus lateralis (Bergstrom, 1975) and the tissue sample may not fully represent the changes that occur during an intervention. This is because fibre type characteristics and protein abundances may differ from one biopsy to the next, even within the same muscle of one individual (Elder et al, 1982). Thus, even four or five biopsies may not fully represent the adaptations that occur throughout the entire muscle.

A unique strength of our analysis is that whole muscle measurements were used to enable us to report absolute data that reflects the level of whole muscle adaptation. Almost without exception, previous work using biosynthetic labelling techniques in either animals or humans only report relative data (Wagenmakers, 1999) i.e. fractional synthesis rate (FSR). Whilst FSR is used extensively in the literature, it is a relative measurement and does not give insight to whether absolute changes, i.e. we do not know if the whole from which the fraction is reported has changed. For example, we report FSR is consistent between control and stimulated muscle during chronic low-

frequency stimulation (10.40 %/d in Ctrl and 9.86 %/d in Stim). However, when we compare absolute synthesis values, we can establish that the muscle is actually making less protein and synthesis rates have decreased (Figure 3.5). For purposes of comparison we have reported FSR throughout this thesis but all data were conducted on absolute values to provide context of how changes to protein turnover affect whole muscle adaptation.

Our two exercise stimulation models produced varying results. Initially, at the whole muscle level, CLFS induced a typical (Jarvis et al, 1996) 50 % reduction in wet muscle mass, whereas CHFS produced 20 % increase in wet muscle mass, consistent with previous work (Schmoll et al, 2018). Both absolute and relative protein synthesis rates were affected accordingly in each of the models. CLFS maintained the rate of relative protein synthesis in Stim (9.86 %/d) compared to the Ctrl (10.4 %/d) over the 30 days of CLFS suggesting that the smaller muscle (Stim) is still making a similar amount of protein as the larger Ctrl muscle. Whereas during CHFS the rate of relative protein synthesis increased in Stim (6.71 %/d) from the Ctrl (4.61 %/d), suggesting the larger muscle (Stim) is making a greater amount of protein than the smaller Ctrl. However, the interpretation is different when the absolute rate of synthesis is calculated for whole muscle in each experimental model. Absolute protein synthesis decreased by ~50 % over the 30 days of CLFS and increased by ~20 % during the 30 days of CHFS. Not only can this account for changes in muscle mass, but means that as the muscle size changes, at the whole muscle level, the absolute rate of newly synthesised protein responds in-line with muscle mass. Therefore, we can be confident that any changes in the abundance of an individual protein not accompanied by a change in synthesis can be attributed to protein degradation.

Top-down proteomic analysis was able to resolve a similar amount of myofibrillar proteins between experiments, resulting in 30 common 2D-gel spots across sampling points for the CLFS intervention and 35 protein spots for the CHFS experiment. This corresponded to 23 non-redundant protein identifications with 10 spots resolved as separate proteoforms in the CLFS investigation. Similarly, 10 individual proteoforms were resolved from 18 protein identifications in the CHFS experiment. The interesting findings from this analysis revealed that resistance exercise training largely effects the whole protein and not the proteoforms, which is in contrast to endurance type exercise. Generally, we see a substitution of specific proteoforms more specialised to slow-twitch muscle in response to our endurance stimulus. This is consistent with

transformation from a fast-to-slow muscle phenotype. Whereas, in response to resistance exercise training the main response is protein accretion resulting in the maintenance of the muscle phenotype. It can be reasoned that there is no need to change the muscle phenotype in response to such a stimulus, as the muscle is already highly specialised to deal with high intensity contraction. Hence, the blanket response of the proteoforms and no evidence of proteoform-specific changes. Furthermore, the response of the muscle to CLFS (Figure 3.4) was more immediate than in CHFS (4.5). This provides evidence for the argument made of proteoform-specific changes may be the early indicators of phenotypic change. Moreover, this makes sense from a physiological position as the abundance of a whole protein takes longer to change than the abundance of a proteoform that could be a result of a post-translational modification. Granata et al, (2017) documents phosphorylation, the most commonly known post-translational modification, to occur immediately after aerobic exercise training in proteins associated with adaptation. Hojlund et al, (2009) were the first to map large scale phosphoproteomics in human muscle and found 306 distinct phosphorylation sites in 127 proteins with 26 % of phosphoproteins belonging to the sarcomere. Despite this large catalogue of information on specific sites of phosphorylation the functional importance, specific kinases and phosphatases involved have yet to be determined for the majority of this work. The site-specific phosphorylation we have discovered through work in this thesis (Figure 3.10), has led to the proteoform-specific degradation of myosin light chain (Figure 3.9). Future work could further support this by providing more quantitative evidence for peptide-specific degradation. This could be achieved by a work flow similar to Xu et al, (2010), in order to identify specific sites of ubiquitination on myosin light chain peptides following endurance type exercise. Xu et al, (2010) generated a monoclonal antibody that can enrich for peptides containing lysine residues modified by di-glycine, an adduct left at sites of ubiquitination after trypsin digestion. This would be an obvious line of follow-up investigation given that there is a lysine residue close by (Lysine 31) to our site-specific phosphorylation at Serine 20.

Upon interrogation of our findings, we can also report interesting differences in the regulation of abundance changes (or lack of in CHFS) between the two experiments. Protein turnover is the fundamental mechanism that both maintains proteome quality and enables muscle adaptation/ changes in protein abundance to occur. We document the regulation of changes in protein abundance to be induced by different

patterns of turnover seemingly bespoke to each mode of programmed exercise. Firstly, protein synthesis of proteins in the soluble fraction appears to elicit very similar responses between CLFS and CHFS. We report increases in synthesis from Ctrl to Stim for 20 proteins in CLFS and 36 proteins in CHFS. For endurance type exercise, this seems generally related to the phenotypic change of the muscle, increases in the synthesis of mitochondrial (Figure 3.14) proteins and decreases in the glycolytic proteins (Figure 3.15). However, when we analyse changes in the abundance of these proteins, there are clear contrasting differences. Consistent with changes in synthesis soluble proteins in the CLFS experiment display both positive and negative net changes in abundance (Figure 3.12) which are consistent with the phenotypic changes described earlier. The unique finding amongst these proteins is that the relative contributions of synthesis and degradation is highly individualised and it appears there is no uniform way to predict this (Fig. 3.14 and 3.15). Conversely, in the resistance exercise training experiment we see almost no changes in abundance (Figure 4.11). The reason for this response is there is an increase in protein turnover and therefore the quality control of the proteins. It is important to appreciate that the abundance of a protein can also be modulated by changes to its rate of degradation as well as synthesis. This provides important information evidencing that both measures are required to provide the correct context for muscle adaptation. It is possible and highly likely that these changes to the rate of protein turnover may influence muscle function even in the absence of changes protein abundance. Indeed, there is a growing awareness of the importance of 'quality control' particularly regarding the biology of ageing and as a mechanism of disease (Lopez-Otin et al, 2013), and this is driving the development for methods such as Dynamic Proteome Profiling to investigate protein homeostasis (i.e. proteostasis) and dynamics.

The reasons underpinning such changes at the gross fractional level could be due to a number of factors from the myofibrillar proteoforms exhibiting a split response in protein abundance in-line with phenotypic change in response to CLFS and the huge ranges of individual protein synthesis rates in the soluble fraction after CHFS (2.7 – 140.5 pg/d) correlating to increased protein turnover. As a consequence, average synthesis reported across each fraction is a poor indicator of muscle adaptation due to the range of synthesis rates and abundance changes within each fraction. Of which, subsequently appears to be unique for each stimulation intervention. Furthermore, we can show the need for individual protein data, as when reported at the fractional level

the data does not further translate to individual regulation of protein turnover. For example, in the myofibrillar fraction alone there are 8 patterns of protein turnover across experiments with 4 patterns of change bespoke to CLFS and 2 patterns of change only reported in the CHFS study (Figure 5.1). Similarly, in the soluble fraction there are a total of 9 patterns of individual protein turnover with 2 only reported in CLFS and 1 unique to the CHFS intervention (Figure 5.1). Furthermore, this is independently unique for each experimental intervention. For example, in the CLFS investigation proteins that exhibit an increase in protein abundance do so completely independently of gene ontology, protein function or structure. The mitochondrial proteins ACON, IDHP and ATPB all increase in abundance but through the independent responses of partially being accounted for by a greater synthesis rate (ACON), without a detectable change in synthesis rate (IDHP) or being entirely accounted for by an increase in the rate of synthesis in Stim compared to Ctrl muscle (ATPB). Whereas in the CHFS experiment, proteins that increased in abundance such as ABLU and ATPB did so through no detection in synthesis rate (ALBU) or through only increasing the rate of synthesis (ATPB), whilst there were marked increases in protein turnover for other proteins such as CISY and KCRM. Figure 5.1 provides a fully comprehensive overview that compares all of the proteins between experiments, detailing individual protein turnover in response to two different types of muscle adaptation.

A	Synthesis	Increase	KCRS (19), TNNT1 (24), CAH3 (29) MYG, MDHC	ATPB (4), TNNT1 (27), CAH3 (30) APTA, CAH3, HBA, ACADL, ATPB, CASQ1, AATC, HBB1, AATM	ODPA, ACON, ATPO, HSPB6
		No change	MYL1 (8), MLRS (11), G3P (21), G3P (22), TNNT3 (25) LDHA, ALDOA, PRVA, KAD1, MYL1, PGAM2, PGK1, PYGM	PLEC (2), DESM (3), ACTS (5), TPM4 (6), TPM2 (7), MYL1 (9), MYL1 (10), MLRS (12), ENOB (13), ATPA (15), KCRM (16), KCRM (17), KCRS (18), ANXA4 (20), ACTA, PGM1, IDH3A, HBB2, TRY1, SAFB1, VDAC, HINT1, ALDR, KCRM, KYPM, FHL1, PARK7	ACTN1 (1) MDHM, IDHP, CX7A2, AT2A2, ALBU
		Decrease	ENOB (14), TNNT3 (26), TNNT3 (28) G3P, PFKAM, ENOB, TPIS	TNNI2 (23) KCRB, PYGB	
		Increase	No change	Decrease	
Degradation					
B	Synthesis	Increase	PLEC (1), KCRM (15), KCRM (16), KCRM (17) CAH3, ODPB, ECHA, QCR1, ATPG, EFIA2, MDHM, CISO, IDHP, AATC, QCR2, ATPO, COX2, ACON, KCRM, KAD1, ODPB, CYC, FABPH, AATM	ATPB (6), DESM (7), ATPA (13), ACTS (14), TPM1 (21), TPM2 (22), TNNT3 (23), TNNT3 (24), TNNT3 (25), TNNI2 (26), TNNI2 (27), TNNT3 (28), MYL1/3 (31), MYL1/3 (32), CAH3 (33), MLRS (34), MLRS (35) COF1, ATPA, ATPB	
		No change	HBA	PYGM (3), PFKAM (4), PFKAM (5), ENOA (9), ENOB (10), ENOB (11), ENOB (12), KCRS (18), KCRS (19), KCRS (20), MYL1/3 (29), MLY1/3 (30) PRDX5, MDHC, MYL1, HSP7C, PARK7, TRY1, ATP5H, HS90B, GPDA, VDAC1, CASQ1, HBB2, PRVA, HBB1, ADT1, MYG, MPCP, AT2A1	ALBU
		Decrease		PYGM (2), ENOA (8) LDHA, PYGM	PFKAM, G3P, KPVM, G6PI, PGM1, TPIS, PYGB, PGK1, PGAM2, ALDOA, ENOB
		Increase	No change	Decrease	
Degradation					

Figure 5.1. Dynamic proteome profiling responses to endurance type exercise and resistance exercise training.

The individual protein turnover responses are described within a matrix for the sum total of proteins reported in the EDL from both the chronic low-frequency stimulation experiment (panel A) and in the TA muscle in the co-contraction high-frequency stimulation experiment (panel B). The matrix reports proteins that either increase, do

not change or decrease for synthesis and degradation rates determined by paired t-tests between the non-stimulated control muscle and the stimulated muscle. Proteins are represented by their Uni-Prot protein I.D. name from the Uni-Prot database, entries returned using the MASCOT search engine. Green text identifies proteins from the myofibrillar fraction (panel A, bracketed number relates to Figure 3.2; panel B, bracketed number relates to Figure 4.3). Blue text identifies proteins from the soluble fraction.

Dynamic Proteome Profiling (DPP) is unique in its ability to provide insight to the individual components of protein turnover (i.e. synthesis, abundance and degradation) on a protein-by-protein basis in skeletal muscle. The present analysis is reproducible but the technique is new so there is undoubtedly scope for further optimisation. The use of heavy water deuterium ($^2\text{H}_2\text{O}$) for biosynthetic labelling is less invasive than infusion of isotope-labelled amino acids and studies can be conducted in free living subjects. Nevertheless, DPP is best suited to studying long term integrated protein dynamics over periods of days or weeks, but it is not optimal for studying the acute short term (e.g. < 1 d) responses due to complex curve fitting and the equilibration of ^2H in body water. Proteomic methods afford the identification of hundreds and sometimes thousands of proteins in any one experiment. However, in any proteomic experiment the number of proteins that can be identified will be largely greater than the number that can be quantified because of issues regarding missing data. That is, to identify a protein it need only be detected in one sample amongst many, but to quantify a protein, peptides that are unique to that protein must be clearly resolved in each biological replicate. Often this issue is partially circumvented by accepting a less than full number of biological replicates for statistical testing of proteomics data, but this is not best practice. Dynamic Proteome Profiling adds a further layer of complexity and requires high quality mass isotopomer distribution profiles to be captured for each peptide during their entire chromatographic profile. Therefore, some peptides may be excluded because co-eluting peptides with similar or overlapping mass isotopomer envelopes contaminate each other and so the number of proteins submitted to statistical analyses is further reduced. Because of the above-mentioned quality control processes, the analysis of some proteins is based on data from single peptides, whereas other proteins may have numerous protein-specific peptides that are well resolved and submitted to statistical analysis. Profiling of the same peptide across

different experimental groups is robust but it is not yet certain how representative one peptide is of the abundance or synthesis rate of the entire protein. Closer inspection of proteins with numerous quantifiable protein-specific peptides sometimes reveals that peptides from the same protein exhibit broadly different rates of synthesis. Given the stringent filtering of data and high level of reproducibility of peptide mass isotopomer analysis, it is unlikely broad differences in peptide synthesis rates occur and it is entirely possible these differences are attributable to technical errors. Furthermore, we have calculated degradation to be the difference between the two processes we measure; synthesis and degradation. Whilst this is likely to be an accurate estimation we cannot ignore the fact DPP fails to directly measure protein degradation. Finally, the time series analyses that is necessary for DPP are well suited to detailed studies such as muscle adaptation. However, the timing of sample collection dictates the sensitivity of the synthesis measurements. Furthermore, to apply this design in human populations that encompass clinical settings may not be appropriate where this technique requires the collection of numerous muscle samples during a short experimental period and may be less well tolerated.

Despite these potential technical limitations, our data reports a mechanistic insight into the regulation of protein abundance within the muscle cell and protein metabolism. Moreover, these data add to the now growing list of evidence indicating whole mixed-muscle protein synthesis give a less than adequate picture of muscle adaptation. We have provided new evidence for selective degradation of individual proteins at varying rates to decrease and/or to maintain the same relative abundance of protein in the muscle and have refined a unique methodology to achieve this. Our work is the first of its kind in rat muscle to document the response of protein-specific turnover during muscle adaptation, providing original evidence to show how protein turnover is increased and decreased by increasing and/or decreasing the relative contributions of synthesis and degradation to coordinate the adaptive response in muscle.

To build on this work, we conclude that our DPP technique is suitable to use in other models that administer significant change to the muscle. For example, future work could continue in this vein to analyse individual protein turnover and utilise further animal models, such as the model of muscle wasting/dis-use, involving silencing of the common peroneal nerve using tetrodotoxin (Dupont Salter et al, 2003). Furthermore, we have provided novel evidence to suggest proteoform-specific degradation may act as an early indicator for phenotypic change. With the current

interest in the field of phosphoproteomics this could build on emerging knowledge (Potts et al, 2017) to answer questions on what modifications may contribute to the adaptive processes over more chronic periods in skeletal muscle. Phosphorylation causes changes in protein conformation that alter functional characteristics (e.g. enzymatic activity, protein-protein interactions and subcellular localisation) of the protein and also change its peptide MS/MS spectra, which can be used to map modifications to specific residues (Roux et al, 2013). Potts et al, (2017) reports almost 6,000 phosphorylation sites on more than 4,800 proteins including low abundance proteins involved in signal transduction. One hour after a bout of maximal intensity contractions there were more than 600 differences in phosphorylation status spread across more than 300 proteins. Less than half of the exercise responsive phosphorylation sites have been previously detected and in most cases the kinases responsible for phosphorylation of these sites have not been defined. Therefore, this work represents a substantial addition to the body of information on muscle responses to resistance exercise. Deciphering which of these signals link contraction to adaptation will be the next challenge and this may not be a straight forward process. For instance, exercise is associated with widespread perturbations to homeostasis, therefore molecular events detected in exercised muscle could be associated with restoration of cellular homeostasis rather than, or as well as, being the signalling events that instigate adaptation. Moreover, such comprehensive information on phosphopeptides is not equivalent to knowing the protein species which are the entities that are actually responsible for biological processes. Indeed, it is uncommon for a protein to be modified at just one site or by just one type of modification (Roux et al, 2013). So, future work will have the demanding task of stitching all the available information together in order to uncover the true nature of the protein species that dictate muscle adaptation.

5.3 Bibliography

References

Bergstrom, J. (1975). Percutaneous needle biopsy of skeletal muscle in physiological and clinical research. *Scand J Clin Lab Invest*, **35**, 609-616.

Biolo, G.; Maggi, S. P.; Williams, B. D.; Tipton, K. D.; Wolfe, R. R. (1995). Increased rates of muscle protein turnover and amino acid transport after resistance exercise in humans. *Am. J. Physiol*, **268**, 514–520.

Burniston, J.G. (2008). Changes in the rat skeletal muscle proteome induced by moderate-intensity endurance exercise. *Biochem. Biophys. Acta*, **178**, 1077-1086.

Burniston, J.G.; Connolly, J.; Kainulainen, H.; Britton, S.L.; Koch, L.G. (2014). Label-free profiling of skeletal muscle using high-definition mass spectrometry. *Proteomics*, **14**, 2339-2344.

Chesley, A.; macDougall, J.D.; Tarnopolsky, M.A.; Atkinson, S.A.; Smith, K. (1992). Changes in human muscle protein synthesis after resistance exercise. *J. Appl. Physiol*, **73**, 1383–1388.

Colberg, S.R.; Sigal, R.J.; Fernhall, B.; Regensteiner, J.G.; Blissmer, B.J.; Rubin, R.R.; Chasan-Taber, L.; Albright, A.L.; Braun, B. (2010). American College of Sports Medicine; American Diabetes Association, Exercise and type 2 diabetes: the American College of Sports Medicine and the American Diabetes Association: joint position statement. *Diabetes Care*, **33**, 147–167.

Dupont Salter, AC.; Richmond FJ.; Loeb, GE. (2003). Effects of muscle immobilization at different lengths on tetrodotoxin-induced disuse atrophy. *IEEE Trans Neural Syst Rehabil Eng*, **3**, 209-217.

Elder, G.C.; Bradbury, K.; Roberts, R. (1982). Variability of fiber type distributions within human muscles. *J. Appl. Physiol*, **53**, 1473-1480.

Granata, C.; Oliveria, RS.; Little, JP.; Renner, K.; Bishop, DJ. (2017). Sprint-interval but not continuous exercise increases PGC-1 α protein content and p53 phosphorylation in nuclear fractions of human skeletal muscle. *Sci Rep*, **10**, 442-447.

Haskell, W.L.; Lee, I.M.; Pate, R.R.; Powell, K.E.; Blair, S.N.; Franklin, B.A.; Macera, C.A.; Heath, G.W.; Thompson, P.D.; Bauman, A. (2007). Physical activity and public health: updated recommendation for adults from the American College of Sports Medicine and the American Heart Association. *Med. Sci. Sports Exerc*, **39**, 1423–1434.

Hojlund, K.; Bowen, BP.; Hwang, H.; Flynn, CR.; Madireddy, L.; Geetha, T.; Langlais, P.; Meyer, C.; Mandarino, L.J.; Yi, Z. (2009). In vivo phosphoproteome of human skeletal muscle revealed by phosphopeptide enrichment and HPLC-ESI-MS/MS. *J Proteome Res*, **11**, 4954-65.

- Jarvis, J.; Mokrusch, T.; Kwende, M.; Sutherland, H.; Salmons, S. (1996). Fast-to-slow transformation in stimulated rat muscle. *Muscle and Nerve*, **19**, 1469-1475.
- Kraemer, W.T.; Ratamess, N.A. (2004). Fundamentals of resistance training: progression and exercise prescription. *Med Sci Sports Exerc*, **36**, 674-688.
- Lopez-Otin, C.; Blasco, M.; Partridge, L.; Serrano, M.; Kroemer, G. (2013). The hallmarks of aging. *Cell*, **6**, 1194-1217.
- Pette, D.; Smith, M.E.; Staudte, H.W.; Vrbova, G. (1973). Effects of long-term electrical stimulation on some contractile and metabolic characteristics of fast rabbit muscles. *Pflugers Arch*, **338**, 257-272.
- Pette, D.; Staron, RS. (2001). Transitions of muscle fiber phenotypic profiles. *Histochem Cell Biol*, **5**, 359-372.
- Phillips, S.M.; Tipton, K. D.; Aarsland, A.; Wolf, S. E.; Wolfe, R. R. (1997). Mixed muscle protein synthesis and breakdown after resistance exercise in humans. *Am. J. Physiol*, **273**, 99–107.
- Potts, G.; McNally, R.; Blanco, R.; You, J.; Herbert, A.; Westphall, M.; Coon, J.; Hornberger, T. (2017). A map of the phosphoproteomic alterations that occur after a bout of maximal-intensity contractions. *Journal of Physiology*, **15**, 5209-5226.
- Roux, PP.; Thibault, P. (2013). The coming of age of phosphoproteomics-from large data sets to inference of protein functions. *Mol Cell Proteomics*, **12**, 3453-64.
- Salmons, S.; Vrbova, G. (1969). The influence of activity on some contractile characteristics of mammalian fast and slow muscles. *J Physiol*, **201**, 535-549.
- Schmoll, M.; Unger, E.; Sutherland, H.; Haller, M.; Bijak, M.; Lanmuller, H.; Jarvis, J.C. (2018). SpillOver stimulation: A novel hypertrophy model using co-contraction of the plantar-flexors to load the tibial anterior muscle in rats. *PLoS ONE*, **13**, 1-19.
- Staron, RS. (1997). Human skeletal muscle fiber types: delineation, development and distribution. *Can J Appl Physiol*, **4**, 307-327.
- Thiebaud, D.; Jacot, E.; DeFronzo, R.A.; Maeder, E.; Jequier, E.; Felber, J.P. (1982). The effect of graded doses of insulin on total glucose uptake, glucose oxidation and glucose storage in man. *Diabetes*, **31**, 957-963.
- Wagenmakers, A. J. M. (1999). Tracers to investigate protein and amino acid metabolism in human subjects. *Proceedings of the Nutrition Society*, **58**, 987-1000.
- Xu, G.; Paige, JS.; Jaffrey, SR. (2010). Global analysis of lysine ubiquitination by ubiquitin remnant immunoaffinity profiling. *Nat Biotechnol*, **8**, 868-73.

Chapter 6. Future directions

We can conclude that our Dynamic proteome profiling (DPP) technique is suitable to bring new insight to muscle adaptation and could be used in other models that result in changes to skeletal muscle phenotype. To build on data generated from this thesis, it would be interesting to investigate other models of adaptation, including pathological changes associated with diseases or ageing. For example, future work could utilise DPP to measure individual protein turnover during muscle wasting/dis-use, in response to silencing of the common peroneal nerve using tetrodotoxin, reported in Fisher et al, (2017). In particular, it would be of interest to know whether the dominant regulators of changes in protein abundance i.e. synthesis driven, degradation driven or a combination of them both, are of a similar weighting during muscle atrophy in comparison to an endurance-type stimulus (Chapter 3), that was also associated with a decrease in muscle mass. Such information will help us to understand if during muscle adaptation, individual protein responses are highly individualised/ specific to the protein, or subject to the specific nature of the stimulus used to induce adaptation. We provided novel evidence to suggest proteoform-specific degradation may act as an early indicator for phenotypic change (Chapter 3). However, we did not uncover the function of the unique site-specific phosphorylation that was identified in the specific myosin light chain 2 (MLRS) proteoform. A key area for future investigation could be focused to discovering the kinase(s) responsible for such contrasting differences between MLRS proteoforms. It would also be of interest to provide quantitative evidence for peptide-specific degradation that may be regulated differently between each proteoform. Such work could be achieved by a workflow similar to Xu et al, (2010), in order to identify specific sites of ubiquitination on MLRS peptides following endurance type exercise. Xu et al, (2010) generated a monoclonal antibody that can enrich for peptides containing lysine residues modified by di-glycine, an adduct left at sites of ubiquitination after trypsin digestion. This type of analysis could test the hypothesis that unique phosphorylation at Serine 20 is a precursor to ubiquitination of the nearby lysine residue (K31) and subsequent degradation. Di-glycine remnant profiling is relatively new, whereas phosphoproteome profiling methods are becoming more widely established. The growing interest in the field of phosphoproteomics could build on emerging knowledge (Potts et al, 2017) to answer questions regarding which modifications contribute to the adaptive processes during

longer term/ chronic interventions in skeletal muscle. Potts et al, (2017) reports almost 6,000 phosphorylation sites on more than 4,800 proteins including low abundance proteins involved in signal transduction. One hour after a bout of maximal intensity contractions there were more than 600 differences in phosphorylation status spread across more than 300 proteins. Less than half of the exercise responsive phosphorylation sites have been previously detected and in most cases the kinases responsible for phosphorylation of these sites have not been defined. However, although these phosphorylation sites are associated with maximal contractions it is not yet clear how they might contribute to changes in specific muscle functions. It is likely some of the acute changes in phosphorylation status are a result of increased mechanical stress, a greater metabolic demand or functional changes associated with force production. Informed from our current work (Chapter 3) it could also be reasoned that some of these phosphorylation could be associated with proteoform-specific degradation and could lead to new molecular insight to muscle adaptation.

Future directions in work arising from this thesis could focus on addressing some of the limitations associated with the DPP technique. DPP is highly novel and allows us to investigate skeletal muscle during adaptation at the individual protein level. However, the data generated from DPP were averages from periods of several days, which raises questions whether the data could be confounded by hour-to-hour fluctuations in synthesis and/or degradation of individual proteins. There is evidence to suggest that there are tissue-specific oscillations in the mechanisms that regulate protein synthesis during a 24-hour cycle, for example changes in the phosphorylation of the mTOR/p70S6K and ERK intracellular signalling pathway (Chang et al, 2017). Interestingly, p70S6k and ERK phosphorylation exhibited circadian variation in the fast-twitch muscle, but not in the slow-twitch muscle and this could provide a means to interrogate whether circadian oscillations affect DPP data. However, knowledge regarding the wider phosphorylation networks in fast- and slow-twitch muscle will be required alongside di-glycine remnant profiling to uncover the true regulatory mechanisms responsible. Such work could provide an important avenue of research to help us understand if circadian variation in protein synthesis-related intracellular signalling networks contribute to circadian rhythms in various muscle specific functions and/or homeostasis.

Whilst DPP is a highly novel and robust technique (Srisawat et al, 2019). We provide no data to link the DPP data presented in this thesis with physiology or histology data

that would enable wider interpretation. It would be beneficial to investigate the contractile properties and physiological characteristics in future investigations that employ DPP to correlate quantitative changes in individual protein turnover with quantitative assessments of strength, endurance and fatigue. For example, CLFS results in a marked slowing of the isometric twitch characteristics and maximum shortening velocity in rat muscle (Jarvis et al, 1996). Likewise, it will be important to know how increases in muscle hypertrophy induced by our co-activation model in Chapter 4 contribute to changes in maximal contractile force, e.g. is the amount of hypertrophy proportional to the maximal contractile force gain?

Finally, some of our own previous work (Hesketh et al, 2016) and others (Kim et al, 2012) provide evidence that suggests the rank order of protein synthesis changes when individual proteins are measured in different types of skeletal muscle and tissue. It would be pertinent to utilise DPP to investigate the several muscles across animal models, in the interest of repeatability and to understand if the individual responses documented in this thesis are a true result of the experimental intervention or as a result of inter-tissue variability.

References

Chang, S.; Yoshihara, T.; Machida, S.; Naito, H. (2017). Circadian rhythm of intracellular protein synthesis signalling in rat cardiac and skeletal muscles. *Biochemistry and Biophysics Reports*, **9**, 153-158.

Fisher, A.G.; Seaborne, R.A.; Hughes, T.M.; Gutteridge, A.; Stewart, C.; Coulson, J.M.; Sharples, A.P.; Jarvis, J.C. (2017). Transcriptomic and epigenetic regulation of disuse atrophy and the return to activity in skeletal muscle. *FASEBJ*, **31**, 5268-5282.

Hesketh, S.; Srisawat, K.; Sutherland, H.; Jarvis, J.; Burniston, J. (2016). On the rate of synthesis of individual proteins within and between different striated muscles of the rat. *Proteomes*, **4**, 1-12.

Jarvis, J.; Mokrusch, T.; Kwende, M.; Sutherland, H.; Salmons, S. (1996). Fast-to-slow transformation in stimulated rat muscle. *Muscle and Nerve*, **19**, 1469-1475.

Kim, S.T.Y.; Wang, D.; Kim, A.K.; Lau, E.; Lin, A.J.; Liem, D.A.; Zhang, J.; Zong, N.C.; Lam, M.P.Y.; Ping, P. (2012). Metabolic Labelling Reveals Proteome Dynamics of Mouse Mitochondria. *Molecular & Cellular Proteomics*, **11**, 1586– 1594.

Potts, G.; McNally, R.; Blanco, R.; You, J.; Herbert, A.; Westphall, M.; Coon, J.; Hornberger, T. (2017). A map of the phosphoproteomic alterations that occur after a bout of maximal-intensity contractions. *Journal of Physiology*, **15**, 5209-5226.

Srisawat, K.; Hesketh, K.; Cocks, M.; Strauss, J.; Edwards, B.; Lisboa, P.; Shepard, S.; Burniston, J. (2019). Reliability of protein abundance and synthesis measurements in human skeletal muscle. *Proteomics*, **2**, 194-198.

Xu, G.; Paige, JS.; Jaffrey, SR. (2010). Global analysis of lysine ubiquitination by ubiquitin remnant immunoaffinity profiling. *Nat Biotechnol*, **8**, 868-73.